PHOTOMETRIC STUDIES IN INFRARED ASTRONOMY

A Thesis Submitted to

The Devi Ahilya Vishwa Vidyalaya of Indore

for

THE DEGREE OF DOCTOR OF PHILOSOPHY

IN

PHYSICS

by

SAM RAGLAND

PHYSICAL RESEARCH LABORATORY

AHMEDABAD 380 009

INDIA

FEBRUARY 1996

CERTIFICATE

I hereby declare that the work presented in this thesis is original and has not formed the basis for the award of any degree or diploma by any University or Institution.

Sam Ragland

Sam Ragland Prabaharan D.
(Author)

Certified by:

T. Chandrasekhar

Dr. T. Chandrasekhar
(Thesis Supervisor)
Reader
Astronomy & Astrophysics Division
Physical Research Laboratory
Ahmedabad 380 009, India.

Contents

Acknowledgements

To begin with, I wish to express my gratitude to my supervisor, Dr. T.Chandrasekhar, whose tolerant attitude, inspiring nature and competent guidance has helped me immensely in this endeavor. I consider it a privilege to have been associated with him. I am also profoundly thankful to Dr. N.M.Ashok for his guidance. Being the first research student of Drs. T.Chandrasekhar and N.M.Ashok, I enjoyed privileges both in academic and non-academic fronts. I thank them for all the knowledge I gained during my tenure as a research student. Their company on many observational trips to Kavalur and Mt. Abu was enjoyable and stimulating.

My sincere thanks and gratitude to Prof. J.N.Desai for the useful discussions I had with him in the field of Optics. It was for me an honor to have the opportunity to work with him and thereby learn various aspects of 'atmospheric scintillation' and 'astronomical photography'. I am also grateful to Prof. M.R.Deshpande for his valuable suggestions and comments for betterment of the thesis, for showing interest in my work and providing me the necessary facilities both at Thaltej and PRL.

I am grateful to Dr. A.Richichi of Arcetri Observatory, Italy, for the useful discussions I had with him in the field of High Angular Resolution Studies and also for his keen interest in the work carried out in this thesis. I am grateful to Prof. R.Sridharan for his continued interest in my work and for his encouragement, suggestions and useful discussions. It was a pleasure working with Dr. H.C.Bhatt of IIA, Bangalore. I thank him for the encouragement and support. I am grateful to Jerry (Dr. P.Janardhan) and Ban (Dr. D.P.K. Banerjee) for their company, useful discussions and for critically going through portions of this manuscript. I thank Prof. B.G.Anandarao for showing keen interest in my work.

I am grateful to Drs. Shyam Lal, Subbu (K.P.Subramanian), Ramesh & Sai Iyer for their interest in my progress. I am indebted to them for helpful advice they used to give me whenever the occasion demanded. I thank Profs. Masahiko Hayashi and Yuki Kobayashi of NAOJ, Japan for the interest they had shown in my work.

I express my sincere thanks to the Director, Prof. G.S.Agarwal for his keen interest in the High Angular Resolution program at PRL. I thank Prof. J.C.Bhattacharya and R.Cowsik of IIA, Bangalore for granting adequate telescope time for the Kavalur observations presented in this thesis.

I am grateful to the general encouragement given by Profs. Raghavarao, B.H.Subbaraya, *S.K.Bhattacharya, J.N.Goswami, Drs. U.C.Joshi, H.O.Vats, Ashok Singal, B.R.Sitaram, Profs. Rengarajan of TIFR, Ram Sagar and Parthasarathy of IIA and Drs. S.K.Ghosh of TIFR and T.P.Prabhu of IIA. My sincere thanks are due to Prof. Maheshwari of Devi Ahilya Vishwa Vidyalaya, Indore for his ever-ready and self-less help.*

I am grateful to Mrs. S.Jani for her computational assistance in the prediction of occultation events. I am thankful to Messrs. K.S.B.Manian, N.S.Jog & R.K.Mahadkar for technical support. I accord my thanks to the staff members of Gurushikhar and Kavalur observatories, Mr. G.G.Dholakia and other staff members of computer center, staff members of library and workshop for their excellent service.

I appreciate gratefully, Kunu, my friend and colleague who has done for me more than what one should expect, especially, for critically going through the whole manuscript. I am grateful to Watson for his enjoyable company, otherwise, many frustrating cloudy nights at Kavalur would have been hell and also for his support in collecting data and very useful long discussions. My special thanks are due to my friend Aparna, for her timely encouragement and help, especially at the crucial last stages of this thesis. It has been a memorable experience to have been associated with her.

I am thankful to my senior colleague and friend, Seema for her company, useful discussions and for her continued contact, encouragement through letters and e-mail. I am thankful to my seniors Drs. K.P.Raju and Debi (Debi Prasad), Mac (Maqbool) and Supriyo for their encouragement and useful discussions.

I will always cherish the cheerful and unforgettable company of my pals Krish, Ramani, Bhushee, Rama, Guru and Siva. Heart-felt thanks to my friends Jyoti, Navin, Yags, Nanda, Manish, Chakko, Yadav, Prabir, Tarun, Poulose and Biju. The joyful company of Anshu, Arul, Biswa, Chetan, Deba, Debabrata, Devashis, Gautam, Ghosh, Himadri, Jagadheesha, Kamath, Manoj, M.Lal, Mitaxi, Muthu, Pallam, Prahlad, Prashant, Ramaswamy, Ratan, Rath, Rathin, Sandeep, Santha, Sarangi, Sarkar, Shibu, Shikha, Somesh, Srini, Sushma, Varun, Viju and Vijay is acknowledged. Their fond memories will echo in my mind.

I thank my college friends Tom (Thomas), Elizabeth, Jeyaseeli and Christopher for their encouragement. I am grateful to my friends Maria of Bulgaria, Jung-kyu Lee of Korea and Ali of Iran for their company during my stay with them and also for keeping me cheerful through contact by e_mail. I thank my friend Neeti Tolia for her letter correspondence and her *encouragement.*

I thank Mr.&Mrs. Prabhu for their encouragement, affection and hospitality, especially, during special occasions, I felt as if I am at home. I thank Mrs. Revathi Chandrasekhar, Mrs. Aruna Ashok, Mrs. Jayashree Ramani, Mrs. Navin, Mrs. Shravani Bhushan, Mrs. Jerry, Mrs. Subbu, Mr.& Mrs. Jebakumar, Mr.& Mrs. Israel, Dr.& Mrs. Sekar, Mr.&Mrs. Narayanan, Mukul and Archana for their affection and hospitality on many occasions during my stay here at Ahmedabad.

Finally, I am grateful to my parents who made it all possible, my brother Jos, my sister Kiruba and brother-in-law Jebaraj for their encouragement, support and love and to my sweet niece Jency for her affection. I am indebted to their sense of optimism.

Research Publications

1. Near infrared observations of Nova Herculis 1991.
   Chandrasekhar, T., Ashok, N.M. & **Sam Ragland**, MNRAS, 1992, **255**, 412.

2. A high speed photometer in the optical region for lunar occultation studies.
   Chandrasekhar, T., Ashok, N.M. & **Sam Ragland**, JAA, 1992, **13**, 195.

3. Near infrared coronal line emission in Nova Her 1991.
   Chandrasekhar, T., Ashok, N.M. & **Sam Ragland**, JAA, 1993, **14**, 7.

4. A high speed near infrared photometer for lunar occultation studies.
   Ashok, N.M., Chandrasekhar, T., **Sam Ragland** & Bhatt, H.C., Experim. Astron., 1994, **4**, 177.

5. Near Infrared High Angular Resolution Observations of Stars and Circumstellar regions by the technique of Lunar Occultations.
   Chandrasekhar, T., Ashok, N.M. & **Sam Ragland**, Proc. of IAU Symposium on *Very High Angular Resolution Imaging*, 1994, 376.

6. SAO 75669: a late-type giant behind the molecular cloud MBM 12.
   Bhatt, H.C., Sagar, R., Subramaniam, A., Gorti, U., Chandrasekhar, T., Ashok, N.M. & **Sam Ragland**, 1994, A&A, **289**, 946.

7. Near Infrared High Angular Resolution Observations of Stars and Circumstellar regions by the technique of Lunar Occultations.
   Chandrasekhar, T., Ashok,N.M. & **Sam Ragland**, Proc. of IAU Symposium on *Astronomical and Astrophysical Objectives of sub-milliarcsecond Optical Astrometry*,1994 (In press).

8. Sub-milliarcsecond resolution observations of two carbon stars: TX Psc and Y Tau revisited.
   Richichi, A., Chandrasekhar, T., Lisi, F., Howell, R.R., Meyer, C., Rabbia, Y., **Sam Ragland** & Ashok, N.M., 1995, A&A, 301, 439.

9. Detection of Circumstellar Dust Shell around Supergiant TV Gem from Milliarcsecond Resolution Near Infrared Observations.
   Sam Ragland, Chandrasekhar,T. & Ashok,N.M, 1996, A&A (To appear).

10. Milliarcsecond Resolution Observations of M giants in the near infrared by Lunar Occultations.
    Sam Ragland, Chandrasekhar,T. & Ashok,N.M, 1996, (To be communicated).

Abstract

This thesis is a high angular resolution study of the central star and its circumstellar region in the case of a few late-type stars which emit predominantly in the infrared part of the spectrum. This study has been carried out by perfecting the novel technique of lunar occultation, in which the motion of the airless limb of the moon, moving relative to the star, provides a straight edge diffraction pattern on the earth in which is embedded the high angular resolution information. This thesis work has involved the design and development of a dedicated high speed infrared photometer for lunar occultations, actual observations of occultations at a wavelength of 2.2 μm using the telescopes at the Gurushikhar and Kavalur observatories, development and use of a detailed software package for analysing occultation light curves and astrophysical interpretation of the results.

As a direct result of these lunar occultation observations, the circumstellar dust shell at a distance of $\sim$ 20 stellar radii from the central star has been detected, for the first time, around the M1 supergiant star TV Geminorium. Two lunar occultations of the carbon star TX Piscium, which have been successfully observed in the course of this thesis work, have in conjunction with other lunar occultation observations on the same source led to the scenario of an asymmetric dust shell very close to the photosphere of the star. In addition to these two special objects, seven stars are clearly resolved from occultation observations and stringent upper limits to the angular size have been derived for six other stars.

Apart from lunar occultation observations, infrared temporal study of the fast nova, Nova Herculis 1991 was also carried out during the initial phase of the thesis work. Important results on the early grain formation and the detection of an infrared forbidden coronal emission line at 1.98$\pm$0.02 μm attributable to silicon ion [Si VI] in this nova are incorporated in this thesis.

High Angular Resolution Studies in the Infrared

Chapter 1

Introduction

In recent times there has been a remarkable advancement in many fields of 'Observational Astronomy'. But surprisingly, there are only few observational data available on the stellar angular sizes. The reason for this dearth of data is the great difficulty encountered in measuring the extremely small angles involved. Stars generally have angular diameters much less than one hundredth of an arcsecond, except for a few supergiants which have angular sizes less than one tenth of an arcsecond. Moreover, the earth's turbulent atmosphere limits the angular resolution of ground based optical observations, known as 'seeing limit', to about an arcsecond. Hence no star, barring the Sun, can be resolved from direct ground based imaging observations. Overcoming the 'seeing limit' and reaching the telescope diffraction limit has been the dream of the astronomers from the time of William Herschel. The term 'High Angular Resolution' has been used throughout this thesis to mean the angular resolution below the 'seeing limit'.

High Angular Resolution observations, at the level of a few milliarcseconds, on stellar systems and their circumstellar regions in our galaxy provide important and often crucial information about the nature of these sources. Apart from measuring the angular size of the central source, such observations in the near infrared region can provide direct evidence of circumstellar material around a source. Knowledge of stellar angular size and bolometric flux can yield the effective temperature of the occulted star. High angular resolution observations can also establish whether the source is single or multiple at a very fine level of separation ($\sim$ 10 milliarcseconds).

The primary objective of this thesis is to resolve the stellar photospheres and the circumstellar dust envelopes around a few evolved stars at a few milliarcsecond levels of angular resolution in the near infrared region using the technique of lunar occultation. The thesis work consists of the designing and development of a dedicated instrument for lunar occultation observations, observations of occultation events, development of a detailed computer code for analysing the light curves and interpretation of the results. When the instrument (developed for the present study) was under field test, a fast nova, Nova Herculis 1991 erupted and was observed with this instrument by the author. Infrared photometric and spectrophotometric studies which were carried out on this nova have also been included in this thesis.

1.1 Different methods of achieving High Angular Resolution

The problem of measuring the small angles subtended by stars at the earth is a very old one in the history of astronomy. Attempts have been made from the times of Galileo to determine these angular sizes. His work *Dialogue concerning the Two Chief World Systems* gives a brief description of a simple experiment wherein a fine vertically suspended cord was used to occult the star Vega and to measure the distance at which this occurs. Though, skillfully conducted, this experiment gave a very large spurious value of 5 arcseconds. Was it the angular scintillation due to the atmosphere, that he was measuring? Later, Newton also made an attempt to theoretically calculate the angular size of stars by assuming that the Sun is an object identical to the stars. If it is placed at a distance where it appears to be of the same magnitude as Vega, then the angle subtended will be 2 milliarcseconds, which closely approaches the presently accepted value of 3 milliarcseconds.

Fizeau's idea of observing Young's fringes had resulted in the development of various interferometric techniques during last century. Michelson (1920) had shown that the angular size of a star can be measured from the interference fringes caused by superposing star light coherently from two well separated mirrors. The first stellar interferometer was built by Michelson and Pease in 1920 and had a baseline of 20 ft.

Later, Hale and Pease designed an interferometer having a 50 ft baseline with separate mounts for the mirrors. However, this experiment was not very successful. As the phase of the fringes are not observed, some model has to be assumed for the stellar brightness distribution. The major difficulty with the instrument was maintaining the two light paths equal to within a fraction of the wavelength of the light. The other problem was the effect of atmospheric scintillation on the precision of the measurements. Nevertheless, angular diameters of 6 cool giants/supergiants had been measured by their interferometer. The interferometer had reached an angular resolution of ~ 20 milliarcseconds with a measurement error in the range $10 - 20$ % (Hanbury Brown, 1974).

Hanbury Brown and Twiss (1956) proposed the Intensity Interferometry as an alternative to Michelson Interferometry. This method was fairly free from some of the technical problems associated with the Michelson Interferometry. Unlike in the case of the Michelson Interferometer, the light received at the two spaced mirrors were separately recorded and the interference carried out electrically. The technique works on the principle that if there is coherence between the light at two spaced points, there will also be a correlation between the fluctuations in the intensity at these points. The only Intensity Interferometer built till today was the one at Narrabri, Australia having two 6.5m telescope apertures at baselines in the range $10 - 150$ m. The major advantage of the technique is that mechanical stability is not as stringent as in the case of Michelson Interferometry and the technique is relatively insensitive to atmospheric scintillations. The major drawback however is the relatively low sensitivity of the technique compared to Michelson Interferometry and hence the need for large aperture telescopes. The technique could be applied to only hotter bright stars ($m_b < +2.5$) as the maximum possible signal-to-noise ratio (SNR) of the technique drops below the detection limits for cooler stars. Due to these limitations, the technique was abandoned in the 60's. In spite of these limitations, angular diameters of 32 southern early type stars had been measured with the technique which could go below 1 milliarcsecond angular resolution for the first time (Hanbury Brown et al., 1974).

Labeyrie (1970) proposed Speckle Interferometry which consists of recording the fast-moving fine structures inside the seeing disc and performing statistical analysis to recover the diffraction limited high angular resolution information. Initial observations by Gezari et al. (1972) on Betelgeuse with the technique confirmed Pease's angular size measurements and also added hints on color dependence and limb-darkening effects on the angular size. Speckle Interferometry can be used as a focal plane instrument and hence has been used with almost all the large aperture telescopes around the globe.

Currie et al. (1974) introduced a version of Michelson Interferometry referred to as 'Amplitude Interferometry'. This is very similar to classical Michelson Interferometry with the difference that the re-collimated beams are combined for interference in a parallel fashion so as to produce a field of uniform illumination thereby enabling the efficient use of photoelectric detectors. The technique resulted in determining the angular diameters of 12 cool giants which includes α Bootes, α Orionis, α Tauri & β Pegasi (Currie et al., 1974) and α Herculis (Knapp et al., 1975). The mean internal error in their measurements are $\sim 15\%$. Tsuji (1976) pointed out that the measured angular sizes are larger than that derived from other methods. The technique has no added advantage when multi-pixel sensors are used instead of single sensors.

Breckinridge (1972) suggested Rotating Shearing Interferometry. In this technique, high angular resolution information is obtained from the interference fringes observed on a plane conjugate to the telescope pupil plane where two pupil images are superposed, one being rotated at a given angle (0 - 180 degrees) with respect to the other. The primary advantage of Rotating Shearing Interferometry with respect to Speckle Interferometry is that the visibility of the perfectly frozen fringes is insensitive to atmospheric scintillations and telescope induced aberrations. When the exposure time is increased, the visibility is uniformly depressed by the same amount at all frequencies except close to zero. Therefore, the uncertainity due to the need of a reference star can be avoided. Also, the interferogram is free from speckle noise. High angular resolution observations of α Orionis with a Rotating Shearing Interferometer has revealed the presence of a circumstellar dust envelope and departure from circular symmetry (Roddier & Roddier, 1983, 1985; Roddier et al., 1986). There are not many Shearing Interferometers routinely used, probably being relatively difficult to use in comparison with Speckle Interferometers.

As early as 1953, Babcock suggested an attractive approach to obtain diffraction limited imaging using the concept of adaptive optics (Babcock, 1953). Modern adaptive optics systems consist of wavefront sensors to measure the wavefront distortion and an optical component (generally a deformable mirror) to compensate for the wavefront distortion caused by the turbulent atmosphere. The wavefront distortion is measured using either the object under study at a different wavelength, a nearby stellar source, or an artificial source (Laser-guide star adaptive optics). Adaptive optics allows imaging without the complications of image reconstructions applied to short-exposure noisy images and hence provides diffraction limited images of much fainter and complex objects. In the case of unresolved images, the technique puts most of the collected photons in as a small image as possible, thereby allowing, among other things, better discrimination against the sky background, improving high spatial and spectral resolution spectroscopy and enhancing interferometric imaging with telescope arrays (Beckers, 1993).

Despite the limitations imposed by the earth's turbulent atmosphere, remarkable progress has been made in the past decade in long-baseline interferometry in the optical and infrared wavelengths Shao & Colavita (1992). Modern Optical Long-BaseLine Interferometry (OLBI) begins with the interferometer of Labeyrie (1975), I2T, which was the first interferometer which provided direct interference fringes using separate telescopes, over a baseline of 12m. Some of the many long-baseline interferometers operational currently include the Mark III in USA (Shao et al., 1988), GI2T in France (Labeyrie et al., 1986), Sydney University Stellar Interferometer (SUSI) in Australia (Davis, 1994), the Infrared/Optical Telescope array (IOTA) interferometer (operated at 2.2 μm) in USA (Dyck et al., 1995) and the Infrared Michelson Array (IRMA) in USA (Dyck et al., 1993). In addition, the I2T interferometer in France (which was originally designed for optical wavelengths) was also successfully used at 2.2 μm (Di Benedetto & Rabbia, 1987). Diameters of stars of different spectral types have been measured by Mark III including cool giants in and out of TiO bands (Quirrenbach et al., 1993a), carbon stars with optically thin dust emission (Quirrenbach et al., 1994a), Be stars (Quirrenbach et al., 1994b), Nova Cygni 1992 (Quirrenbach et al., 1993b) and Mira (Quirrenbach et al., 1992). The precision of the best measurements is about 1% (Mozurkewich et al., 1991). Stellar angular diameters at 2.2μm were obtained from

IRMA system for o Cet (Ridgway et al., 1992), α Ori (Dyck et al., 1992) and α Her (Benson et al., 1991).

In 1974, Johnson and his co-workers constructed a Heterodyne Interferometer using the two 81cm McMath auxiliary telescope at Kitt Peak at a baseline of 5.5 m (Johnson et al., 1974). In this technique, after heterodying to an intermediate frequency, the signal processing is identical to that of a radio interferometer. Several bright infrared sources have been observed with the interferometer to study the spatial distributions of dust and their positions (Sutton et al., 1977,1978,1979,1982). In 1988, Townes and co-workers built a dedicated Infrared Spatial Interferometer (ISI) located at Mt. Wilson, operating in the $9 - 12$ μm atmospheric window (Bester et al., 1994). The spatial distribution of dust around a sample of 13 well known evolved stars have been studied with the interferometer (Danchi et al., 1994). In this thesis an alternative to the above discussed interferometric techniques viz. the technique of lunar occultation, has been used for high angular resolution studies and is described in the following section.

1.2 The Phenomena of Lunar Occultations

1.2.1 A Historical outline

Lunar occultation of a stellar body is one of the most ancient of astronomical observations. Pre-telescopic observations by Aristotle date back to 350 BC. The earliest recorded lunar occultations of stars are documented in Ptolemy's Almagest. White & Feierman (1987) have pointed out that the Almagest lists seven occultations reported by different observers over the period 294 BC to AD 98. These seven occultations were of only three objects, α Vir, β Sco and the stars of the Pleiades cluster. Copernicus observed an occultation of Aldebaran (α Tau) in 1497. These pre-telescopic observations showed the relative closeness of the moon and the small angular sizes of stars. The first telescopic observation was reportedly made by Bullialdus in 1623 AD. Jeremiah Horrocks in 1662, from observations of the passage of moon through the Pleiades, noted that rapidity of occultation would imply a small angular size for the star. On 21 April, 1720 Cassini observed occultation of the double star γ Vir and noted the 30 seconds time separation between the disappearance of the components. It was probably William Herschel in

1850 who had realised the ability of the occultation process to reach higher angular resolution than the diffraction limit of the telescope, particularly in relation to resolving binaries. As early as in 1834, Bessel had concluded from the suddenness of occultation the absence of any appreciable lunar atmosphere. Compilation of early observations of lunar occultations can be found in Newcomb (1878) and in Morrison et al. (1981).

The next generation of lunar occultation studies began towards the end of $19th$ century with the advent of photographic emulsions. On 25 Feb 1898, E.S.King at Harvard obtained the first photographic record of an occultation event with a series of exposures with exposure time as short as 60 milliseconds. Using a rotating plate holder similar to King's but with a much fast rotation rate (60mm/s) Arnulf in Paris in 1936 was able to record two fringes during the occultation of Regulus. Arnulf inferred from his data a diameter between 1.5 and 2 milliarcseconds which proved to be an inspired guess, as the value measured by intensity interferometry was 1.3 milliarcseconds, which even today, is at the limit of the occultation technique.

The nature of the occultation process began to be understood with the simple ideas of Major McMahon in 1909. Considering it to be a purely geometric process he reasoned that 1 milliarcsecond star should be occulted by the moon in a finite time $\sim 1/500$ seconds. Eddington (1918) immediately pointed out that lunar occultation of pseudo point source is a diffraction process. He calculated correctly the fringe amplitude and spacing from simple diffraction theory but concluded wrongly that all stars in the visible region would show angular diameter of atleast 8 milliarcseconds, this being the angular size of the central fringe. It was only much later in 1939 that J.D.Williams of Princeton observatory and A.E.Whitford working independently showed that for a finite source size though the spacing between the fringes remain the same as that of a point source, the amplitude of the fringes is reduced (Whitford, 1939 & Williams, 1939). A high speed photometer and sensitive detector could detect this departure from a point source. The development of photocells and high gain amplifiers mark the beginning of the third chapter of the occultation observations wherein, photoelectric measurements became feasible. Whitford, in fact developed a photocell, used it at the 100 inch Mt. Wilson telescope and recorded the output photographically from the oscilloscope. In Sept., 1938 Whitford successfully recorded diffraction fringes of β Cap and ν Aqr. It is an interesting coincidence that ν Aqr has also been observed as part of this thesis. The successes of Whitford coupled with the availability of photomultipliers and amplifiers stimulated lunar occultation observations in the years after World War II. A new series of occultations of α Sco began in 1950 and was observed by David Evans in South Africa. The discovery of radio pulsars in 1967–68 and the growing awarness of the importance of rapid variability in white dwarfs and cataclysmic variable stars led to developments of high speed photoelectric photometry and a revival on interest in occultation observations in 1968. This began the modern era of lunar occultation with Nather & Evans introducing the then new technique of digital recording (Nather, 1970) and the application of least squares method to modelling the light curve (Nather & McCants, 1970).

The observations of the lunar occultations in the near infrared region with its inherent advantages was pioneered by Ridgway and Joyce in mid 1970s at the 1.3 m telescope of Kitt Peak National Observatory (Ridgway et al., 1977). In spite of being one of the oldest techniques, it is remarkable that lunar occultation is still one of the most powerful and productive techniques for achieving high angular resolution in the optical and near infrared regions. At present, IR arrays have reached a level of performance where their use for lunar occultation is expected to improve the limiting magnitude and accuracy of the technique (Richichi, 1994b). The scope of IR arrays for lunar occultation studies has been discussed in the last chapter.

1.2.2 Technique

One of the most impressive sights in the heavens is the dramatic contrast between the slow approach of the dark edge of the lunar limb and the near instantaneous extinction of a star during an occultation. The technique consists of recording a fast photometric time sequence of a star disappearing (or emerging from) behind the moon's limb. The lunar limb acts as a plane diffracting edge which diffracts the light from a distant star which is considered to be a pseudo point source. Like a total solar eclipse (lunar occultation of Sun), lunar occultation of a star has all the excitement and drama of a fleeting astronomical event. The schematic diagram of the phenomena of lunar occultation is shown in the Fig. 1.1.

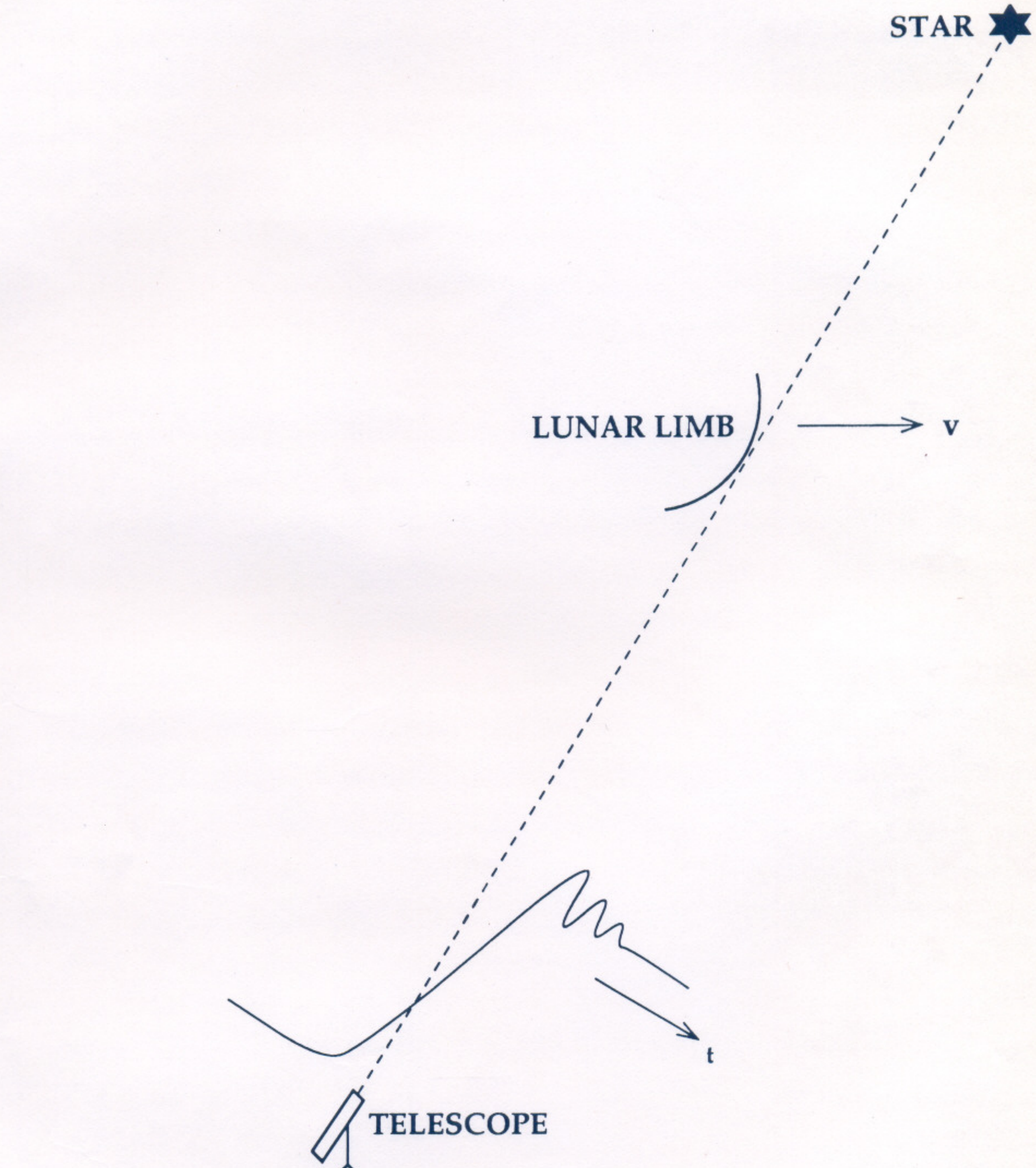

Figure 1.1: *Schematic diagram of the phenomena of Lunar Occultation.*

The intensity pattern expected when a monochromatic point source is obscured by lunar limb is given by

$$I(t) = 0.5 I_o \left[(0.5 + C(\omega))^2 + (0.5 + S(\omega))^2 \right] \tag{1.1}$$

(Born & Wolf, 1959), where I_o is the stellar brightness and C(ω) and S(ω) are the Fresnel integrals defined as,

$$C(\omega) = \int_0^\omega cos\left(\frac{\pi}{2}t^2\right) dt \tag{1.2}$$

$$S(\omega) = \int_0^\omega sin\left(\frac{\pi}{2}t^2\right) dt \tag{1.3}$$

and ω, the dimensionless Fresnel number given by

$$\omega = \left(\frac{2}{\lambda d}\right)^{\frac{1}{2}} x \tag{1.4}$$

where x represents the actual distance on the ground from the observer to the geometric point of occultation, d is the distance to the moon and λ is the wavelength of observations. The geometric point of occultation is where the stellar intensity reduces to 25% of its value.

The maximum intensities occur at ω = 1.22, 2.34, 3.08, ... and minimum intensities occur at ω = 1.88, 2.74, ... For a wavelength λ = 2.2μm and distance, d = 400,000km, using eqn. 1.4, we obtain $x = 20.98\omega$ metres. The angular width to the first minimum is (1.88/d) (λ d/2)$^{\frac{1}{2}}$ = 20.33 milliarcseconds.

In a formal sense, the occultation process at a wavelength 2.2μm is equivalent to a diffraction limited telescope having an aperture of (1.22 λ)/(1.88 $(\frac{\lambda d}{2d})^{\frac{1}{2}}$) $\sim$ 27 m.

More generally we can write,

$$a = 43 \left(\frac{\lambda}{2.2}\right)^{\frac{1}{2}} \left(\frac{d}{10^6}\right)^{\frac{1}{2}} \tag{1.5}$$

where a is in m, λ and d are in km.

The schematic diagram of the geometry of lunar occultation is shown in the Fig. 1.2. If V is the velocity with which the moon moves to occult the distant star at a point P on the lunar limb, the velocity component in the direction of occultation, V_{comp} is given by V cos(θ_{CA}), where θ_{CA} is the contact angle. Moon's orbital motion being $\sim 13^o$/day, the lunar rate relative to star is $\sim 0.5''$/sec. The resulting fringe pattern sweeps over the

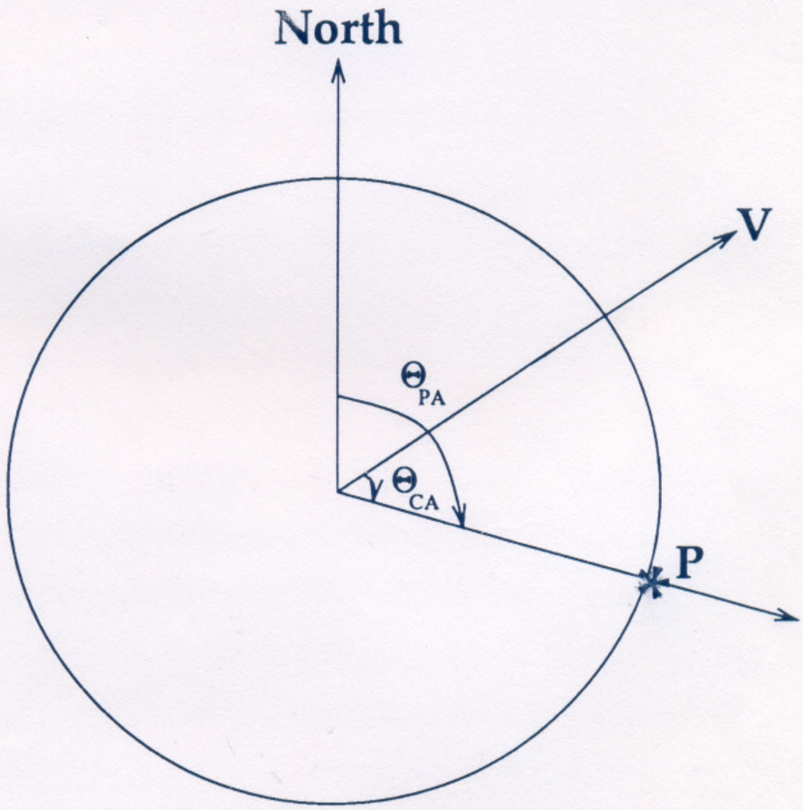

Figure 1.2: *Schematic diagram of the geometry of Lunar Occultation.*

Table 1.1: *Terrestrial length and time scales of the lunar occultation fringes.*

Fresnel number ω	Fringe	Length scale (metres)		Time scale (millisec.)	
		@0.5 μm	@2.2 μm	@0.5 μm	@2.2 μm
1.22	Max.	12.2	25.6	24	51
1.87	Min.	18.7	39.2	37	78
2.35	Max.	23.5	49.3	47	99
2.74	Min.	27.4	57.5	55	115
3.08	Max.	30.8	64.6	62	129

earth's surface as fast as ~ 1 km/sec, the distance to the moon being $\sim 4\times 10^5$ km. The speed of the diffraction fringes which sweep across the telescope objective depends on many factors like the exact distance to the moon, the position angle of occultation, the direction of the lunar velocity vector, altitude of the moon and the latitude of the observatory. Table 1.1 shows the fringe maxima and minima distances in metres from the point of occultation for visible (0.5 μm) and near IR (2.2 μm) wavelengths. The last two columns in Table 1.1 list the time of crossing of the detector plane of a particular maxima or minima taking typical value of ~ 0.5 km/s for the speed of the diffraction pattern on the ground. It is clear that it takes only little more than 120 millisec for 3 maxima to cross the detector plane at 2.2 μm. The conditions of visible light occultations are more stringent by a factor of two. The need for high speed and sensitive detectors to record the fringes is thus evident. Since the event is a very fast one and lasts for only a few hundred milliseconds, one can successfully record the event, only if the telescope is tracking the star during the event and is equipped with a High Speed Photometer which samples the light curve at ~ 1 KHz. The high angular resolution information is embedded in the Fresnel diffraction pattern which is scanned by the telescope as the pattern sweeps past. The most attractive aspect of this technique is that high angular resolution down to 1-2 milliarcseconds can be achieved in the optical and near infrared with very high accuracy of ~ 0.1 milliarcseconds (Ridgway et al., 1977, Richichi et al., 1988).

This theoretical diffraction pattern is averaged out by various factors. Among them are the instrumental smearing effects like the finite optical filter bandwidth, finite telescope aperture and finite time response of the detector system. The spectral distribution and finite size of the source also influence the light curve. All these effects should be carefully considered and very accurately taken care of in the data reduction procedure which consists of the standard Nonlinear Least Squares technique.

1.2.3 Advantages of lunar occultations

The lunar occultation method has two very important facts that need to be appreciated. Firstly, the phenomena takes place well outside the earth's atmosphere. So, in principle it is unaffected by atmospheric turbulence and more specifically, it is not limited by 'seeing'. Further the technique can be used even in a unfavorable atmospheric conditions (partially cloudy skies) unlike other interferometric techniques, as the event is over in a few hundred milliseconds. Secondly, the angular resolution is not limited by the diffraction limit of the telescope unlike other high angular resolution techniques like Speckle Interferometry. The angular resolution obtained far exceeds the theoretical diffraction limit of the telescope used. Here, the telescope acts only as a flux collector to collect the diffracted star light. Hence, telescopes in the 1-2m class suffice for excellent occultation work (although a larger aperture increases the SNR). It is also not absolutely necessary to have telescopes of the highest optical quality. We have shown in this thesis that even with a telescope of relatively poor optical quality having a point spread function of $\sim$ 8 arcsec one can do excellent lunar occultation work to reach milliarcsecond levels of resolution in the near infrared wavelengths. The various smearing effects being taken care of in the data analysis procedure, the finite SNR ratio in the light curve is the one which finally limits the achievable angular resolution. The SNR is defined (in all further discussion in this thesis) as the ratio between the signal of the unocculted star and the standard deviation (1 σ) of the best fit to the data. A SNR of $\sim$ 50 is sufficient to resolve the central star. A SNR $\sim$ 10, though inadequate in measuring fringes, can detect binaries. Of course, the ultimate limit is constrained by the various observational parameters like distance to the moon, wavelength of observation and lunar velocity component in addition to finite SNR.

One can thus clearly see the advantage that lunar occultation has over other high angular resolution techniques. Techniques like speckle interferometry and wavefront shearing interferometry require a large telescope while long-baseline techniques require two or more telescopes with a unique design. The instrumentation, data acquisition and data reduction techniques involved in these methods are also far more complicated. These methods are also greatly affected by seeing and require an exceptionally good astronomical site. Another major difference is that most of these high angular resolution techniques require a calibration source, whereas lunar occultation does not need one.

The technique of lunar occultation has many more advantages when observing in the near infrared region compared to the visible region. We have seen from actual measurements that the scattered lunar background light is less in the near infrared by a factor of ~ 20 relative to that in the optical region. As is evident from eqn. 1.4, the fringe pattern scales as the square root of the wavelength of observation. Hence, the fringes spread out wider by a factor of 2 resulting in easier sampling. In the near infrared, the possibility of daytime observations increases the rate of favorable events in this region of the spectrum. Late-type giants emit most of their radiation in the near infrared. In addition most of the cool giants do have detectable IR excess. This infrared excess has generally been attributed to warm dust particles in the circumstellar envelope.

1.2.4 Disadvantages of lunar occultations

It must be admitted, though, that the lunar occultation technique has some inherent disadvantages. The most obvious drawback is the limited sky coverage. Only stars that lie in the moon's path in the celestial sphere can be observed. Hence, observationally one is restricted to the zodiacal belt only. But this is not a very stringent drawback. The moon in its orbit covers about 10 % of the whole sky. The number of sources which is covered in the Two Micron Sky Survey (Neugebauer & Leighton, 1969) in the declination zone of $\pm 30^o$ amounts to ~ 3500, which is quite a large number for most of which angular diameter is not known. Hence, important and interesting events can be observed unless the interest is focussed only on a particular type of object. Secondly, a single lunar occultation observation yields only a one dimensional source structure along the direction of occultation. But if occultations are taken at different sites or the source is occulted repeatedly, one can get observations involving different occultation geometries i.e. different position angles. From this it is possible to obtain some two dimensional information of the occulted source. As an example, two dimensional brightness information have been recovered for a carbon star TX Psc from multiple observations at different position angles and are discussed in chapter 3. Finally, the most severe drawback with this technique is that it is event based. Though the lunar cycle is such that a given star is often occulted several times within a few lunations, this occurs at different locations on earth. Hence each event is a unique one. The cycle, with identical circumstances, repeats every 18.6 years and corresponds to the period of precession of moon's nodes. The parallax of the moon is large ($\sim 1^o$) and hence an occultation event is observable only at a few places around the globe.

1.2.5 Scope of the technique

Lunar occultation observations have been used widely. Apart from the study of the theory of lunar motion, the existence of a lunar atmosphere, study of lunar limb irregularities and astrometry of radio and X-ray sources, lunar occultation has very important high angular resolution applications. According to the review of high angular resolution techniques by McAlister (1985), the great majority of all known stellar angular diameters have been obtained by means of lunar occultation.

A fundamental parameter in the understanding of stellar atmosphere is the effective temperature (T_{eff}). Its accurate determination observationally is crucial in testing the validity of different models of stellar atmospheres. Various methods leading to indirect determinations of T_{eff} based on photometric or spectroscopic data exist and have been reviewed by Böhm-Vitesse (1981). A direct determination of T_{eff} without any hypothesis is however possible only from measurements of angular diameter and apparent bolometric flux of the star (F), from the definition,

$$T_{eff} = \left[\frac{F}{\sigma\phi^2}\right]^{\frac{1}{4}} \tag{1.6}$$

where, σ is the Boltzmann constant and ϕ is the angular diameter of the star.

T_{eff} determinations accurate to $1 - 2$ % are generally required to discriminate between different stellar models. The major drawback in achieving this level of accuracy in direct determination of T_{eff} arises due to the non availability of accurate stellar angular diameters rather than bolometric flux.

Apart from Michelson's pioneering efforts on a few supergiants, observational programs on stellar diameter measurements have been carried out for a limited number of early type stars (hotter than F8) by intensity interferometry (Hanbury Brown et al., 1974). For cooler stars, lunar occultations, and in recent years, optical interferometric methods have been used. As we discussed earlier, due to reduced lunar background and better signal strength, lunar occultation in the infrared region can provide much more accurate angular diameter estimates than in the optical region for late-type stars (due to improved SNR) and this advantage has been exploited in the present work.

Ridgway et al. (1980) gave an effective temperature scale for cool giants in the spectral range K0 to M6 from lunar occultations observations of 20 stars. This calibration is presently very widely used in a variety of astrophysical scenarios, and is the only direct effective temperature calibration that includes cool M giants. Di Benedetto & Rabbia (1987) suggested a revision in this temperature scale in the spectral region M0 – M2 from long-baseline interferometric observations of 11 stars. Determination of T_{eff} to the accuracy of 1% or lower still remains a challenging task for any technique.

The effective temperature of a star may also be derived by indirect methods like colour index method (CIM), flux distribution method (FDM) and Infrared flux method (IRFM). In the case of CIM, the observed photometric colour indices are compared with the model-atmospheric colours. FDM is a method in which the observed spectra of the source is compared with the model spectra. In the case of IRFM, the ratio of the total integrated stellar flux to the monochromatic flux at a chosen wavelength is used as a temperature indicator.

Bell & Gustafsson (1989) have presented model-atmospheric colours for K giants. Recently, Blackwell & Lynas-Gray (1994) have revised effective temperature determination by IRFM using Kurucz LTE line blanketed model atmosphere in the temperature range 4000 – 8500 K. Calibration based on visual colours have been given by Buser & Kurucz (1992). The overall agreement between T_{eff} derived from direct angular diameter measurements and the indirect methods like IRFM for F to early M stars is satisfactory. However, stars significantly cooler than 4000 K lack detailed photospheric models to compare with the observations. Tsuji derived effective temperature scales for the M giants from both FDM (Tsuji, 1978) and IRFM (Tsuji, 1981a). IRFM has been used by Tsuji (1981b) for carbon stars. These indirect methods are fairly consistent with the direct measurements.

Apart from the more challenging task of determining stellar angular diameters, lunar occultation observations can also readily resolve binary and multiple systems at a few milliarcseconds. While single occultation observation of a binary system provides only the projected separation between the components in the direction of occultation, multiple (atleast two) occultation measurements are required to get the plane of the sky separation.

As stars evolve from the main sequence into the asymptotic giant branch of the Hertzprung-Russell diagram they exhibit mass loss which can be due to cool winds (Salpeter, 1974), thermal pulses (Schwarzschild and Härm, 1962) or some other types of mass ejection. It is known that the dust formation is intimately related to mass loss, but little direct evidence exists about the dust forming zone. Observing evolved giants and supergiants in the infrared, with sufficiently high angular resolution to resolve the stellar surface and immediate surroundings can answer some of the most interesting questions related to grain condensation, mass loss and hence stellar evolution. The direct detection of the circumstellar dust shells at few stellar radii has been mainly done by lunar occultation (Richichi et al., 1991; Richichi et al., 1995b; Sam Ragland et al., 1996).

As one can infer from the above discussion, lunar occultation with its simple observing technique, relatively straight forward data analysis, and accurate results has provided an effective method of resolving late type giants and supergiants comparable in accuracy to the much more elaborate modern techniques like long baseline interferometry and offered the best angular resolution ever achieved in the near infrared.

1.3 Motivation for the present Study

Circumstellar envelopes in the angular scales of a few arcmin have been well studied from millimeter observations of emission lines of CO and other molecules and also from IRAS imaging. However, the process occurring in the dust envelope close to the stellar photosphere (approximately a few stellar radii) or processes that involve the photosphere itself (such as pulsation and dust formation) can be addressed only from high angular resolution studies which can reach milliarcsecond levels of angular resolution to resolve the stellar photosphere and its immediate surroundings.

The largest angular diameter stars ($\sim$ 50 milliarcseconds) are very few and have already been studied in some detail with various interferometric techniques. To study a sample of cool giants, one needs to go down to $\lesssim$ 5 milliarcseconds angular resolution and the inner dust shell at few stellar radii is expected to be at $\lesssim$ 20 milliarcseconds. The diffraction limit ($1.22\lambda/D$) for the Gurushikar 1.2 m telescope (used for much of the work in this thesis) at 2.2μm is $\sim$ 450 milliarcseconds. The largest optical telescope in India, the 2.3 m Vainu Bappu Telescope at Kavalur as well as Hubble Space Telescope (HST) can resolve down to $\sim$ 240 milliarcseconds at the same wavelength. Clearly, increasing telescope aperture is not the solution to achieve milliarcsecond levels of angular resolution. As far as interferometric techniques are concerned, only the long-baseline interferometry has the capability to reach the required angular resolution (a few milliarcseconds) for these studies. However, long-baseline optical interferometric techniques are extremely demanding in terms of sophisticated technology of path difference control and beam mixing and are also required to be installed at a site with excellent seeing.

From this point of view, an attractive alternative to reach milliarcsecond angular resolution is by using the technique of lunar occultation. Lunar occultation is the only presently available technique which provides milliarcsecond angular resolution using a single 1 m class telescope. This interesting feature of the lunar occultation was the motivation behind developing this technique in the near infrared using 1 m class telescopes available in India.

In India, the technique of lunar occultation has been extensively used in the radio wavelengths at 327 MHz using the Ooty Radio Telescope. A number of sources from

3C catalog has been resolved at the resolution in the range 0.6 – 4 arcseconds (Joshi & Gopal-Krishna, 1977). In India, high angular resolution astronomy in the visible and infrared is still in a stage of infancy. The Indian Institute of Astrophysics (IIA), Bangalore in the past had observed lunar occultations of a few bright stars in the visible region. Several occultations in the V, R and I band were also observed by us in the initial phases of the project (Chandrasekhar et al., 1992a). Projected angular separation between two close stars in the triple system SAO 075999 of 55 milliarcseconds was derived from the optical light curve. In the near Infrared we at the Physical Research Laboratory (PRL) have pioneered the technique of lunar occultations in India.

1.4 Thesis Outline

A high speed near infrared photometer has been designed and developed for lunar occultation as part of this thesis work and is discussed in the chapter 2. Also discussed are the computer codes developed for analysing the occultation light curves. A sample of 15 cool giants/supergiants have been observed as part of this thesis by lunar occultations in the near infrared using the 1 m class telescopes available in India. These observations include two interesting and rare objects viz. TV Gem which is a M1 super giant and TX Psc which is a carbon star. Circumstellar dust around these two cool giants have been studied and are discussed in chapter 3. Among the remaining late-type giants, seven are resolved from our observations and upper limits on the angular diameters in the case of unresolved sources have been derived. These sources are discussed in chapter 4. The instrument developed for studying lunar occultation by the author has also been used to carry out the infrared observations of a fast nova – Nova Herculis 1991. These infrared studies provide a direct means of detecting the formation of dust and coronal line emission in the nova ejecta. These aspects are discussed in detail in chapter 5. The final chapter briefly describes the summary and scope for future work and the directions that can be explored with the use of currently available 'state-of-the-art' infrared arrays and other recent developments.

Chapter 2

Lunar Occultations: Instrumentation and Data Analysis

2.1 Instrumentation

A dedicated near infrared fast photometer with millisecond sampling capability has been designed and developed for this thesis work and is discussed here in some detail. This instrument was built with the considerable experience gained in using a photomultiplier based, occultation photometer for V, R, I filter bands. The details of the earlier instrument and the results obtained therein are given in Chandrasekhar et al. (1992a). Also discussed in this chapter is the data reduction computer code developed in Fortran for analysing the observed occultation light curves.

2.1.1 Optical System

The schematic diagram of the infrared fast photometer is shown in Fig. 2.1. The F/13 optical beam from the telescope after a right angled reflection at plane chopper mirror M_3 is focussed on a cooled aperture wheel with selectable apertures located inside a liquid nitrogen cooled dewar. A plane mirror M_1 can be flipped into the optical path when necessary to deflect the light onto a field eyepiece E_1 for centering the source. The mirror M_1 can be replaced by a cold mirror (dichroic beamsplitter) which reflects visible light while transmitting IR with some loss. The cold mirror is used when accurate guiding of the star is needed. The details of the beam splitter are given in Table

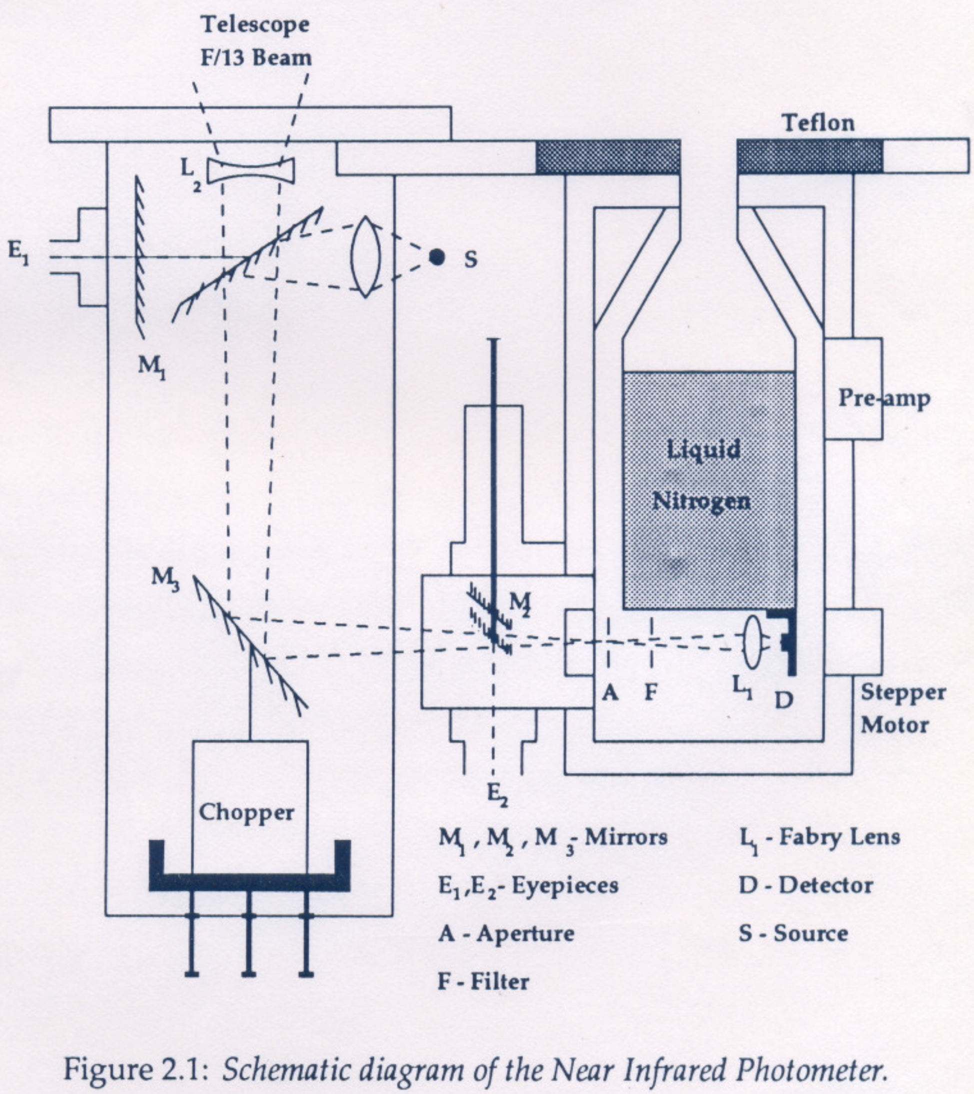

Figure 2.1: *Schematic diagram of the Near Infrared Photometer.*

Table 2.1: *Cold mirror specifications.*

Dimensions	50mm$\times$50mm$\times$50mm
Material	Polished pyrex
Transmission at 2.2 μm	$\sim$80%
Angle of incidence	45^o
Cutoff wavelength	2.7μm

2.1. The mirror M_3 is mounted at 45° on the shaft of a mechanical vibrator permitting its oscillation at a frequency between 10 and 15 Hz with a maximum vertical displacement of $\sim$ 2 mm. In the absence of a vibrating secondary mirror, this tertiary mirror chopper arrangement is needed for background sky subtraction when the system is used for regular photometric observations. In such a case, phase sensitive detection technique with a lock-in amplifier permits the signal to be extracted at the chopper frequency and chopper phase and the background and detector noise to be largely rejected. Details of the chopper system are given in Table 2.2. Mirror M_2 permits light to be deflected into an eye piece arrangement E_2 rigidly attached to the dewar and is used for fine tuning the optical alignment. The InSb IR detector is housed in a liquid nitrogen cooled dewar (Infrared Labs Inc.) and is extensively baffled to reduce background radiation falling on it. At the cold plate bottom of the dewar are mounted the aperture wheel (A), filter wheel (F), Fabry lens (L_1) and InSb detector (D), the details of which are given in Table 2.3. The Fabry lens ensures that all the light falling on the focal plane aperture falls uniformly on the detector. Presently, two IR dewars are available ; Dewar 1 (called CVF dewar) incorporates in addition to standard J, H, K filters, a circularly variable filter for spectrophotometric measurements between 1.7 to 3.4 μm with a resolving power ($\lambda/\Delta\lambda$) of $\sim$ 70. Dewar 2 (called fast dewar) incorporates the standard J, H, K, L and M filters. Dewar 2 has two switchable feed back resistors, either of which can be selected externally through a relay. Details of these optical filters and feed back resistors are given in Table 2.3. A lens L_2 is used to divert light from a mercury lamp, S, into the detector system after double reflection – one at the back surface of Mirror M_1 (which

Table 2.2: *Chopper unit specifications.*

Model No.	201 Ling Dynamic Systems
Rated peak sinusoidal force	17.8 Newtons (1.81Kg)
Usable frequency range	DC to 13 KHz
Max. displacement (Rated travel)	$\pm$ 2.5 mm (0.1 inch)
Rated peak sinusoidal velocity	1.83 m/s
Max. acceleration	892 m/s^2
Weight, shape and size	1.81 Kg, Cylindrical (r = 39 mm, h = 89 mm)
Operating frequency	10-15 Hz
Operating amplitude	2 mm
Focal plane displacement	26 arcsec on the sky
	at the Gurushikhar 1.2 m telescope (F/13 beam)

is flipped into the telescope beam) and the other at Mirror M_3. This arrangement is required only occasionally with the CVF dewar for wavelength calibration.

The aperture plane of the photometer is at about 50 cm (when measured along the optical axis) from the instrumental plate. Since the focal plane of Kavalur 1m telescope can't reach this distance (which was designed basically for optical work), a tele-expander is used, when this photometer is mounted on this telescope. The tele-expander, labelled as L_3 is a CaF_2 negative lens of focal length -40 cm which is fixed at the top entrance of the photometer and can be easily removed when not required. This arrangment is needed only at the 1 m Kavalur telescope and doesn't degrade the instrument performance.

2.1.2 Mechanical System

The flip mirror assembly and the vibrator are enclosed in a rectangular alluminium box which can be rigidly coupled to the Cassegrain plate attached to the telescope. The vibrator rests on a metallic plate whose height and tilt with respect to the bottom of the box can be minutely adjusted by three screws at the bottom. In addition to these,

Table 2.3: *Electrical and Optical characteristics of the two dewars.*

Components	specifications	Dewar 1 (CVF)	Dewar 2 (FAST)
1. Detector:	Material	Photovoltaic InSb (0.5mm diameter)	
	Spectral range	$1 - 5\ \mu$m	
	Impedance @77K (R_D)	$2\times 10^9\Omega$	$1.2\times 10^9\Omega$
	NEP	$4\times10^{-15}W/\sqrt{Hz}$	$5.6\times10^{-15}W/\sqrt{Hz}$
		(20Hz,K)	(40Hz,K)
2. Pre Amp:	Feedback resistor (R_F)	$5.7\times 10^{10}\Omega$	$1.87\times 10^8\Omega$ /
	@77K		$2.12\times 10^{10}\Omega$
	Voltage Responsivity	5×10^{10}V/W	-
	Current Responsivity	-	0.54A/W
	Pre amp noise	$2\times10^{-4}\mathrm{V}/\sqrt{Hz}$	$0.31\times10^{-6}\mathrm{V}/\sqrt{Hz}$
	with feedback resistor	@20Hz	@40Hz
3. Filter:	Band/$\lambda_{eff}(\mu$m)	Bandwidth(μm) (FWHM)	
	J/1.25	0.30	0.32
	H/1.65	0.30	0.34
	K/2.20	0.40	0.40
	CVF_{min}/1.7	~ 0.03	-
	CVF_{max}/3.4	~ 0.03	-
	L/3.8	-	0.66
	M/4.71	-	0.64
4. Focal plane aperture:	size (mm)	arcsec on the sky (1.2 m; F/13 beam)	
	0.5	6.6	
	1	13.2	
	2	26.4	

there are two screws attached to the aluminium box which rotates the vibrator about the telescope axis. A locking arrangement ensures that adjustment once made is not disturbed accidentally. This is important because often the instrument has to be used at low elevations during occultation observations especially disappearance events a few days after new moon. The net effect is that the orientation of the IR beam after reflection at the chopper mirror can be precisely adjusted during alignment.

The dewar is independently coupled to the Cassegrain plate through an intermediate plate. The small size of the detector and the inaccessibility of the final stage of the optical path inside the dewar make optical alignment of the system for maximum and stable signal strength a difficult task. Presently, there is no provision to fill liquid nitrogen into the dewar when it is attached to the telescope. However, the dewar coupling plate has been carefully configured to permit removal of the dewar and its reattachment after filling liquid nitrogen without loss of optical alignment. In order to have a constant check on the crucial optical alignment, a second removable eyepiece mirror assembly (M_2) rigidly attached to the dewar has been incorporated. Mirror M_2 when inserted into the optical path diverts star image to a high power eyepiece assembly (E_2) provided with XY movements and adjustable crosswire illumination. Once satisfactory optical alignment has been reached, the eyepiece crosswires are adjusted to center the star image.

2.1.3 Electrical System

The different subsystems associated with the photometer are shown in Fig. 2.2. The output from the InSb detector is fed to a preamplifier having cooled first stage of matched FETs (Model LN-7). The bias to the detector is externally adjustable for minimum noise. However, this adjustment is not possible always for occultation observations due to background light level from the moon. The preamplifier output is directly given to the data acquisition system in the high speed photometry mode. In the conventional photometry mode the preamplifier output is fed to a lock-in amplifier followed by the data acquisition system. The preamplifier output can also be monitored on the scope. The ready switchability between the conventional photometry mode and the high speed photometry mode is very useful in practice, as it permits the J, H, K

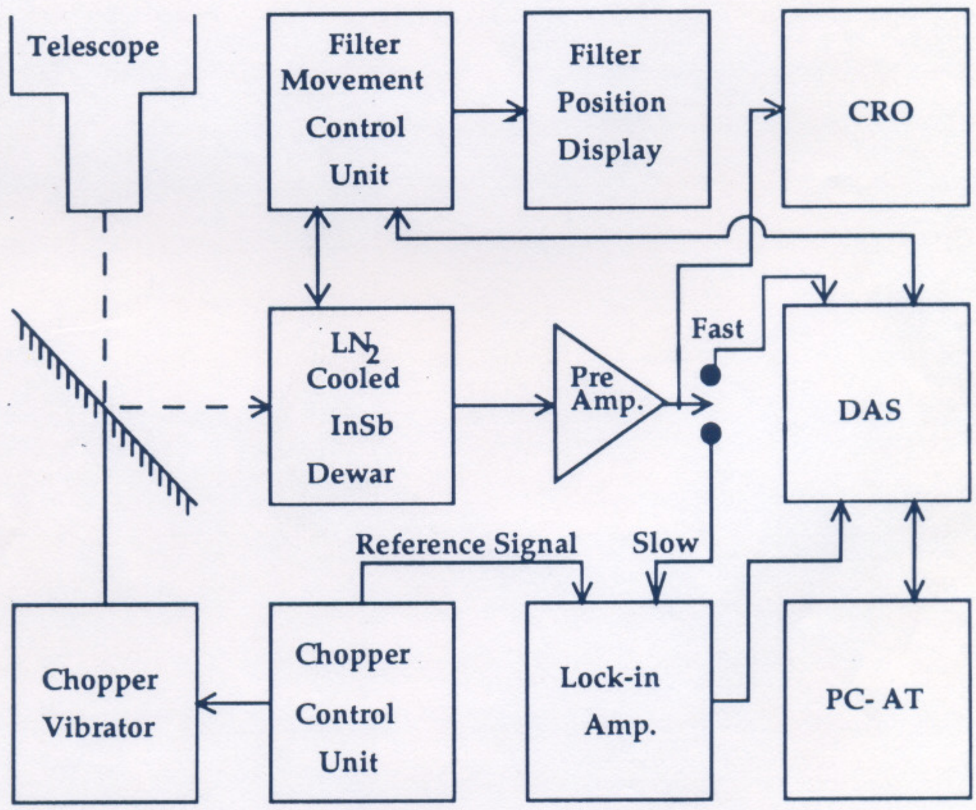

Figure 2.2: *Block diagram of the High speed Infrared Photometer.*

fluxes and CVF spectrophotometry of the occultation sources to be measured in the same night and optimises the use of telescope time.

A serious problem for high speed photometry with this photometer mounted on the telescope which was encountered during the initial runs was the strong and persistent 50 Hz (Mains frequency) modulation in the preamplifier output. The problem is not serious for slow photometry because the lock-in amplifier rejects the 50 Hz modulation to a great extent. The peak to peak voltage of this modulation can be as large as 3.5V (CVF detector noise level $\sim$ 10 mV). Attempts were made by using a notch filter to filter out the 50 Hz and also by taking differential output from the preamplifier instead of single ended output, but these resulted in no significant improvement. With ground isolation, the modulation could be reduced to $\sim$ 350 mV level. Some slow photometric observations as well as lunar occultation of a few bright sources were observed in this phase. Attempts made by providing a low resistance path through a thick short copper cable from the telescope chassis to the electronics ground reduced the pickup amplitude levels comparable to the detector noise. However, the thick and rigid copper cabling needed made it inconvenient to use in practice. The problem was later elegantly resolved completely by electrically isolating the dewar assembly from the telescope and other parts of the photometer. Teflon pieces were suitably machined and introduced in the dewar coupling supports to achieve the electrical isolation of the dewar.

A Keithley unit (System 575) is used for data acquisition and system control, which can be interfaced with an IBM PCs like PC XT or PC AT. Initially a system 570 unit with 12 bit A/D was used. System 575 unit provides 16 single-ended (or 8 differential) channels for analog input, 2 high speed channels for analog output and 32 TTL compatible channels for digital input and digital output. In addition, it provides 16 programmable channels for power relay control. It uses a 16 bit high speed A/D converter for analog data aquisition which can be sampled at a maximum rate of 50 KHz and has a programmable electrical filter (100 KHz/2 KHz) for the analog input. Two analog input channels - one for detector output and the other for CVF position readout are used. Also two digital output ports are used - one to provide input pulses for the stepper motor drive and the other to provide one or zero state to the CVF stepper motor drive to sense the required direction of rotation.

The CVF is driven with a 4 phase stepper motor with a potentiometric readout of its angular position. Each fine step corresponds to a wavelength shift of 0.008 μm, while one coarse step corresponds to four fine steps and is approximately the achievable resolution with the CVF. In actual operation, the stepper motor movement is hindered at certain positions of the CVF filter wheel and in those positions its movement has to be assisted manually. This exercise causes at times a jitter in the motor movement resulting in jumping over a few fine steps but never greater than one coarse step. Spectral calibration of this potentiometer is carried out with a low pressure mercury vapour lamp with strong narrow lines in the region of interest and is discussed in a separate section in this chapter.

Presently, the occultation data is recorded for 60 seconds at the sampling interval of one millisecond, well centered on the predicted time of the event. The 'System 575' incorporates a powerful graphics program which enables any portion of the 60,000 samples acquired during a run to be displayed and studied. The data acquisition software has the provision to start the data acquisition at the pre-defined event time automatically and is found to be very convenient especially when a single observer had to attempt 'difficult-to-observe' events.

2.1.4 System Time Response Calibration

The Dewar 1 and its InSb detector were acquired earlier for the purpose of regular photometric observations of IR sources. The time constant of the detector system i.e. the time taken for the signal to reach $\frac{1}{e}$ (i.e. 0.36787944) of its initial value, is $T_c \sim$ 18 ms. Dewar 2 which was acquired for high speed photometry has relatively fast time response ($T_c \sim 7$ ms) with R_f high. R_f low could not be used due to its reduced sensitivity. As lunar occultation light curve is sampled at a frequency of 1 KHz, the frequency response of both Dewar 1 and Dewar 2 are not flat up to the sampling cut off frequency set by the sampling interval. The averaging effect due to this finite system time constant has to be accurately taken care of in the data reduction procedure to extract the high angular resolution information present in the observed light curves. Hence, the system time response curve is experimentally determined accurately using two independent methods which are discussed below.

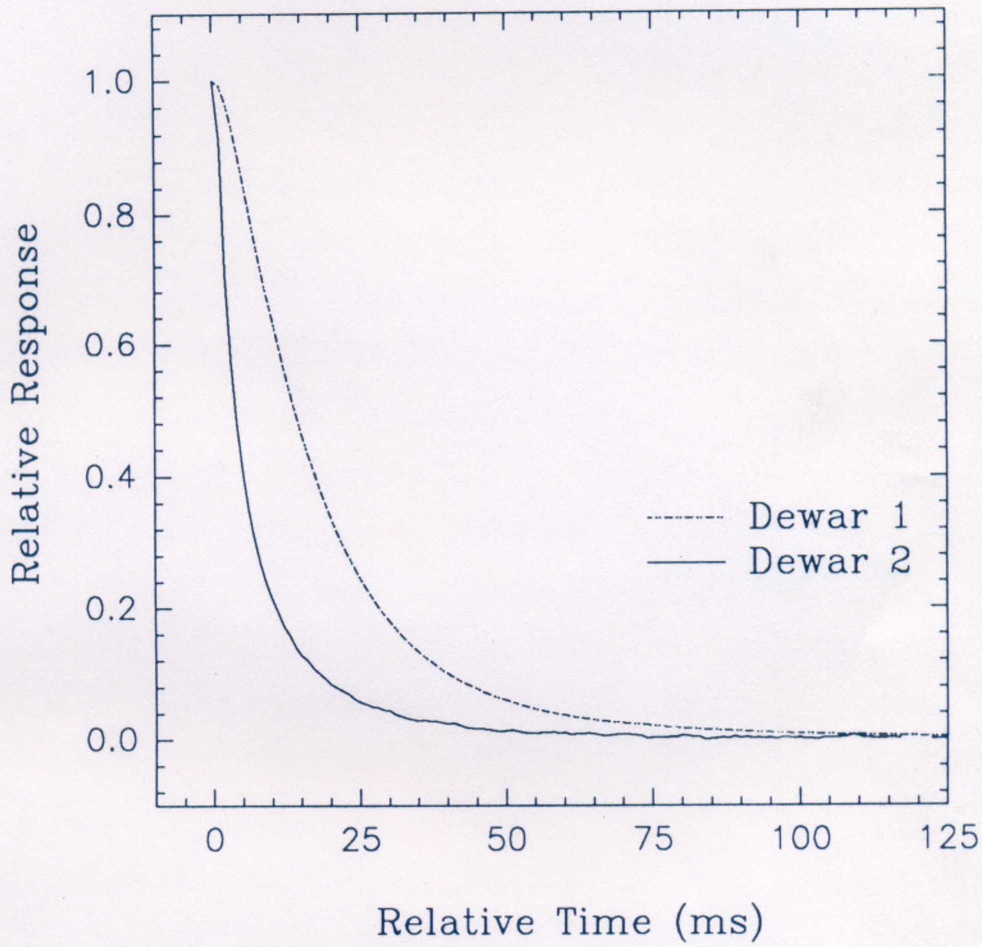

Figure 2.3: *Relative time responses of Dewar 1 and Dewar 2.*

Rotating chopper setup

A nearly point source (≤ 0.1 mm spot size) was produced on a rotating chopper wheel blade by reimaging a well illuminated aperture of 1 mm by good quality camera lens of focal length 25 cm. Even at small chopper frequencies of a few Hertz, the imaged spot could be blocked by the blade in < 50 μsec. This setting could be verified by observing the transition in the R_f low mode (Very fast mode) of Dewar 2. In the occultation mode (R_f high) the transition showed a measurable time response which is plotted in Fig. 2.3. Also plotted is the time response of the Dewar 1 used initially with a relatively poorer time response.

Infrared Light Emitting Diode (LED) setup

Since the time response calibration is very crucial to resolve sources at 2-3 milliarc second levels of angular sizes, it was felt that the calibration carried out with rotating chopper setup should be cross checked with some other independent method. A fast infrared LED was used for this purpose and the system response to a step input is recorded. In the absence of infrared LEDs of known spectral characteristics readily with us, locally available LEDs were tried out. A LED which is used in Television and VCR remote control set was found to be well suited for our purpose in the near infrared region (J, H, and K filters), although the manufacturer's specification for this LED shows only negligible response in the wavelength range beyond 1 μm. The step voltage input for this LED is provided by a pulse generator through a current limiting resistor. Care is taken so that the applied voltage and the current are in the linear response region of the LED. One major advantage of this method compared to the rotating chopper method is that the optical alignment is very easy to achieve and is very convenient for field use to obtain a calibration just after a successful occultation observation. Repeated calibrations of our system were carried out, keeping different values of the detector bias voltage and at different background and signal levels. The system time response and the gain are found to change appreciably when the bias voltage and/or the background light level are changed. Fig. 2.4 and 2.5 shows the range of possible system response curve respectively for Dewar 1 and 2. It was also noticed that the CVF dewar has undergone changes in the system response and the gain over a period of about five years. The reason for this change in the detector characteristics is believed to be caused by the aging of the electronic components, more specifically the load resistor.

2.1.5 CVF Spectral Calibration

The spectral calibration of the CVF dewar is required while using it for spectrophotometry. Usually spectral lamps which emit well defined lines in the region of interest are used for this purpose. A serious problem in performing such calibration is the overwhelming contamination of the line emission by the broad thermal emission of the quartz envelope of the spectral lamp. The standard sky chopping technique used for regular infrared photometry can not be used, since the dimension of the source of

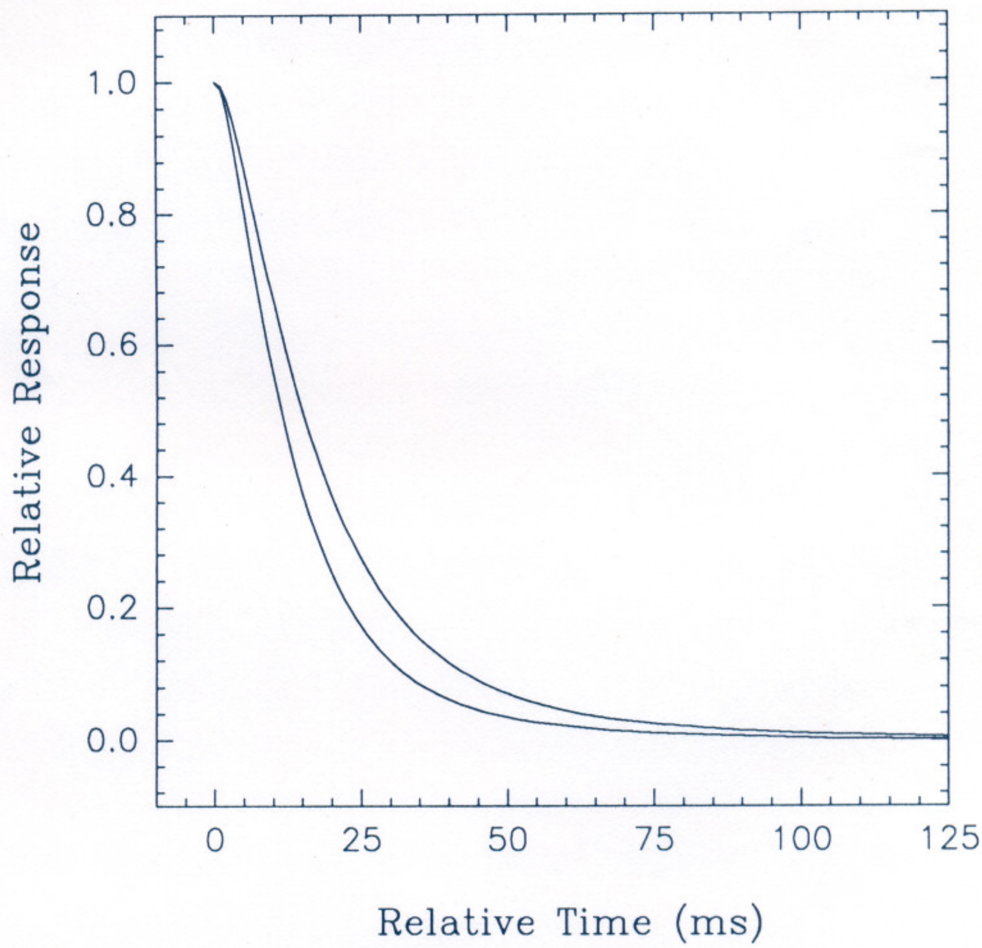

Figure 2.4: *Shown is the range of possible time response curves of Dewar 1.*

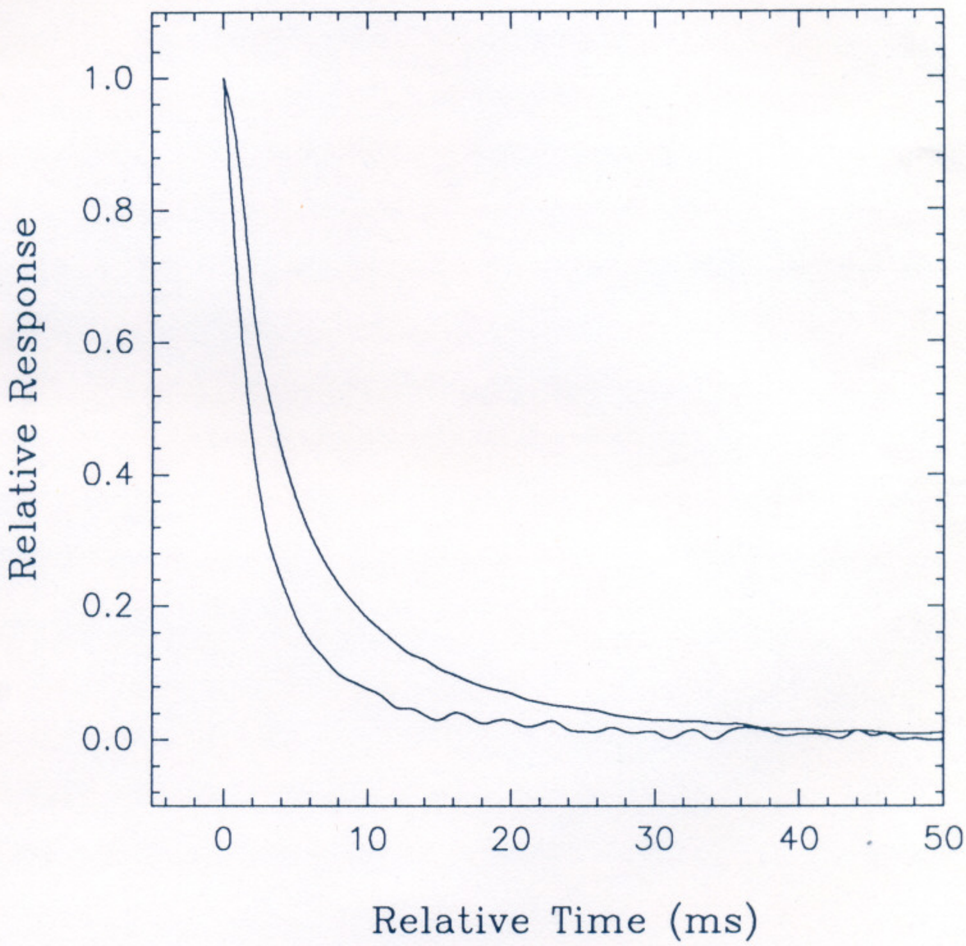

Figure 2.5: *Shown is the range of possible time response curves of Dewar 2.*

line emission is comparable to that of the source of thermal emission. A simple and inexpensive method introduced by Chandrasekhar et al. (1984) is followed for the spectral calibration of CVF Spectrometer. The method uses an already-present internal modulation to effectively discriminate the emission of the plasma discharge of the source from the thermal emission of the envelope. A standard low-pressure Hg lamp (Philips, Type 93123 E/E27) with a quartz window operating at 50 Hz at a discharge current of 0.9 A is used. Radiation from this source after suffering 90° reflections at mirrors M_1 and M_3 is incident on the InSb detector after passing through the aperture, optical filter and Fabry lens. Due to a.c. operation, the current through the discharge tube is modulated at 50 Hz and the plasma emission of the Hg source which includes the various line transitions superposed on the continuum emission is strongly modulated at 100 Hz. The preamplifier output is fed to a lock-in amplifier along with an electromagnetic pick-up from the Hg lamp as a reference signal. The lock-in amplifier locks the signal at the reference signal frequency and phase and thereby the continuum thermal emission from the envelope at all other frequencies are rejected.

2.1.6 The Infrared Sky Background in the vicinity of the Moon

In the near infrared the brightness of the sky near the moon has the following contributions:

1. Solar light reflected by the bright limb of the Moon and scattered through the Earth's atmosphere into the telescope beam
2. Thermal emission from the sky
3. Thermal emission from telescope structures etc.

These components have different intensities and different wavelength dependences. Scattered light intensity depends upon the phase of the moon and on the aerosol content of the atmosphere above the observing site. Thermal emission from the sky has a wavelength dependent emissivity which drops to a few percent in the atmospheric windows. Due to atmospheric turbulence, this emission fluctuates in time and along different lines of sight resulting in a granularity which is an important source of noise

(Lena, 1978). Contributions to the thermal emission from the telescope structures is due to emissivity of telescope mirrors, central obscuration, spiders and structures around the primary mirror if the secondary is oversized. In Cassegrain configuration, it has been pointed out that telescope emissivity could be optimized to ~ 0.09 (Moorwood, 1986).

Fig. 2.6 shows the idealised spectral radiance curves between the wavelengths of 0.5 and 5 μm for different components in the direction of the moon. In this figure curve A and B refer to scattered light from full Moon and Moon at quadrature, respectively. The thermal emission corresponding to a temperature of 390 K (Low and Davidson, 1965) at the subsolar point of the full moon is depicted in curve C. It can be readily seen that thermal contribution begins to dominate beyond a wavelength of 2.5 μm. Curve D represents the terrestrial atmospheric thermal contribution corresponding to a temperature of 300 K.

Fig. 2.7 shows the expected relative contributions to the night sky near full moon from the scattered light of the moon and the thermal emission due to the atmosphere for an exceptionally clear (Coronal) sky and for a more frequently seen normal sky with some dust. As we are concerned only with occultation observations, close to the limb of the moon the scattered sky brightness contribution is a large value and variable with phase of the moon and position angle of occultation. The actual infrared brightness measurements made by us at 25″ from the bright limb of the moon are shown for two wavelengths 2.2 μm and 3.35 μm in the same figure. Also shown is the day time Gurushikhar sky brightness at 2.2 μm at an angle of 50° from the Sun.

Fig. 2.8 shows the variation of this brightness with increasing distance from the bright limb in units of magnitude per square arcsec. These sky brightness measurements were carried out with a 40 arcsecond diaphragm on the sky at Kavalur with 1 second integration on the 0.75 m telescope. Age of the Moon at the time of observations was 1.5 days after full moon. Intensity calibration was done using a nearby standard star HR 4450 (m_k = 1.471). These observations are consistent with the earlier reported range of 0 – 7 magnitude in K band with a 15 arcsec diaphragm (Richichi, 1989b).

15608

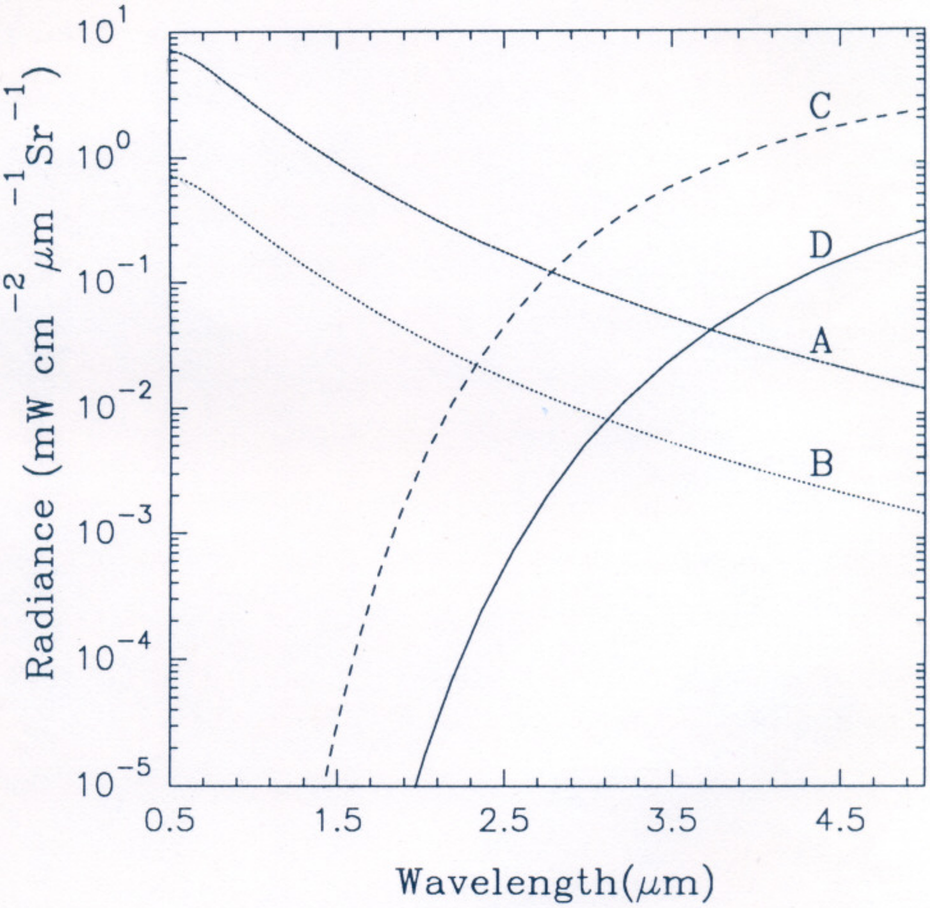

Figure 2.6: *Spectral radiance curves in the direction of moon. The curves A, B, C and D refers to scattered light from full Moon, Moon at quadrature, thermal emission at the subsolar point of the full moon and terrestrial atmospheric thermal contribution, respectively.*

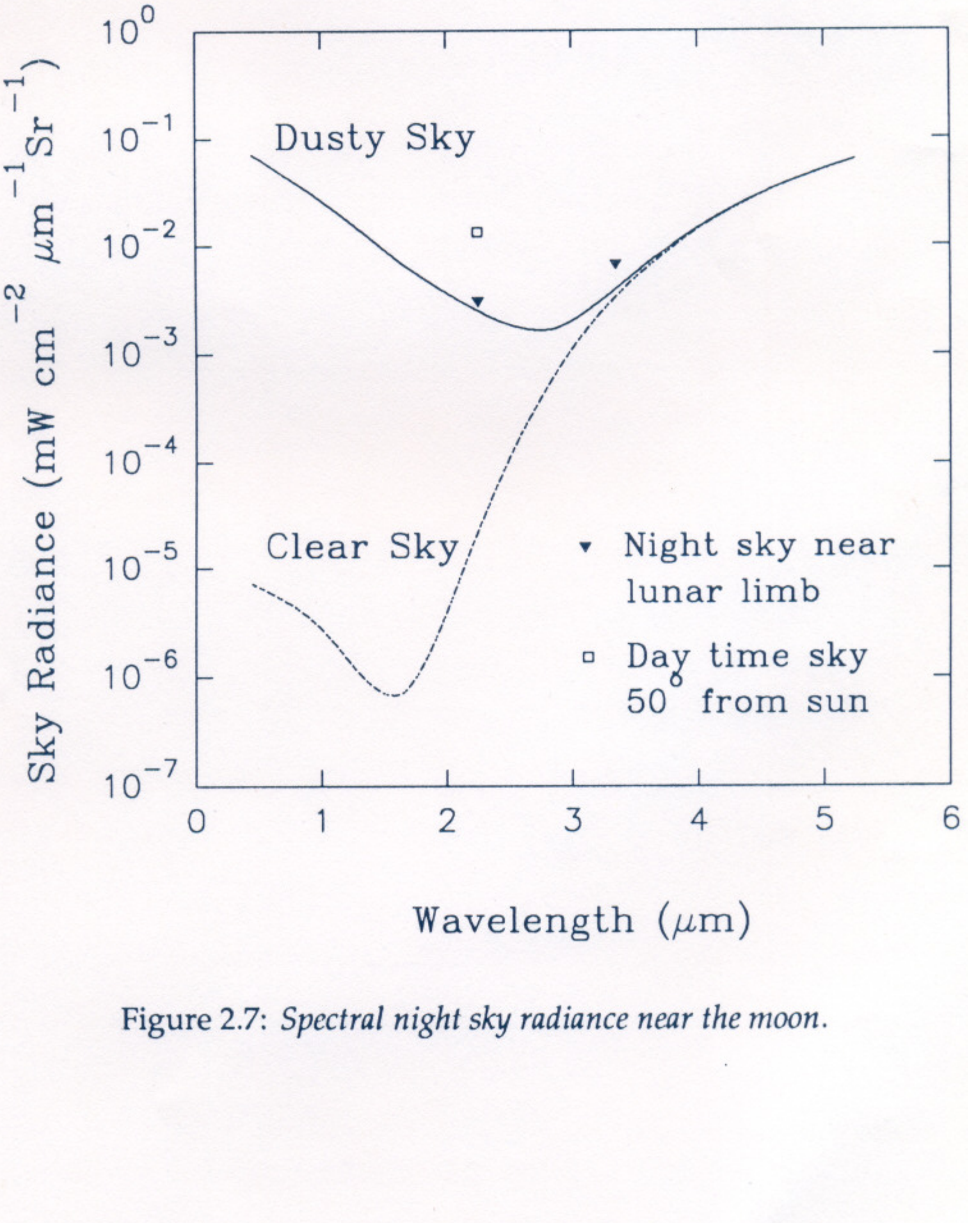

Figure 2.7: *Spectral night sky radiance near the moon.*

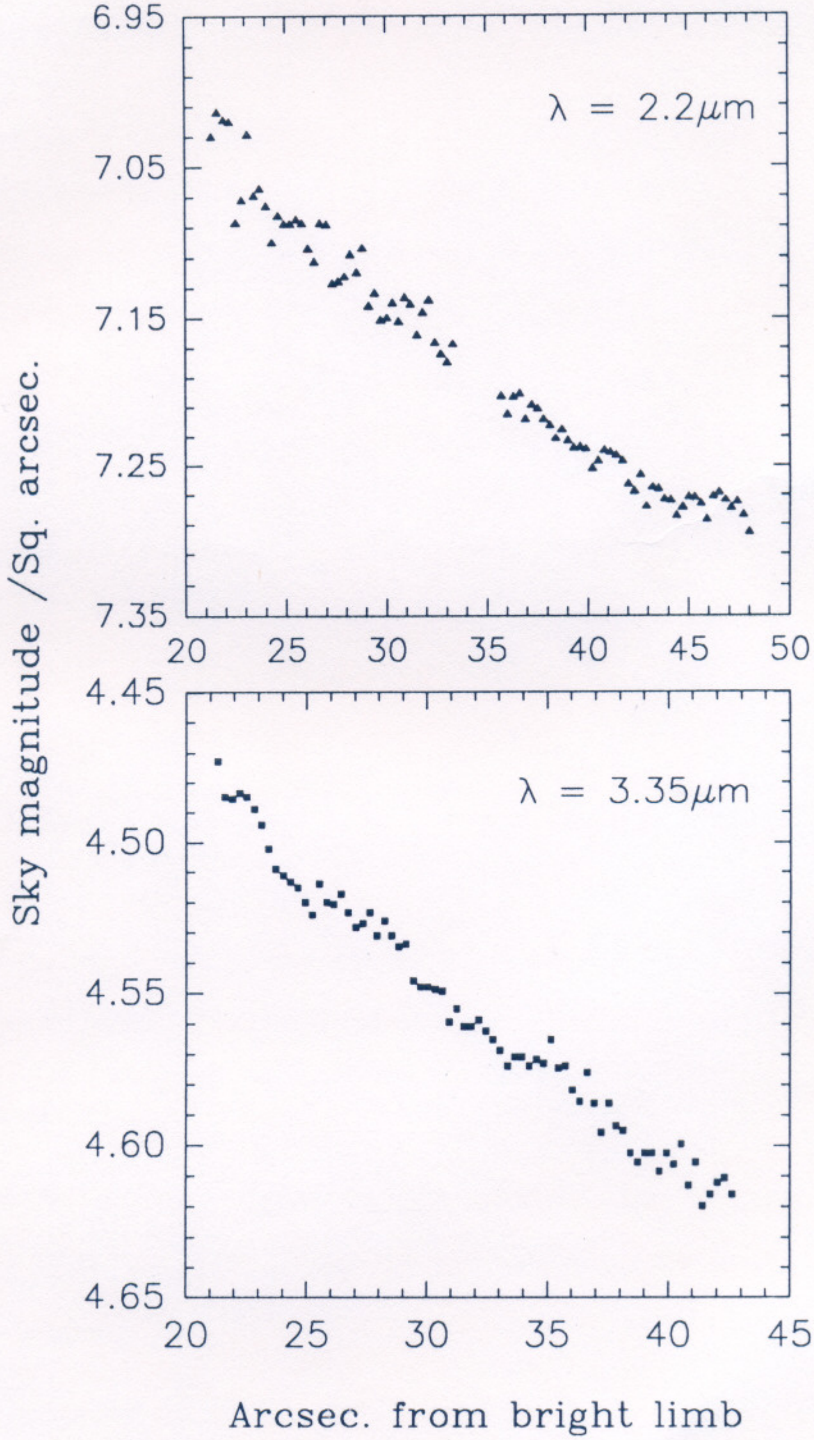

Figure 2.8: *Variation of sky brightness with increasing angular distance from the bright limb of the moon at 2.2 μm and 3.3 μm (Moon's age is 1.5days after full moon).*

2.1.7 System Performance

The instrument in the present form has been used to observe several occultation events including a few, difficult-to-observe, daytime disappearance and nighttime reappearance events apart from the usual nighttime disappearance events. Nearly a hundred sources have been attempted.

Being fixed time events, lunar occultation demands a very high quality performance from telescope and allied system which is not always met. Apart from cloudiness factor other difficulties encountered in observing lunar occultation events which needs mention are:

1. Data Acquisition system malfunction – System 575 cannot be accessed in field locations at all PCs.

2. Power failures minutes before the event without time to switch on Diesel generator.

3. Telescope malfunctions.

4. Inability to locate source in time; true for evening events a few days after new moon.

5. System saturation in the case of events close to full moon. Thin clouds also cause system saturation in day time events.

6. Loss of source and inability to reacquire it in the crucial moments before an event.

7. Source not being in the aperture in reappearance events.

8. 50Hz pickup problems. High frequency problems - difficulty in centering using oscilloscope.

Fig. 2.9 shows the occultation light curve (squares) of ζ Gem observed with Kavalur 1 m telescope. The solid line is the result of a detailed model fit which is described in the next chapter. Shown in the lower panel is the residual (data - model) suitably magnified for clarity. The source is just at the verge of the resolving capability of our instrument. We have estimated an upper limit of $\phi \leq 2$ milliarcseconds (mas) for the

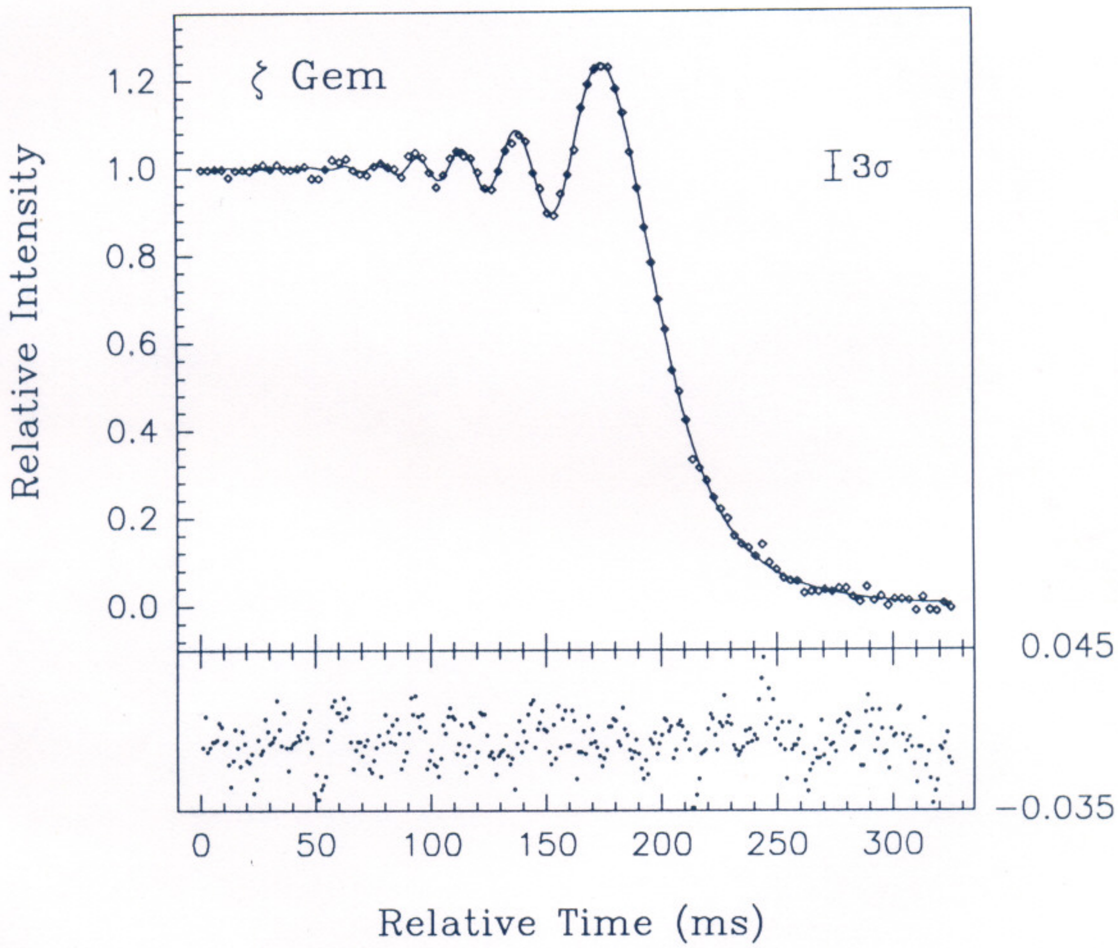

Figure 2.9: *Occultation light curve of ζ Gem (squares) and the model fit (solid line). The SNR in the observed light curve is ∼ 90. Lower panel shows the residue of the model fit i.e. Data − Model.*

angular diameter of the source. These observations show that the present state-of-the-art of our instrument fine tuned at the telescope is ~ 2 mas angular resolution for light curves observed with good SNR (~ 100) (Ashok et al., 1992).

Recovering high angular resolution information from the observed light curve is a difficult inverse problem. Detailed analysis is essential to reach mas levels of angular resolution. The numerical techniques adopted to analyse the observed occultation light curve is discussed in the following section in some detail.

2.2 Data Analysis

The observed lunar occultation light curve can be depicted as

$$I(t) = \int_{-\infty}^{\infty} \int_{-A/2}^{A/2} \int_{\lambda_1}^{\lambda_2} \int_{-\Delta\tau}^{0} S(\phi) F(\omega) O(\alpha) \Lambda(\lambda) T(\tau)\, d\phi d\alpha d\lambda d\tau + \beta(t) \tag{2.1}$$

where $F(\omega)$ is the diffraction pattern of a monochromatic point source, $S(\phi)$ is the brightness profile of the source along the direction of occultation, $O(\alpha)$ is the projected telescope aperture function along the direction of occultation, $\Lambda(\lambda)$ is the wavelength response of the system, $T(\tau)$ is the time response of the detector and $\beta(t)$ is the time varying background light level.

$$F(\omega) = 0.5\left[(0.5 + C(\omega))^2 + (0.5 + S(\omega))^2\right] \tag{2.2}$$

where C(ω) and S(ω) are the Fresnel integrals given in eqn. 1.2 and 1.3 and ω is the Fresnel number given by,

$$\omega = \left(\frac{2}{\lambda d}\right)^{\frac{1}{2}} [v(t - t_0) + (d \;\; tan(\phi)) + \alpha] \tag{2.3}$$

where d is the distance to the moon, λ is the wavelength of observation, t_o is the time of geometrical occultation, v is the velocity of shadow motion and α is the linear displacement term to account for the telescope averaging effect.

2.2.1 Nonlinear Least Squares technique

Nather & McCants (1970) introduced a Nonlinear Least Squares (NLS) method for analysing optical occultation light curves. Since then, this method has been widely used in both optical and near infrared region. Essentially, a model is assumed for the one dimensional brightness distribution of the source (along the direction of occultation) with a set of physical parameters and the problem is to obtain best statistical estimation for these parameters along with other scaling parameters like source intensity, background intensity, velocity component of the moon along the direction of occultation and the time of geometric occultation. In the case of stars, the assumed source function has the form,

$$S(\phi) = I_o \frac{\frac{2}{\pi}\left[1-\left(\frac{\phi}{\Omega}\right)^2\right]^{\frac{1}{2}} + \frac{1}{2}k\left[1-\left(\frac{\phi}{\Omega}\right)^2\right]}{1+\frac{2}{3}k} \tag{2.4}$$

where Ω is the stellar angular radius and k is the limb darkening coefficient. The finite SNR in the light curve doesn't allow the limb darkening coefficient to be treated as a free parameter in the model and hence appropriate value has to be assumed for k depending on the spectral class of the object and wavelength of observation. However, same results can be obtained by assuming a uniformly illuminated stellar disk model (k = 0) while modelling the light curve and use correction factors to convert from uniform disk diameter to limb darkened diameter using model atmospheres. Evans et al. (1980) have remarked that this indirect approach could introduce systematic error in the angular diameter estimation. However, it is safe to use this approach in the near infrared as the effect of limb darkening in near infrared wavelengths is small. Schmidtke et al. (1986) have shown that the ratio of limb darkened to uniform disk (k = 0) is 1.028 in K band for K4 giants and this value is generally used for any cool giants. In this thesis limb darkening effects are not considered and uniformly illuminated stellar disk is assumed.

2.2.2 Varying Background Light

The background light level, $\beta(t)$ is often found to vary during the event. In the case of disappearance events, in general, the varying background can be depicted as a positive gradient, as the bright portion of the moon approaches the instrument field of view with time. The steepness of the gradient depends on various factors like lunar phase, position angle of occultation, position angle of lunar terminator, wavelength of observation, air mass and atmospheric aerosol characteristics and is very difficult to predict. Occasionally, the varying background light can't be accounted with a single gradient. Keeping this in mind, the background light level has been modelled by a polynomial series of adjustable order, which has the form

$$\beta(t) = \sum_{i=0}^{n} a_i x^i(t) \tag{2.5}$$

The degree of the polynomial, *n* is chosen depending on the characteristics of the varying background light level. Rapid scintillation effects are dealt with separately later.

2.2.3 Effect of Finite Source size

The modelling approach of this smearing effect is shown in Fig. 2.10. Essentially, the source is sliced into smaller pieces along the direction of occultation. Now each slice can be assumed as a point source of intensity proportional to the area of the slice.

In practice, the integration in eqn. 2.1 has to be performed numerically, i.e.

$$S_i'(\phi_i) = \int_{\phi_i-\delta\phi}^{\phi_i+\delta\phi} S(\phi)\, d\phi \tag{2.6}$$

$$S_i(\phi_i) = \frac{S_i'(\phi_i)}{\sum_i S_i'(\phi_i)} \tag{2.7}$$

where S(ϕ) is the source function given in eqn. 2.4. The step size is chosen depending on the required numerical angular resolution in the computation. Generally, for initial run, we set $\delta\phi$ as 0.2 mas and for final run, we set it to 0.05 mas.

Fig. 2.11 shows the light curves of angular sizes 2 mas, 5 mas, 10 mas, 20 mas and point source.

2.2.4 Effect of Finite Optical Bandwidth and System Wavelength Response

The wavelength response of the instrument is defined by the optical filter characteristics f(λ) and the wavelength response of the detector l(λ) used. In addition, the spectral energy distribution of the star b(λ) also needs to be considered when broad band filters are used. The resultant system wavelength response has the mathematical form,

$$\Lambda(\lambda) = f(\lambda)\, l(\lambda)\, b(\lambda) \tag{2.8}$$

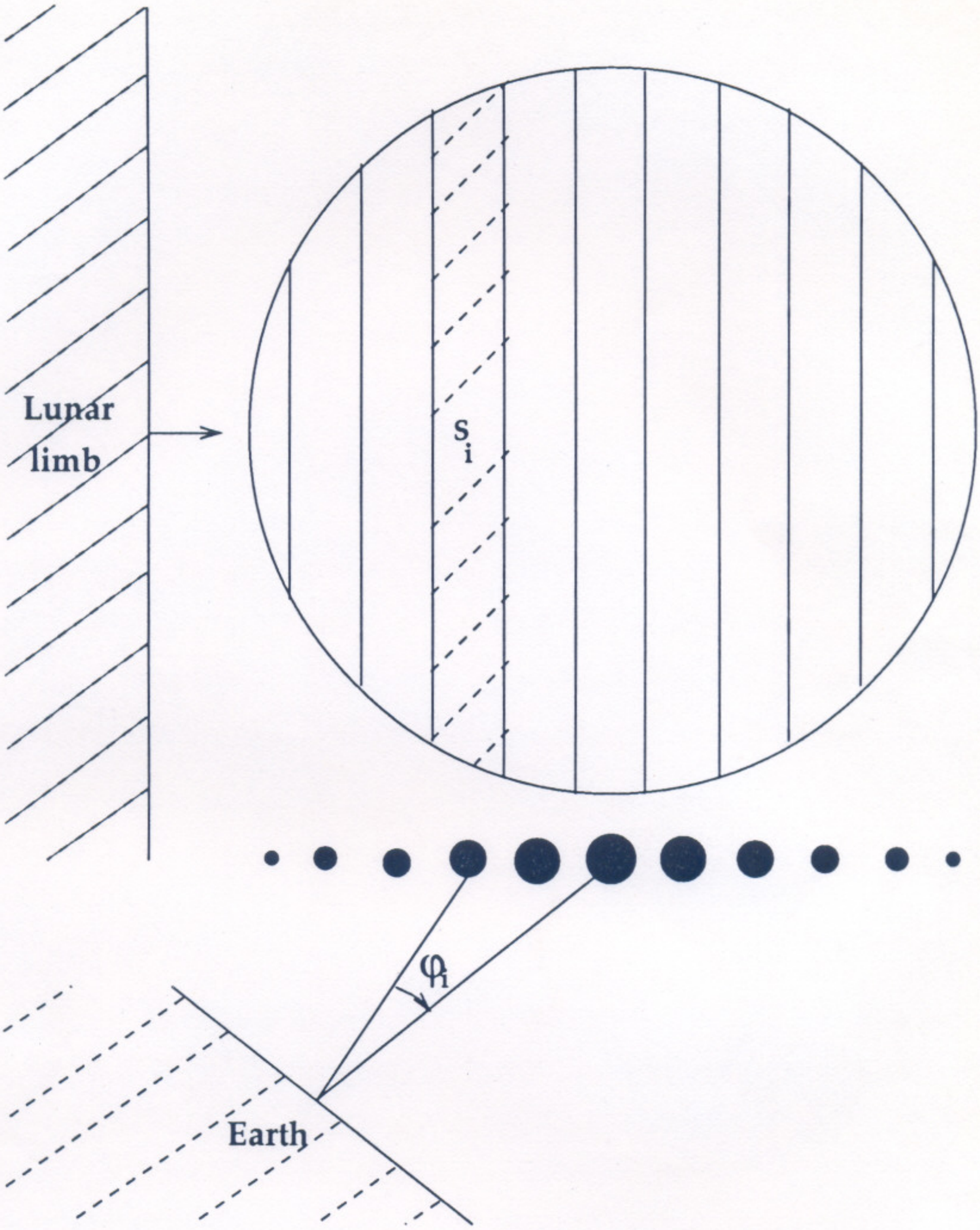

Figure 2.10: *Modelling approach to account for the finite source size. Stellar disk is sliced into pieces along the direction of occultation and are replaced by point sources of appropriate brightness. Resultant light curve is the sum of all these point source patterns. Here brightness is indicated by the size of the spot.*

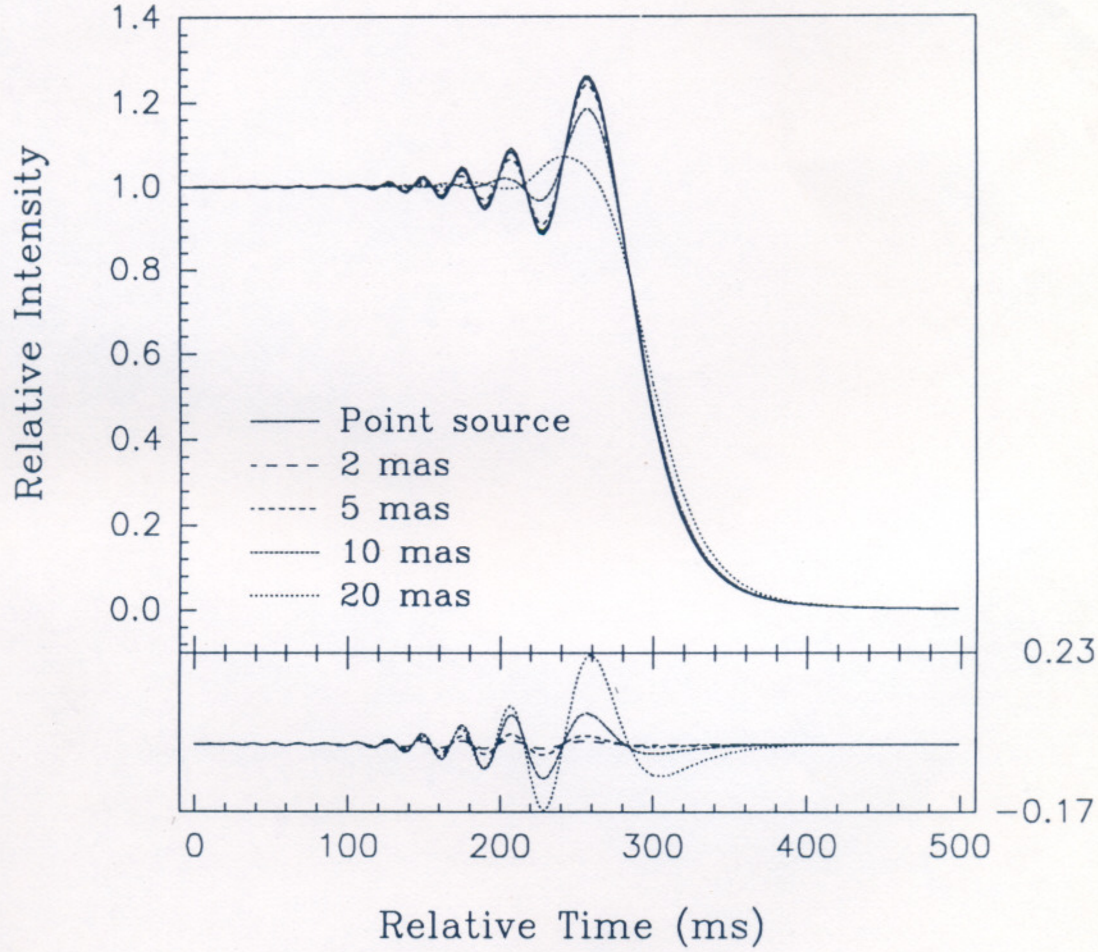

Figure 2.11: *Simulated light curves (disappearance event) assuming K band filter for different source sizes. Lower panel shows the difference between the point source light curve and the light curves of source sizes, 2 mas, 5 mas, 10 mas and 20 mas.*

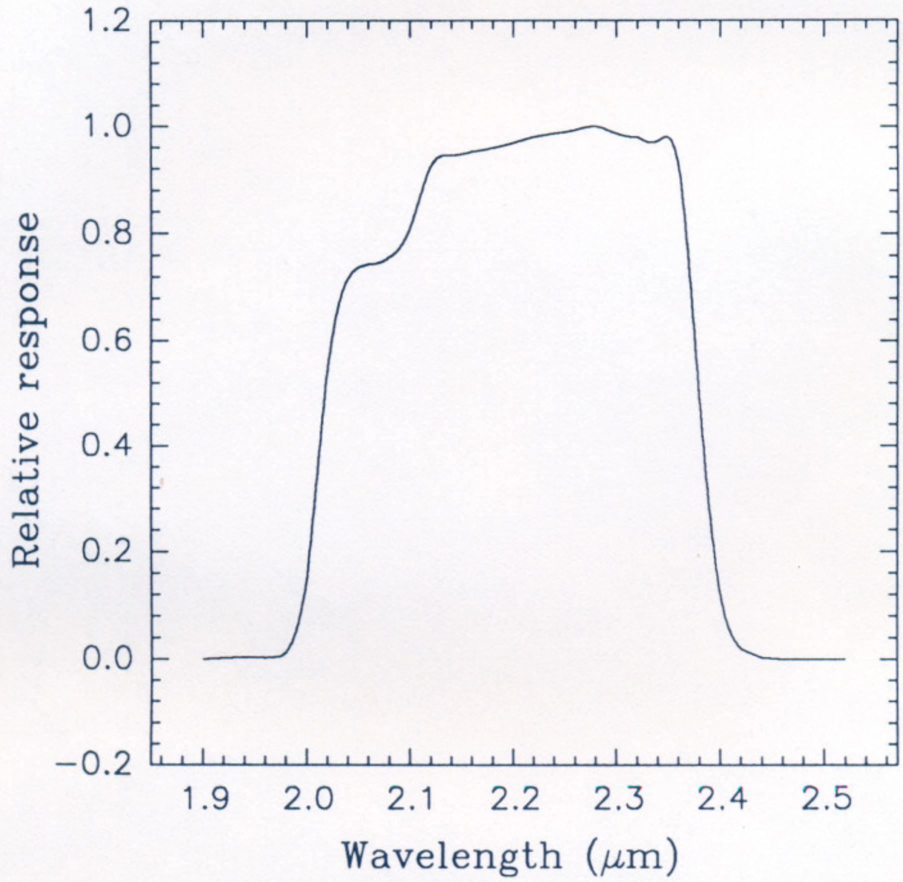

Figure 2.12: *The system wavelength response when standard broad band K filter is used.*

The function $f(\lambda)$ can be obtained from filter calibration and $l(\lambda)$ for InSb detector can be approximated within K band as,

$$l(\lambda) \propto \lambda \tag{2.9}$$

Fig. 2.12 shows the system wavelength response when K filter is used (i.e. K filter transmission curve multiplied by the detector wavelength response).

Fig. 2.13 shows the point source light curve averaged by our instrumental wavelength response where a standard K filter (λ_{eff} = 2.2 μm, $\Delta\lambda$ = 0.4 μm) is assumed. Also shown in the figure is the monochromatic point source light curve at 2.2 μm.

The function $b(\lambda)$ is generally assumed as a blackbody spectrum when observed

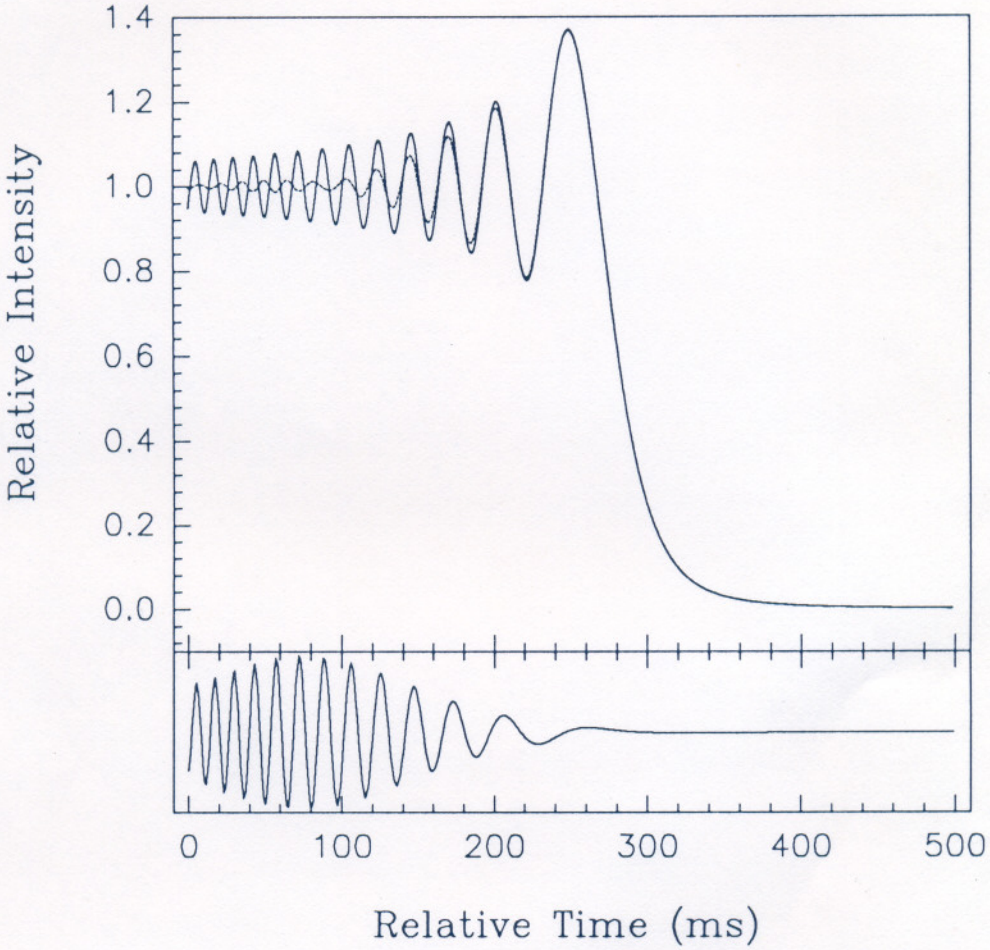

Figure 2.13: *The theoretical monochromatic point source occultation light curve at 2.2 μm (solid curve) along with another light curve averaged by the finite bandwidth of the standard broad band K filter (dotted curve). The difference between these two light curves is shown in the lower panel.*

spectrum of the source is not available in the wavelength of interest and has the form,

$$b(\lambda) = c_1 \times \frac{\lambda^{-5}}{e^{\frac{c_2}{\lambda T}} - 1} \tag{2.10}$$

where $c_1 = 2\pi hc^2 = 3.7415 \times 10^4 W cm^{-2} \mu^4$, $c_2 = \frac{ch}{k} = 1.43879 \times 10^4 \mu\ ^\circ K$ and T is the temperature of the star in Kelvin. The $d\lambda$ integration in eqn. 2.1 is replaced by summation. $\Lambda(\lambda)$ is evaluated at a fixed point by integrating the function,

$$\Lambda_i'(\lambda_i) = \int_{\lambda_i - \delta\lambda}^{\lambda_i + \delta\lambda} \Lambda(\lambda)\, d\lambda \tag{2.11}$$

$$\Lambda_i(\lambda_i) = \frac{\Lambda_i'(\lambda_i)}{\sum_i \Lambda_i'(\lambda_i)} \tag{2.12}$$

$\delta\lambda$ is set as 0.05 μm for initial runs and the final run is carried out by setting $\delta\lambda$ as 0.025 μm. We find from our occultation light curve of ζ Gem that this averaging effect can bias the angular diameter estimation (of a 1.8 mas source) by $\sim$ 115 % when not taken care in the data reduction procedure.

2.2.5 Effect of Finite Telescope Aperture

The diffraction pattern which is sweeping over the Earth surface is averaged by the finite telescope aperture. This effect can be neglected when 1 m class telescope is used, but for large aperture telescopes this effect has to be accurately modelled. In the case of Cassegrain reflectors, the secondary obscuration also has to be taken into account. The telescope aperture along the direction of fringe motion is sliced into small pieces as shown in fig. 2.14. The function has the mathematical form,

$$\begin{aligned} O(\alpha) &= \left[1 - \left(\frac{\alpha}{T_p}\right)^2\right]^{\frac{1}{2}} - \left[1 - \left(\frac{\alpha}{T_s}\right)^2\right]^{\frac{1}{2}} \quad when \quad \alpha \leq T_s \\ &= \left[1 - \left(\frac{\alpha}{T_p}\right)^2\right]^{\frac{1}{2}} \quad when \quad T_s \leq \alpha \leq T_p \end{aligned}$$

Where T_p and T_s are respectively the radius of the telescope primary and secondary mirrors.

Like the other averaging effects, the integration in eqn. 2.1 has to be performed numerically, i.e.,

$$O_i'(\alpha_i) = \int_{\alpha_i - \delta\alpha}^{\alpha_i + \delta\alpha} O(\alpha)\, d\alpha \tag{2.13}$$

$$O_i(\alpha_i) = \frac{O_i'(\alpha_i)}{\sum_i O_i'(\alpha_i)} \tag{2.14}$$

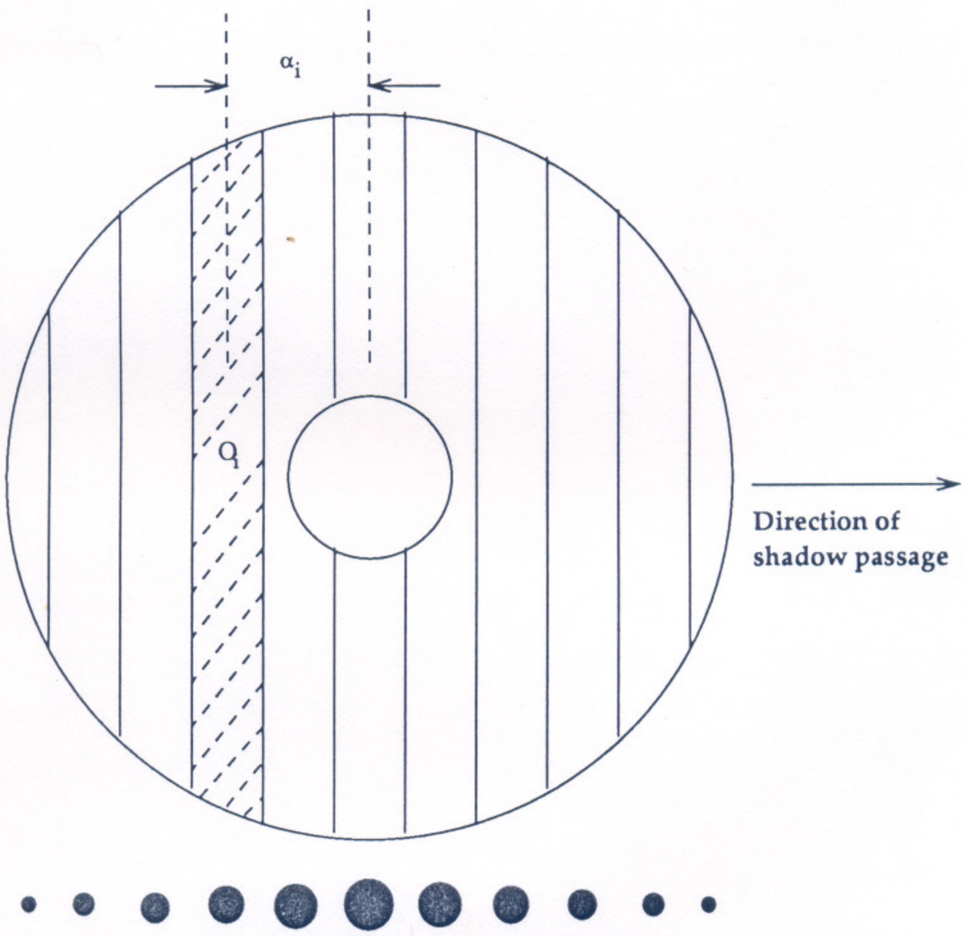

Figure 2.14: *Modelling approach to account for the telescope smearing effect. Here brightness is indicated by size of the spot.*

$\delta\alpha$ is fixed for required numerical resolution of the model calculations knowing the distance and the velocity of the moon. For the initial runs, when $\delta\phi$ is set as 0.2 mas, $\delta\alpha$ will be $\sim$ 40 cm assuming typical values for the distance to the moon and the lunar velocity component. For the final run, when $\delta\phi$ is taken as 0.05 mas, $\delta\alpha$ will have a value of $\sim$ 10cm.

Fig. 2.15 shows the monochromatic point source light curve for two cases - a telescope of negligibly small diameter (10 cm) and 4 m telescope, wherein the secondary obscuration is assumed as 10 % of the primary area. Occultation light curve of ζ Gem observed with 1 m telescope shows that the model fit overestimates the angular size by $\sim$ 12 % when telescope averaging effect not accounted in the analysis procedure.

2.2.6 Effect of Finite System Time Response

As discussed in section 2.1.4, finite system time response has to be carefully accounted for, to reach milliarcsecond level of angular resolution. For simplicity, initially we modelled our system time response as an exponential response of the form $e^{-\frac{t}{\tau}}$ (where τ is the system time constant). The residue curve (model – data) suggested that this approximate form of the time response doesn't account for the averaging effect satisfactorily and accurate knowledge of accurate system time response function is essential to recover the high angular resolution information contained in the data. Hence, the system time response was experimentally determined and convolved with the point spread function to account for this instrumental smearing effect. Fig. 2.16 shows the monochromatic point source light curve for an ideal system (whose frequency response is flat up to the sampling cut off frequency) along with the corresponding light curve for the detector system Dewar 1 and Fig. 2.17 shows the corresponding plots for the detector system Dewar 2. Occultation light curve of θ Cnc (of angular diameter 3.3 mas) observed with Dewar 1 shows that this averaging effect overestimates the angular size by $\sim$ 350 % when not accounted for in the data reduction procedure. Occultation light curve of ζ Gem observed with Dewar 2 shows that the finite system time response averaging effect overestimates the angular size by $\sim$ 250% and hence has to be accurately taken care in the analysis.

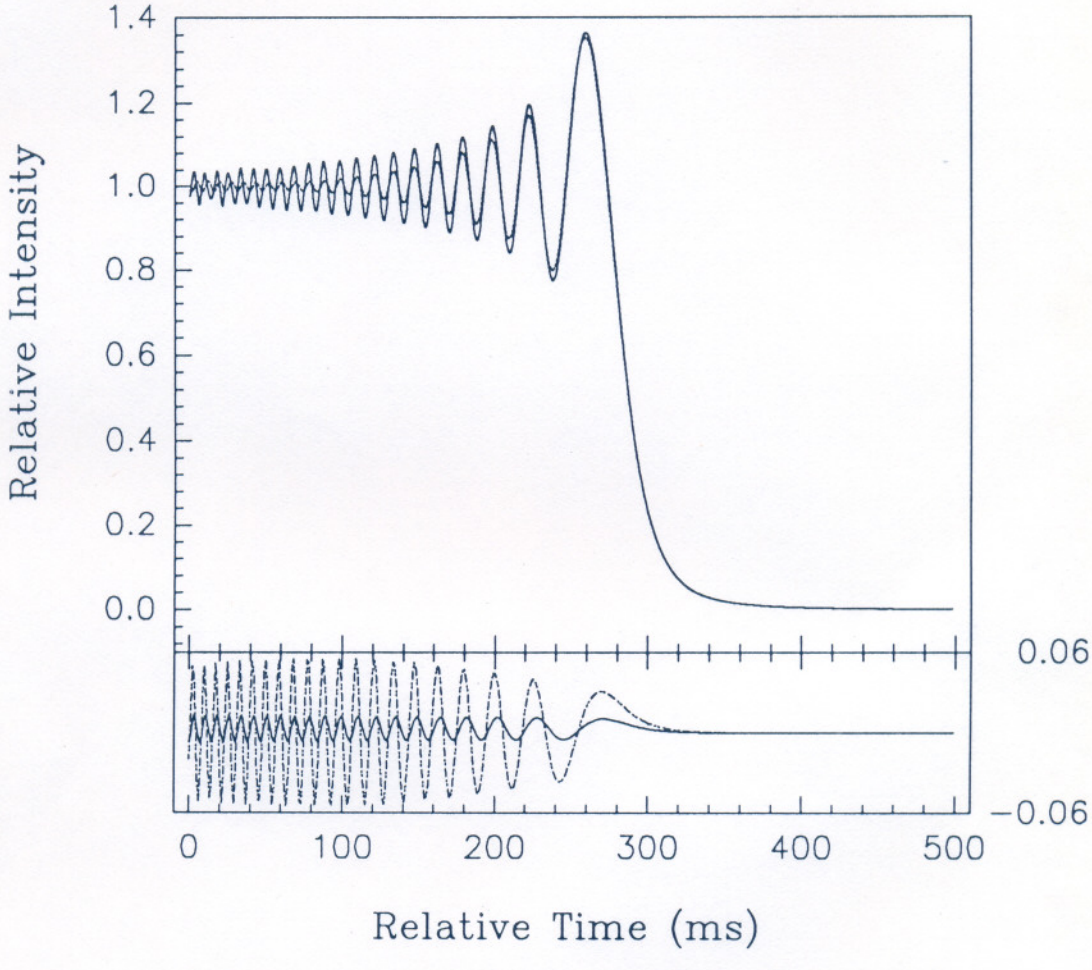

Figure 2.15: *Simulated monochromatic point source light curve (disappearance event) with a 1.2 m telescope (solid curve) and a 4 m telescope (dotted curve). Difference between each of these light curves and an ideal light curve with zero telescope diameter are shown in the lower panel.*

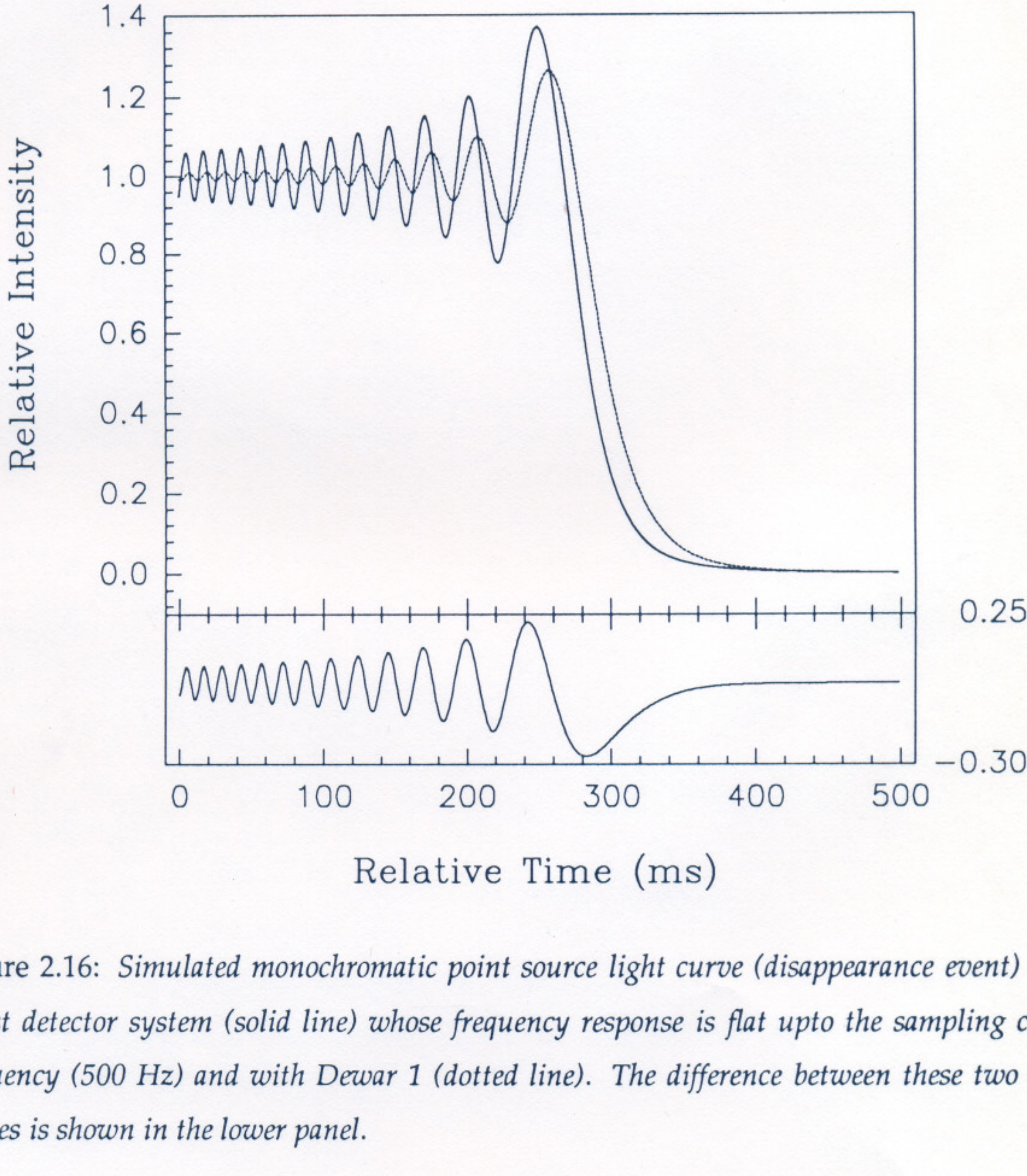

Figure 2.16: *Simulated monochromatic point source light curve (disappearance event) with a fast detector system (solid line) whose frequency response is flat upto the sampling cutoff frequency (500 Hz) and with Dewar 1 (dotted line). The difference between these two light curves is shown in the lower panel.*

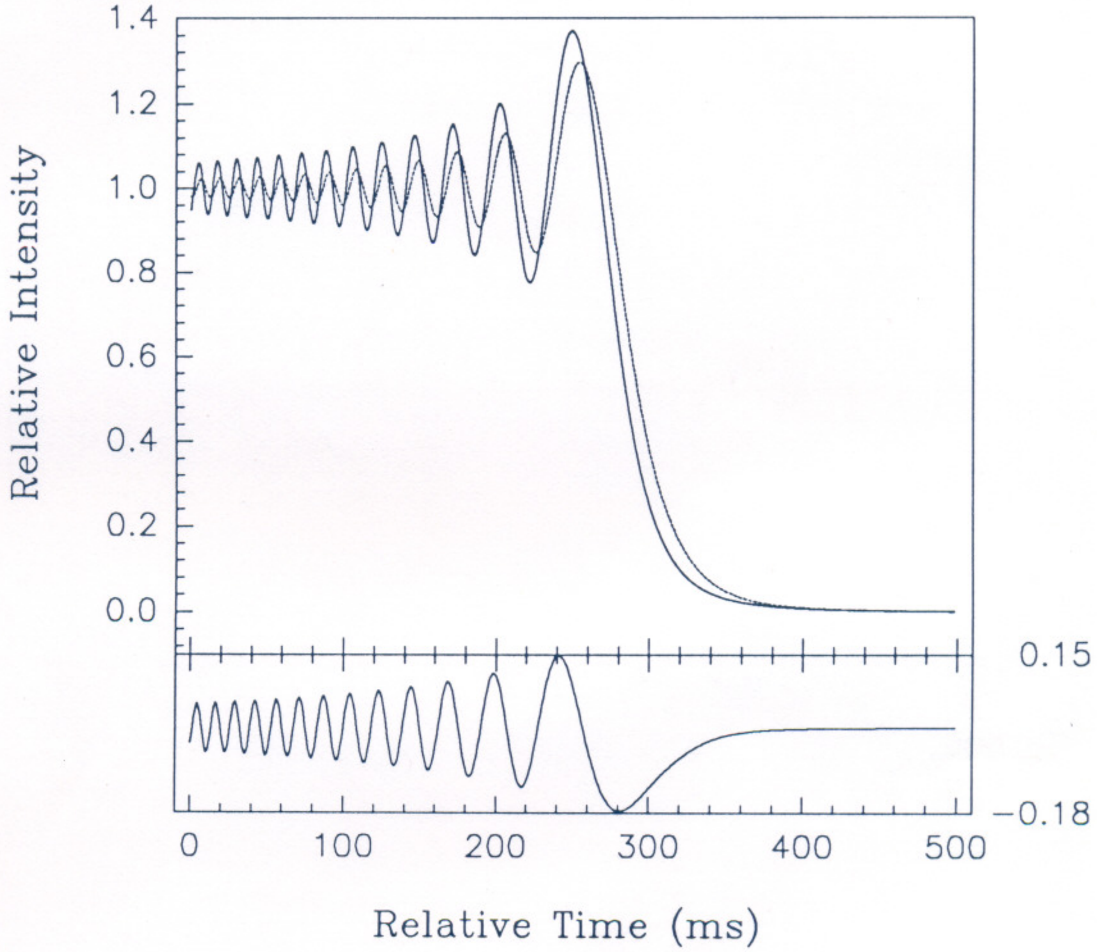

Figure 2.17: *Simulated monochromatic point source light curve (disappearance event) with a fast detector system (solid curve) whose frequency response is flat up to the sampling cutoff frequency (500Hz) and with Dewar 2 (dotted curve). The difference between these two light curves is shown in the lower panel.*

2.2.7 Effect of Scintillation Noise

Lunar occultation being a fast event, the effect of atmospheric seeing and scintillation on the light curve is, in general, not very severe. However, often these effects are noticed in the light curves of bright sources recorded with (a) small aperture telescopes and (b) unfavourable observing conditions like high air mass, daytime event or bad weather. The effects like improper centering of the object in the focal plane aperture, telescope tracking failure, thin low level passing clouds, changes in the sky transmission (if any) can also cause scintillation like noise in the light curve. This problem was addressed by Knoechel & Van der Heide (1978) and they have shown with numerical simulations that these effects can bias the angular diameter determinations very severely. For example, one such simulation with a 60 cm telescope at a zenith distance of 69° shows that the angular diameter estimation has as large as 220 % error. They also introduced a mathematical procedure to account for this effect and have shown with numerical simulations that this procedure works efficiently.

Essentially the scintillation effect on the occultation light curve is modelled by a normalized Legendre polynomial of the form,

$$L'(t) = \left[1 + \sum_{i=1}^{m} b_i L_i(t)\right] \tag{2.15}$$

which is multiplied with the theoretical Fresnel diffraction pattern expected for the source in the absence of any background light; where m is the order of the Legendre polynomial used and b_is are treated as free parameters in the model along with the other model parameters.

The procedure was applied to the real data only recently by Richichi et al. (1992a, & b). Richichi et al. (1992a) suggested to damp the portion of this Legendre term L(t) after geometrical occultation to obtain a stable solution. Since, the scintillation effect vanishes when star disappears, this suggestion makes physical sense. The damping function has the form,

$$\begin{aligned} \rho(t) &= 1 && when && t \leq t_o \\ &= I(t) - \beta(t) && when && t > t_o \end{aligned}$$

Hence, the light curve (eqn. 2.1) takes the form,

$$I(t) = L'(t)\,\rho(t) \int_{-\infty}^{\infty} \int_{-A/2}^{A/2} \int_{\lambda_1}^{\lambda_2} \int_{-\Delta\tau}^{0} S(\phi)\,F(\omega)\,O(\alpha)\,\Lambda(\lambda)\,T(\tau)\,d\phi d\alpha d\lambda d\tau + \beta(t) \tag{2.16}$$

The degree of these Legendre polynomials is chosen taking into account the correlations between all free parameters used in the model as well as the relative errors of these parameters (Richichi et al., 1992b). Care should be taken in choosing the order of the polynomial, since adding more and more parameters to a model will arbitrarily improve the model fitting, which may be spurious. Another approach is wherein different portions of the light curve of equal length as that of the event portion are fitted with a Legendre polynomial of adjustable order. The average polynomial order required to fit these portions meaningfully is compared with the other procedure mentioned earlier.

The occultation light curve of NSV 1529 is shown in Fig. 2.18. The initial fall seen in the light curve is due to low frequency scintillation noise present in the data. A 5^{th} order Legendre polynomial was used to model the scintillation noise present in the light curve. The source is resolved from our observations. The results from this light curve are dicussed in chapter 4.

2.2.8 Model Independent retrieval of brightness profiles from lunar occultation light curves

Although the technique of lunar occultation provides very high one dimensional angular resolution, it suffers from a major drawback that, the brightness profile of a source can't be directly extracted from the light curves (at least in optical and near infrared wavelengths), unless some apriori knowledge of the shape of the source is given. In order to overcome this difficulty, Richichi (1989a) introduced a deconvolution algorithm which provides the *most-likely* brightness profile from a set of all possible profiles for a given light curve which is unique.

Technique

The technique is essentially a composite algorithm which uses both nonlinear least squares fitting and Lucy's deconvolution algorithm. Lucy introduced an iterative

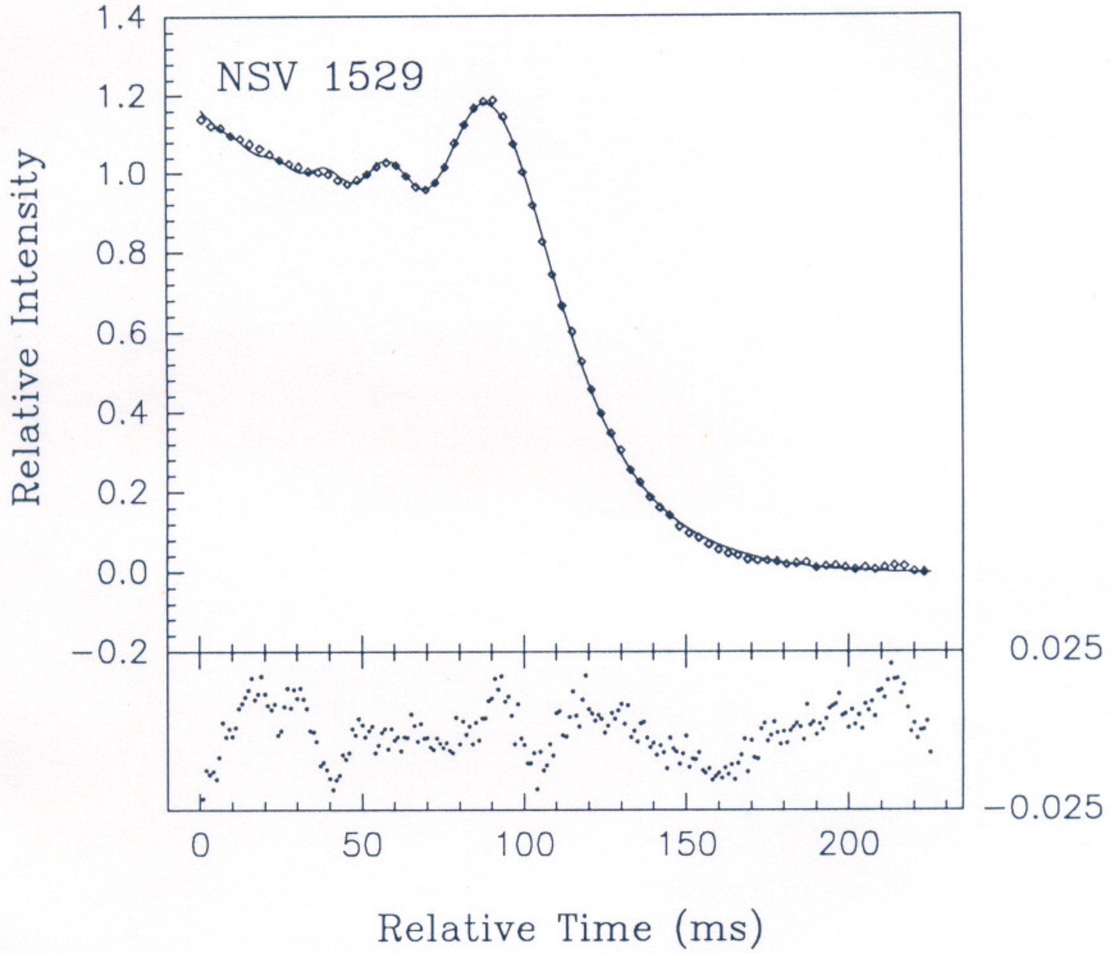

Figure 2.18: *Occultation light curve of NSV 1529 (squares) observed on 12 Feb 1991 with 1m telescope at Kavalur and the model fit (solid line) to the data.*

algorithm to solve deconvolution problems in statistical astronomy (Lucy, 1974). The required function is $\chi(\epsilon)$, while, the measurable quantity is its 'representation' ϕ(x) given by

$$\phi(x) = \int \chi(\epsilon) P(x, \epsilon) d\epsilon \tag{2.17}$$

where, P(x, ϵ)dx is the probability (presumed known) that x′ will fall in the interval (x, x+dx) when it is known that $\epsilon' = \epsilon$.

Lucy has shown that if $\chi(\epsilon)$ satifies positivity and normalisability, it can be found iteratively using following expression,

$$\chi^{r+1}(\epsilon) = \chi^{r}(\epsilon) \int \frac{\Phi(x)}{\phi^{r}(x)} P(x, \epsilon) dx \tag{2.18}$$

where suffix r denotes rth iteration, Φ(x) is the observed value of ϕ(x) and ϕ^r(x) is the rth approximation to the data. It can be shown that when r $\rightarrow \infty$, the solution $\chi^r(\epsilon)$ is also the solution of the equivalent maximum-likelihood problem, and that it is unique.

Eqn. 2.1 can be rewritten now as

$$I(t) = \int S(\phi) \Pi(t, \phi) d\phi + \beta \tag{2.19}$$

where,

$$\Pi(t, \phi) = \int_{-A/2}^{A/2} \int_{\lambda_1}^{\lambda_2} \int_{-\Delta\tau}^{0} F(\omega) O(\alpha) \Lambda(\lambda) T(\tau) d\alpha d\lambda d\tau \tag{2.20}$$

It is clear that eqn. 2.17 and eqn. 2.19 are the same except for the background term β(t) which can be subtracted from the original data at the data reduction level.

S(ϕ) on physical ground satisfies positivity and normalisability and hence Lucy's algorithm can be applied to solve eqn. 2.19. However, in practice, it is not straight forward since the matrix Π(t, ϕ) is computed from variables such as v, t_o, I_o which can't be theoretically calculated accurately and also the background term β(t) correlates with I_o and thus with S(ϕ). Nevertheless an iterative scheme can be set up as shown in Fig. 2.19.

First, one has to provide initial guesses for v, t_o, I_o and β(t). Also, the function S(ϕ) has to be assumed. In principle, any random function or a constant can be assumed for S(ϕ). But, closer the guess profile to the actual, faster will be the convergence. Eqn. 2.1 is solved with a reduced version of the classical least squares method, in which S(ϕ) is held fixed. This provides new values for v,t_o, I_o and parameters in the β(t) term which

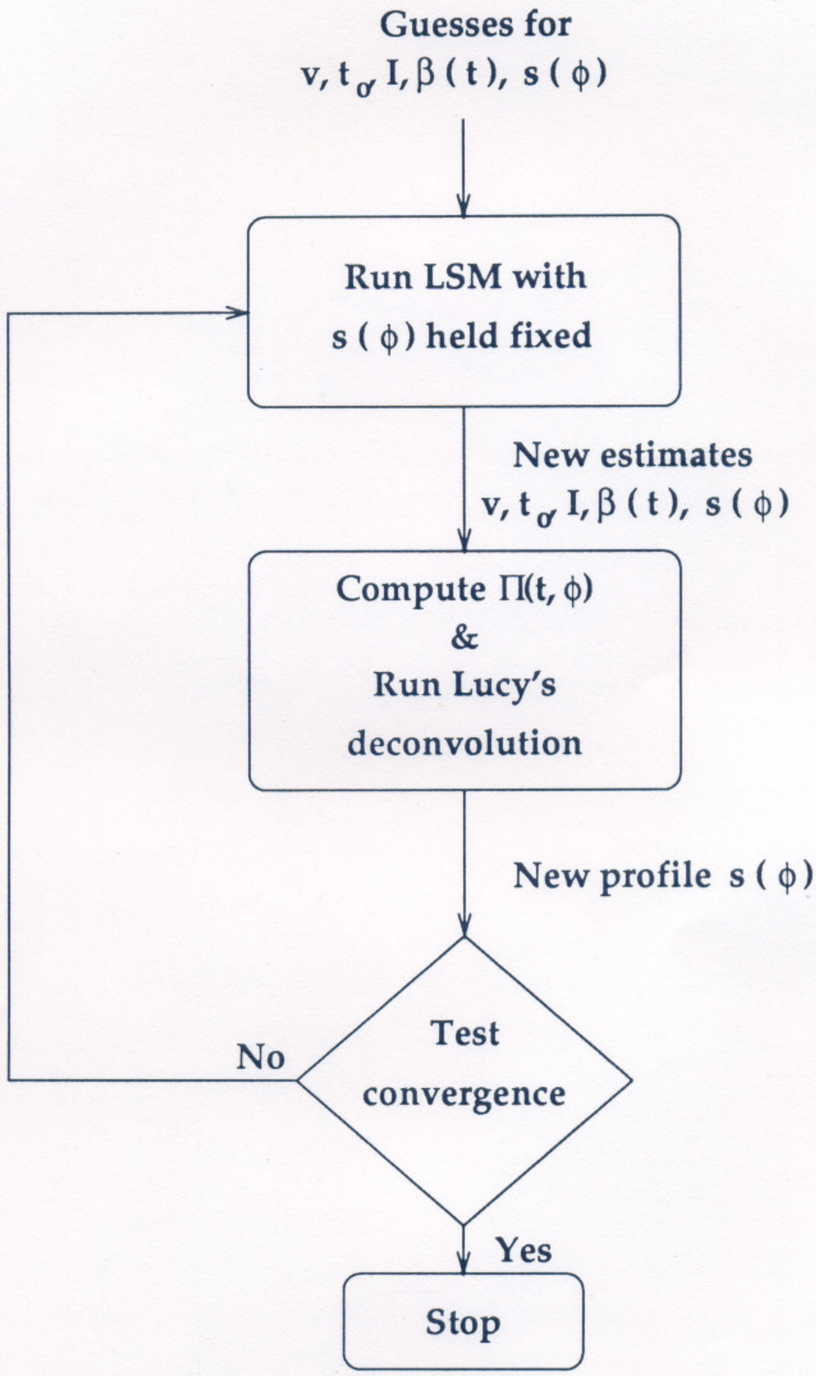

Figure 2.19: *Block diagram of the iterative scheme for brightness profile retrieval from occultation light curves, taken from Richichi (1989a).*

are used along with the old $S(\phi)$ to compute the matrix Π. Then, eqn. 2.19 is solved using Lucy's algorithm and a new determination of $S(\phi)$ is obtained. These steps can now be iterated until satisfactory convergence of $S(\phi)$ has been achieved.

It is important to perform a sufficiently large number of iterations in order to exploit all the information present in the data, but care should be taken to avoid contamination by noise. In fact, if too many iterations are performed, the restored profile tends to develop a structure with fine details which are fictitious and due to the noise in the original data. χ^2 is computed at each iteration to check the convergence.

In summary, a high speed near infrared photometer has been developed for lunar occultation studies successfully with the capability to reach milliarcsecond level of angular resolution. The numerical computer codes for analysing occultation light curves have also been developed. The results obtained from a detailed analysis of occultation light curves of two rare cool objects namely TV Gem (M1 supergiant) and TX Psc (Carbon star) are discussed in the next chapter.

Chapter 3

Circumstellar Dust Shell around Evolved Giants

It has been known for long that cool giants of spectral type M or later have circumstellar gas shells (Deutsch, 1960). Gehrz & Woolf (1971) and Gillett et al. (1971) have shown from 10 μm observations that many shells have dust component as well. However direct observations of these shells around red giants have been very limited. Recent observations in the infrared with a spatial interferometer (Danchi et al. 1994, Townes et al. 1994) on the distribution of dust around a sample of well known late type stars have shown that these stars fall into two categories – one class has inner radii of dust shells very close to the photosphere (3–5 stellar radii) and at a higher temperature ($\sim$ 1200K) than previously measured. This class includes VY CMa, NML Tau, IRC+10216 & o Ceti. The second class of stars has dust shells with large inner radii ($\geq$ 8 stellar radii) and very little dust close to the star. This class includes several supergiants like α Sco, α Ori and α Her. Interestingly, SiO,H_2O or OH maser emission is not seen in these supergiants while it is generally present in the other class. There is also good evidence that for long period variables like o Ceti new dust is formed in the cooling phase close to the star, during each cycle. Recent theoretical work by Winters et al. (1995) on the circumstellar dust shell around long period variables predicts discrete shell-like distribution of dust across the circumstellar shell around carbon stars. For supergiants like α Ori which is an irregular variable gas and dust are emitted episodically and there may not be any dust production for many decades. In this context it is worth while to study other cool giants at HAR to investigate the nature of the dust shells.

Circumstellar dust envelope around an oxygen-rich supergiant, TV Gem and a carbon star, TX Psc have been investigated from milliarcsecond angular resolution studies and the details are presented in the following sections.

3.1 Supergiant: TV Gem

3.1.1 An observational history of TV Gem and its surroundings

TV Gem is a distant oxygen rich supergiant classified as M1 Iab. It is a short period semi regular pulsating variable of variability type SRc with a period of 182 days (Kukarkin et al., 1969). The best estimation of distance to TV Gem is based on interstellar extinction towards eleven stars in the Gem OB1 association to which the star belongs. This yields a value of 1200 pc with an uncertainty of ~ 25 % (Underhill, 1984). The estimated value for the visual extinction is 1.98 magnitude (Radick et al. 1984). The visual magnitude given by Hoffleit & Jaschek (1982) and most widely used is 6.56. However, Keenan & McNeil (1989) gave a value 7.0 $-$ 7.8 for the visual magnitude and the spectral classification M0$-$1 Iab.

TV Gem is a suspected syncretic binary (Buss & Snow, 1988) where the primary is the early M supergiant and the secondary is an early B star. Syncretic (VV Cep) type binaries are a loosely defined class of spectroscopic binaries which exhibit a composite spectrum of an early M supergiant and a hot companion. The hot star orbits inside the stellar wind region of the primary.

The IUE low resolution spectrum in the range 1000 $-$ 3000 $\mathring{A}$ shows a clear bump at 2175 $\mathring{A}$ and Si II, Si III, C II, Si IV, Al II absorptions (Buss & Snow, 1988). Based on IUE data and UBV photometry, Underhill (1984) has suggested a B 3.5 IV companion around the M1 Iab supergiant primary. They estimate an angular separation between the two stars to be ~ 3 arcseconds with a B magnitude difference of 1.6. So far the presence of the companion has not been observationally established by direct imaging. We estimate the magnitude difference in K magnitude between these components to be ~ 6. The secondary, even if present, will be lost in the noise and hence we can't confirm or deny its presence from our occultation observations.

TV Gem has earlier optical occultation observations using y strömgren filter (Radick et al. 1984). The derived value for the stellar angular diameter is 5.31 ± 0.91 mas. Our value for the stellar angular diameter of 4.9 ± 0.3 mas is well within the quoted errors of the previous measurement and is also more accurate due to better SNR on the account of lesser background scattered light level in the K band. Recently, an unpublished occultation light curve of TV Gem in the K band observed by Richichi (1995a) has come to our notice . The derived value for the stellar angular diameter from this light curve is consistent with our value.

The circumstellar gaseous environment of TV Gem has been studied in the CO (1−0) and CO (2−1) lines in the millimeter region (Loup et al., 1993, Heske, 1990). The velocity profile in the CO (1−0) line is weak and flat topped which appears unresolved in the beam width of observations of ~ 23 arcsecond. This is not surprising as the CO envelope size (R_{CO}) limited by the ambient interstellar radiation field is typically 10^{17} cm $< R_{CO} < 6\times 10^{17}$ cm for optically thin cases (Loup et al. 1993). At the distance of 1200 pc assigned to TV Gem for the derived value of $R_{CO} = 1.7 \times 10^{17}$ cm one obtains for the envelope an angular size of 9.7 arcseconds which is well below the beam width of the observations. From the CO velocity profile, an expansion velocity (V_e) of 12 km/s has been derived. The mass loss rate ($\dot{M} \propto V_e^2\, d^2$) for a distance of 1200 pc to the source is $2\times10^{-6}\ M_\odot\ yr^{-1}$, assuming a $[CO/H_2]$ ratio of 5×10^{-4} typical of oxygen rich stars.

Stencel et al. (1989) have studied the infrared fluxes and spatial and spectral characteristics of over a hundred supergiants including TV Gem. They find that about one fourth of these objects are spatially resolved in the coadded (ADDSCAN) IRAS data at 60 μm and possess extended circumstellar shells with implied expansion for $\sim 10^5$ yr at a typical rate of ~ 10 km/s. Empirically, the IRAS point source response function at 60 μm is 2.3 − 2.5 arcminutes in terms of full width at 10% of the maximum intensity ($W_{10\%}$). With this criterion, TV Gem is just resolved at 60 μm with a full width at 10% value of 2.9 arcminutes. It must be pointed out, however, that Young et al. (1993a & b) have examined IRAS 60 μm and 100 μm data for spatially resolved structure in a large number of stars. TV Gem does not figure in their final list of resolved objects as in their classification, it falls into a set of stars which are near other sources or embedded in regions of extended emission resulting in curved base lines. Hence, there is no conclusive but conflicting evidence of the extended source structure around TV Gem from IRAS imagery at the level of arcminutes. However, the 9.7 μm silicate emission feature seen in IRAS LRS and the infrared excess present in the IRAS photometric data for TV Gem unambiguously points to the presence of dusty circumstellar shell which can be probed only by HAR methods.

It is known from early broad band IR observations that onset of silicate excess in oxygen rich stars is seen for all stars later than M6 III, M5 II, M1 Iab, K3 Ia and G0 Ia–O supergiants (Merrill & Stein, 1976). Supergiants redder than V$-$K$\sim$6 invariably exhibit silicate feature. Many warmer supergiants with V$-$K $<$ 6 have IR excess as shown by the ratio $\left(\frac{f_{25}}{f_{12}}\right)$ indicative of dusty circumstellar envelopes but do not generally exhibit a silicate feature. However, as shown by Stencel et al. (1989) the broad band warm dust indicator $\left(\frac{f_{25}}{f_{12}}\right)$ peaks among these stars with lowest LRS continuum ratio. Cooler stars have more dust. The cooler photosphere and the greater quantity of dust contribute to a shallower LRS continuum. The emission strength of the feature at 9.7 μm is also known to correlate with $\left(\frac{f_{25}}{f_{12}}\right)$ ratio because both relate to newly formed warm dust. TV Gem is an exception to the rule or a border line case where both IR excess and silicate feature are present although the V$-$K value is 5.6. We estimate the mass loss rate from the 9.7 μm silicate feature strength (Skinner & Whitmore, 1988) to be $\dot{M}$ = $1.8\times10^{-6}M_{\odot}yr^{-1}$, which is consistent with that derived from CO observations.

3.1.2 Observations and Data Analysis

The lunar occultation observations presented here were carried out at the 0.75 m telescope at Kavalur (78° 49′ 45″E, 12° 34′ 35″N, 725 m) during March 1993. Table 3.1 lists the circumstances of the event. Table 3.2 lists the source identifications in different catalogs. The occultation event reported here was a disappearance event at the dark limb of the moon.

The instrument used was a LN_2 cooled InSb based high speed infrared photometer which is described in chapter 2. A standard K filter (λ = 2.2 μm,$\Delta\lambda$ = 0.4 μm) and a 2 mm circular diaphragm which corresponds to 42″ field on the sky were used. Data sampling was at a rate of 1 KHz for 30 seconds using a 16 bit high speed A/D converter (Keithley system 575). The absolute timing of the event was not recorded, since it is

Table 3.1: *Predicted Circumstances of Observed event.*

Date	30 *Mar* 93
Time (UT)	14 : 30 : 28
Predicted Position Angle (deg)	95
Predicted Contact Angle (deg)	11
Lunar Phase (days since new moon)	7.1
Altitude (deg)	59.4
Shadow vel. comp. (km/s)	0.6456

Table 3.2: *Cross identifications of TV Gem.*

IRC	IRAS	BS	SAO	*HD*
+20134	06088+2152	2190	78092	42475

not relevant for the present work.

Near infrared photometry of TV Gem has been carried out using the same high speed IR photometer with 1.2m telescope at Gurushikhar (72°47′E, 24°39′N,1680m) and the photometric values are listed in Table 3.3.

Data analysis was performed using both the Nonlinear Least Squares method (NLS) and the Model Independent Algorithm (MIA) described in Chapter 2. Averaging effects due to finite optical filter bandwidth and telescope aperture have also been accurately taken into account. The analysis takes into account the CVF spectrum of TV Gem reported by Arnaud et al. (1989) in the spectral range 2 − 2.4 μm while accounting for the smearing effect caused by the finite optical filter bandwidth. The data analysis

Table 3.3: *JHK Photometry of TV Gem.*

Filter band	J	H	*K*
Magnitude	2.13 $\pm$0.05	1.17$\pm$0.1	0.93 $\pm$ 0.05

procedure also accounts for the finite bandwidth of the detector system.

3.1.3 Direct detection of dust shell

Observed occultation light curve of TV Gem (Fig. 3.1), fitted with a simple uniformly illuminated disk stellar model does not yield a completely satisfactory fit. The nature of the residuals suggests that the model fit is likely to improve if an extended source is present in addition to the central star. Since the nature of the extended source is not known, MIA has been used to obtain the shell brightness profile. We decompose the model light curve into stellar and shell components. For the stellar component a uniformly illuminated disk model is assumed, while for the shell a flat guess profile is assumed. The shape and the extent of this assumed profile (for the shell) is not critical to achieve convergence, except that, the extent should be larger than the true extent of the circumstellar envelope present in the data. First, NLS fit is carried out to estimate the stellar angular size and the star to shell flux at 2.2 μm along with the scaling parameters. Now, the stellar component is removed from the observed light curve and Lucy's deconvolution algorithm is used to modify the shell brightness profile. A three point binning of the data is made to improve the SNR while performing Lucy's deconvolution which sets the angular resolution of the recovered brightness profile at $\sim$ 1.1 mas. The whole procedure is repeated till it converges. Five iterations of the MIA algorithm are sufficient to achieve good fit to the data.

The portion of the observed light curve, most sensitive to the angular size, can be determined by plotting the partial derivative of the best fit model curve with respect to the angular diameter. Such an approach has been used earlier by Ridgway et al. (1979). The partial derivative of the best fit model with respect to the angular size of the star and shell are shown in Fig. 3.2. It can be seen that the most sensitive points correspond to the maxima and minima of the light curve. From SNR ratio consideration a sensitivity zone can be defined for the TV Gem occultation from 100 – 300 milliseconds.

The data fitted using MIA is shown in Fig. 3.3. The shell component of the observed light curve and the corresponding model fit are shown in Fig. 3.4.

The recovered brightness profile for the source is shown in Fig. 3.5. The broad feature recovered is well above the noise level and is the signature of the dust shell

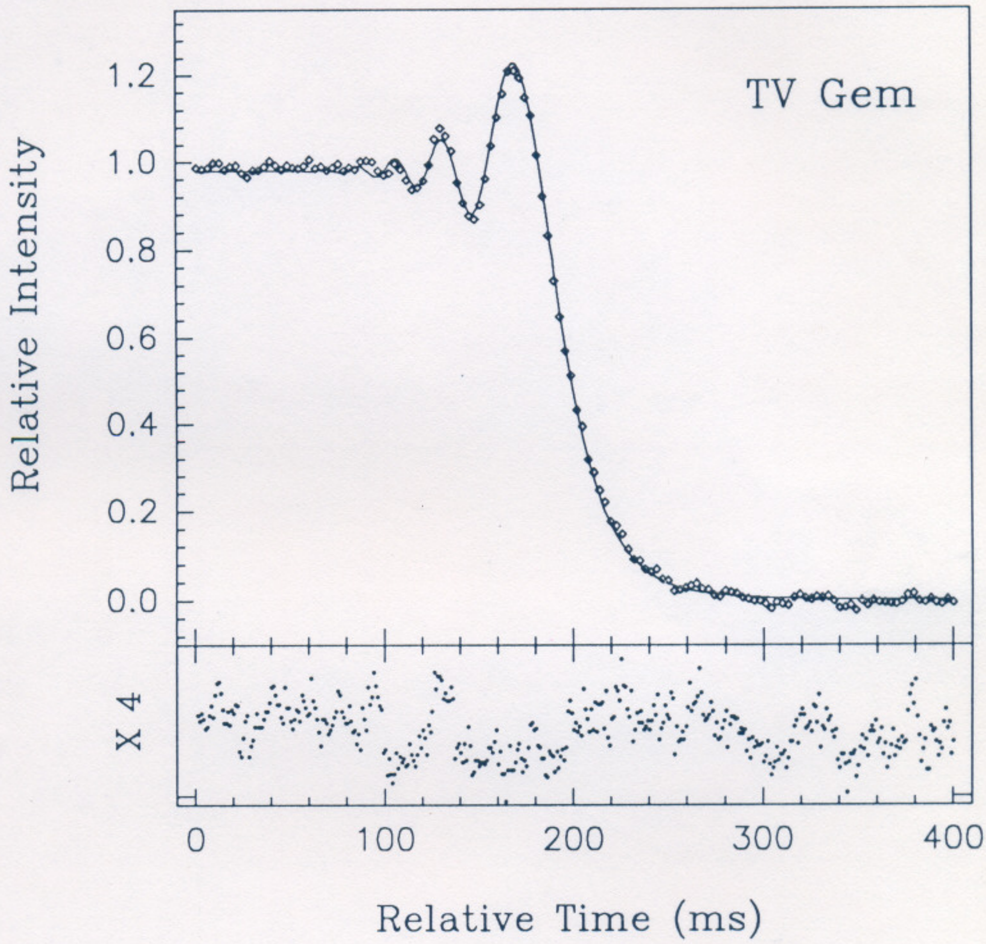

Figure 3.1: *Occultation light curve of TV Gem (open squares) fitted with a uniformly illuminated stellar disc model using NLS method (solid line) is shown in the upper panel. Lower panel shows the residuals of the fit enlarged by a factor of 4.*

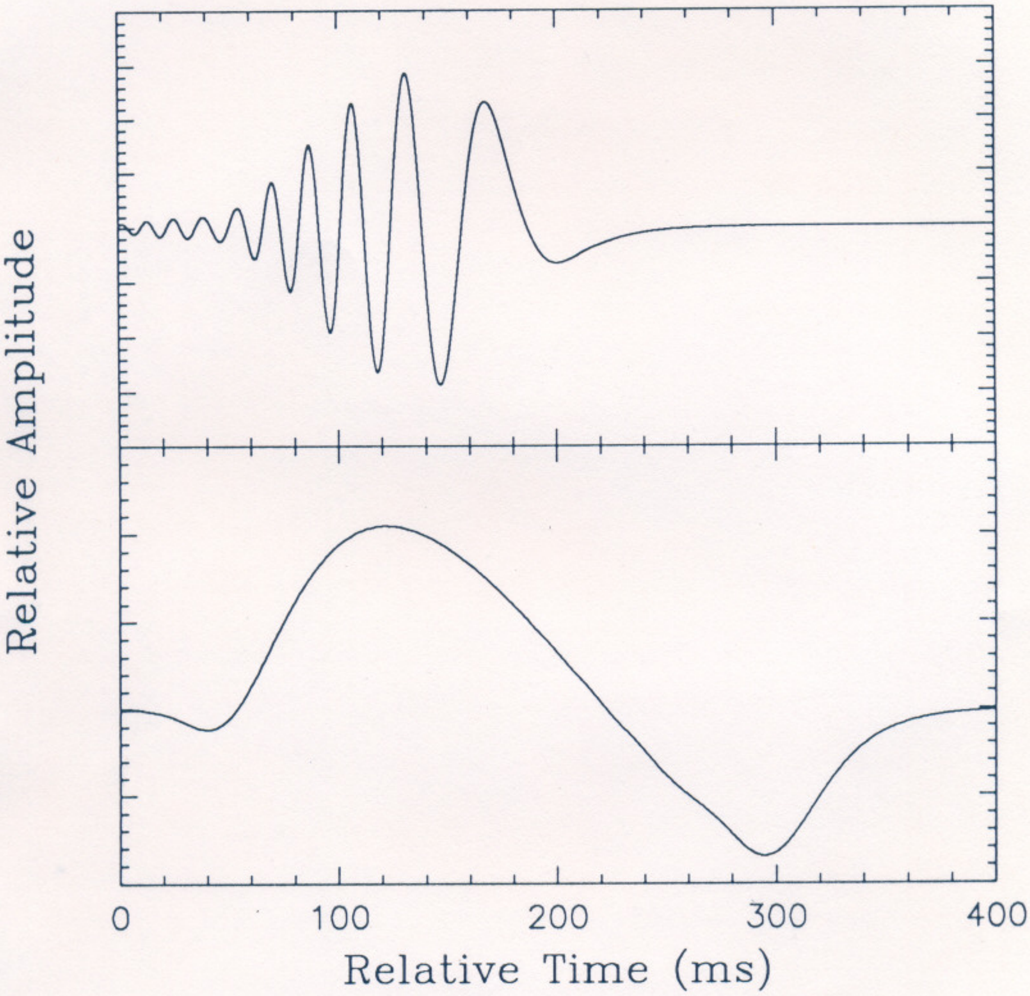

Figure 3.2: *The partial derivative of the best fit model with respect to the angular size of the star and shell are shown respectively in the top and bottom panel.*

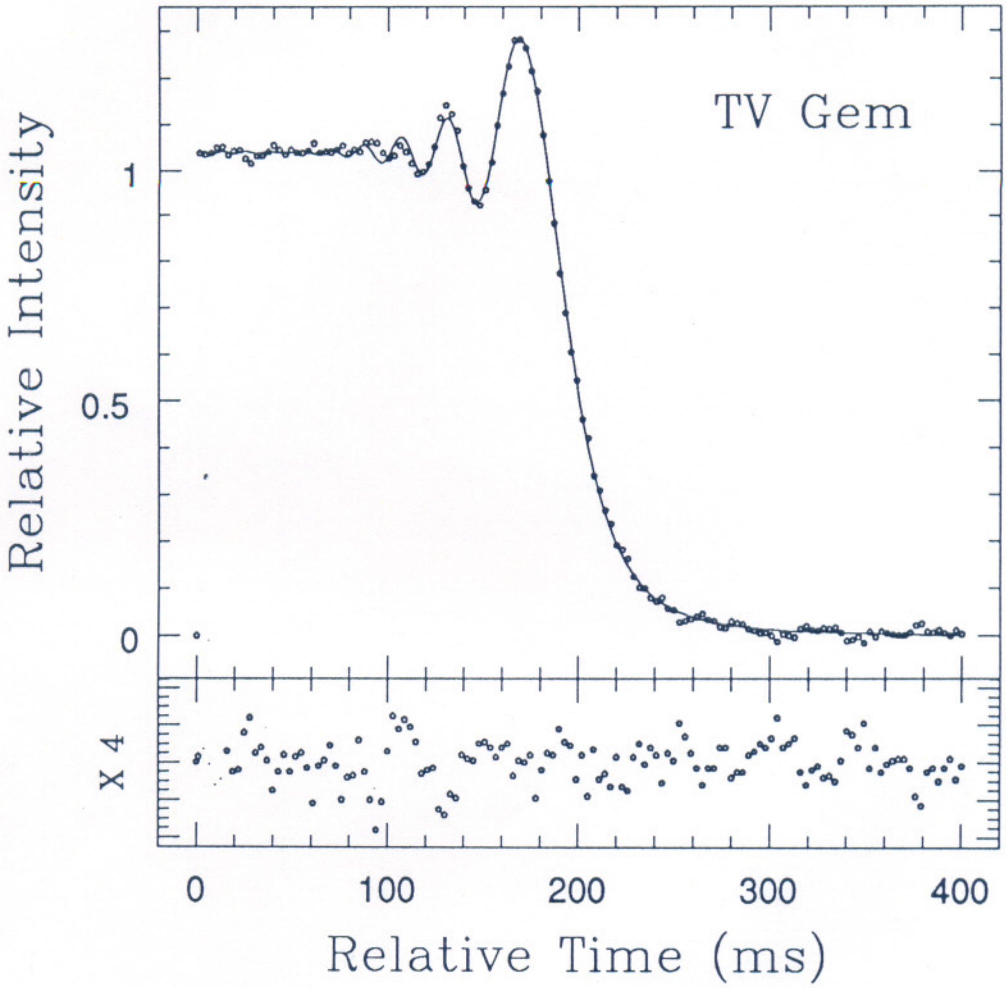

Figure 3.3: *Occultation light curve of TV Gem (open circles) fitted using MIA (solid line) is shown in the upper panel. Lower panel shows the residuals of the fit enlarged by a factor of 4.*

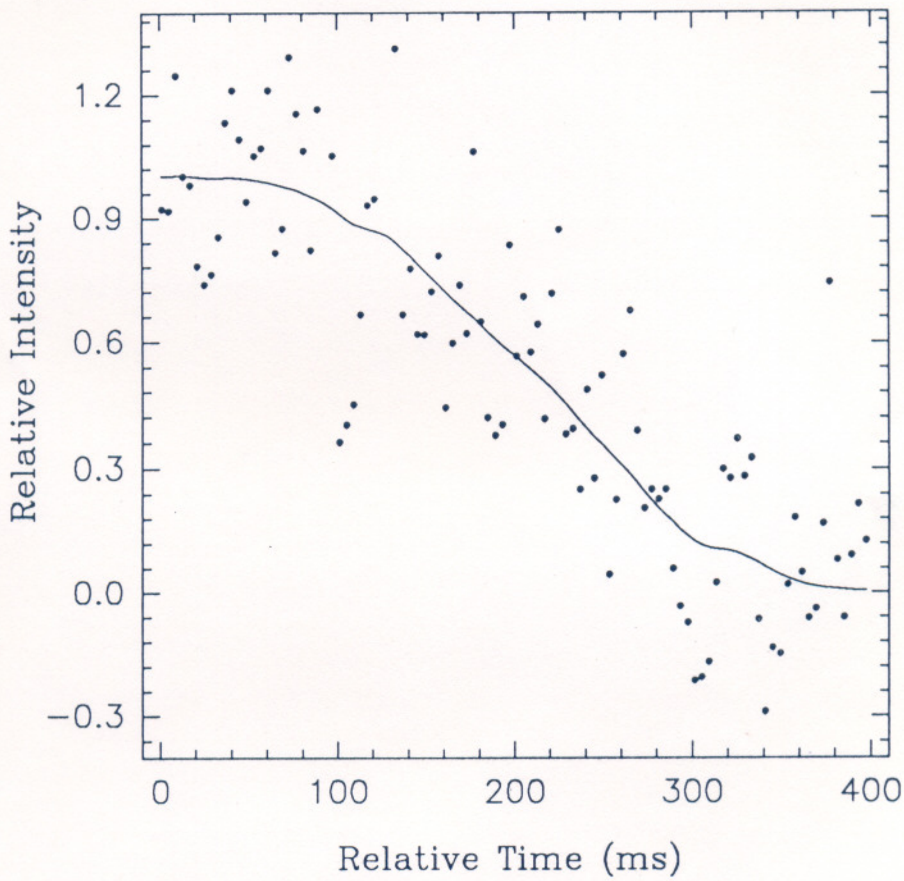

Figure 3.4: *The contribution to the light curve of TV Gem due to the extended component alone recovered using MIA (dots) and the corresponding fit (solid line).*

around the central star. The shape and the amplitude of this recovered profile is very stable against initial guess values of the model fitting procedure.

Fig. 3.6 shows the residuals (data – model) for a uniform disk model using NLS and a uniform disk plus circumstellar shell model using MIA. It can be seen that the uniform disk model has an oscillatory residue pattern which is indicative of an unaccounted more extended source. The residuals after invoking circumstellar extended feature do not exhibit this oscillatory pattern and the noise pattern is now random. The solid lines drawn in Fig. 3.6 are not due to any least squares fitting and are plotted to merely show that inclusion of a shell makes the residue more random.

The recovered brightness profile is fairly symmetric. For the best fit model we derive the FWHM of the shell extent to be 100 $\pm$ 20 mas and the star to shell flux ratio at 2.2 μm to be 35. The derived value for the stellar angular diameter is 4.9$\pm$0.3 mas. U, B & V photometric values of TV Gem are corrected for the presence of a companion (Underhill, 1984). Bolometric flux has been derived by integrating numerically the available optical and infrared photometric data in the literature (Hoffleit & Jaschek, 1982; Underhill, 1984; Gezari et al., 1993) in addition to our JHK values. Thus derived value for the bolometric flux for TV Gem is 1.53×10^{-6} erg/cm^2/s and the estimated error in this bolometric flux is 10%. From the derived stellar angular size and bolometric flux, we derive a stellar effective temperature of 3670$\pm$125K for TV Gem.

3.1.4 Circumstellar dust distribution

The dust distribution around TV Gem is investigated taking into account our occultation observations, 9.7 μm silicate feature seen in the IRAS LRS and the 12, 25 and 60 μm far infrared fluxes from IRAS. A simple radiative transfer model of an optically thin isothermal shell composed of grains of a single size is invoked.

The following are the observational constraints imposed in the model:

1. The radius of the dust shell around TV Gem derived from our lunar occultation data analysis is 20$\pm$5 $R_\star$.

2. The estimated value for the shell flux at 2.2 μm is 5.7×10^{-16} W/cm^2/μm.

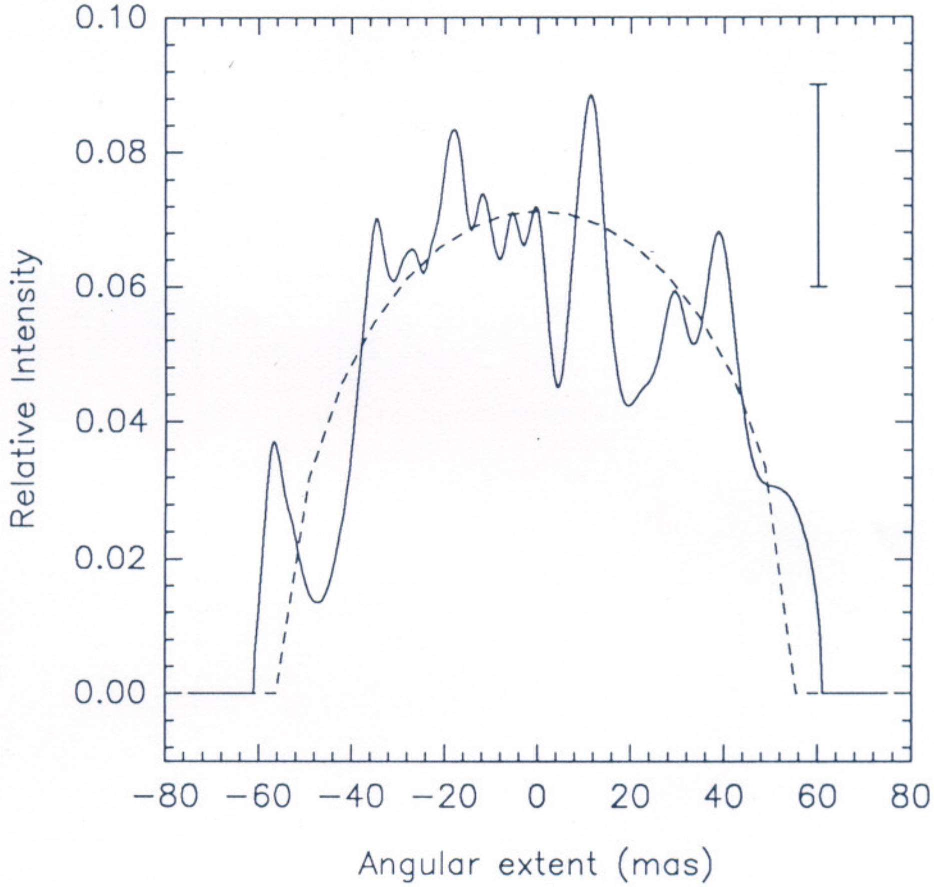

Figure 3.5: *The recovered one dimensional brightness profile of the extended component of TV Gem (solid line) recovered using MIA. Also shown is a uniform disk brightness profile of 55 mas angular radius (dashed line).*

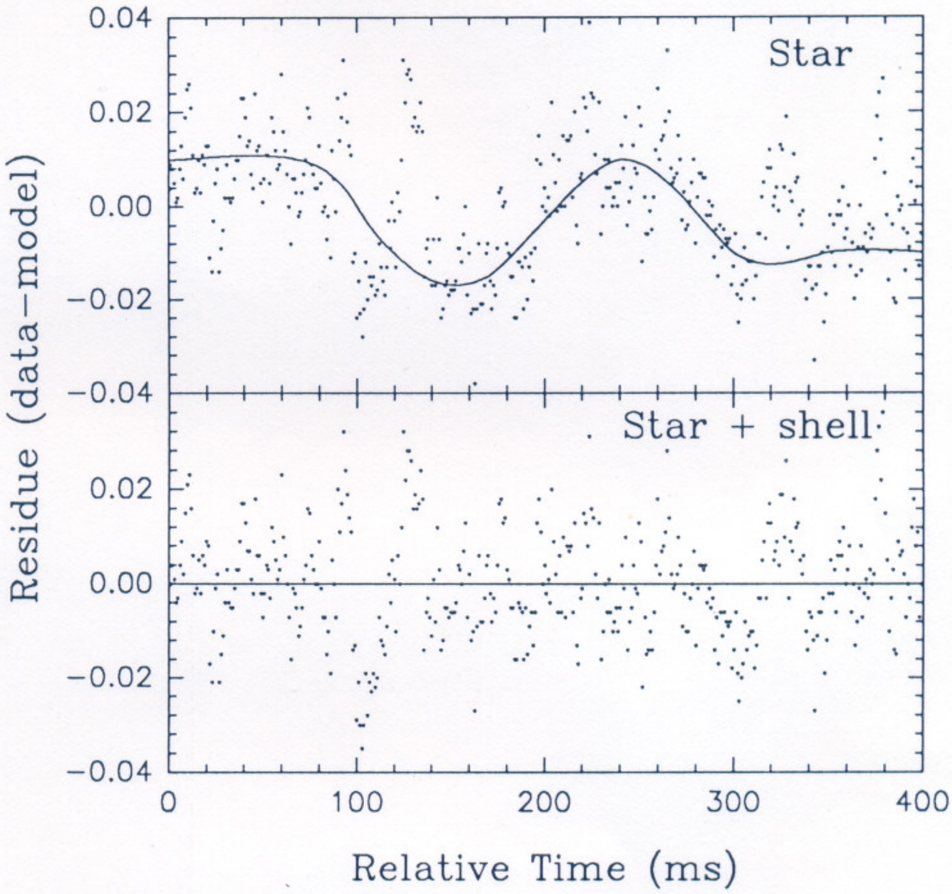

Figure 3.6: *Residuals of the 'star only model' using NLS is shown in the upper panel and the lower panel shows the residuals of the 'star plus shell model' using MIA.*

3. In addition, the shell flux at 9.7 μm, 12 μm, 25 μm and 60 μm are estimated from IRAS data by subtracting stellar contribution which is calculated from the stellar parameters derived from our occultation light curve. These fluxes are respectively 3.6×10^{-16}, 1.7×10^{-16}, 1.7×10^{-17} and 4.1×10^{-19} W/cm^2/μm. The stellar contribution to the total flux at these wavelengths are in the range 15 – 22 %.

The flux (F_λ) at wavelength λ is given by

$$F_\lambda = \frac{4\pi a^2 Q_{emit} B(\lambda, T)}{4\pi d^2} N, \tag{3.1}$$

where B(λ,T) is the Planck function (blackbody flux) at temperature T and wavelength λ, d is the distance to the source, N is the total number of grains in the shell, Q_{emit} is the emission efficiency of the grain and a is the size of the grain. We assume the grains to be bare silicates without mantles. The spectral signature of the silicate features at 10 and 20 μm are characteristic of the Si-O stretch and bend in rocky materials. Recently, there has been considerable discussion on the definition of true astronomical silicate in an interstellar sense. Greenberg & Li (1995) have interpreted 9.7 μm and 18 μm interstellar features not in terms of pure silicate but by a pure silicate core-organic refractory mantle grains. While this core-mantle model provides a better fit to the interstellar absorption 10 μm feature, for regions of grain formation relatively close to the stellar photosphere, wherein 10 μm silicate feature is in emission, a bare silicate model may be adequate. Accordingly, Draine and Lee (1984) model to obtain Q_{emit} values in the region of interest has been used. A constant grain size of a = 0.1 μm and a grain density of 3.3 gm/cc (Skinner & Whitmore, 1987) are assumed.

Assuming radiative equlibrium in the circumstellar environment, the shell flux ratio (2.2 μm to 9.7 μm) as a function of radial distance from the star is computed using eqn. 3.1 and shown in Fig. 3.7. It can be seen that the flux ratio in the range 0.4–1.8 corresponds to a shell radius in the range 15 – 25$R_\star$. Even taking into account the errors involved in the estimation of shell flux value at 2.2 μm from our occultation observations, the actual ratio is expected to lie well within this range. The conclusion is that the dust shell radius is sharply confined to the zone of 15 – 25 $R_\star$. These results also suggest that both 2.2 μm and 9.7 μm fluxes mainly arise from the same dust zone

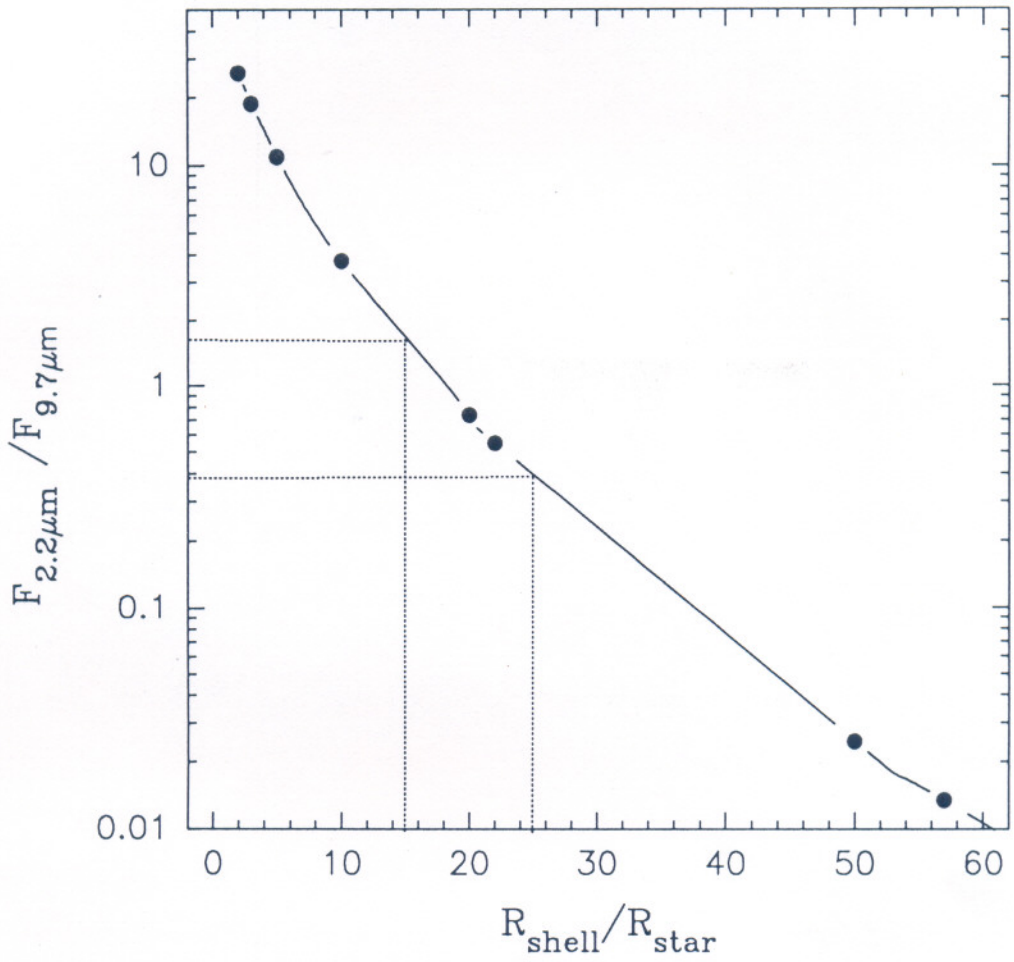

Figure 3.7: *Calculated 2.2 μm to 9.7 μm flux ratio as a function of radial distance from the central star using a simple radiative tranfer shell model.*

existing at $\sim 20 \pm 5$ $R_\star$.

The shell maximum temperature can range from $\sim$ 950K at 15$R_\star$ to $\sim$ 730K at 25$R_\star$. There exist no agreement on the precise condensation temperature of silicate dust grains (Griffin, 1993). Some authors favour values as high as 1500 K (Volk & Kwok, 1988), others a value of 1000 K (Skinner & Whitmore, 1988; Danchi et al, 1994), while a value as low as 500 K was used as the inner dust shell temperature of some stars (Rowan-Robinson & Harris, 1983; Hagen, 1982; Onaka et al., 1989). Refractory compounds condense first in the ejected hot gas envelope, close to the central star as their condensation temperature is high. The compounds of Al, Ti, Ca and probably

Fe will form the seed of the grains. The condensation temperatures of Al_2O_3, $CaTiO_3$, $Ca_2MgSi_2O_7$ & Metallic Fe are respectively 1720K, 1650K, 1580K & 1450K. These 'seed' nuclei subsequently grow by becoming clad by more abundent Mg-silicates which condenses at relatively lower temperature. The condensation temperature of Mg_2SiO_4, Mg_2SiO_3 & SiO_2 is 1350K (Turner, 1991).

We now consider a uniform dust mass loss rate of $2\times10^{-8}M_\odot$ yr-1 and an expansion velocity of 10 km/s for the circumstellar material around TV Gem, consistent with CO observations in the outer regions of TV Gem (Loup et al. 1993, Heske, 1990).

The number density of silicate grains, for this situation has a R^{-2} dependence and can be written as

$$n\left(R\right) = \frac{3.18 \times 10^{-3}}{\left(\frac{R}{R_\star}\right)^2} cm^{-3}. \tag{3.2}$$

The model flux from the shell with boundaries R_1 and R_2 are estimated by integrating between the limits R_1 and R_2 using eqns. 3.1 & 3.2. Although the observed shell flux at 2.2 μm and 9.7 μm can be explained with the inner dust shell detected from our occultation light curve, the far infrared excess, particularly at 60 μm, can be fitted only by invoking cooler dust at $\sim$ 500 $R_\star$. There is no evidence of dust in the intermediate region (Fig. 3.8). An immediate conclusion of this confinement of dust to two isolated shells is that the dust condensation in TV Gem and the consequent mass loss is not a continuous process. While the void in the inner zone $\lesssim 15R_\star$ can be attributed to temperatures higher than the condensation temperature of silicate material, the absence of material beyond $25R_\star$ can only be explained by considering the mass loss rate in TV Gem to be a sporadic process. The dust seen in the $15 - 25R_\star$ zone has an estimated mass of $\sim 10^{-7}M_\odot$ from its 2.2 μm shell flux values and it would have formed in a time frame of a few decades. The mass estimated for the cooler outer shell is 6×10^{-6} $M_\odot$ with a shell thickness of $\sim$ 200 $R_\star$. It would have condensed $\sim 10^3$ yrs back.

Finally, we compare our results on the circumstellar dust shell around TV Gem with that of α Ori, since both the supergiants are of similar spectral and luminosity class. The dust shell around α Ori has been studied in great detail with various interferometric observations (Sutton et al., 1977; Howell et al, 1981; Roddier & Roddier, 1983; Bloemhof et al., 1984; Bloemhof et al., 1985; Christou et al., 1988; Bester et al., 1991). Recently,

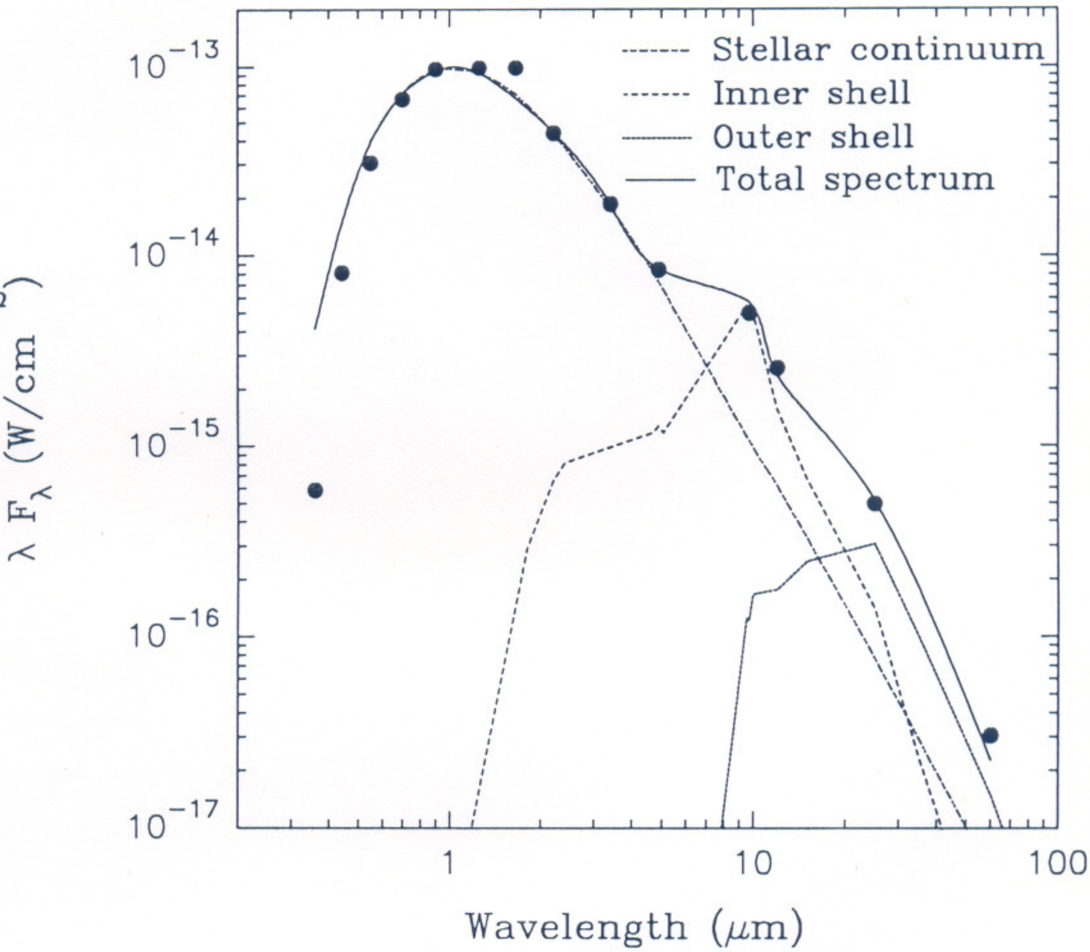

Figure 3.8: *Observed photometric values (dots) fitted with a three component (star + double shell) model is shown. In addition to our measured near infrared photometric values, values are also taken from the literature (Hoffleit & Jaschek, 1982; Underhill, 1984; Gezari et al., 1993). The spectra of the individual components are shown as dashed lines.*

Danchi et al. (1994) reported two dust shells present around α Ori – one at $\sim 25R_\star$ with a shell thickness of $\sim 2R_\star$ and inner shell temperature of 381K and the other at $\sim 50R_\star$ with a shell thickness of $\sim 5R_\star$ and inner shell temperature of 266K from infrared spatial interferometric observations suggesting a sporadic dust condensation in α Ori. We suggest that the circumstellar dust shell properties of these two supergiants are somewhat similar, though the time interval between two episodes of mass loss may be different. Sporadic mass loss and dust condensation with a time scale of a few decades could be a general phenomenon in early M supergiants.

3.2 Carbon star: TX Psc

Carbon stars are, on the evolutionary scale, advanced stars that lie high on the asymptotic giant branch, poised to become long period variable (many already are) and then planetary nebula (Johnson et al., 1995). The abundance of carbon in the photosphere of carbon stars is greater than the abundance of oxgygen. These carbon stars are characterized by extreme red colours, low effective and colour temperatures and detectable infrared excess. Carbon stars have extended and cool atmospheres. Infrared and radio observations reveal that most of them are embedded in dust and molecular clouds. This implies mass loss at a very large rate. As the matter flows out away from the star, adiabatic expansion and radiative cooling take place and this sets up an ideal environment for the formation of dust grains. This leads to the formation of circumstellar shells.

Stellar and circumstellar dust shell parameters of carbon stars have been studied in detail in a series of papers by Bergeat et al. (1976a,b & c) with a sample of 29 carbon stars by modeling the observed spectral energy distribution of these stars. They have classified the carbon stars from their samples into two categories. The first class consists of 4 carbon stars, including TX Psc, which doesn't show the evidence of circumstellar dust atleast upto 2.2 μm. The other class consists of the rest 25 stars, including a cool carbon star T Cnc, which show the evidence of circumstellar dust shell from their work. The predictions of the stellar and circumstellar dust shell parameters have also been made for these 25 stars by these authors (Bergeat et al., 1976b). However, direct HAR observations are few to compare these model predictions on the circumstellar dust shell parameters.

HAR studies of carbon stars have been carried out, so far, mainly by lunar occultation as most of these stars are too faint in the visible region for interferometric techniques to observe. The compilation of angular diameters from lunar occultations by White & Feierman (1987) contains nine carbon stars namely CW Leo, IRC-20420, TW Oph, SS Vir, SZ Sqr, TX Psc, Y Tau, X Cnc & RT Cap. Recently, compact circumstellar dust shell around T Cnc (a cool carbon star) has been detected by Richichi et al. (1991) using lunar occultations. CW Leo is the only carbon star, observed with various interferometric techniques (Ridgway & Keady, 1988; Dyck et al., 1991 & Danchi et al., 1994), in addition to lunar occultations (Toombs et al., 1972 & Ridgway & Keady, 1988). Recently, optical long-baseline interferometry has resolved for the first time three bright carbon stars namely UU Aur, YCVn & TX Psc (Quirrenbach et al., 1994a). As the technique is limited to bright stars ($m_v \sim 5.3$), only a few of carbon stars can be observed. However, repeated observations of very limited sources are possible by long-baseline interferometry.

Being a rare class of objects, there is a paucity of observational data on carbon stars, especially at high angular resolution. Accurate knowledge of intrinsic properties are necessary to support theoretical models. High angular resolution studies to resolve the stellar surfaces and hence the accurate determination of the stellar effective temperature can form the foundation for pursuing problems related to the carbon stars.

3.2.1 Observations

The lunar occultations of TX Psc reported in this thesis have been carried out on two occasions, one from Gurushikhar and the other from Kavalur at 2.2 μm. Table 3.4 lists the circumstances of these events. Both the events were observed under extremely difficult observing conditions. The Gurushikhar event was a day time disappearance event (local time $\sim 14^h{:}30^m$) and was observed with a small telescope of 0.35 m diameter, while, Kavalur event was observed with a 1m telescope at very large air mass of ~ 8. The observations of TX Psc have been carried out as part of an international campaign organised by Dr. Andrea Richichi to investigate the central star and its immediate surroundings from multiwavelength lunar occultations at different position angles

Table 3.4: Predicted Circumstances of Observed events.

Parameters	*Gurushikar event*	*Kavalur event*
Date	27 *Jan* 93	13 *Feb* 94
Time (UT)	08 : 59 : 32	14 : 29 : 17
Predicted Position Angle (deg)	91	56
Predicted Contact Angle (deg)	−39	13
Lunar Phase (days since new moon)	4.3	3.0
Altitude (deg)	59.3	7.6
Shadow vel. comp. (km/s)	0.4913	0.8949

Table 3.5: Cross identifications of TX Psc.

IRC	IRAS	BS	SAO	*HD*
+00532	23438+0312	9004	128374	223075

during 1992-94, when star underwent a series of lunar occultations.

The light curves were recorded with the instrument described in chapter 2. The standard broad band K filter was used and the instrumental field of view was 100″ & 21″ respectively for the Gurushikhar and Kavalur events. Table 3.5 lists the source identifications in different catalogs.

3.2.2 Detection of asymmetry in the brightness profile

Lunar occultation light curve of TX Psc, observed at Gurushikhar, fitted with a uniform disk model using NLS is shown in Fig. 3.9. Being a day time event and observed with a small aperture telescope, the data was dominated by background sky noise as well as scintillation noise due to small telescope aperture (35 cm). Nevertheless, the source has been resolved from our observations and the best fit model provides an angular diameter of 7.5 ±0.5 mas. The Gurushikhar occultation is probably a unique day time event, observed with the smallest single telescope ever used in the infrared to provide

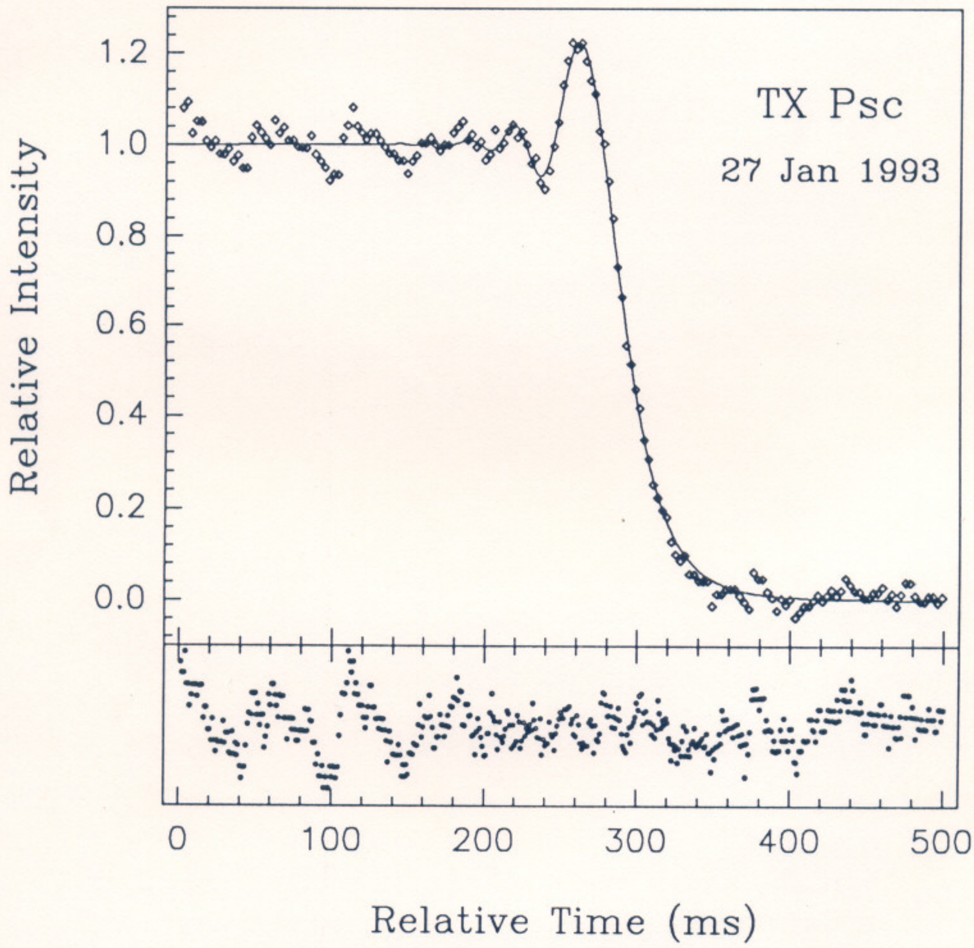

Figure 3.9: *Occultation light curve of TX Psc observed on 27 Jan 1992 with 14″ telescope at Gurushikhar and the model fit using NLS.*

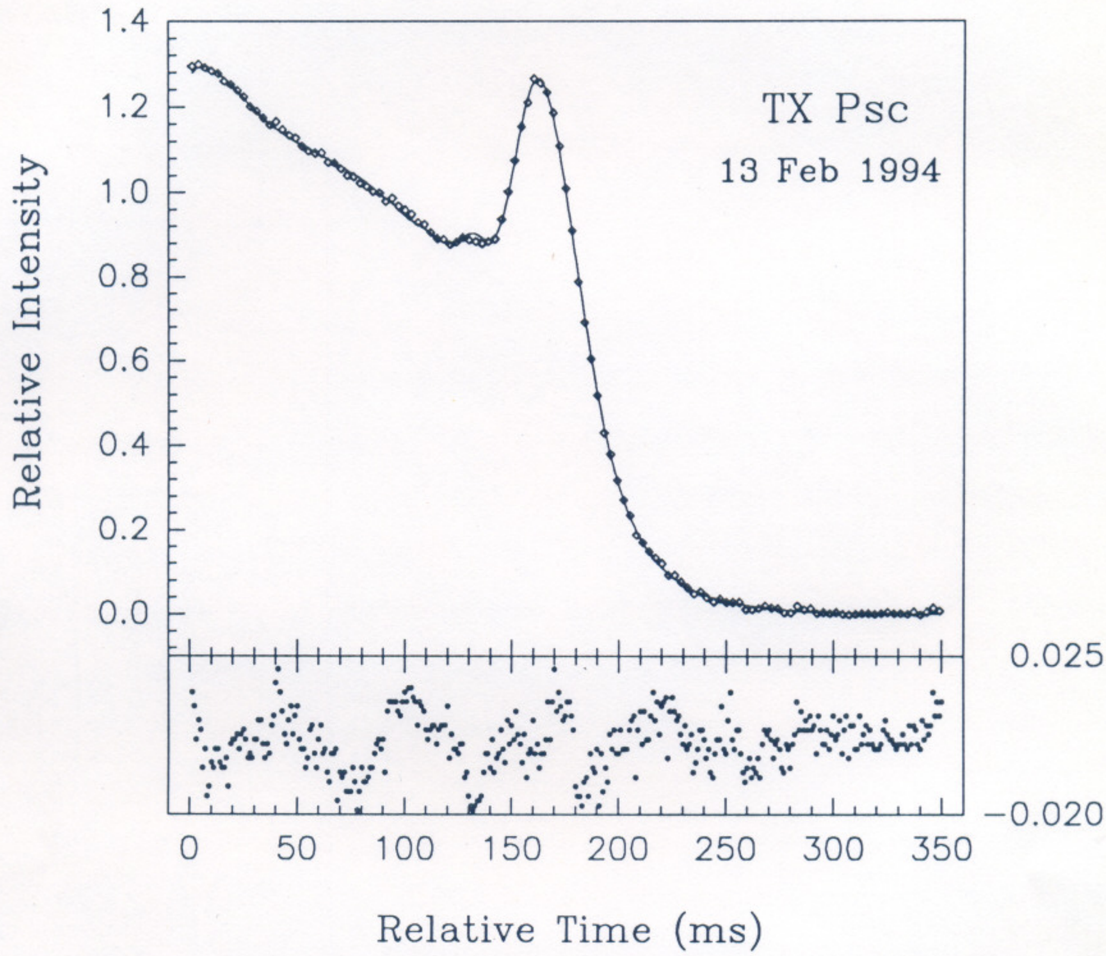

Figure 3.10: *Occultation light curve of TX Psc observed on 13 Feb 1993 with 1m telescope at Kavalur and the model fit to the data using NLS.*

mas angular resolution. The occultation light curve of TX Psc observed from Kavalur is shown in Fig. 3.10. The steep fall in the signal level (Fig. 3.10) just before the event is due to scintillation noise present in the data, as the event was observed at very large air mass. The scintillation effects in the data has been modeled with a 7^{th} order Legendre Polynomial using the procedure outlined in chapter 2. The uniform stellar disk model fit to the observed light curve using NLS method is also shown in the same figure. The source has been resolved from our observations and the angular diameter has been estimated to be 9.3±0.5 mas. Both the light curves clearly show the capability of the lunar occultation technique, atleast in the near infrared, to provide astrophysically valuable results even under bad observing conditions unlike other HAR techniques which need excellent sky conditions for an extended period of time.

The angular sizes derived from these independent light curves provides different values and the difference is well above the measurement errors. As both the events were observed at different epochs separated by about one year, it may appear that the variable angular size could possibly explain the observed difference in the angular size.

Temporal variability in cool giants has been suggested by Ridgway et al. (1982) to explain the difference in the derived angular diameters from independent occultation events. In the case of Y Tau (which is a carbon star), Schmidtke et al., (1986) reported temporal variability in the stellar angular diameter and was strengthened recently by Richichi et al. (1995b).

Earlier, Peery et al. (1976, 1977) had reported a variability in the radius of TX Psc of $\sim 15\%$ from radial-velocity measurements at a shorter period of ~ 31.5 days. However, there is no HAR observations available presently to confirm or deny variability at such a fast time scale.

Recently, Quirrenbach et al. (1994a) have proposed the possibility of variable angular diameter of TX Psc from the correlation existing between the derived angular diameters and the V magnitude. Mark III interferometer was used for their angular diameter measurements during 1989 – 1992 at 712, 754 and 800nm. However, we don't believe that this alone can explain the observed discrepancy in the angular size of TX Psc, as the difference in the angular size is as large as $\sim 40\%$, while, the variability in the brightness is only ~ 0.16 magnitude and hence the need for the stellar effective temperature to drop by ~ 400 K. We propose that the relatively small brightness variations, which are known to be irregular, are produced by local obscuration by dense clumps of circumstellar matter or by the presence of cold/hot spots on the stellar photosphere, without necessarily a change in diameter. Alternatively, the scattered light from an asymmetric circumstellar dust shell itself can explain the observed discrepancy. The position angle of both our occultation observations are different (separated by $\sim 35^{o}$) and hence asymmetry in the stellar disk and/or asymmetry in the warm dust existing very close to the stellar photosphere could also explain the difference in the derived angular diameter. Following Richichi's suggestion of possible asymmetry in the brightness profile of TX Psc from Gurushikhar light curve (Richichi, 1994a), we carried out a detailed analysis of the light curve using MIA. Unlike in the case of TV Gem, MIA has been carried out here in a different way. For the source brightness profile, a flat guess profile was assumed. First, NLS fit was carried out to estimate the scaling parameters like source brightness, background light level, time of geometric occultation and shadow velocity component in the model. Then, Lucy's deconvolution algorithm is performed to modify the source brightness profile. The combined algorithm of NLS and Lucy's deconvolution was repeated till it converges. Three iterations of this combined algorithm were sufficient to make a good fit to the data.

The recovered brightness profile of TX Psc from our Gurushikhar light curve is shown in Fig. 3.11. The recovered profile shows possible asymmetry in the stellar brightness distribution. Unfortunately, MIA could not be carried out to Kavalur data due to severe scintillation present in the data.

TX Psc has been observed earlier on three occasions in the optical wavelengths. The derived angular diameter from these observations are ϕ_{UD} = 9$\pm$1 mas (Lasker et al., 1973), ϕ_{UD} = 8.9$\pm$1 mas (de Vegt, 1974) and ϕ_{LD} = 10.2$\pm$2.5 mas (Dunham et al., 1975). Both Lasker et al. (1973) and de Vegt (1974) have remarked that the model fit to the data is less optimum and irregularity at the lunar limb was suggested by these authors as the possible cause.

Earlier, Lasker et al. (1973) had suggested that the possible departure from simple uniform disk stellar model could also explain the poorer quality of their fit to the data. Later, Bogdanov (1979) had reported evidence of an envelope or extended atmosphere with a diameter of 14.4 mas by reanalysing the lunar occultation light curves of TX Psc by Lasker et al. (1973) and de Vegt (1974). However, the poorer quality of the optical light curves makes these detections questionable.

3.2.3 Circumstellar Envelope around TX Psc

TX Psc has a spectral type between $C_{5,2}$ and $C_{7,2}$ (Richichi et al., 1995b). The distance is estimated to be 230 pc by Bergeat et al. (1978). Alternative values reported are 280 pc by Olofsson et al. (1988) and a larger value of 370 pc by Loup et al. (1993).

Young et al. (1993a & b) reported to have resolved the circumstellar dust around

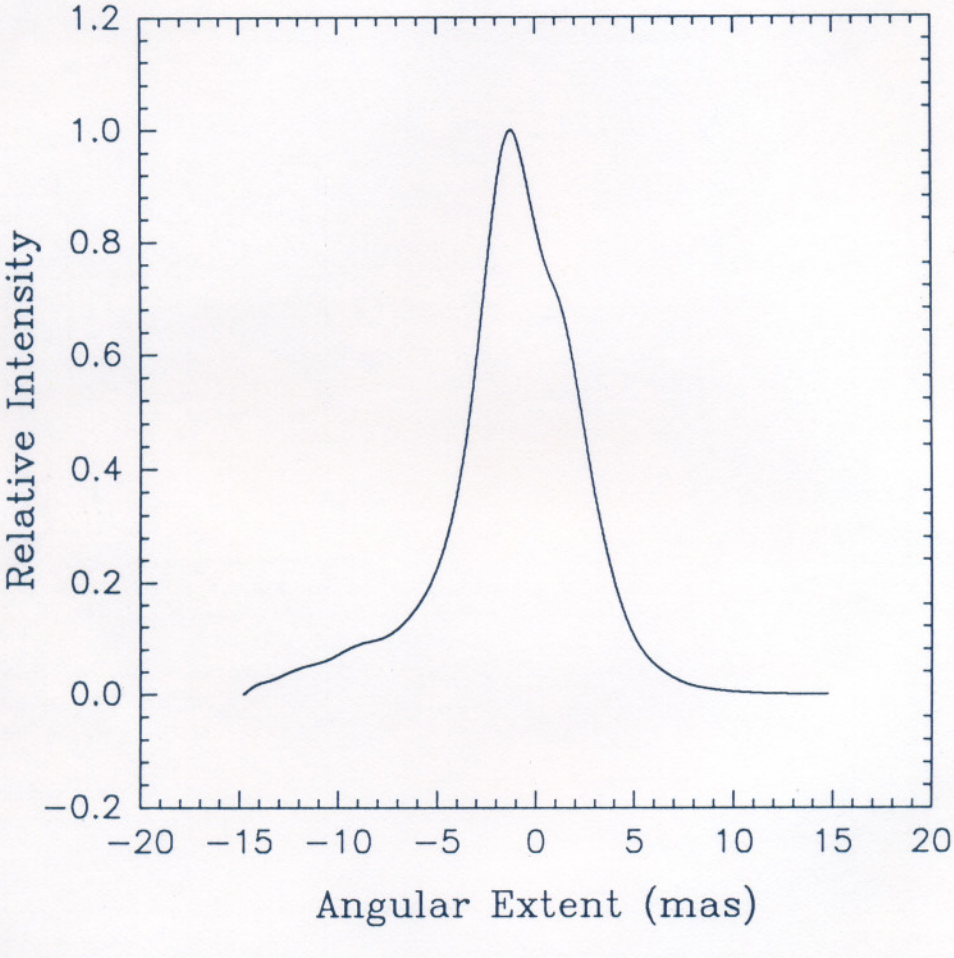

Figure 3.11: *The recovered brightness profile of TX Psc from the occultation light curve observed from Gurushikar using MIA.*

Table 3.6: Observational details of the observed events.

Sl. No.	*Observatory*	*UT Date*	*Filter band*	λ_o (μm)	$\Delta\lambda$ (μm)	*PA* (*deg*)	ϕ_{UD} (*mas*)
1	*Calern*	12 – 03 – 92	*V*	0.55	0.06	98	9.5±1.1
2	*Calern*	12 – 03 – 92	*R*	0.71	0.09	98	8.8±0.7
3	*Tirgo*	12 – 03 – 92	*K*	2.21	0.35	92	9.82±0.10
4	*Gurushikhar*	27 – 01 – 93	*K*	2.2	0.4	76	7.5±0.5
5	*WIRO*	27 – 10 – 93	*K*	2.18	0.38	5	7.72±0.06
6	*CalarAlto*	20 – 12 – 93	*L*	3.56	0.86	50	9.7±0.2
7	*Kavalur*	13 – 02 – 94	*K*	2.2	0.4	40	9.3±0.5

TX Psc from IRAS 60 μm image and the outer and the inner radii of the dust shell are 3″ and 0.1″ respectively.

Looking at all the light curves observed during the period 1992 – 1994 from different observatories, at different wavelengths (in the range 0.55 μm to 3.6 μm) enabled us to reach a level of angular resolution ($\sim$ 0.6 mas) which was never achieved on TX Psc. The results from these studies have already been published by Richichi et al. (1995b).

Observational details of all the observed light curves during this campaign is listed in Table 3.6. The recovered brightness profile using MIA from six of the observed light curves has been shown in Fig. 3.12.

The departure from circular symmetry is apparent in all six profiles. In spite of the poor SNR, the optical profiles (V & R band profiles) indicate a central compact source surroundered by more extended, possibly asymmetric, structure. The brightness profile gets more and more complicated as we go towards longer wavelengths. Infrared profiles (K & L band profiles) show two side peaks in addition to the central compact source. The brightness of the side peaks is comparable to that of the central source in the K profile and it dominates in the L profile suggesting that the side peaks are at relatively lower temperature with respect to the central source.

The three K profiles observed at different position angles suggest an asymmetry in the circumstellar structure i.e. more extended along the E–W than the N–S direction.

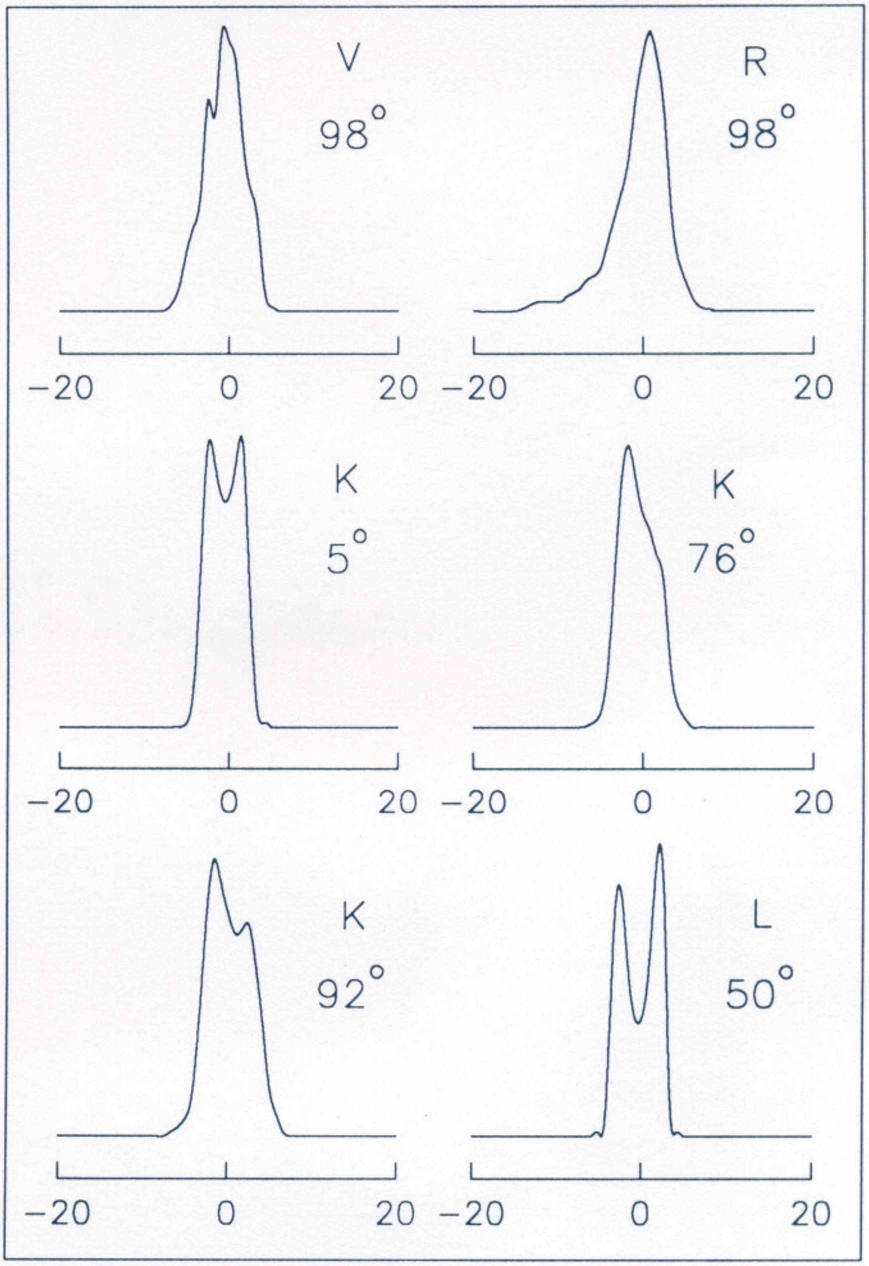

Figure 3.12: *The recovered brightness profiles of TX Psc (Richichi et al., 1995b) derived from occultation light curves obtained at different telescopes around the globe.*

The recovered profiles also suggest that the detected side peaks are located close to the stellar photosphere of the central star.

The observed profiles can be explained invoking the presence of circumstellar dust shell with an inner radius of $\lesssim 2\,R_{\star}$. In the visible wavelengths, the scattered star light by dust, while in the infrared, the thermal emission from the dust could explain the observed profiles. The dust temperature can be constrained to be < 1300K from the relative strength of the side peaks at K and L profiles with respect to the strength of the central star at these wavelengths and also considering the location of the dust from the stellar photosphere. As the central star is seen in the optical, the dust detected has to be optically thin and/or occur in clumps.

Alternatively, the observed features can be explained assuming large spots on the stellar surface. The spots could either be a lower temperature region on the stellar surface or resulting from obscuration by interventing dust clumps very close to the star. Such spots could be dark in the optical, but emit significantly in the infrared. It is also possible that both these possibilities do co-exist as they are closely related.

Richichi et al. (1991) have reported the evidence of circumstellar dust shell around T Cnc from lunar occultations at 2.2 μm and have compared the Bergeat's model predictions with their derived stellar and circumstellar parameters. They have shown that the stellar diameter and effective temperature predicted by this model are comparatively close to their derived values. However, the predicted shell size and star-to-shell flux ratio at 2.2 μm are highly inconsistent with the observations.

Our observations on TX Psc gave another opportunity to test this model for the other class of hotter carbon stars. Contrary to T Cnc, the model had predicted no shell around TX Psc. However, the intensive campaign on TX Psc from different observatories, of which this work is a part, clearly detected asymmetric circumstellar structure close to the photosphere. Bergeat's models of circumstellar structures around carbon stars clearly require a revision in the light of these observations.

In the presence of the extended structure, the derived stellar angular diameter of TX Psc (Table 3.6) based on uniform disk model may not be the true estimation. Qualitatively we can state that the angular diameter of TX Psc is ~ 9 mas and the effective temperature is ~ 3050K. There are discrepancies related to the model predictions of the effective temperature of TX Psc. While, Bergeat et al. (1976c) assumes a value as a low 2560 K, Scargle & Strecker (1979) obtain a higher value of 3790 K. However, recent work by Jorgensen (1989) provide a value of 3100 K which is consistent with our results. The effective temperature derived from optical long-baseline interferometry of 2805K (Quirrenbach et al., 1994a) is probably an under estimate as simple uniform disk model was assumed in their model fit. TX Psc is a suitable candidate to observe continuously for longer period by long base-line interferometer along with accurate photometric observations. The occultation international campaign has also brought out the importance of observations in the L band for recovering at good SNR, signatures of outer (cooler) structures around the star.

In summary, circumstellar dust shell around the M super giant TV Gem and the carbon star TX Psc have been investigated from milliarc second resolution observations in the infrared by lunar occultations. In addition to these two cool giants, seven more M giants, three K giants and five G giants have also been studied by lunar occultaions in the infrared and are discussed in the next chapter.

Chapter 4

Milliarcsec Resolution studies of Late-type Giants

A sample of six M giants, three K giants and three G giants have been studied as a part of this thesis work by lunar occultations in the near infrared region at 2.2μm and are discussed in this chapter.

4.1 Observations and Data Analysis

Three of the light curves reported here namely NSV 1529, IRC+00198 and BQ Ori were observed with the 1m telescope at Kavalur and IRC+10194 was observed with 0.75m telescope at Kavalur, while, the rest were observed with the 1.2 m telescope at Gurushikhar. Table 4.1 lists the source identifications. All observations reported except the occultation of NSV 4308 were disappearance events at the dark limb of the moon. The instrument used was the LN2 cooled InSb based high speed infrared photometer described in chapter 2. First six events in Table 4.1 namely, θ Aqr, ι Ari, IRC+20190, θ Cnc, NSV 1529 and IRC+00198 were observed with Dewar 1 and the rest six events were observed with Dewar 2.

All occultation light curves were observed in the standard K filter (λ = 2.2μ m,$\Delta\lambda$ = 0.4μ m). A 26″ circular diaphragm was used for Gurushikhar observations, while, 21″ & 42″ diaphragms were used respectively with the 1m & 0.75m telescopes at Kavalur. The strong sky background light level was offset as and when required to avoid the

Table 4.1: *Cross identifications of Occulted Sources.*

Sl. No.	Source	TMSS	IRAS	SAO	HD	BS
1	θ Aqr	-10578	22142-0801	145991	211391	8499
2	ι Ari	+20034	01546+1734	92721	11909	563
3	IRC+20190	+20190	07513+2114	79782	64351	–
4	θ Cnc	+20200	08287+1815	97881	72094	3357
5	NSV 1529	+20073	04123+2357	76523	26816	–
6	IRC+00198	+00198	–	118558	94252	–
7	BQ Ori	+20129	05540+2250	77756	39983	–
8	IRC+10194	+10194	08459+1243	98143	75156	–
9	IRC+10024	+10024	01598+1314	92763	12479	601
10	ν Aqr	-10557	21068−1134	164182	201381	8093
11	NSV 4308	+10197	08531+1149	98235	76351	3550
12	IRC+00529	+00529	–	128156	220406	8897

Table 4.2: *Predicted Circumstances of Observed events.*

Event No.	Source Name	Date	UT	PA (deg)	CA (deg)	Phase[1]	Alt (deg)	Vel. (km/s)
1	θ Aqr	25 Nov 1990	14:02:54	348.6	-299	8.2	55.0	0.3323
2	ι Ari	23 Jan 1991	15:34:54	32.8	35.3	9.2	52.5	0.5791
3	IRC+20190	25 Feb 1991	16:50:48	57.1	57.8	11.0	78.5	0.3596
4	θ Cnc	25 Mar 1991	14:34:48	74.9	41.9	9.3	75.5	05927
5	NSV 1529	12 Feb 1992	17:59:28	100.8	-7.0	8.9	25.1	0.8558
6	IRC+00198	17 Mar 1992	17:30:41	93.2	36.5	13.2	77.5	0.5606
7	BQ Ori	3 Feb 1993	14:44:54	88.0	5.2	11.9	71.4	0.6090
8	IRC+10194	23 Mar 1993	15:49:48	125.4	-6.6	11.4	85.0	0.6248
9	IRC+10024	13 Dec 1993	14:33:57	32.3	-30.6	10.6	70.2	0.5179
10	ν Aqr	07 Dec 1994	12:07:15	68.7	7.1	4.5	51.7	0.6581
11	NSV 4308	21 Dec 1994	21:28:20	150.3	34.8	18.9	74.5	0.4953
12	IRC+00529	06 Jan 1995	13:55:56	42.0	-18.4	5.1	46.7	0.6608

[1] days since new moon

Table 4.3: *JHK Photometry of the sources observed from Kavalur.*

Source	J	H	K
IRC+20190	3.5 ± 0.1	2.7 ± 0.2	2.5 ± 0.1
NSV 1529	2.2 ± 0.1	1.3± 0.2	1.0 ± 0.1
IRC+00198	3.8 ± 0.1	3.0 ± 0.2	2.9 ± 0.1
IRC+10194	2.9 ± 0.1	2.2 ± 0.2	1.9 ± 0.1
IRC+10024	2.3 ± 0.1	1.5 ± 0.2	1.3 ± 0.1

Table 4.4: *JHK Photometry of the sources observed from Gurushikhar.*

Source	J	H	K
θAqr	2.60± 0.05	2.07± 0.1	1.97 ± 0.05
ιAri	3.48± 0.05	3.00± 0.1	2.95 ± 0.05
θCnc	2.27± 0.05	1.55± 0.1	1.40 ± 0.05
BQ Ori	2.18 ± 0.05	0.70 ± 0.1	0.93 ± 0.05
νAqr	3.05± 0.05	2.43± 0.1	2.37 ± 0.05
NSV 4308	3.07± 0.05	2.39± 0.1	2.33 ± 0.05
IRC+00529	3.54± 0.05	2.62± 0.1	2.41 ± 0.05

system saturation.

Near infrared photometry of the occultation sources has been carried out with the 1m telescope at Kavalur and 1.2m telescope at Gurushikhar. The derived values are listed in Tables. 4.3 & 4.4 for Kavalur and Gurushikhar observations respectively. Gurushikhar being relatively a better site for near infrared observations (higher altitude and lower water vapour content), better photometric accuracy could be obtained for Gurushikhar photometry in comparsion to Kavalur observations.

Observed light curves are analysed with the NLS method detailed in chapter 2. We have computed χ^2, using the expression,

$$\chi^2 = \left[\sum_{i=0}^{n} \left(\frac{I(t_i) - I_m(t_i)}{\sigma_i} \right)^2 \right]^{\frac{1}{2}} \tag{4.1}$$

where $I\,(t_i)$ is the ith data point of the observed light curve, $I_m\,(t_i)$ is the corresponding model value and σ_i is the error in $I\,(t_i)$.

Lunar occultation being a one-shot experiment, modeling the noise (i.e. σ_i) as a function of time is a difficult task. Observed sources from our sample are of different brightness and are observed under different observing conditions and hence the noise characteristics of different observed light curves are very different.

The noise characteristics of different light curves are very different as the sources in our sample are of different brightness and are observed from different observing sites with variable telescope aperture size, field of view and detector systems, in addition to extreme observing conditions. Hence different procedure is followed for different light curves in modeling the noise during the event. There are few very good quality light curves where scintillation noise is not present. Light curves of sources like IRC+10024, IRC+00529 belong to this set. For this set of light curves, a small portion of the data (of ~ 30 ms) before and after the event is taken and the standard deviations for these sets, σ_1 and σ_2 are calculated. Now in computing χ^2 (eqn. 4.1), σ_1 is used for the portion of the light curve before the event and σ_2 is used for the portion of the light curve after the event.

Many light curves are dominated by scintillation noise. Some light curves in this class have scintillation noise in the portion of the light curve before the event but the event portion is fairly free from such noise. The light curves of sources like BQ Ori, IRC+00198, ν Aqr and IRC+10194 belong to this class. In such case, very large value (say 100 times σ_2) is assumed for this portion affected by scintillation noise and σ_2 is used for the rest data points while computing χ^2.

There is another class of light curves where the scintillation noise is present during the event. This class includes the light curves of the sources like TX Psc (Kavalur data), NSV 1529 and IRC+20190. In such cases, scintillation noise is accounted for using the procedure outlined in chapter 2. In computing χ^2, we used σ_2 for all data points.

It is known that often the quoted error in the angular diamter measurements reported in the literature is only formal error and is highly underestimate of the actual error in the measurement. Hence we followed different approach to estimate the measurement error. We denote the formal error derived from model fit as $\Delta\phi_1$. The finite error in the time response calibrations causes noticable error in the derived angular size and is denoted as $\Delta\phi_2$. Cases where scintillation correction is done, the uncertainty in the order of the Legendre polynomial used, also introduce uncertainity in the angular size measurement and is denoted by $\Delta\phi_3$. The resultant error in the derived angular size is,

$$\Delta\phi = \left[\sum_{i=1}^{3} (\Delta\phi_i)^2\right]^{\frac{1}{2}} \tag{4.2}$$

These values are given in Tables 4.5.

The SNR given in Tables 4.5 is defined as in chapter 1 and not in conventional sense and hence it may appear larger than what one would expect looking at the light curves. The SNR also may appear to be uncorrelated with the measurement errors. The reason is that two different detector systems were used to record these light curves. For example, the light curve of θ Cnc has the largest SNR ($\sim$ 250) from our sample. However, the light curves of NSV 4308 and IRC+00529 recorder with relatively low SNR of $\sim$ 100 also have comparable measurement error. This is because, θ Cnc was observed with a detector system which has relatively larger time constant and hence the light curve has a better SNR at the expense of low sensitivity of the light curve to the angular size. In the case of NSV 1529, the large quoted measurement error in spite of good SNR is due to the presence of scintillation noise in the data.

χ^2 as a function of angular size is computed for all sources. Resolved sources show a well defined single minima, while, unresolved sources show a constant χ^2 upto $\sim$ 2 mas and beyond this an asymptotic increase in χ^2 with increasing angular diameter.These curves are shown as an inset in the figure showing the observed light curve with the model fit. Regarding NSV 4308 and IRC+00529, although their χ^2 curves show a dip, they can be considered to be only mariginally resolved from our observations because they are close to the limit of the resolving capability of the instrument. Certainly more observations are required for these giants to confirm our derived stellar parameters.

We estimate the distance to the observed giants using an iterative process assuming a spectral class and hence the absolute magnitude (Schmidt-Kaler, 1982) for the source. Initially the interstellar extinction, A_v is assumed as zero and the distance is estimated from the absolute and apparent visual magnitudes. Then, A_v is obtained for the corresponding distance from the work of Lucke (1978) and is used to update the distance.

This procedure is repeated till it converges. We have derived stellar bolometric flux from the available photometric data in the literature in addition to our JHK values using numerical integration.

4.2 Effect of 50 Hz modulation

Some of our initial lunar occultation light curves were affected by 50 Hz modulation of the mains power supply. At that time electrical isolation of the dewar had not been done. The power spectrum of the light curve shows clearly the fundamental frequency along with some of its harmonics. These modulations interfere with the diffraction pattern, as the diffraction pattern too contain power at these modulation frequencies. Hence, these modulations had to be filtered before performing any detailed light curve analysis. These modulations are filtered using a least squares analysis which is similar to the one Peterson & White (1984) and Richichi et al. (1992a) used in similar circumstances.

Essentially, the modulation characteristics are obtained from the portion of the light curve before/after the event and this information is used to filter the modulations in the event portion of the light curve. Generally, sinusoidal components at 50, 100, 150, 200, 250 & 300 Hz are present in the affected data. The amplitudes and phases of these 6 components along with two more scaling parameters (totally 14 parameters) are estimated using least squares method. The equation used has the form,

$$I\left(t\right)=\sum_{i=1}^{6}a_{i}sin\left[\left(i\omega\Delta t\right)t+\phi_{i}\right]+\beta \tag{4.3}$$

where, ω is the fundamental harmonic of the modulations which is very close to 50 Hz. Δt is the sampling interval, which is one millisecond in our case; a_i and ϕ_i are the amplitudes and phases of the modulations. The exact value of the fundamental frequency do differ from data to data by about one percent, probably because of locally generated power being used for these observations. Hence the fundamental frequency was treated as a free parameter in the model fit. A portion of the light curve after the event of $\sim$ 300 ms in length is fitted to estimate the amplitudes and phases. These values are used to extrapolate the modulation characteristics for the event portion of the light curve and is subtracted from the original data. Fig. 4.1 shows the observed light curve suffering from 50 Hz modulations along with the light curve after removing

Table 4.5: *Results from lunar occultation light curves of resolved giants observed at 2.2μm.*

Source	ϕ_{UD} mas	T_{eff} K	SNR	V	K	Sp. type
θ Cnc	3.3±0.3	3665±180	247	5.34	1.42	K5 III
NSV 1529	3.3±0.4	3380±160	120	8.3	0.90	M2–M7 III
BQ Ori	4.2±0.2	3460±100	85	6.9	0.92	M5 III
IRC+10194	4.2±0.5	2760±170	30	6.61	1.845	M3.3 III
IRC+10024	3.2±0.2	3650±100	110	5.87	1.2	M2 III
NSV 4308	2.6±0.3	3975±260	91	5.41	2.24	K5 III
IRC+00529	2.4±0.3	3747±260	103	6.31	2.48	K2

these modulations using least squares method. The power spectrum obtained for the processed light curve confirms the performance of the filtering procedure.

4.3 Occultation Results

4.3.1 Resolved Sources

Seven of the observed sources are resolved from our occultation observations in addition to TV Gem and TX Psc discussed in the previous chapter. Results from our lunar occultation light curves for these seven giants are listed in Table 4.5 along with some source details.

θ Cnc (IRC+20200)

Occultation light curve of θ Cnc was observed under very good sky conditions. The observed light curve was affected by 50 Hz modulation of the mains power supply. The light curve after filtering these modulations is shown in Fig. 4.2 along with the model fit. The SNR ($\sim$ 250) in the recorded light curve is good enough to detect even a small amplitude ($\sim$ 2% of signal strength) sky gradient apparent while fitting the data. Sky gradient is corrected for in the model fitting. The best model fit provides a value

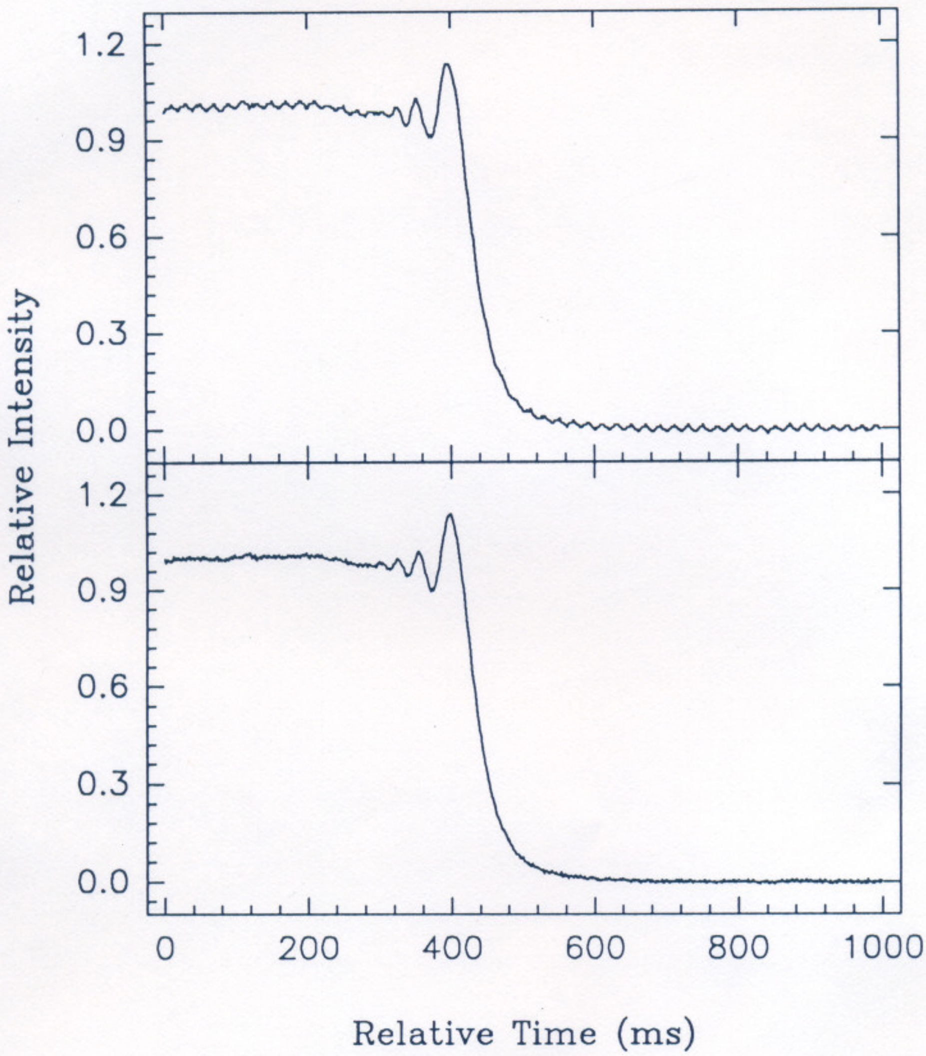

Figure 4.1: *Occultation light curve of θ Cnc affected by 50Hz modulations is shown in the upper panel and the processed light curve which is free from these modulations is shown in the lower panel. Note the recovery of the 4^{th} fringe.*

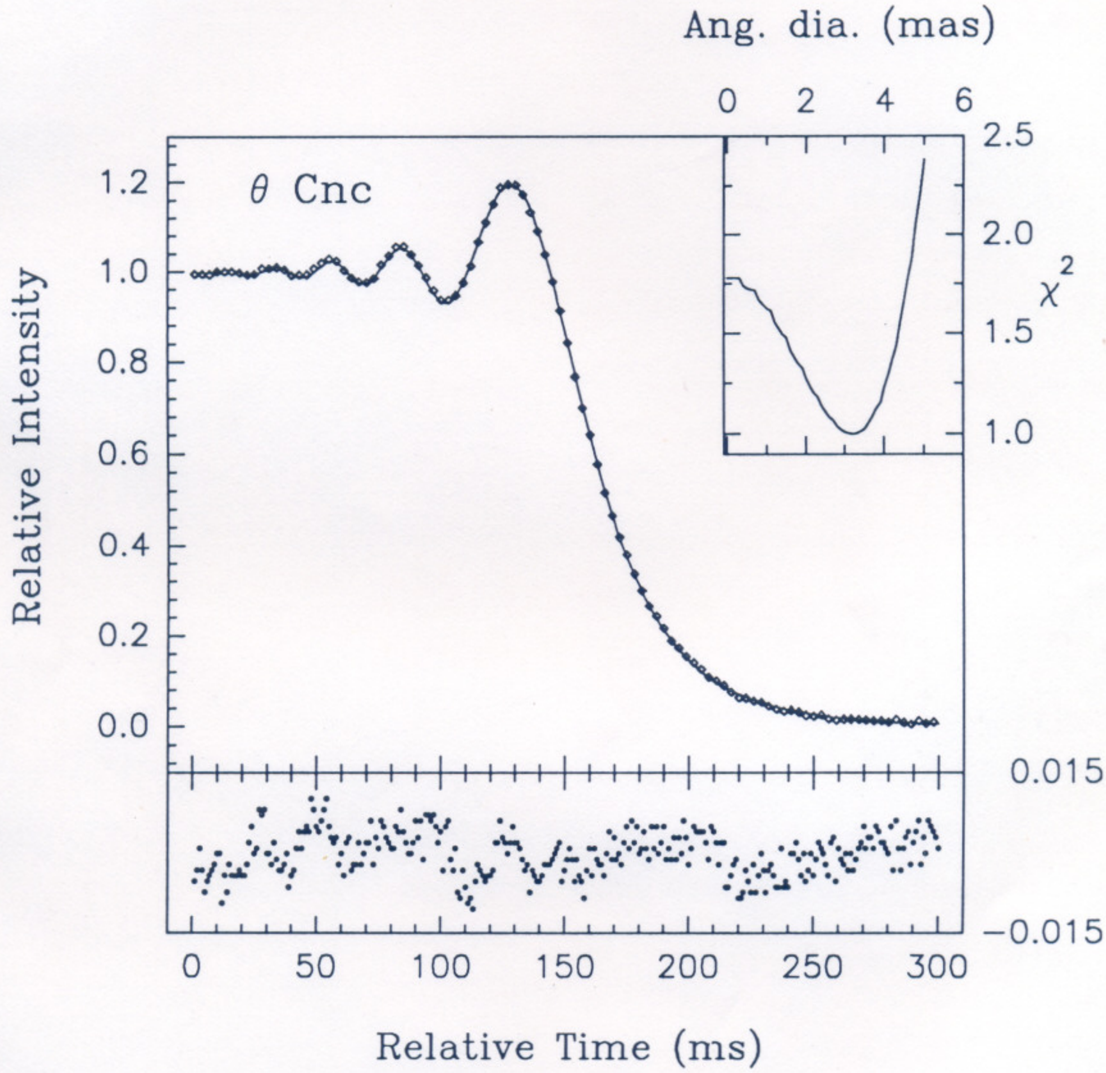

Figure 4.2: *Occultation light curve of θ Cnc (squares) observed on 25^{th} Mar 1991 using 1.2m telescope at Gurushikhar and the model fit (solid line) to the data.*

for the angular diameter of 3.3 $\pm$ 0.3 mas. The effective temperature is derived to be 3665$\pm$180K.

This bright giant is classified as K5 III (Hoffleit & Jaschek, 1982). The alternative classification of M0 III can be found in IRAS catalog. This object was searched for Li I line at 6709$\mathring{A}$ and the line is probably detected, but not strong enough for any abundance measurements (Merchant, 1967). We estimate the distance to the source to be 128 pc assuming a K5 III spectral classification. However, the distance estimation based on photometric values at 1.02μm (Eggen, 1967) would give a value of 158 pc.

θ Cnc is a visual double star system of angular separation, $\Delta\phi \sim 1'$ and visual magnitude difference, Δm = 4.4 (Hirshfeld & Sinnott, 1982b). Earlier visual occultation observation had suggested that the primary component may be an occultation binary of angular separation $\sim$ 0.3 $''$ (Hoffleit & Jaschek, 1982; Hartkopf & McAlister, 1984). However the photographic speckle observation carried out with 30 mas limiting angular resolution have not detected any multiplicity (Hartkopf & McAlister, 1984). Also the photoelectric optical occultations (Eitter & Beavers, 1974) and near infrared occultations (Ridgway et al., 1982) have not detected any multiplicity in this primary component.

The angular size of the primary component has been derived earlier by Ridgway et al. (1982) from multiwavelength lunar occultation observations. The derived values at 0.94 μm, 1.6μm & 2.2μm are respectively 3.21$\pm$0.34, 3.35$\pm$0.36 & 3.13$\pm$0.15 mas. Our own observation, 3.3$\pm$0.3 mas, agrees well with Ridgway's results. There is no signature of any occultation binarity of the primary upto $\Delta m_k \sim 3$.

NSV 1529 (IRC+20073)

The occultation light curve of NSV 1529 is shown in Fig. 4.3. The initial fall seen in the light curve is due to low frequency scintillation noise present in the data. This event is the fastest event in our sample (V_{comp} = 0.86 km/s). The uniform disk stellar model fit shown in the figure takes into account this scintillation effect on the light curve. The amplitude of scintillation noise in the data is relatively large and can partly be attributed to the larger air mass ($\sim$ 2.4) and partly to the poor sky condition during the event.

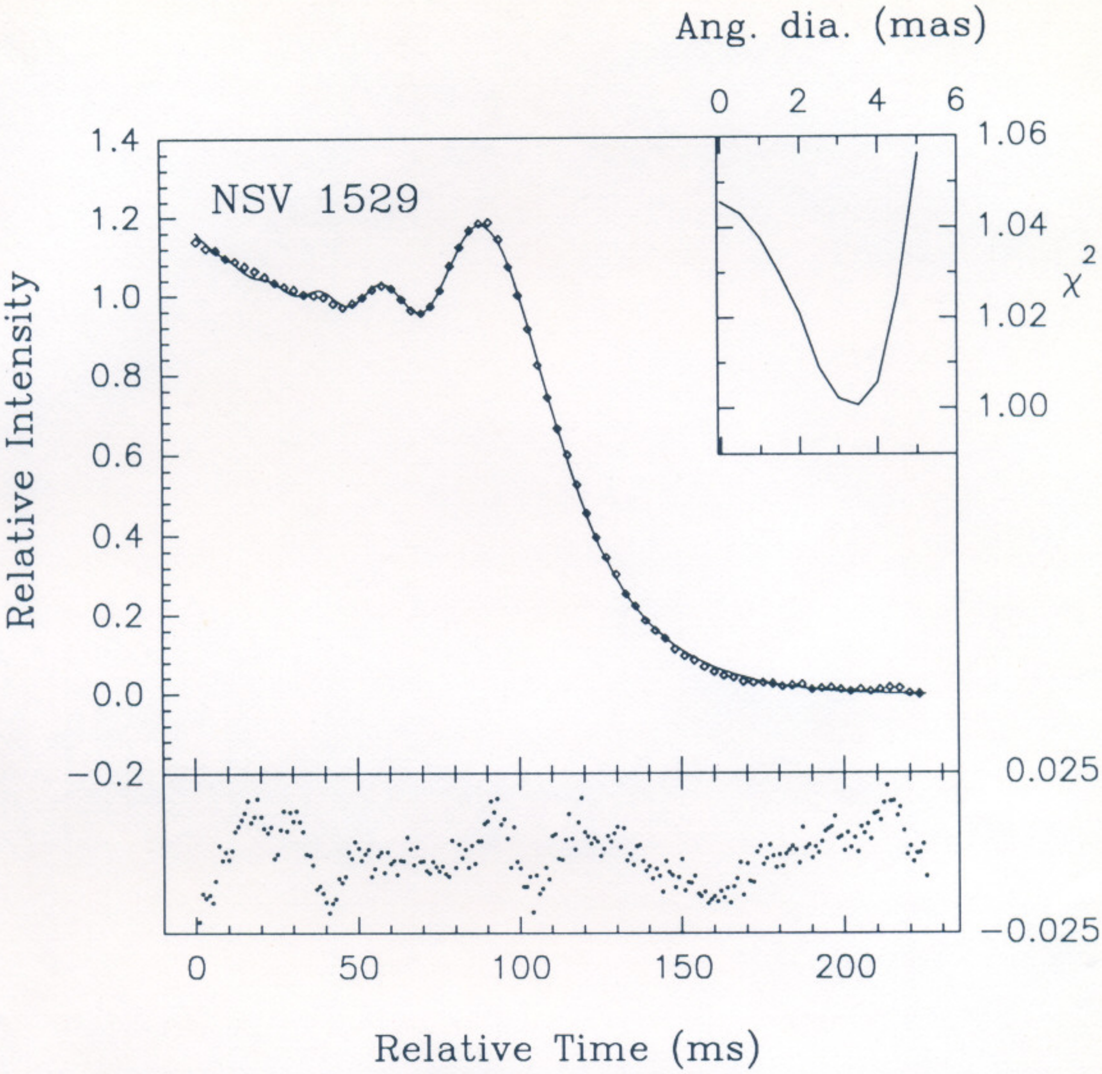

Figure 4.3: *Occultation light curve of NSV 1529 (squares) observed on 12 Feb 1991 with 1m telescope at Kavalur and the model fit (solid line) to the data.*

The value of stellar angular diameter derived from our light curve is 3.3±0.4 mas. Also shown in Fig. 4.3 (lower panel) is the residual of the model fit to the data (data – model) and plot showing the sensitivity of the model to the stellar angular size as a inset (top right). Adopting a value of 5×10^{-7} erg/cm^2/s for the stellar bolometric flux (Richichi et al., 1988), we estimate the stellar effective temperature to be 3380±160K.

Kukarkin et al. (1969) classified this source as M2 giant of variability class Lb with visual magnitude at maximum of 8.5 and the amplitude of photographic visual magnitude variations of 0.7 mag. However the source is classified by Bidelman (1980) as M7 giant.

This source was earlier resolved by Richichi et al. (1988) from lunar occultations at 2.2 μm and they obtain a value of 3.00 $\pm$ 0.11 mas for the angular diameter and 3500 K $\pm$ 150 K for the stellar effective temperature.

Richichi et al. (1988) suggest from their lunar occultation observations that the spectral class of this source is in the range M4-M6. Adopting M5 spectral class, we estimate the distance to the source to be 0.4 kpc. Richichi et al. (1988) have shown that in colour-colour diagram [(12-25) μm - (25-60) μm] this source falls in a region where only carbon stars are present suggesting that it is a peculiar source. From the Low resolution IRAS spectra, the source was classified by Volk & Kwok (1991) as 'stellar blackbody' class suggesting that there is no significant circumstellar envelope around this giant.

BQ Ori (IRC+20129)

The observed occultation light curve of BQ Ori is shown in Fig. 4.4 along with the model fit. As can be seen in the residual plot, the noise is more before the event, when source is in the beam, implying that the high frequency scintillation noise is the dominant source of noise in this light curve. However, unlike in the case of NSV 1529, the noise frequency is comparable to frequency of the fringes and hence the correction procedure used for NSV 1529 could not be applied here. The SNR in the observed light curve is $\sim$ 85. The best fit model provides a value for the stellar angular diameter of 4.2$\pm$0.2 mas.

This semi-regular variable star is classified by Sharpless (1956) as M5 III and alternative classification of M5e III can be found in Houk (1963). BQ Ori is a SRa type variable of period 110 days (Houk, 1963) and the amplitude of visual magnitude variations, $\sim$ 2 (Sharpless, 1956). We have derived the distance to be 370 pc.

Evans & Edwards (1983) observed an occultation of this source in the optical wavelength. The source was not resolved from their observations and binary detection limits have been reported by the authors. Schmidtke et al (1986) resolved this source from occultation observations carried out at three wavelengths namely 0.96μm, 1.6μm and 2.2μm. The derived values for the stellar angular size are respectively 6.14$\pm$1.37 mas, 4.16$\pm$0.41 mas and 4.04$\pm$0.48 mas. The light curve at 0.96μm is relatively noisier than the infrared light curves, which is apparent in the large error quoted for the angular

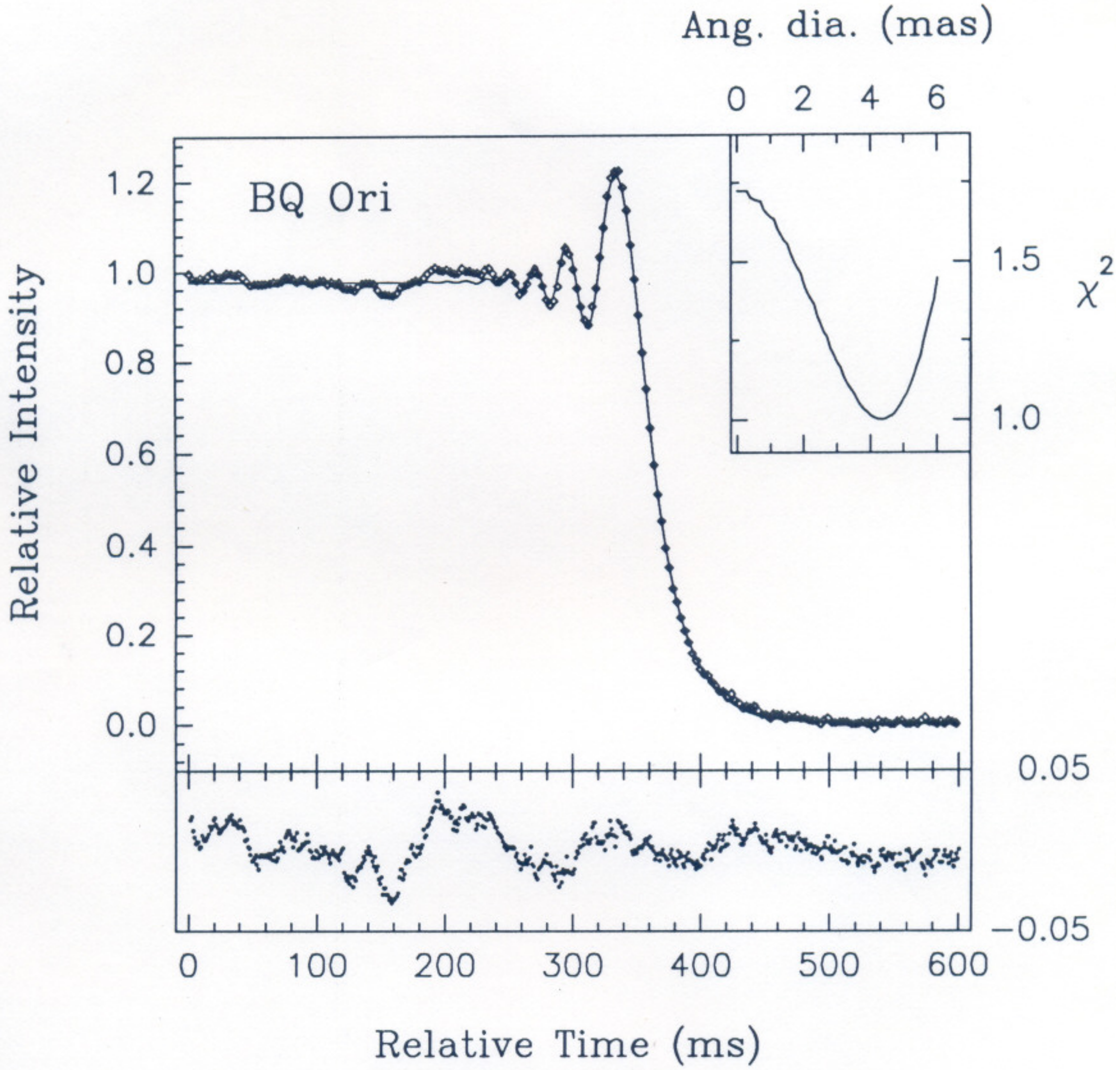

Figure 4.4: *Occultation light curve of BQ Ori (squares) observed on 3 Feb 1993 with 1m telescope at Kavalur and the model fit (solid line) to the data.*

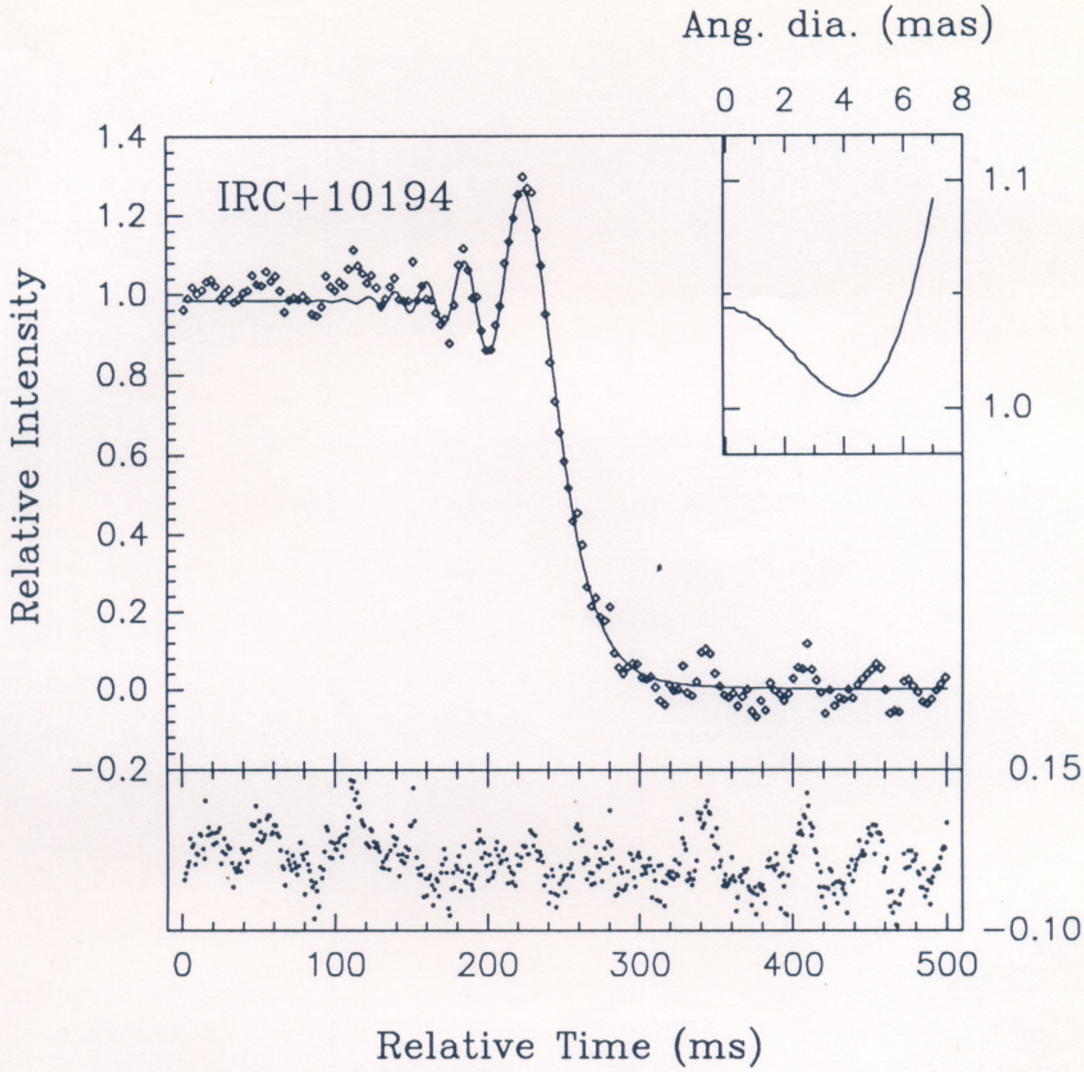

Figure 4.5: *Occultation light curve of IRC+10194 (squares) observed on 23 Mar 1994 with 0.75m telescope at Kavalur and uniform stellar disk model fit (solid line).*

diameter measurement. Our derived angular diameter at 2.2μm is more accurate than the earlier reported values. The derived stellar effective temperature is 3460$\pm$100 K.

IRC+10194

The observed occultation light curve of IRC+10194 fitted with a uniform disk model is shown in Fig. 4.5. This source was observed with a small telescope (0.75m telescope at Kavalur) and hence has a relatively lower SNR ($\sim$ 30). Nevertheless, two fringes are well recorded. The light curve is dominated by the background noise apparent from the residual plot which shows similar noise level before and after the event. The light curve reported here appears to be the first high angular resolution observation of this source at 2.2μm. The best fit model provides a value for the angular diameter of 4.2$\pm$ 0.5 mas. Stellar effective temperature has been derived from our occultation observations, adopting a value for the bolometric flux of 35.6 $\times 10^{-8}$ erg/cm^2/s (Ridgway et al., 1980). The value is 2760$\pm$170 K.

This old disk population red giant is classified as M3.3 III by Ridgway et al (1980) and M3 II - III by Keenan & McNeil (1989). We estimate the distance to be 280 pc.

The source has been observed in two occasions in the optical wavelength by Africano et al. (1977,1978). The source was not resolved from their observation and binary detection limits have been reported. Later the source has been resolved by Ridgway et al (1977, 1979) on two occasions at 1.65μm and by White (1978) once at 0.75μm. The reported values are 3.84$\pm$0.55 and 4.49$\pm$0.59 at 1.6μm and 4.00$\pm$0.49 at 0.75μm. All these early light curves are more noisier than our light curve observed at 2.2 μm. Ridgway et al (1980) have estimated the effective temperature of this source from these occultation observations as 2810 $\pm$ 110 K. However, Tsuji (1981a) estimate the stellar effective temperature to be 3570K from infrared flux method (IRFM) which is inconsistent with the direct HAR observations. Our observations are consistent with the earlier occultation results and confirm the discrepancy. We suggest that the apparent discrepancy could be due to the presence of warm circumstellar dust close to the stellar photosphere. Alternatively, the presence of a close secondary of similar spectral class could also explain the observed discrepancy. Unfortunately, the SNR in our light curve is not good enough to support or deny these possibilities. IRC+10194 is an ideal source for further HAR observations both at K and longer wavelengths.

IRC+10024

A good quality (SNR $\sim$ 110) occultation light curve of IRC+10024 fitted with a uniform disk model is shown in Fig. 4.6. The derived value for the stellar angular diameter is 3.2$\pm$0.2 mas. Adopting a bolometric value of 64.3 $\times$ 10 $^{-8}$ erg/cm^2/s (Richichi et al., 1992b), we derive the stellar effective temperature to be 3650 $\pm$ 100 K.

This M giant is classified as M2 III (Hoffleit & Jaschek, 1982). Alternative classifications reported are M3 III (Eggen, 1992) and M3.3 III (Kenyon & Fernandez-Castro,

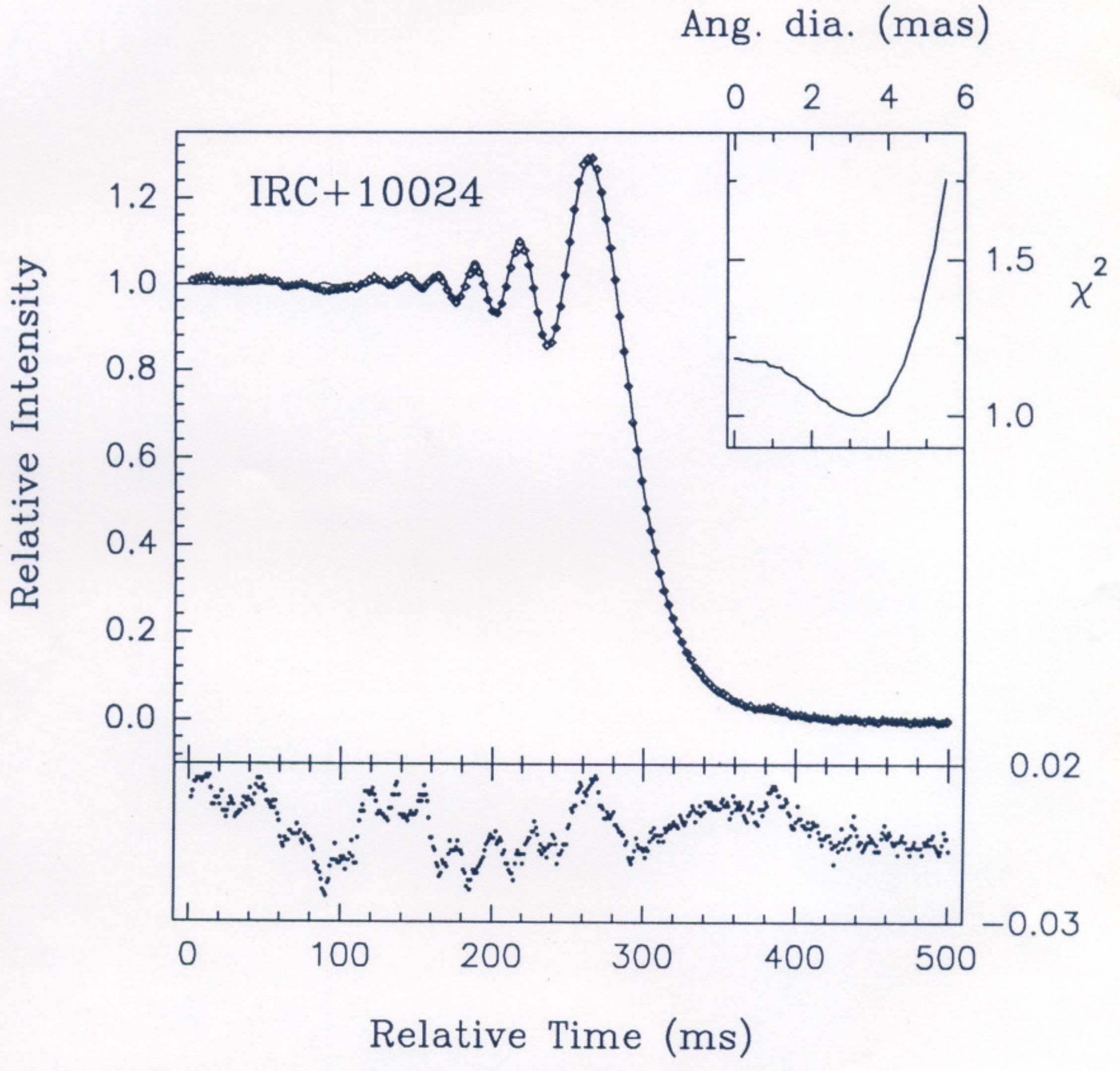

Figure 4.6: *Occultation light curve of IRC+10024 (squares) observed on 13 Dec 1994 with 1.2m telescope at Gurushikhar and uniform stellar disk model fit to the data (solid line).*

1987). Lunar occultations of this source was observed earlier on two occasions in the optical and once in the near infrared. Africano et al. (1976) resolved the source in the optical region and the derived fully darkened stellar disk diameter is 2.6±0.5mas. Two-color optical occultation observations by Beavers et al. (1982) on two occasions (totally 4 light curves) provide a value for the fully darkened stellar disk diameter of 3.9±0.6 mas. Uniform disk diameter can be estimated from these observations and the value is 2.82±0.33 (Richichi et al., 1992b). Richichi et al. (1992b) resolved this source at 2.2μm and the derived value for the uniform disk stellar diameter is 3.3±0.17 mas. The resultant stellar effective temperature is 3730 ± 100 K. Our derived value for the stellar parameters are consistent with this earlier observation at 2.2μm. Tsuji (1981a) estimate the stellar effecive temperature using IRFM to be 3630 K assuming M3.3 spectral classification.

NSV 4308 (IRC+10197)

A good quality (SNR $\sim$ 90) reappearance light curve of NSV 4308 fitted with uniform stellar disk model is shown in Fig. 4.7. Our observations constitute the first HAR observation of this source at the infrared wavelengths. The derived stellar angular diameter is 2.5 ± 0.3mas. The effective temperature is derived to be 3975±260K.

IRC 10197 is classified as K5 III. We estimate the distance to be 84pc. This source has been observed earlier in the optical region. The source was not resolved from earlier three optical occultation observations (Africano et al., 1976; Africano et al., 1978). Later, White (1978) resolved the source in the optical wavelength and derived a uniform stellar disk angular diameter of 3.3± 0.4 mas. Their derived value for the stellar angular diameter is slightly higher than our value but consistent within errors.

IRC+00529

An occultation event of IRC+00529 has been observed under good sky condition. The SNR is very good ($\sim$ 100). There is no earlier HAR observation available for this source. The observed light curve fitted with a uniform stellar disk model is shown in Fig. 4.8. The derived value for the stellar diameter is 2.4±0.3mas. The effective temperature is derived to be 3747±260pc.

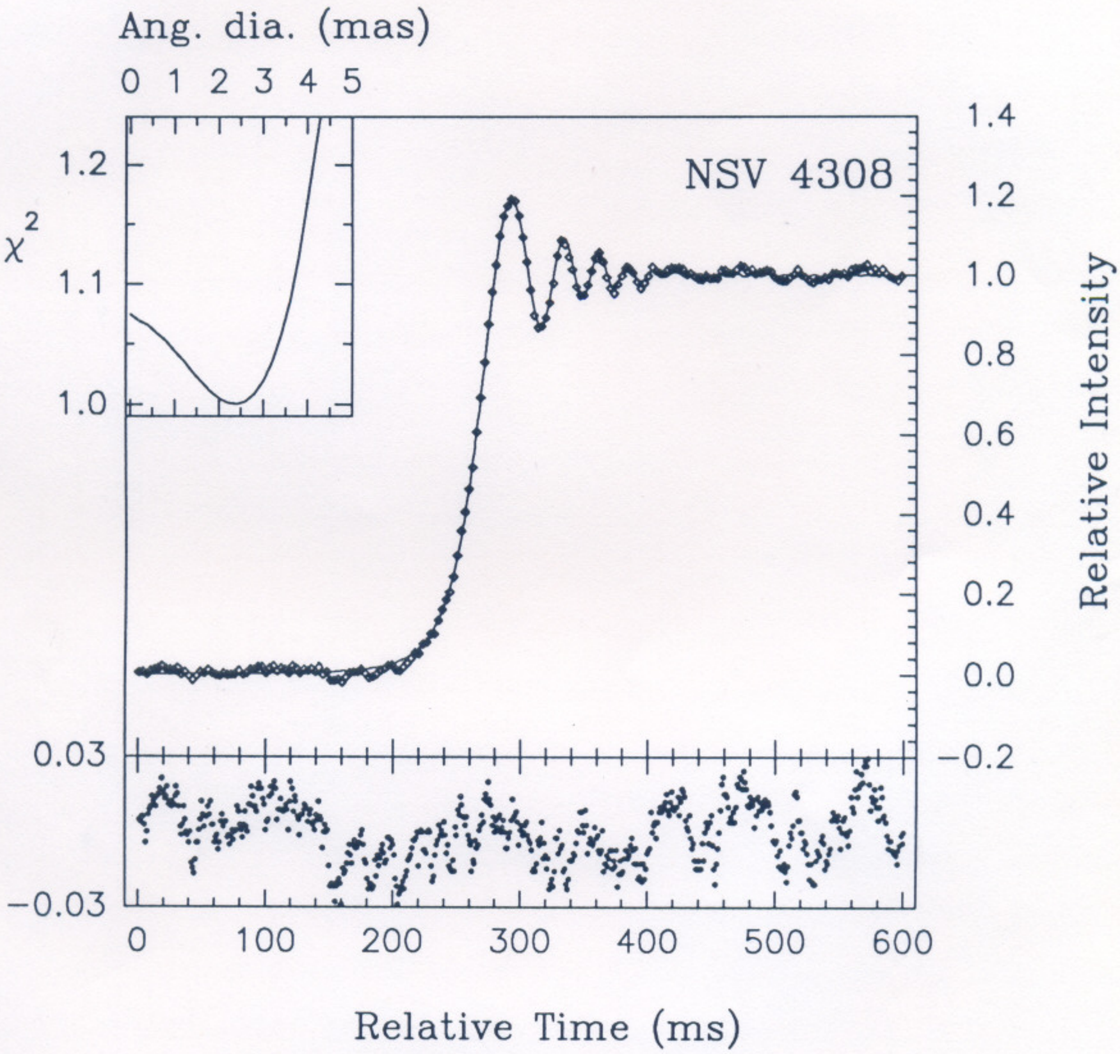

Figure 4.7: *Occultation light curve of NSV 4308 (squares) observed on 21*st *Dec 1994 with 1.2m telescope at Gurushikhar and the model fit (solid line).*

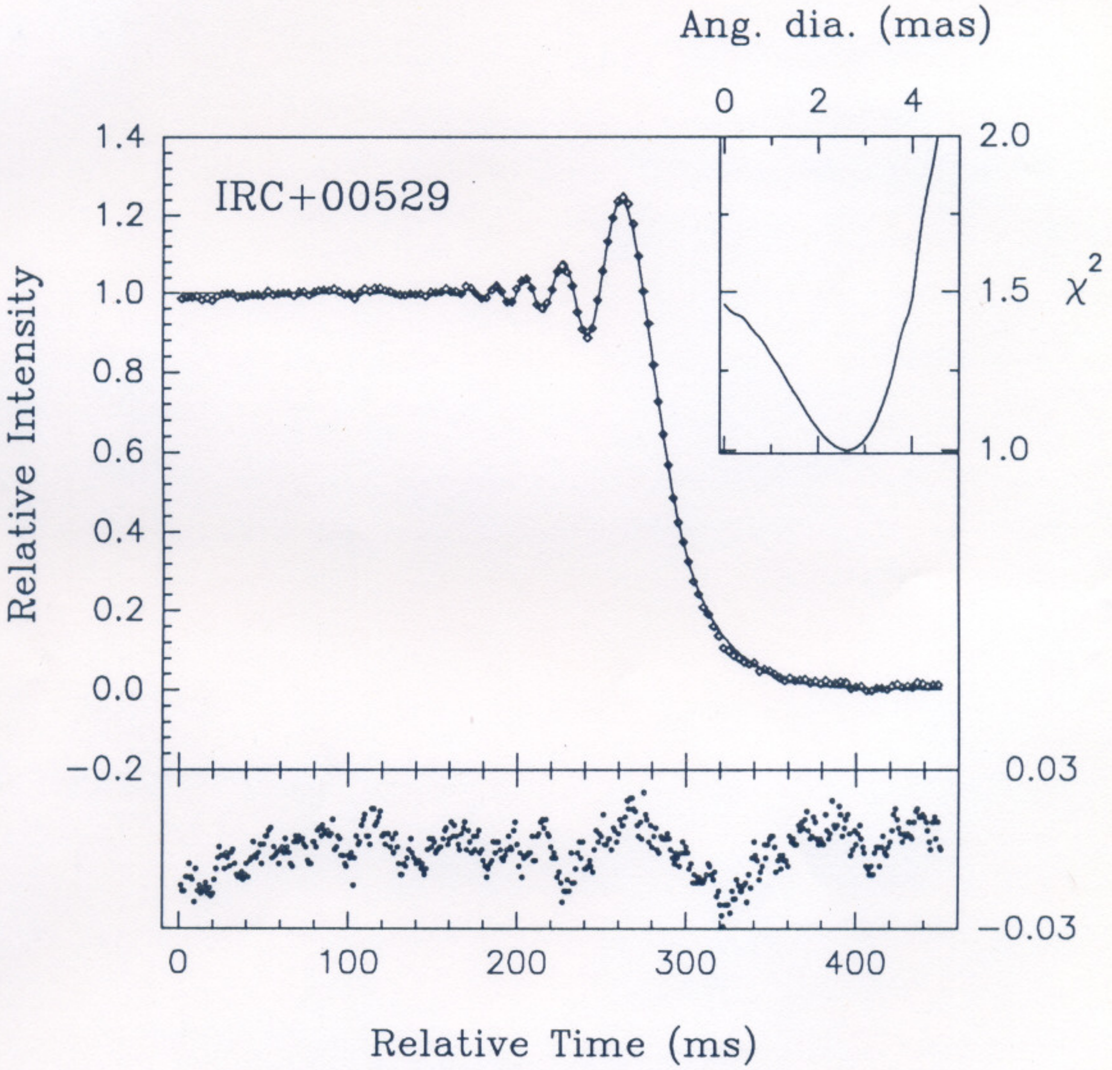

Figure 4.8: *Occultation light curve of IRC+00529 (squares) observed on 6^{th} Jan 1995 with 1.2m telescope at Gurushikhar and the model fit (solid line).*

Table 4.6: *Details of lunar occultation light curves of sources unresolved from our observations carried out at 2.2μm.*

Source	ϕ	SNR	V	K	Sp. Type
θ Aqr	$\leq$2	22	4.16	2.11	G9 III
ι Ari	$\leq$2	78	5.10	2.93	G8 III
IRC+20190	$\leq$2	75	6.84	2.53	M2 III
IRC+00198	$\leq$2	73	7.2	2.85	M2 III
ν Aqr	$\leq$2	75	4.51	2.42	G8 III

The spectral class of IRC+00529 is K2 (Griffin, 1972) and the luminosity class is not known. Assuming luminosity class III, we estimate the distance to be 145 pc. This source is a visual double with angular separation between the components of $\sim 42''$ and visual magnitude difference of 4 (Hirshfeld & Sinnott, 1982b).

4.3.2 Unresolved Sources

Five of the observed sources are unresolved from our occultation observations and are listed in Table 4.6 along with source details.

θ Aqr (IRC-10578)

The occultation of this young disk population giant θ Aqr marked the beginning of near infrared occultation observations from Gurushikar, Mt. Abu, India. The observed light curve of this source is shown in Fig. 4.9. This source doesn't have any earlier HAR observations and is not resolved from our observations. We have estimated an upper limit of $\phi \leq 2$ mas for the angular diameter of the source.

Keenan & McNeil (1989) classified this source as G9 III. Alternative classification by Roman (1952) is G8 III - IV. Absolute visual magnitude is derived from Ca II H & K line width to be 1.3 $\pm$ 0.3 (Wilson, 1976). We estimate the distance to be 37 pc. θ Aqr is the nearest giant in our sample. This object was searched for lithium with negative results. (Brown et al., 1989).

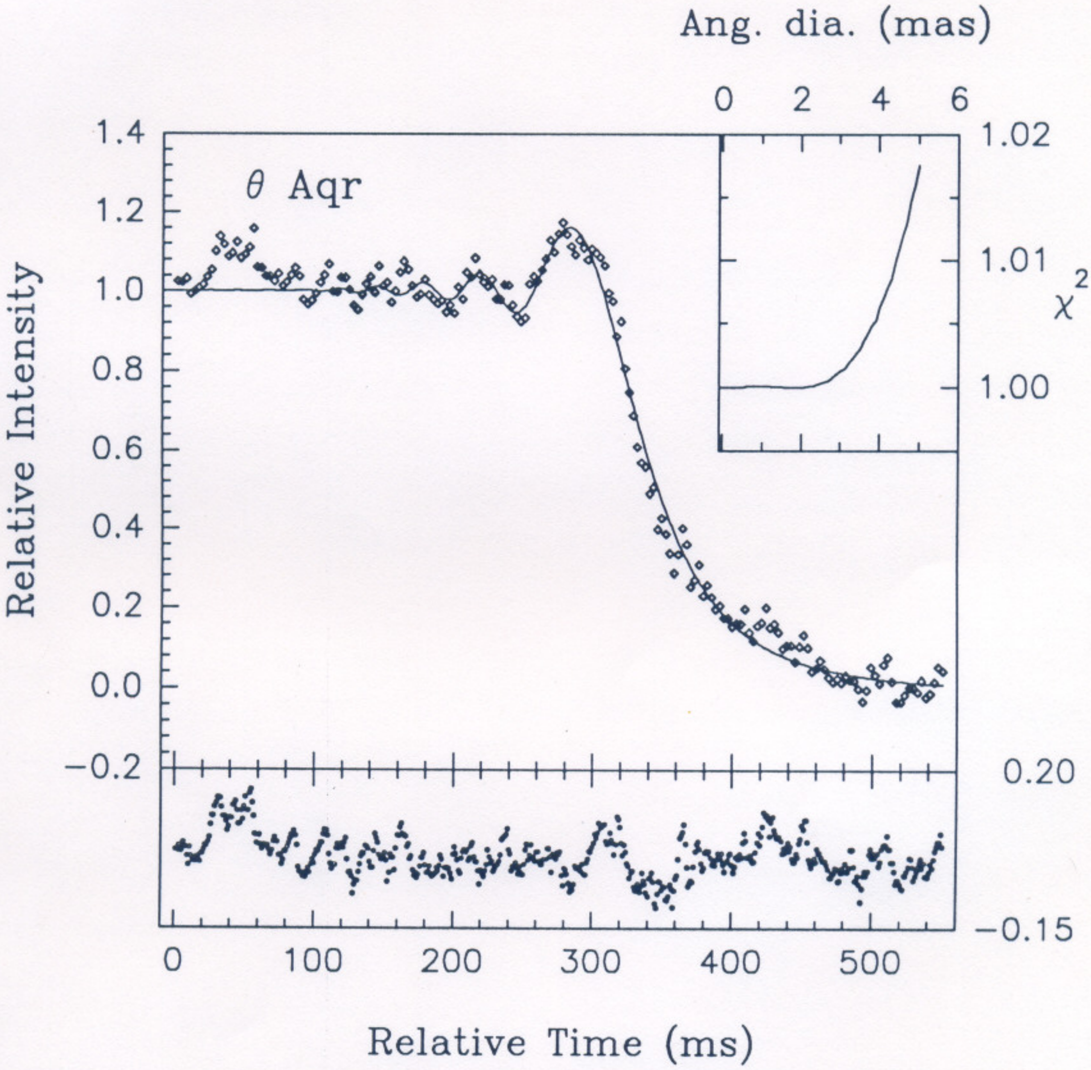

Figure 4.9: *Occultation light curve of θ Aqr (squares) observed on 25th Nov 1990 with 1.2m telescope at Gurushikhar and the model fit (solid line).*

IRFM provides the angular diameter of the source, $\phi = 1.84 \pm 0.03$ mas and the stellar effective temperature, $T_{eff} = 4979 \pm 50$ K (Blackwell et al.,1990). Effective temperature derived from DDO photometric calibrations is 4970 K (Claria et al., 1994).

Barnes relations based on $(B\text{-}V)_o$,$(V\text{-}R)_o$ and $(R\text{-}I)_o$ colour indices discussed later in this chapter provide an angular diameter of 2.28 mas.

ι Ari (IRC+20034)

The observed occultation light curve of ι Ari is affected by 50 Hz modulation of mains power suppy. The data is processed to filter these modulations and is shown in Fig. 4.10 along with the best model fit to the data. The source is not resolved from our observations. Detailed analysis of the light curve provides an upper limit for the angular diameter of ≤ 2 mas.

Visual occultation observations had suggested that this stellar system could be a occultation binary with an angular separation (along the direction of occultation) of ~ 10 mas. However, speckle observation carried out in the optical region with ~ 30 mas angular resolution does not detect any multiplicity in this system (Hartkopf & McAlister, 1984). This source is a spectroscopic binary with a period of 1567.66 days (Gordon, 1947).

Barnes relations, based on $(B\text{-}V)_o$ and $(R\text{-}I)_o$ colour indices, provide an angular diameter estimation of 1.4 mas.

IRC+20190

The lunar occultation light curve of IRC+20190 was affected by 50 Hz and its harmonic modulations of the mains power supply. Occultation light curve of IRC 20190 after filtering the 50Hz modulation is shown in Fig. 4.11 along with the uniform stellar disk model fit to the data. Low frequency scintillation noise is present in the light curve and is accounted for in the data reduction procedure. The source is not resolved from our observations. Detailed analysis of the light curve provides an upper limit for the angular diameter of ≤ 2 mas.

This source is classified as M2 III (Hirshfeld & Sinnott, 1982a). We estimate the distance to this giant to be 310 pc. Visual occultation timing observations of this source

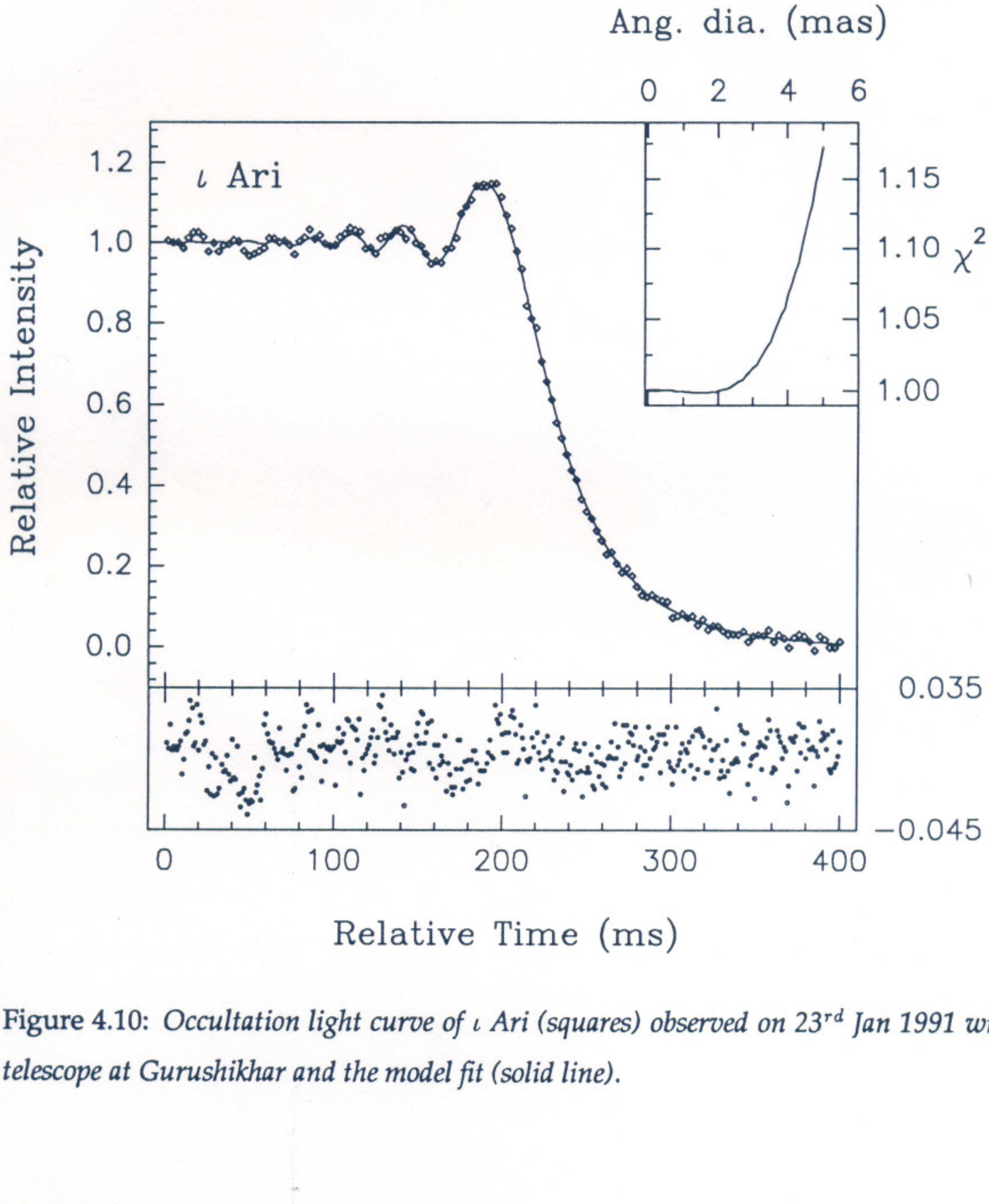

Figure 4.10: *Occultation light curve of ι Ari (squares) observed on 23rd Jan 1991 with 1.2m telescope at Gurushikhar and the model fit (solid line).*

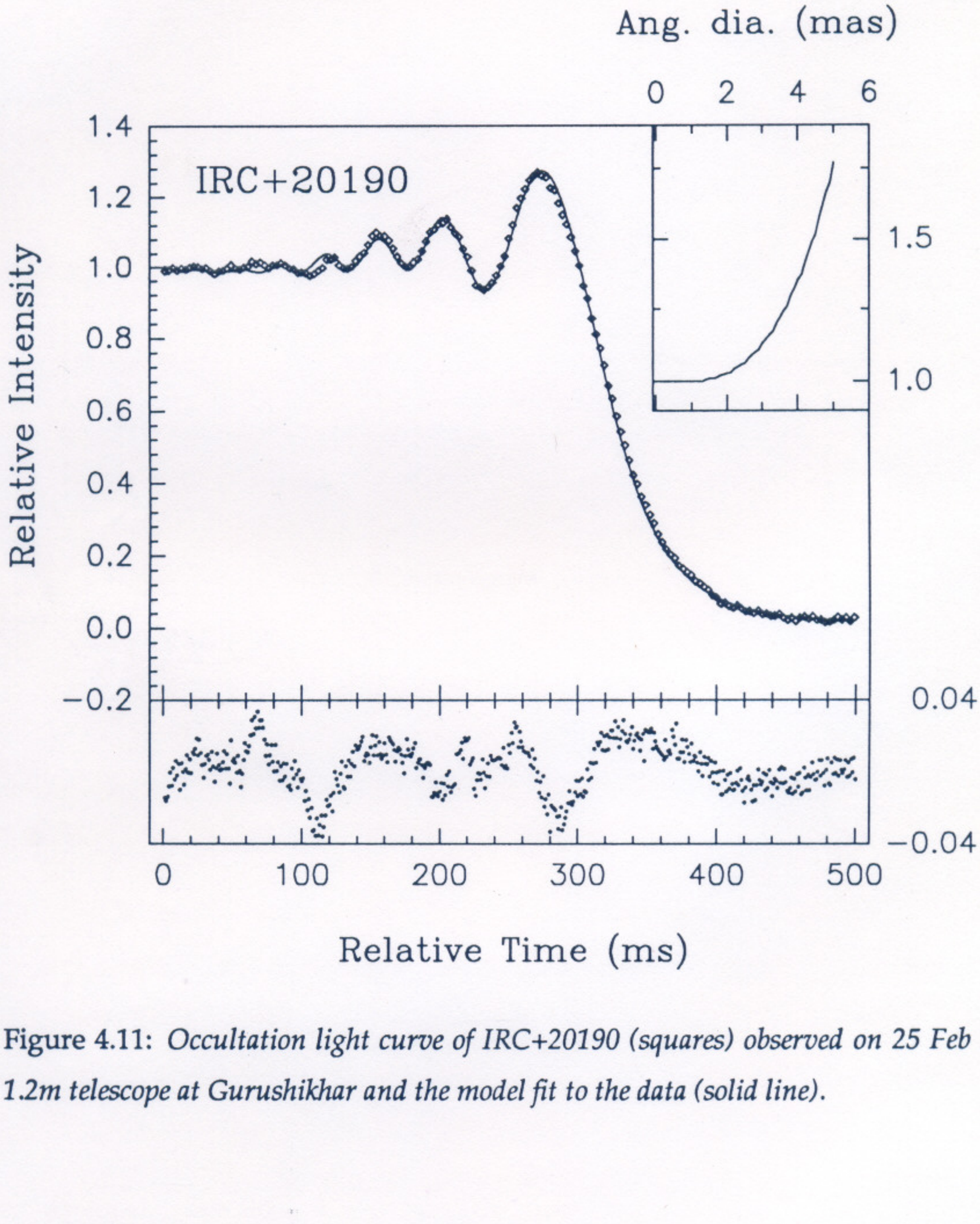

Figure 4.11: *Occultation light curve of IRC+20190 (squares) observed on 25 Feb 1991 with 1.2m telescope at Gurushikhar and the model fit to the data (solid line).*

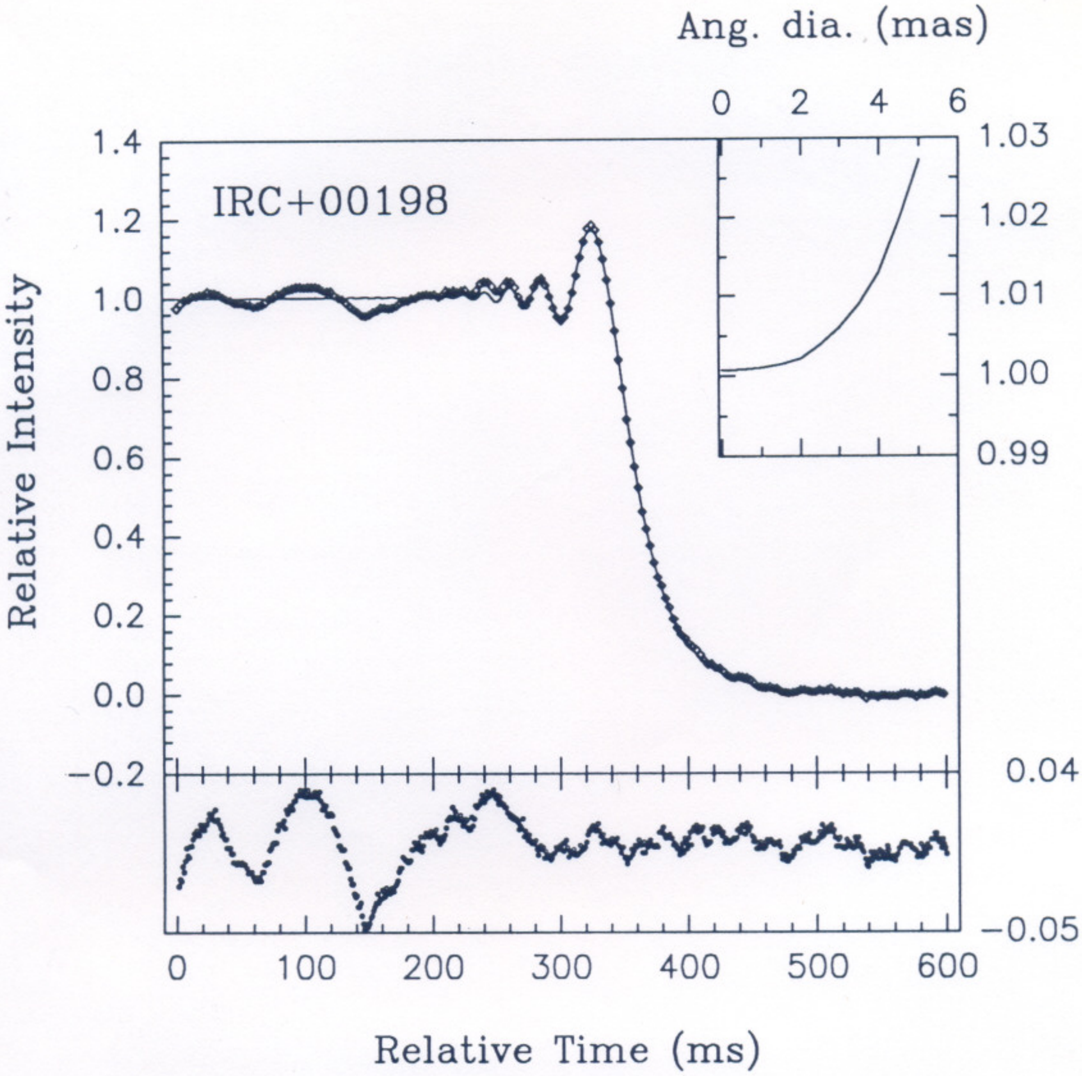

Figure 4.12: *Occultation light curve of IRC+00198 (squares) observed on 17 Mar 1992 with 1m telescope at Kavalur and model fit to the data (solid line).*

suggests that the source is probably not an occultation binary (Hilaire, 1974).

IRC+00198

Occultation light curve of IRC 00198 is shown in Fig. 4.12 along with the model fit to the data. The source is not resolved from our observations. Detailed analysis of the light curve provides an upper limit for the angular diameter of ≤ 2 mas.

This source is classified as M2 III (Gottlieb, 1978). Eitter & Beavers (1979) recorded 4 occultation light curves (2 in red and 2 in blue wavelengths) of two occultation events and they have not detected any multiplicity from their light curve at the position angles

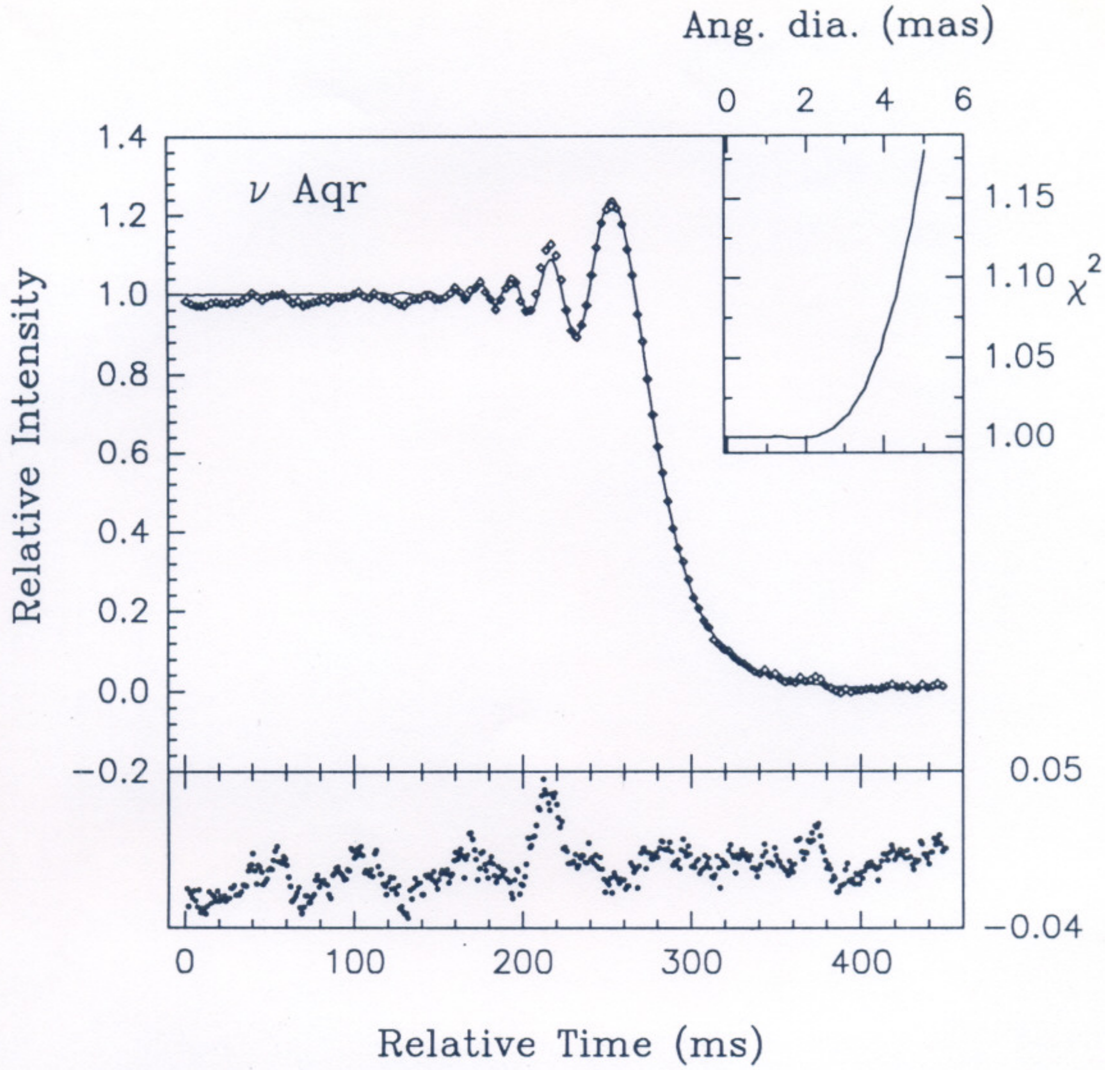

Figure 4.13: *Occultation light curve of ν Aqr (squares) observed on 7th Dec 1994 with 1.2m telescope at Gurushikar and the model fit (solid line).*

181.3° and 66°.

Detailed analysis of these observations by Beavers et al (1980, 1981) shows that the source is not resolved from their light curves and the angular diameter is likely to be $\leq$ 2 mas. They estimate the angular diameter from Barnes relation as 1.1 mas.

ν Aqr (IRC-10557)

Occultation light curve of ν Aqr along with the model fit is shown in Fig. 4.13. ν Aqr is one of the first sources to be studied by photoelectric method by Whitford in 1930s. No angular diameter is reported. ν Aqr is not resolved from our observations. Upper limit on the angular diameter of ≤ 2 mas has been derived.

ν Aqr is classified as G8 III by Roman (1952). Absolute visual magnitude has been derived from the width of chromospheric Ca II emission line and also from narrow band photometric calibrations. The values are respectively $M_v(K) = 1.2$ (Wilson, 1976) and $M_v(DDO) = 1.8$ (Brown et al., 1989). Adopting an average value of 1.5 for the absolute magnitude, the distance is derived to be ~ 40 pc. However, the distance modulus given by Eggen (1974) would give a distance estimation of 60 pc. This source was searched for lithium and is not detected (Brown et al., 1989). The stellar effective temperature has been derived from narrowband photometric calibrations and the value is given by Brown et al. (1989) as 4960 K and by McWilliam (1990) as 5010 K.

4.4 Indirect Angular Diameter estimation

From the basic relation,

$$F_{bol} = \left(\frac{\phi}{2}\right)^2 \sigma T^4, \tag{4.4}$$

we obtain,

$$logT_{eff} + 0.1C = 4.2207 - 0.1V_o - 0.5log(\phi) \tag{4.5}$$

where C is the bolometric correction and V_o is the unreddened V magnitude.

The right hand side of the above equation is defined as stellar surface brightness in visual and is an observable quantity. i.e.

$$F_v = 4.2207 - 0.1V_o - 0.5log\,(\phi) \tag{4.6}$$

Wesselink (1969) discovered a tight correlation existing between visual surface brightness F_v and the unreddened colour index $(B\text{-}V)_o$ independent of luminosity for early type stars from then available angular diameter measurements of 19 stars. The validity of this relationship to late spectral type is shown by Warner (1972) & Harwood et al. (1975) with additional stars for which angular diameters then became available. Later Barnes & Evans (1976a) found that the relationship becomes multivalued for $(B\text{-}V)_o > 1.5$ but a monotonic relationship holds between F_v and $(V\text{-}R)_o$. This was later refined by Barnes et al., (1978) as

$$F_v = 3.841 - 0.321(V - R)_o \tag{4.7}$$

for $(V\text{-}R)_o \geq 0.80$ and tabulated relationship for $(V\text{-}R)_o < 0.8$.

Barnes et al. (1976b) obtained relationships for early type stars based on $(B\text{-}V)_o$, $(V\text{-}R)_o$ & $(R\text{-}I)_o$ indices with a large number of stars.

Studies in this line have proven to have important astrophysical applications like determination of absolute magnitudes and radii of main sequence stars (Wesselink, 1969; Lacy, 1977a), determination of linear radii of white dwarfs (Warner, 1972; Moffett et al., 1978) and distance estimation for novae (Barnes, 1976), eclipsing binaries (Lacy, 1977b) and classical cepheids (Barnes et al., 1977).

The empirical relationship that exist between stellar surface brightness in the visual (F_v) and the infrared color indices, $(V-J)$, $(V-H)$, $(V-K)$ and $(V-L)$ are investigated using a carefully selected sample of angular diameters available in the literature. We found that a single slope expression holds good for the entire range of spectral types and is independent of luminosity class.

The data base for our work is White & Feierman (1987) which contains 138 published angular diameter measurements for 124 stars by lunar occultations. Amoung these 124 stars, 23 are known to be variables and 11 stars do not have either V or K magnitude readily. For simplicity, we excluded these 34 stars for our present work and are hence left with 90 stars. To cover a wider spectral range (O and S type stars), five more stars from Barnes et al. (1978) are also included and hence we have totally 95 stars for the present investigation. Great majority of the sources are late type giants and multiple observations are available for many sources at different wavelengths. It is known that the angular diameters of late giants could be wavelength dependent (Schmidtke et al., 1986). As K band light curves are relatively of good quality, due to reduced background moon light, K band angular diameter is taken when ever possible. In the absence of measurement in K, H band angular diameter is taken and if not then the visible region angular diameter measurement. We feel justified in using angular diameters in infrared as the optical light curves are relatively of poorer quality and the reported measurement errors are probably an under estimate in many cases. Most of the reported angular diameters are uniformly illuminated disk values and are converted to limb darkened values using the correction factor given by Schmidtke et al. (1986). The effects of interstellar extinction have been ignored since it has been proven to be negligible (Barnes, 1976a). The parameter visual surface brightness F_v of our sample stars is derived using eqn. 4.6. The visual magnitudes are taken from White & Feierman (1987) and the near infrared colours are taken from Gezari et al. (1993). A least squares fit has been carried out to establish relationship between the visual surface brightness and the near infrared colour indices. Fig. 4.14 shows the model fit to our samples. We find that there is an excellent linear relationship existing between visual surface brightness and near infrared colour indices. The derived equations are given below.

$$F_v = 3.8608 - 0.1421(V - J)_o \tag{4.8}$$

$$F_v = 3.8931 - 0.1216(V - H)_o \tag{4.9}$$

$$F_v = 3.8471 - 0.1094(V - K)_o \tag{4.10}$$

$$F_v = 3.8809 - 0.1093(V - L)_o \tag{4.11}$$

We have estimated the angular diameters for our occultaion sources using the first three relations and given in Table 4.7. The estimated error involved in the derived angular sizes is in the range 10 – 15%. The surface brightness versus $(V\text{-}K)_o$ colour index relationship has been independently established by Di Benedetto (1993) using angular diameters derived from modern Michelson interferometric observations. They have separated the giants from supergiants. In the case of giants they have shown a difference in the slope of the relationship between K and M giants. The relationships given by Di Benedetto (1993) for giants are,

$$\begin{aligned} F_v &= 3.927 - 0.122(V - K)_o \quad when \quad 1.4 > (V - K)_o < 3.7 \\ F_v &= 3.833 - 0.101(V - K)_o \quad when \quad (V - K)_o > 3.7 \end{aligned}$$

The relationship given for supergiants is

$$F_v = 3.960 - 0.135(V - K)_o \quad when \quad (V - K)_o > 0.6$$

4.5 Model fit to Photometric data

Photometric data for these sources are taken from Johnson et al. (1966), Neugebauer & Leighton (1969), Nicolet (1978), Hoffleit & Jaschek (1982), Häggkvist & Oja (1970; 1987), Oja (1987), Sato & Kuji (1990), Gezari et al. (1993) and Fluks et al. (1994) in

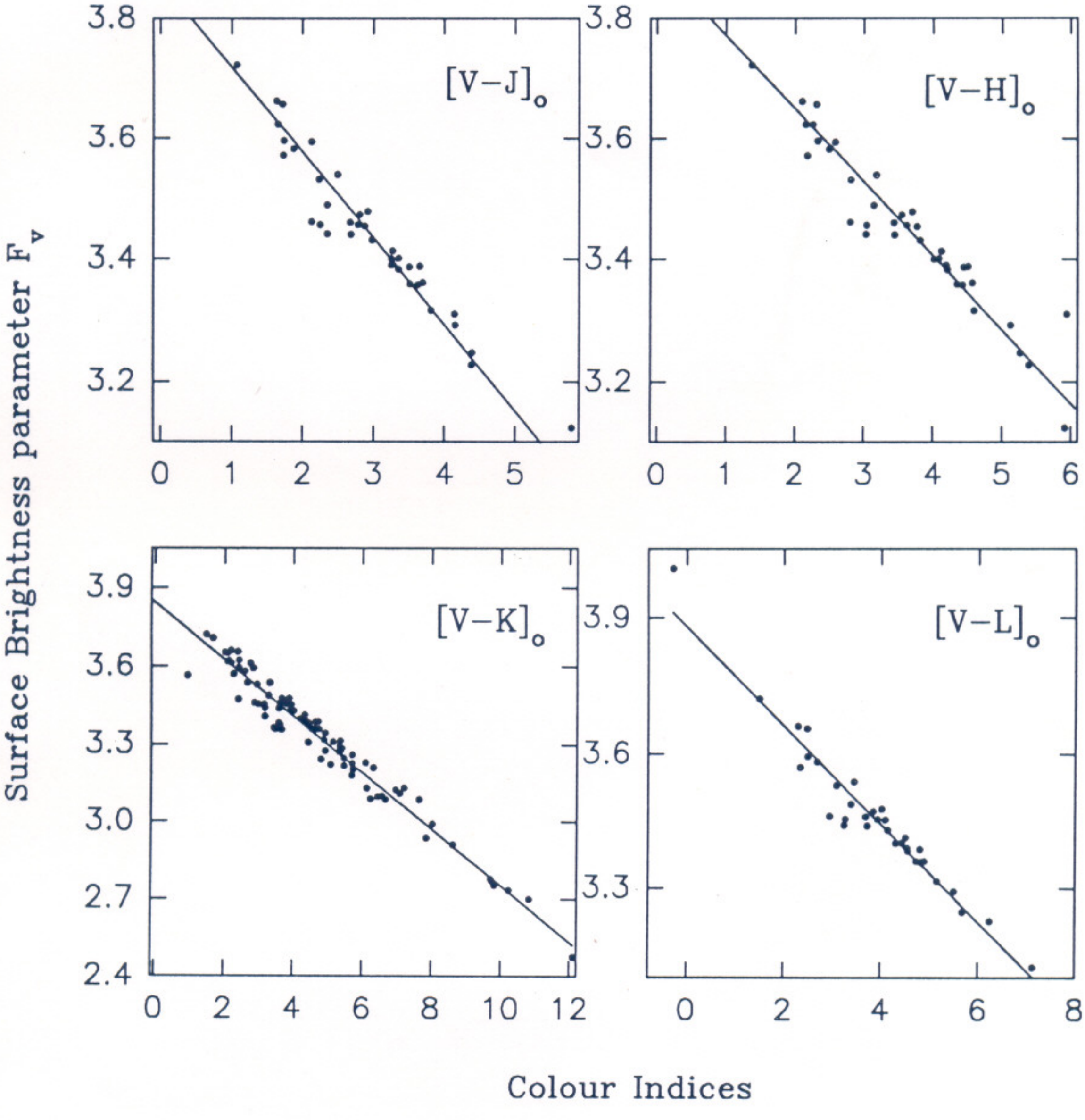

Figure 4.14: *Shown is the correlation existing between the surface brightness parameter and the near infrared colour indices.*

Table 4.7: *Angular diameter estimations from F_v Verses infrared colour indices relationships.*

$Source$	$\phi_{(V-J)}$	$\phi_{(V-H)}$	$\phi_{(V-K)}$	ϕ_{avg}
θAqr	2.1	2.1	2.5	2.3
ιAri	1.4	1.4	1.6	1.5
$IRC+20190$	2.0	2.0	2.1	2.0
θCnc	3.3	3.2	3.5	3.3
$NSV1529$	5.5	4.7	4.7	5.0
$IRC+00198$	1.8	1.7	1.8	1.8
$BQOri$	4.5	5.9	4.6	5.0
$IRC+10194$	2.8	2.5	2.9	2.7
$IRC+10024$	3.6	3.5	3.7	3.6
νAqr	1.7	1.8	2.1	1.9
$NSV4308$	2.0	2.0	2.2	2.1
$IRC+00529$	1.8	2.0	2.2	2.0

addition to our photometric values (Tables 4.3 & 4.4). Interstellar extinction out to 1 kpc along the direction of all our occultation sources except NSV 1529 and BQ Ori is negligibly small. In the case of NSV 1529 and BQ Ori, we estimate the visual extinction to be respectively 0.61 and 0.35 magnitudes (Lucke, 1978). Photometric data of these two giants are corrected for interstellar extinction.

Stellar effective temperature could be derived, in principle, from blackbody model fit to the observed photometric values. However, for late-type stars, this approach may not provide a reliable estimation as the spectra of these stars strongly depart from Planck function. Nevertheless, we used this approach, mainly to look for infrared excess, if any (signifying the presence of dust shells) and also to compare these estimations with values derived directly from our occultation light curves. We have rejected B,V,R,I & H values as these values are systematically biased by molecular line opacities (Tsuji, 1978). We have also rejected U band values as the uncertainity in the interstellar extinction correction is significant in this photometric band. A nonlinear least squares fit has been carried out to fit a blackbody spectra to the rest of the photometric values and are shown

Table 4.8: *Indirect estimations of stellar parameters.*

Source	ϕ_{UD} mas	T_{eff} K	ϕ_{bb} mas	T_{bb} K	$\phi_{F\upsilon}$ mas
θ Aqr	$\leq$2	–	2.1	4790	2.3
ι Ari	$\leq$2	–	1.5	4640	1.5
IRC+20190	$\leq$2	–	2.1	3640	2.0
θ Cnc	3.3$\pm$0.3	3665$\pm$180	3.5	3630	3.3
NSV 1529	3.3$\pm$0.4	3380$\pm$160	5.4	3110	5.0
IRC+00198	$\leq$2	–	1.9	3540	1.8
BQ Ori	4.2$\pm$0.2	3460$\pm$100	7.7	2530	5.0
IRC+10194	4.2$\pm$0.5	2760$\pm$170	2.6	3750	2.7
IRC+10024	3.2$\pm$0.2	3650$\pm$100	3.6	3660	3.6
ν Aqr	$\leq$2	–	1.8	4830	2.4
NSV 4308	2.5$\pm$0.3	3975$\pm$260	2.1	4070	2.1
IRC+00529	2.4$\pm$0.3	3747$\pm$260	2.1	3570	2.0

in Fig. 4.15, 4.16 & 4.17. The stellar parameters derived from our blackbody model fit to the photometric data are shown in Table 4.8 along with the parameters obtained from our occultation light curves. Also listed in the same table are the estimated angular sizes (average value) using the relationship established in the previous section based on stellar surface brightness and infrared colour indices. The estimated errors in the derived angular diameter and blackbody temperature from photometric model fits are respectively 30% and 10 – 15%. The data reduction procedure has the provision to incorporate a second cool blackbody component to fit for the infrared excess if present. None of our sample sources discussed in this chapter has detectable infrared excess from our simplistic blackbody model fit to the photometric data. This signifies the absence of any detectable circumstellar dust around these evolved giants.

In summary, in this chapter, lunar occultation observations and analysis of the light curves have been discussed. A dozen giants ranging from G type to early M

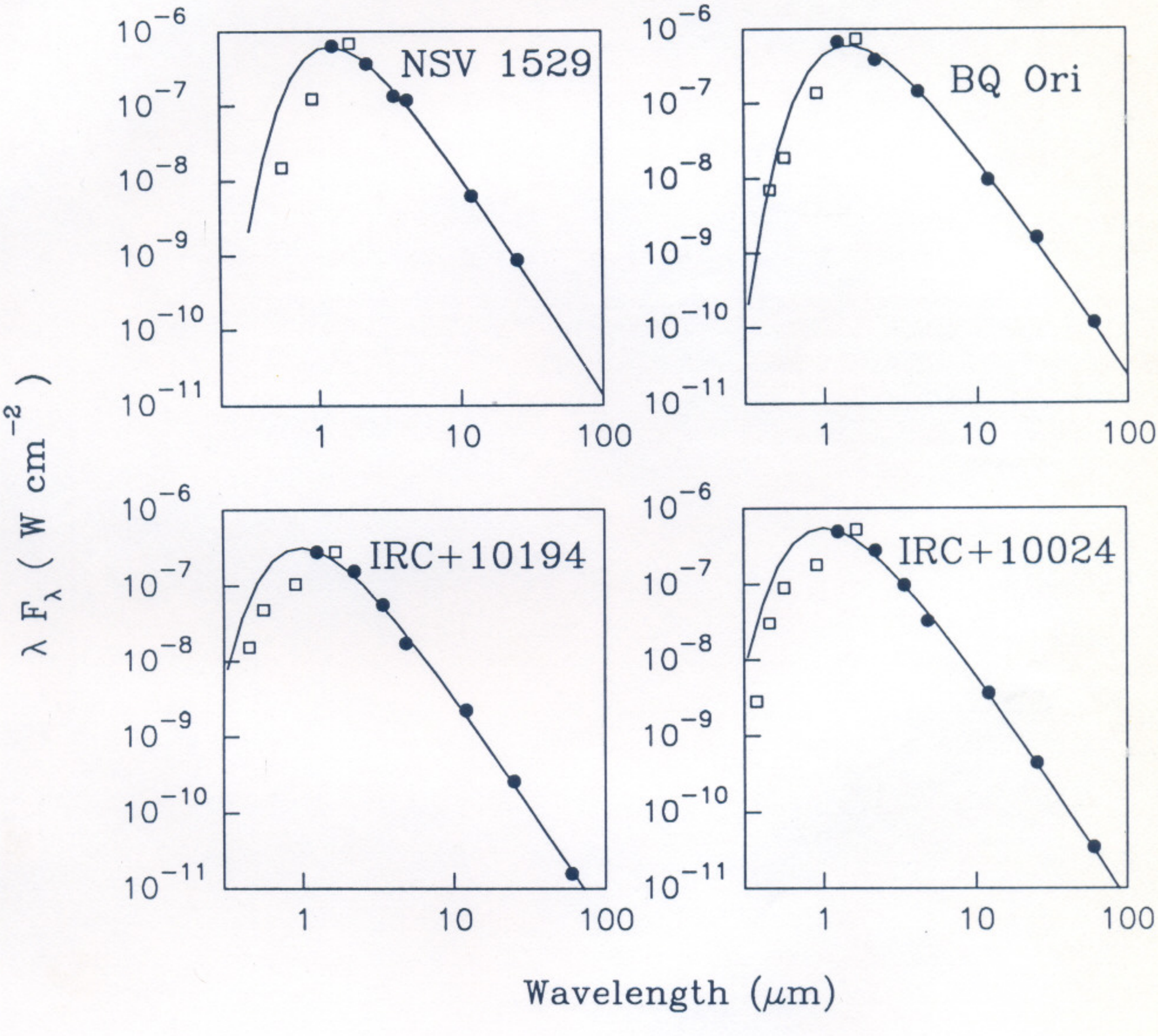

Figure 4.15: *The blackbody model fits to the spectra of four M giants, resolved from our occultation observations. Filled cirles are the points which are used in the model fit and the open squares are rejected points.*

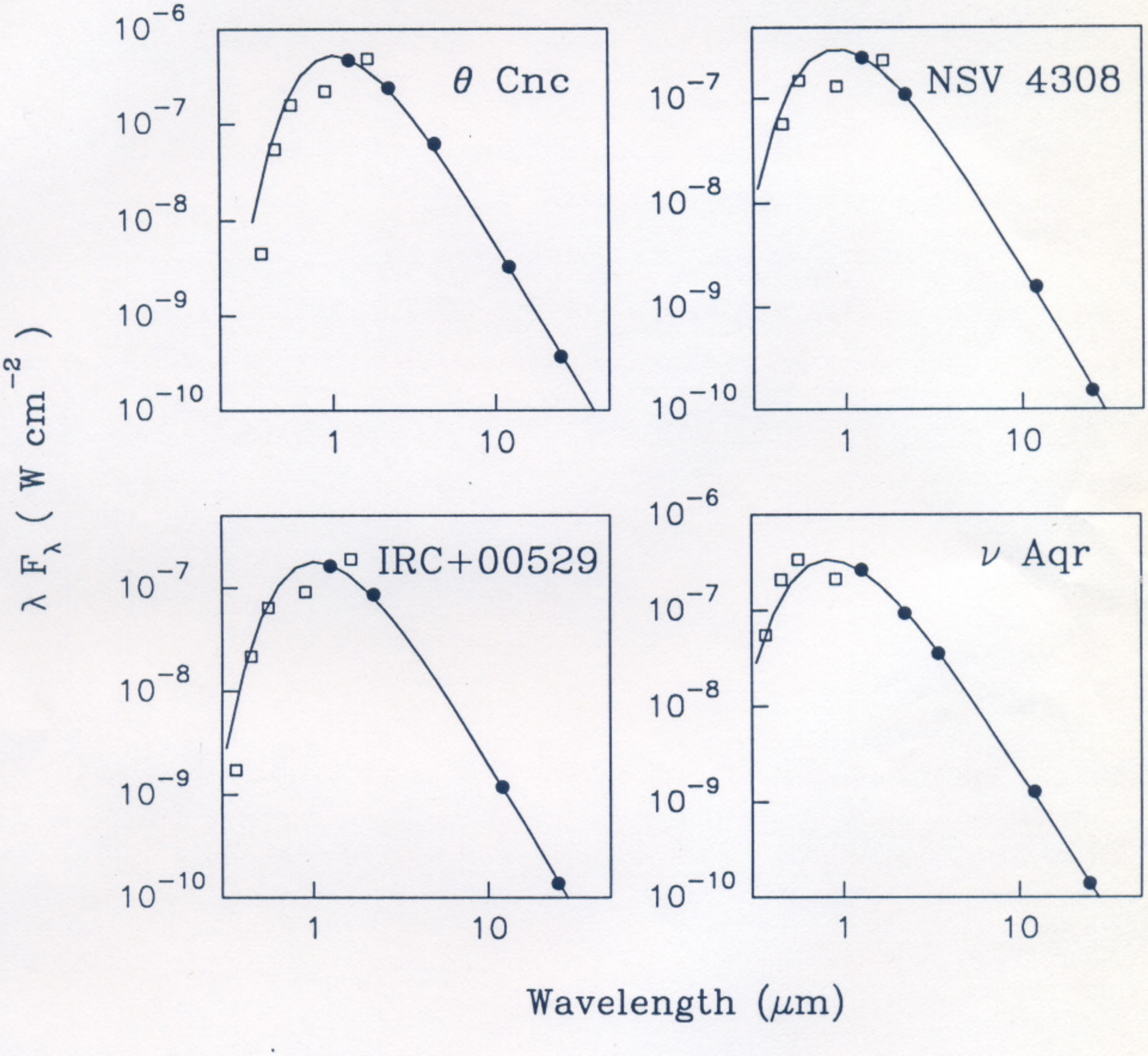

Figure 4.16: *The blackbody model fits to the spectra of four G/K giants. The first three sources are resolved from our occultation observations. Filled cirles are the points which are used in the model fit and the open squares are rejected points.*

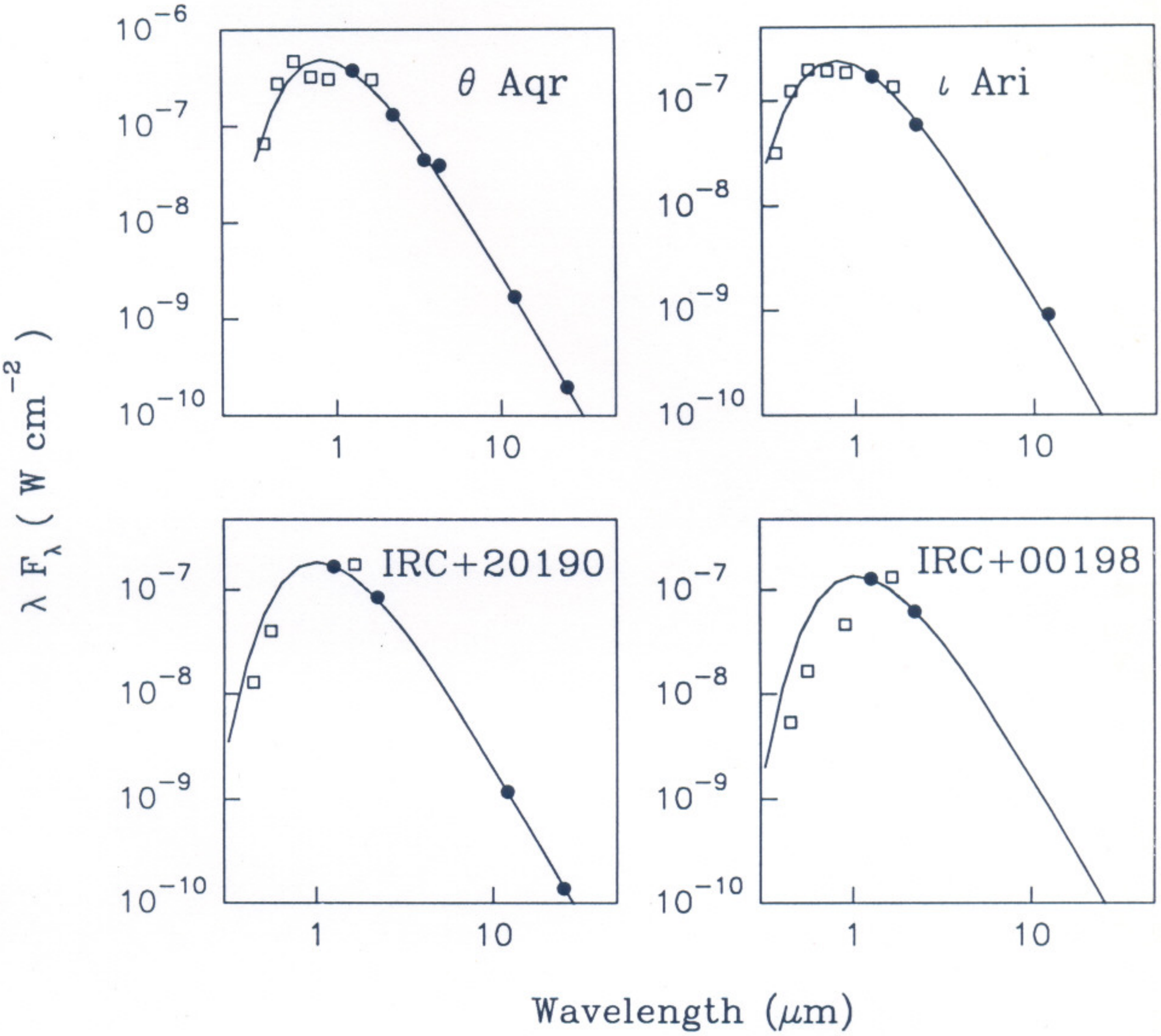

Figure 4.17: *The blackbody model fits to the spectra of four late-type giants, unresolved from our occultation observations. Filled cirles are the points which are used in the model fit and the open squares are rejected points.*

type have been studied of which seven sources have been resolved. Stellar effective temperature has been derived for all the resolved sources using bolometric flux and angular diameter. Derived effective temperatures, when compared with the available temperature scales (discussed in chapter 1), are found to be consistent within the errors involved in the calibrations and the measurements. However, statistically, the sample studied is not large enough to derive any conclusive feature in the existing temperature scale. Nevertheless, with the increasing angular diameter measurements, these results will play an important role in improving the already existing calibration. We have not detected circumstellar dust shell or multiplicity in any of these giants. A few sources like IRC+10194 are peculiar and merit further attention.

The instrument developed for this thesis work has also been used to carry out infrared observations of a fast nova – Nova Herculis 1991 by the author. The interesting results which emerged from these studies have been discussed in the next chapter.

Infrared Temporal Studies of Nova Herculis 1991

Chapter 5

Infrared studies of the fast nova – Nova Herculis 1991 (V838 Herculis)

A classical nova eruption is caused by a thermonuclear runaway in a hydrogen-rich degenerate layer on the surface of a white dwarf in a close binary system. In such a system, the primary is a white dwarf and the companion is either a main sequence star or a late giant. The hydrogen rich degenerate layer is produced by continuous accretion by the white dwarf of matter which is ejected through the inner Lagrangian point by the companion. In a single event, approximately 10^{-4} $M_\odot$ to 10^{-6} $M_\odot$ may be ejected into the interstellar medium at velocities between 10^2 km/s and 10^4 km/s. Such an explosion may occur every several hundred to several thousand years.

Infrared (IR) observations are important in studies of novae because they provide a direct means of detecting the formation of dust in nova ejecta and for studying their subsequent evolution. In particular, temporal studies of novae in the IR are crucial for delineating the different phases of nova evolution viz. psuedo-photospheric expansion, optically-thin gas emission phase and dust formation. Since changes in novae environments occur rapidly, IR observations are required as early as possible after the outburst, followed by frequent subsequent observations, to study all the stages in the development of the ejecta.

The infrared observations of novae carried out so far, particularly their temporal behaviour, are well documented (Gehrz, 1988). A general summary of classical nova outbursts can be found in a recent work (Starrfield, 1988). IR studies of the temporal development of less than 10 novae have been properly followed through, while isolated IR observations exist for a few more cases. Coordinated temporal infrared studies of novae are yet to be carried out on a regular basis.

Novae are classified into speed classes on the basis of the observed velocity of the early ejecta and the light decline. The speed with which novae evolve after the nuclear reactions begin varies enormously depending primarily on the mass of the white dwarf and mass of the accreted material. In 'slow' novae ($v_{exp} \sim 100$km/s), conditions are generally favorable for the condensation of extensive, optically thick dust shells, whereas the ejecta of fast novae ($V_{exp} \geq 10^4$km/s) have insufficient density to permit efficient grain growth, when the hot gas cools below the condensation temperature, $T_c \sim 1000$K. Fast novae are the least understood of all novae because of the severely nonequlibrium processes that take place at the onset. The study of this class of novae are of great interest (Lynch et al, 1992). However fast novae are difficult to study observationally because they are not only unpredictable (like any other nova), but also evolve too quickly to undertake a planned observing program.

An interesting aspect that has emerged from the infrared observations of novae made so far is the wide variety exhibited by these objects in their dust-forming behaviour (Gehrz, 1988). Earlier it was thought that all dust-forming novae formed shells without spectral features and composed of graphite grains only. However a few novae deviated from this general picture and exhibited emission features. While Nova Aql 1982 (V1370 Aql) exhibited a 10 μm feature attributable to SiC, Nova Vul 1984 (QU Vul) exhibited dust composed entirely of oxygen-rich silicates with characteristic 10 and 20 μm spectral signatures in emission, superposed on a complex gas-shell spectrum composed of thermal bremsstrahlung continuum with strong forbidden-line emission (Gehrz et al., 1988). In faster novae like V1668 Cyg (Gallagher et al. 1980; Piirola & Korhonen, 1979) and V1500 Cyg (Ennis et al., 1977) there is only limited evidence for dust formation. V1688 Cyg condensed into an optically thin dust shell with a maximum optical depth of 0.1 in about 60 days while V1500 Cyg exhibited only a weak 10 μm excess after 100 days, attributable to a dust shell. The diversity of IR behavior exhibited by novae makes it very important to study the temporal behavior of every nova in the infrared. Whether fast novae can form substantial dust shells remains to be established.

Some novae exhibit, in addition to optical forbidden line emission commonly seen in novae such as [OII] 3727 Å, [OIII] 4363 Å, [NIII] 4640 Å, [OIII] 4959 Å and [OIII] 5007 Å, optical *coronal* line emission such as [FeVII] 6087 Å, [FeX] 6374 Å and [FeXI] 7892 Å (Starrfield, 1988). In the near IR, forbidden emission lines of coronal origin were first discovered about two decades back in Nova V1500 Cyg (Grasdalen & Joyce, 1976). Subsequently IR spectrophotometry at moderate resolving powers ($\frac{\lambda}{\delta\lambda} \sim 100$) of novae V1500 Cyg, QU Vul, Nova Her 1987 (V827 Her), V1819 Cyg have shown that some novae enter a coronal emission phase characterized by IR forbidden line emission a few hundred days after eruption (Gehrz, 1988). Though the excitation temperatures for these emissions are of the order of $\sim 10^3$ K the temperatures required for the ions to exist are in the range $5\times10^5 - 10^6$ K. The presence of these lines require large energy inputs to the region to sustain the population of high lying states against adiabatic cooling. It has been pointed out by Starrfield (1988) that though the cause of the coronal line emission is not exactly known, X-ray data if present could indicate whether it is emission from shock heated, ejected material.

The eruption of Nova Her 1991 provided a good opportunity for studying its dust formation and coronal line emission behaviour from observations made in the near infrared from the 1.2m telescope at Gurushikhar.

The work detailed in this chapter constitutes the first documentation and exploration of early grain formation in a fast nova environment and has been published (Chandrasekhar et al., 1992b; Chandrasekhar et al., 1993). It is heartening to note that the basic inferences of the work have largely been confirmed by subsequent researchers in the field on this nova (Woodward et al., 1992; Harrision & Stringfellow, 1994).

5.1 An observational history of Nova Her 1991

Nova Her 1991, apart from being one of the brightest and fastest novae in recent times, has also been a very unusual one. Optical detection of the nova was on the night of 1991 March 24.781 at an estimated magnitude of V=5.4 (Sugano, et al., 1991). The presumed precursor has been identified on the blue plate of the Palomar Sky Survey as a 20.6

magnitude star while on its red plate the measured magnitude is 18.25 (Humphreys et al., 1991). Thus the amplitude of the optical outburst is larger than 15 magnitude, which places this nova among the brightest in recent times. Nova Her 1991 faded rapidly in the optical, declining by about 6 magnitudes in $\sim$ 10 days (Woodward et al., 1992). Following the discovery, it was observed extensively at other wavelengths as well. It was detected at milli Jansky level at 14.9, 8.4 and 4.9 GHz by the Very Large Array (VLA) about 11 days after optical maximum (Hjellming, 1991). Near Infrared photometric observations showed a brightening peaking in the K (2.2 μm) band 14 days after the outburst suggesting an unusually early phase of dust formation in the nova. A periodic eclipse like feature at an oribital period of P=0.29764 days was reported by Leibowitz et al. (1992) and confirmed by Ingram et al. (1992). The high initial ejection velocity (Della Valle & Zelinger, 1991) and the later appearance of strong neon lines in the spectra confirmed that Nova Her 1991 was indeed an ONeMg nova (Dopita et al, 1991). Nova Her 1991 has also been detected by ROSAT satellite in the X-ray wavelengths just five days after optical maximum (Lloyd et al., 1992) – the first ever nova to be positively detected in X-rays so early in its evolution. The high temperature zone needed for X-ray emission also constitutes a favourable environment for the production of highly ionized states of elements and for producing detectable coronal line emission from the excited states of these ions.

5.2 Observations

First reports of the Nova Herculis 1991 outburst (Sugano et al., 1991) were received at the Gurushikar observatory only on 1991 April 3 due to failure in our e_mail network. Following this a programme of infrared observations of the nova was quickly formulated and the first observations were made on April 5, 1991 . The observations were continued at intervals of a few days, weather permitting, until the end of 1991 May when overcast skies associated with pre-monsoon conditions set in.

The coordinates of Nova Her 1991 are

$$\begin{array}{ll} Equatorial: & RA = 18^h 44^m 11.83^s \\ (1950\ \ coord.) & Dec. = +12^\circ 10' 45.0'' \\ Galactic: & l^{II} = 43^\circ 18.9' \\ & b^{II} = +6^\circ 37.2' \end{array}$$

The IR photometric observations were carried out using the 1.2m telescope at Gurushikhar (72° 47′E,24° 39′N) with a liquid nitrogen cooled InSb based IR photometer which is described in Chapter 2. The observations reported here cover a span of about 50 days starting from day 13 since visual maximum. Observations were made mainly in the J, H, and K near-infrared filter bands and occasionally at a longer wavelength near 3.3 μm with a narrower circular variable filter (CVF). Sky-chopping with an amplitude of $\sim$ 26 arcsec at a frequency of $\sim$ 10 Hz was accomplished with a tertiary vibrating plane mirror in the light path. A focal-plane aperture of 26 arcsec was generally used. The sky near the nova was also sampled regularly in all the filters to correct for sky gradients. Nearby standard stars (α Leo, α Ser, μ Her, ϵ Her and α Oph.) were also frequently monitored during the observations. α Oph, being observationally conveniently located at about the same declination as the nova, was the most frequently used calibration star with its infrared magnitudes taken as J=1.78, H=1.64, K=1.66 and m $(3.3\mu m) = 1.61$ (Gezari et al., 1987). The flux-density calibration was derived from Johnson's zero-magnitude fluxes (Johnson, 1966). Table 5.1 gives the journal of observations. K band data could be taken on all the observation days, while J and H band observations were discontinued once the nova became fainter than 9 mag in these filter bands. Only a few observations could be taken in the longer wavelength at $\sim$ 3.3 μm. As a narrower bandwidth was used in this case and as this wavelength (3.3 μm) falls in a region of relatively poor atmospheric transmission, the errors of measurement are correspondingly higher.

Nova Her 1991 was observed in the region 1.9 $-$ 2.1 μm in the CVF mode on four days between April 9, 1991 and April 20, 1991. On two days the spectral coverage extends upto 2.4 μm. Details of the spectral line observations made are given in Table 5.2, while Table 5.3 lists the infrared magnitudes measured in the J, H and K bands on the days the spectral line was observed in the CVF mode. Also listed are the blackbody

Table 5.1: *Near infrared Observations of Nova Her 1991.*

1991 UT DATE	DAYS SINCE VISUAL MAX.*	IR MAGNITUDE**			
		J	H	K	3.3 μm
APRIL 5.97	12.97	7.37±0.08	5.59±0.05	4.29±0.03	–
APRIL 6.96	13.96	7.44±0.08	5.69±0.05	4.26±0.03	2.6±0. 2
APRIL 9.95	16.95	7.71±0.08	6.16±0.10	4.51±0.03	2.7±0. 2
APRIL 10.89	17.89	7.81±0.10	5.98±0.05	4.47±0.03	–
APRIL 12.91	19.91	7.98±0.10	5.97±0.05	4.42±0.03	–
APRIL 15.91	22.91	8.00±0.20	6.16±0.05	4.60±0.03	2.8±0. 2
APRIL 16.94	23.94	8.50±0.20	6.26±0.05	4.67±0.03	–
APRIL 17.96	24.96	8.40±0.20	6.30±0.05	4.71±0.05	–
APRIL 20.89	27.89	8.80±0.20	6.83±0.05	4.98±0.05	–
APRIL 21.92	28.92	9.90±0.30	6.80±0.05	5.05±0.05	3.4±0. 2
APRIL 22.96	29.96	9.60±0.30	7.02±0.08	5.20±0.05	–
APRIL 27.86	34.86	9.90±0.30	7.48±0.10	5.42±0.05	–
MAY 4.90	41.90	–	8.90±0.20	6.49±0.08	–
MAY 5.90	42.90	–	8.52±0.20	6.54±0.08	–
MAY 9.90	46.90	–	9.00±0.30	7.02±0.08	–
MAY 18.70	55.70	–	–	7.64±0.1	–
MAY 19.70	56.70	–	–	7.71±0.1	–
MAY 23.70	60.70	–	–	8.20±0.2	–
MAY 28.80	65.80	–	–	8.50±0.2	–

*Date of visual maximum: Mar 24.0 UT

**Zero magnitude fluxes from Johnson (1966) temperature (T_{BB}) fitted to the observed spectrum and the angular extent of the dust zone ($2\theta_{BB}$) obtained from the observed flux $F_\lambda \sim \theta^2 B(\lambda, T)$. The nova spectrum was ratioed with that of α Oph (A5 V), obtained with the same CVF resolution and then multiplied by a blackbody spectrum corresponding to the star's effective temperature of 8500 K in order to remove effects of atmospheric absorption. It was assumed that the nova reached maximum light on March 24.0 at a visual magnitude $m_v = 5.0$. All temporal variations in the IR light curve of the nova are with reference to this date.

5.3 IR light curve of Nova Her 1991

While there are no IR observations of this nova in the pseudo-photosperic phase, early IR observations of this nova have been reported (Hekkert & Harrison, 1991; Doyon & Aycock, 1991; Moneti & Bouchet, 1991; Feast & Carter, 1991 and Gehrz et al., 1991). The early IR observations show a decline in IR flux until about day 6, consistent with a free-free emission phase. Thereafter there is an increasing brightness in the K and L bands, suggesting dust formation. This development has been commented upon (Feast & Carter, 1991) as early and unusual in a fast nova .

Fig. 5.1 shows these early IR observations together with visual observations available in the literature (Mattei, 1991; McNaught, 1991; Schmeer & Royer, 1991). It is clear from Fig. 5.1 that as the optical light sharply declines on about day 6.5, the IR light curve shows a corresponding increase. This type of behaviour was exhibited earlier by Nova Vul 1976 (NQ Vul) and Nova Ser 1978 (LW Ser), which formed optically thick dust shells (Gehrz, 1988). However, what is peculiar is that while these novae exhibited this phenomenon on about day 80, in the case of Nova Her 1991 it happened as early as day 7. Fig 5.2 shows the temporal development of Nova Her 1991 at the early phase.

Fig. 5.3 presents an overview of near-infrared (JHK) observations of the nova. The increase in flux (signifying dust formation) is clearly seen in the K and H bands and, to a lesser extent, in the J band.

Fig. 5.4 plots the J, H, K fluxes as a function of time (t) since visual maximum. The light curve exhibits a slow decline in the flux ($\propto t^{-1}$) until about day 23 followed by a faster decline ($\propto t^{-4}$). It has been remarked (Gehrz et al., 1988) that a t^2 law arises from

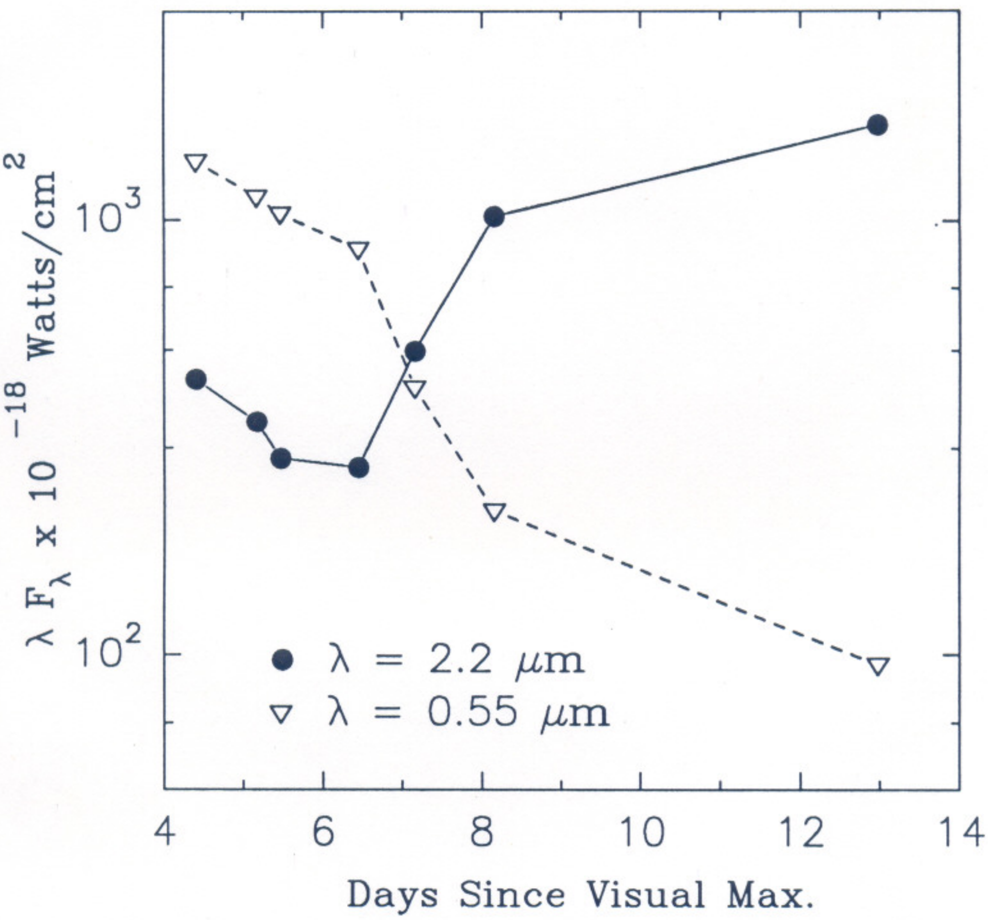

Figure 5.1: *A comparision of K(2.2 μm) and V(0.5 μm) band fluxes from Nova Her 1991. The sudden dip in V and the corresponding rise in K flux at $\sim$ day 7 points to the commencement of the dust formation stage.*

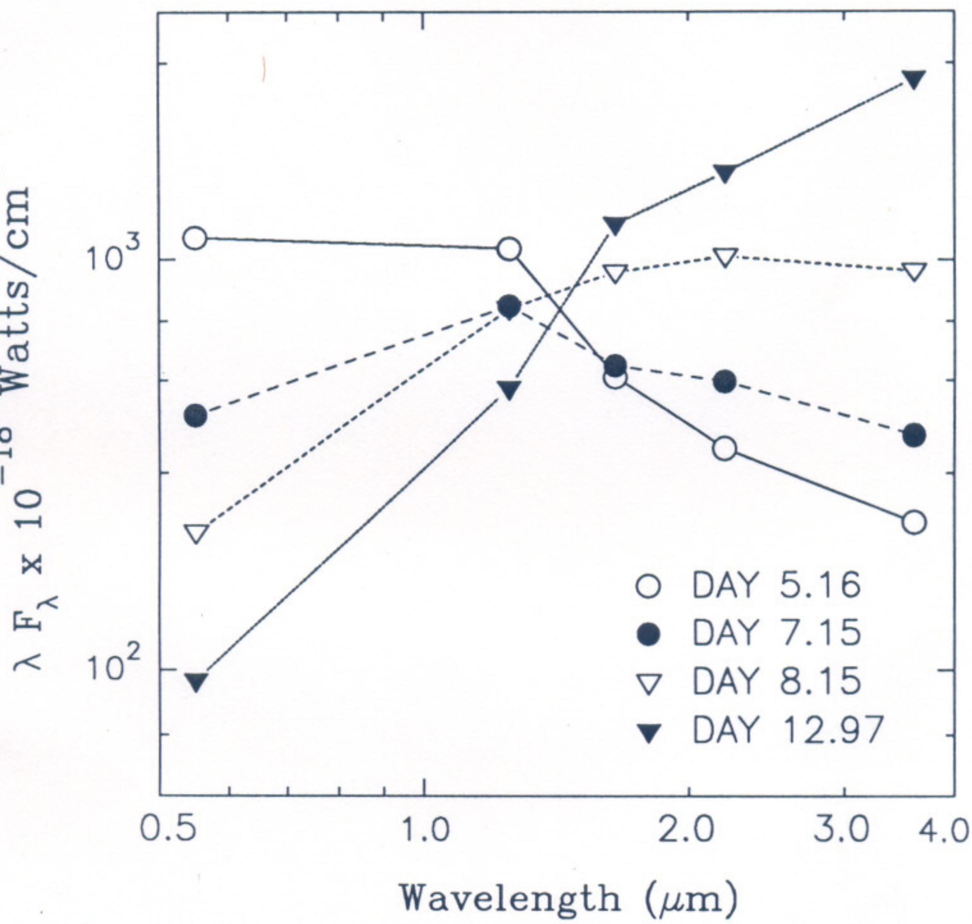

Figure 5.2: *Spectra of Nova Her 1991 shown on different days witnessing the early dust formation.*

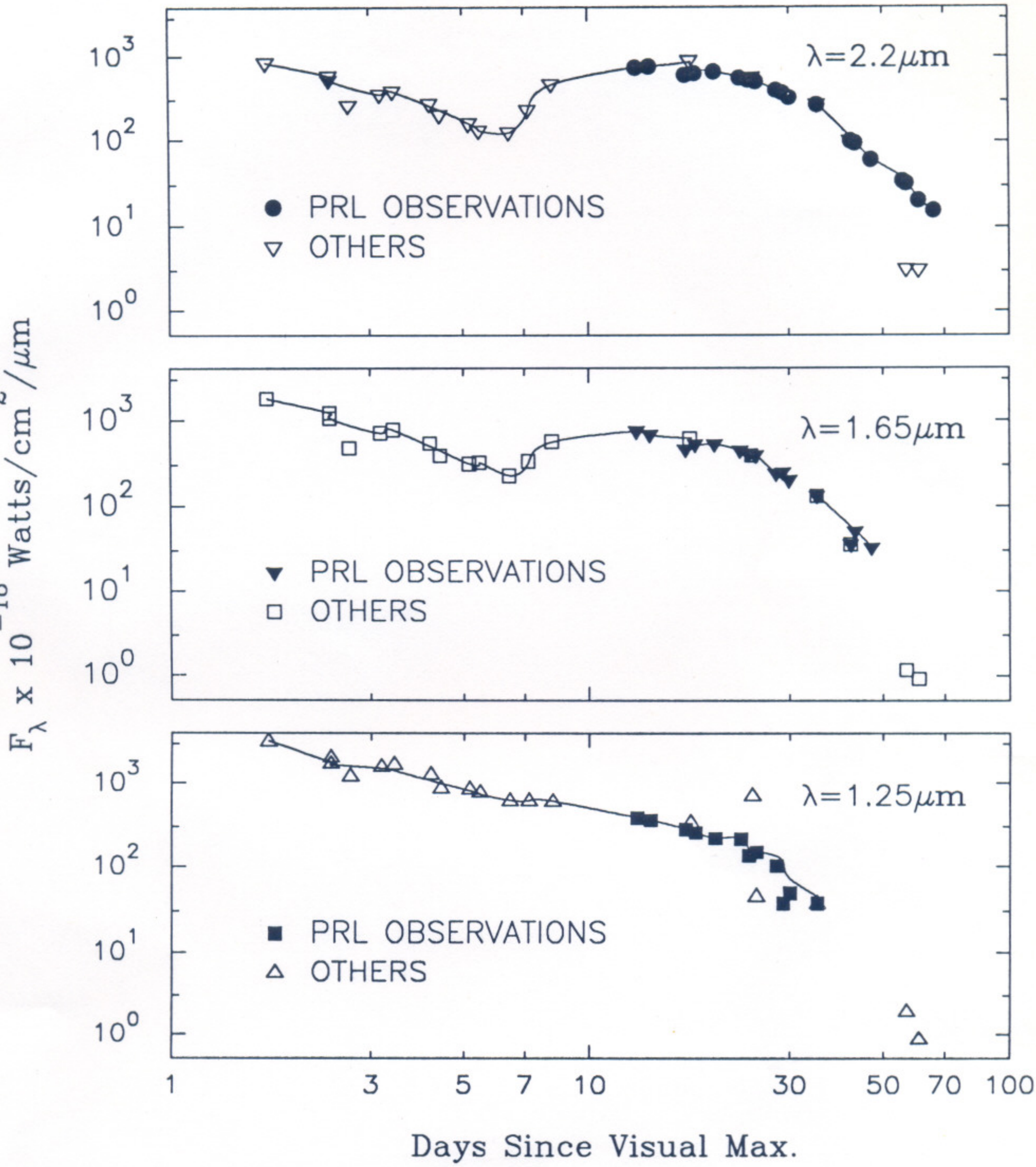

Figure 5.3: *An overview of near-infrared (J,H,K) observations of Nova Her 1991. A dip in the light curve at ~ day 6 and a subsequent rise signifying dust formation can be clearly seen in K(2.2 μm) and H(1.65 μm) and to a lesser extent in J(1.25 μm).*

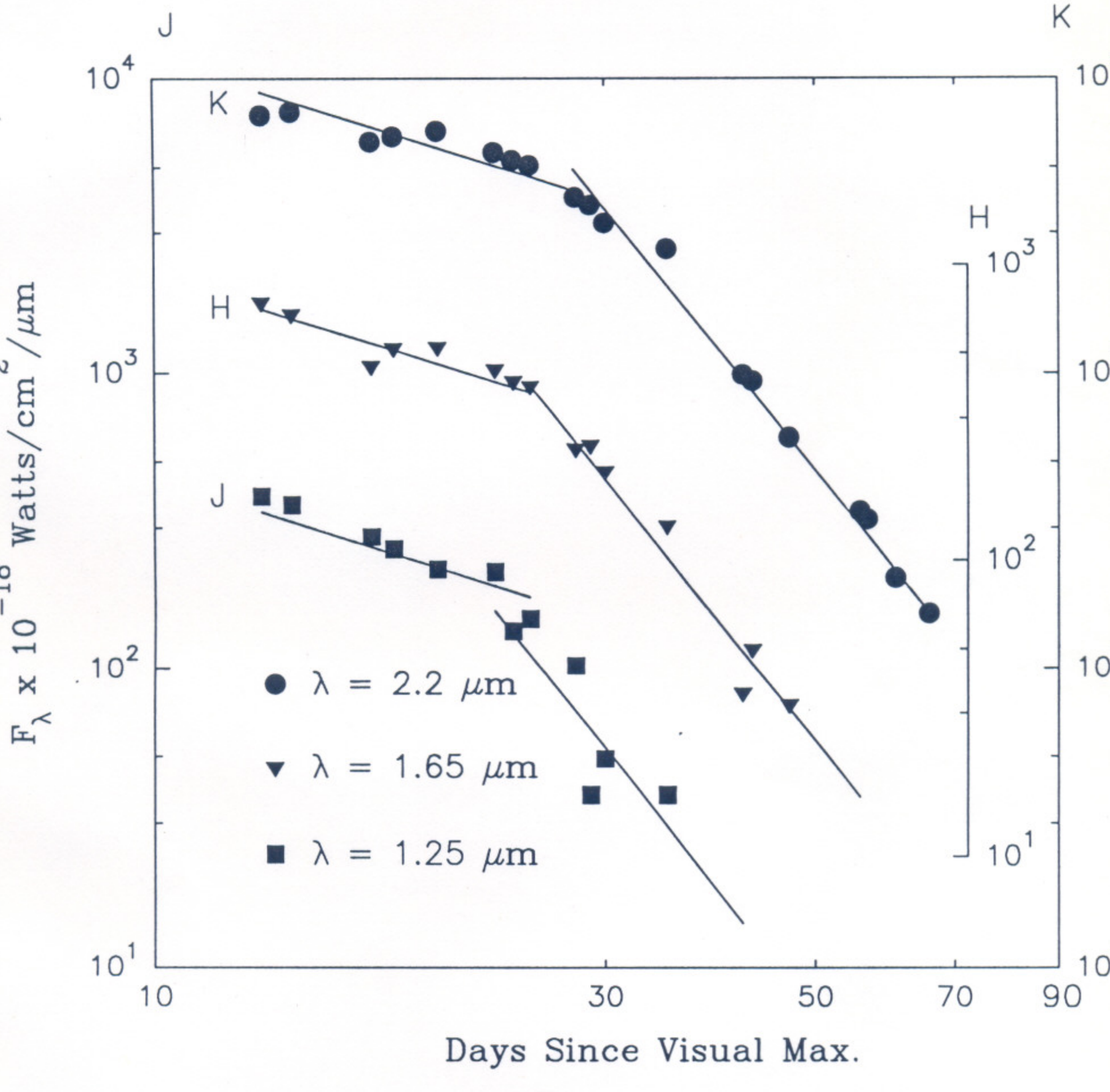

Figure 5.4: *Light curve of Nova Her 1991 in J,H,K filter bands. Observations in K(2.2 μm) cover the period 13 to 66 days since visual maximum. In H(1.65 μm) the coverage is from day 13 to 47 while in J(1.25 μm) it is from day 13 to 35. The data show a sharp change at $\sim$ day 25. Power laws of t^{-1} before day 25 and t^{-4} afterwards are superposed on the observation points.*

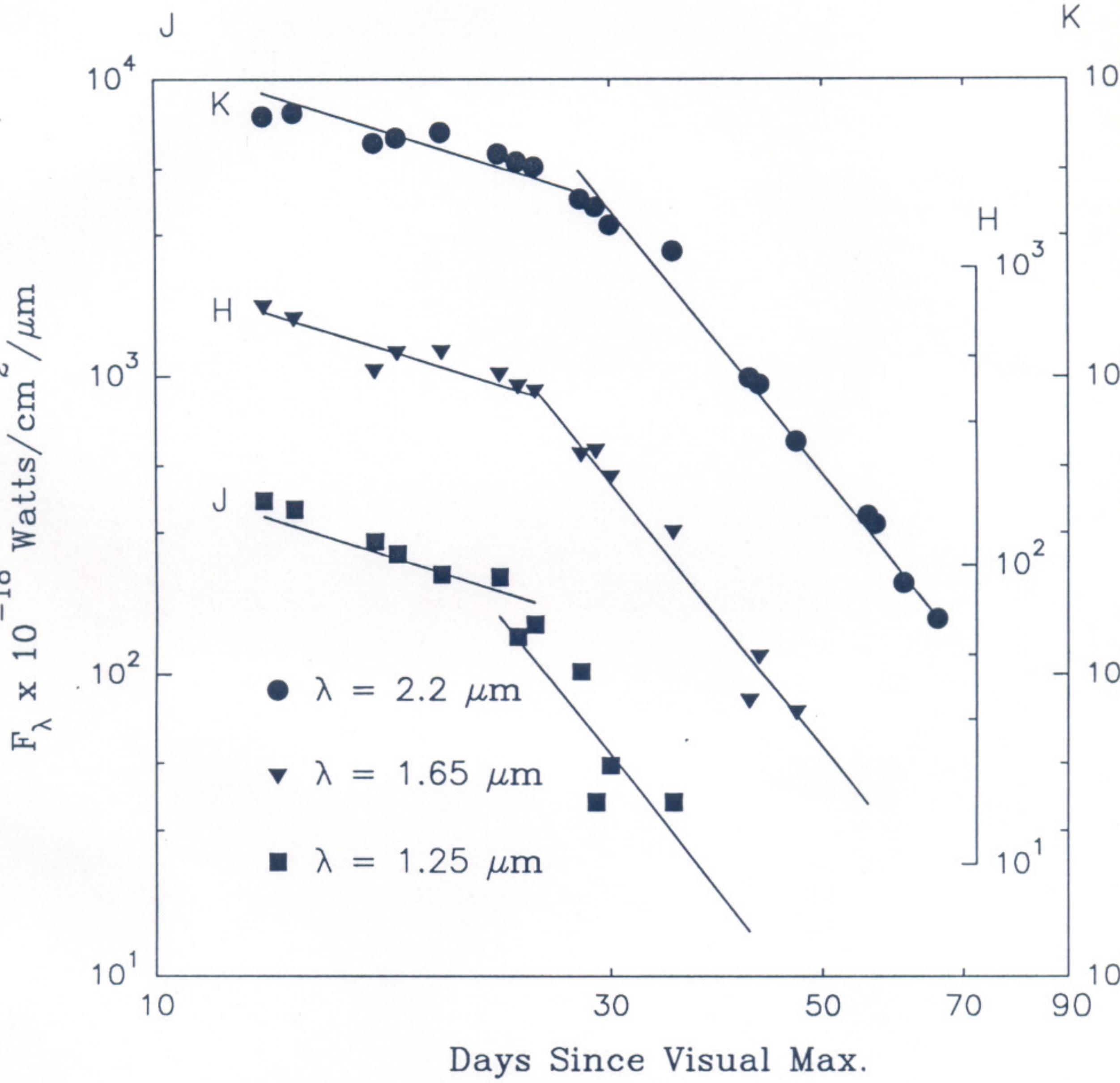

Figure 5.4: *Light curve of Nova Her 1991 in J,H,K filter bands. Observations in K(2.2 μm) cover the period 13 to 66 days since visual maximum. In H(1.65 μm) the coverage is from day 13 to 47 while in J(1.25 μm) it is from day 13 to 35. The data show a sharp change at ~ day 25. Power laws of t^{-1} before day 25 and t^{-4} afterwards are superposed on the observation points.*

an expanding optically thick psuedo-photosphere during the initial stages of a nova outburst while t^{-2} and t^{-3} laws are characteristic of optically thin gas shells in constant-thickness expansion and free expansion, respectively. The slow initial t^{-1} decline in the IR could have been caused by the presence of strong emission lines. Strong IR emission lines in the nova have been reported by Joyce (1991a & b). This is similar to observations of PW Vul by Gehrz et al., 1988. The subsequent temporal behaviour of the IR light of Nova Her 1991, however, is distinctly different from that of PW Vul. Again, the remarkable characteristic of Nova Her 1991 is the extreme rapidity of events. While in the case of PW Vul the transition of free-expansion phase occurred about 100 d after the event, in the case of Nova Her 1991 it occurred in less than 25 d. This early transition is consistent with the steep decline in optical output and subsequent rapid development in the nova.

5.4 Blackbody temperature

Blackbody distributions fitted to the data yield equilibrium dust temperatures which show a steady decline from a peak value of $\sim$ 1400 K. Fig. 5.5 shows the cooling curve, wherein the last two values (shown by open triangles) are from observations by others (Russell & Chatelain, 1991; Joyce, 1991a; Harrison & Stringfellow, 1991). The dust temperature exhibits a slow decline $t^{-1/2}$. For a constant expansion velocity V, this behaviour indicates a constant-luminosity phase, since L $\propto$ (R^2 T_{BB}^4) $\sim$ V^2 $\sim$ constant. Such behaviour has been reported before (Gehrz, 1988) in novae that have formed optically thick dust shells.

5.5 Blackbody angular size

Assuming the newly formed dust around the nova to be a blackbody at temperature T_{BB} distributed in a shell of radius R, the observed flux F_λ is given by

$$F_\lambda \sim \theta_{BB}^2 B(\lambda, T_{BB}),$$

where $B(\lambda, T_{BB})$ is the Planck function at wavelength λ and temperature T_{BB}. Using the deduced dust temperature in the above expression, estimates of θ_{BB} and the angular

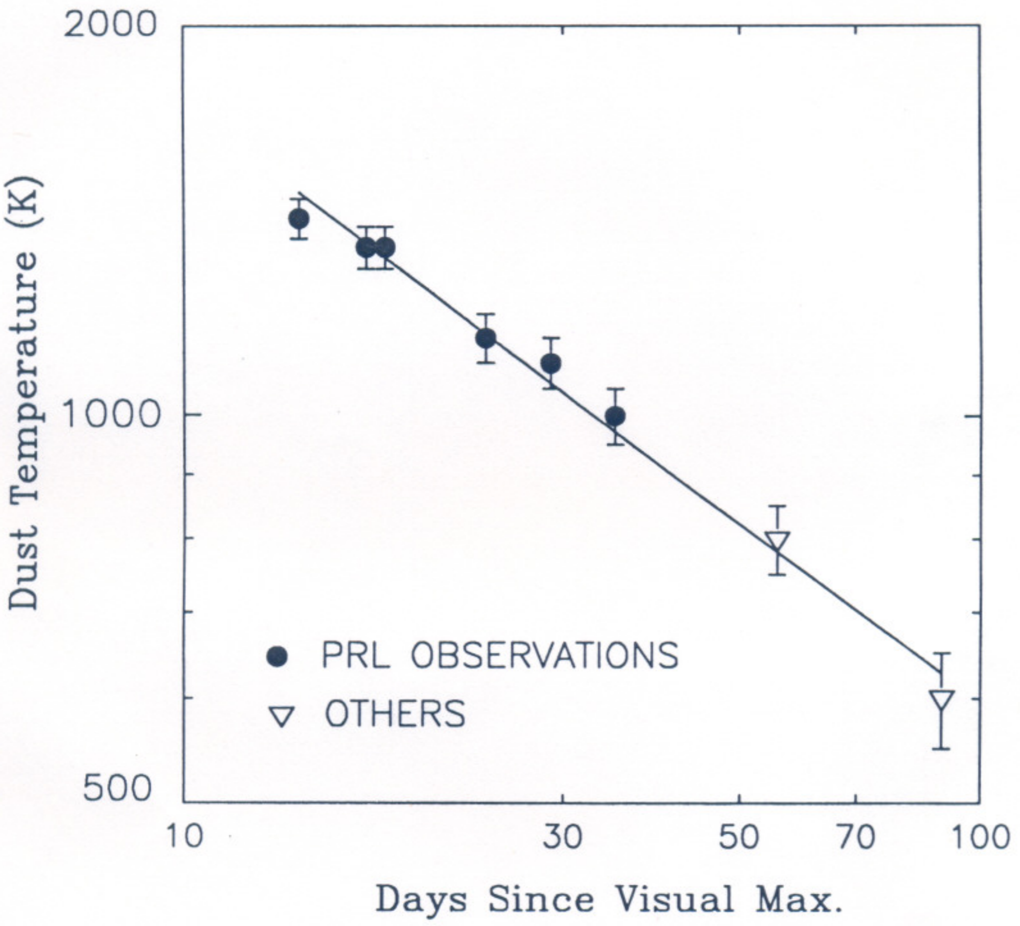

Figure 5.5: *The cooling curve of the dust in Nova Her 1991. A least squares fit to the data gives a slope of ~ -0.5 signifying a constant IR luminosity phase. Maximum temperature observed is $\sim 1420 \pm 50$ K.*

radius, the above can be estimated.

Fig. 5.6 shows the temporal behaviour of angular size ($2\,\theta_{BB}$). It can be seen that after a smooth increase, ($2\,\theta_{BB}$) shows an abrupt change around day 30. This behaviour suggests that dust formation has nearly ceased by this time, with the onset of optical thinness and free expansion. This scenario is consistent with the temporal behaviour of the IR light curve, which steepens at about the same time. Similar behaviour has been exhibited by novae which formed dust shells – NQ Vul, LW Ser and V1668 Cyg (Gehrz, 1988). The transition in these novae, however, occurred at a much later time, 60-80 d after the eruption.

5.6 Distance to the nova

Considering Fig. 5.6, a linear increase in the angular size with time until about day 30 is clearly seen implying uniform expansion velocity. A least-square fit to the linear portion yields an angular expansion rate (ω) of ~ 0.15 milliarcsec (mas) per day. Spectroscopic reports (Della Valle & Zelinger, 1991; Sivaraman et al., 1991) imply a large expansion velocity (V) of ~ 3000 km s^{-1}. From the expression D=V/ω:

$$D(kpc) = \frac{5.8 \times 10^{-4} V(km\ s^{-1})}{\omega(mas\ d^{-1})}.$$

Putting V=3000 km/s and $\omega = 0.15$ mas d^{-1}, we get D $\sim$ 11.5 kpc. This result appears rather large, but it could be due to the uncertainty in the actual value of the angular expansion rate (ω) which is correct only to a factor of about 2. One can also estimate the distance to the nova using the relationship between the absolute visual magnitude M_v and the time t_3 (in days) for the nova to decrease by 3 mag from visual maximum (Payne-Gaposchkin, 1957; Gehrz et al., 1980). M_v is given by the expression

$$M_v = -11.5 + 2.5 \log_{10} t_3.$$

From reports of visual sightings of the nova (Schmeer & Royer 1991; McNaught 1991) one can infer that the nova faded from $m_v \sim 5$ to ~ 8 in about 6 d implying that $M_v = 9.6$. Without assuming any extinction, a distance modulus of $m_v - M_v = 14.6$ can be obtained, leading to a distance, D $\leq$ 8.3 kpc.

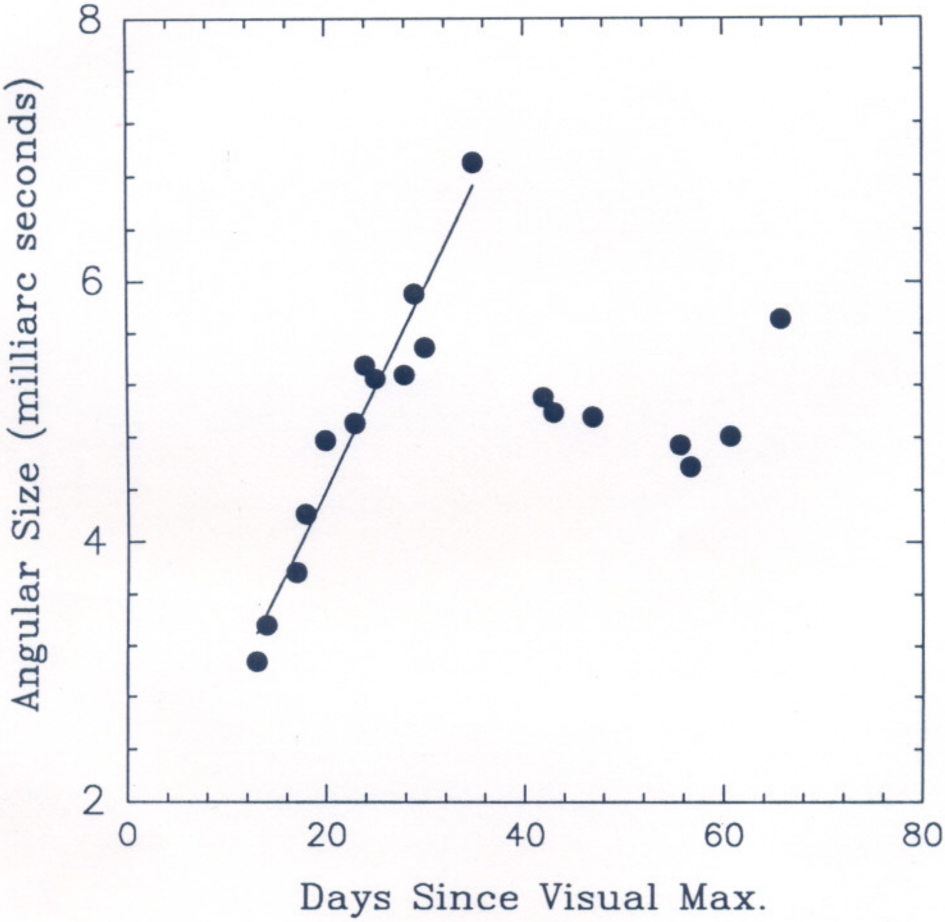

Figure 5.6: *The variation of angular size (in milliarcseconds) with time since visual maximum. Angular size increases linearly with time until $\sim$ day 30 implying expansion of the dust shell with uniform velocity. The abrupt change after day 30 could be attributed to the onset of optical thinness and the end of the dust formation stage.*

Using the value of $(\lambda\ F_\lambda) \approx 1.7 \times 10^{-15}$ W cm^{-2} (λ = 2.2 μm) measured on day 14, a distance of 8.3 kpc would imply that the IR luminosity of Nova Her 1991 was 4 π D^2 [1.34 $(\lambda\ F_\lambda)_{max}$] $\approx 5.2 \times 10^4\ L_\odot$. From initial visual observations, a magnitude m_v ~5 without exitinction would yield an outburst luminosity $L_{max} \sim 6.7\times10^5\ L_\odot$ which is clearly above the Eddington limit. It has been argued that only a fraction of this luminosity would have been transferred to the infrared, while the rest could have resulted in a high-speed stellar wind (Bath & Shaviv, 1976). If we assume that an Eddington Luminosity for a 1 $M_\odot$ star of $\sim 2.5\times10^4\ L_\odot$ appeared as the IR luminosity, then the observed flux implies a distance to the nova of only 5.8 kpc.

A characteristic feature of novae that form optically thick dust shells has been the appearance of an appreciable fraction of the outburst luminosity in the infrared. In case of Nova Her 1991 only a small fraction (10 per cent) of the outburst luminosity appears in the infrared. Considering the peak visual magnitude of $\sim$ 5 and a peak K magnitude of 4.26, we infer a visual optical depth of $\tau_v = (\lambda\ F_\lambda)_{2.2}/(\lambda\ F_\lambda)_{0.55} \sim 0.07$.

5.7 Early Coronal emission in Nova Her 1991

5.7.1 Detection of a spectral emission line

Line profiles of the 1.98 μm line obtained on the four days of observations are shown from Fig. 5.7 to Fig. 5.10. As mentioned in Table 5.2 on three days out of four, the spectral range of observations extends beyond 2.10 μm. The full observed nova spectrum of these days is shown from Fig. 5.11 to Fig. 5.13. The region near our line of interest is also highlighted as an inset in these figures. Instrumental spectral calibration has been carried out by observing a strong spectral line at 1.97 μm in a mercury discharge tube. The CVF instrumental width determined from the calibration is 0.03 μm. The observed line width (Fig. 5.7 – Fig. 5.13) does not exceed the instrumental width and hence no attempt is made to derive a line profile from the observations.

The spectral line and its adjacent continuum are represented respectively by a gaussian of fixed width (FWHM = 0.03 μm) and a line of appropriate slope. This combination is superposed on the data and is also shown in Fig. 5.7 – 5.13. It has the

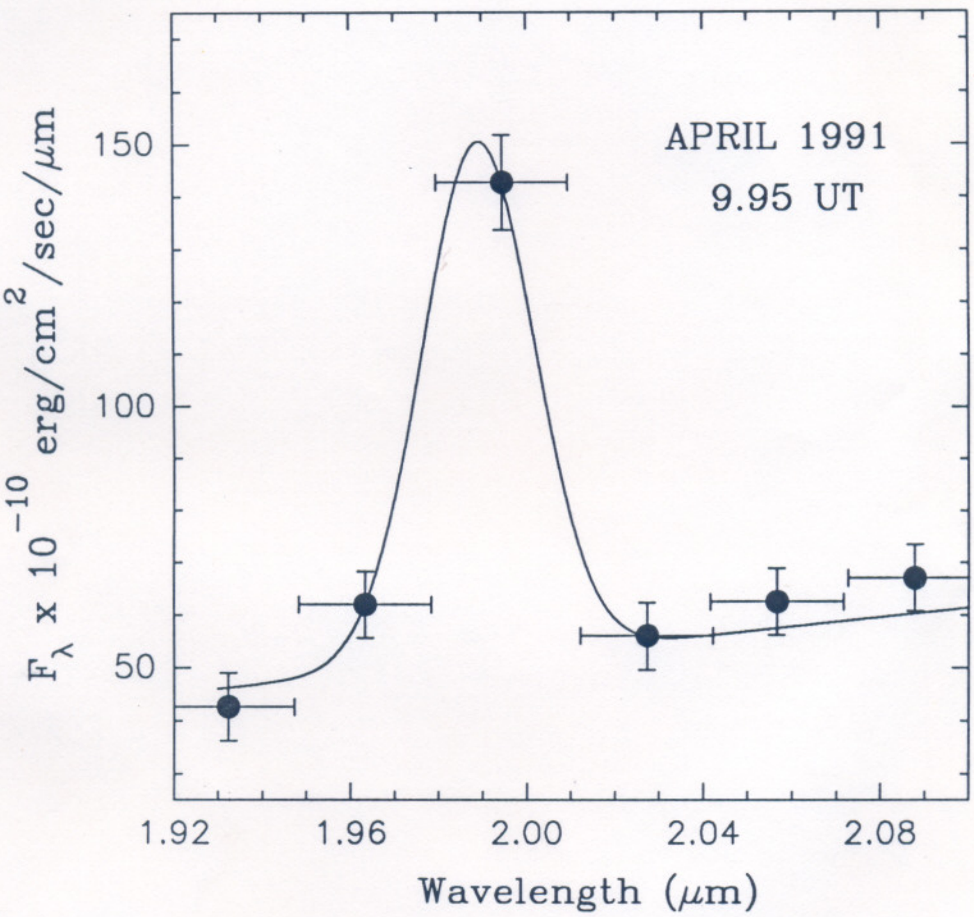

Figure 5.7: *Observed spectral line at ~ 1.98 μm from Nova Her 1991 on day 16.95 after optical maximum.*

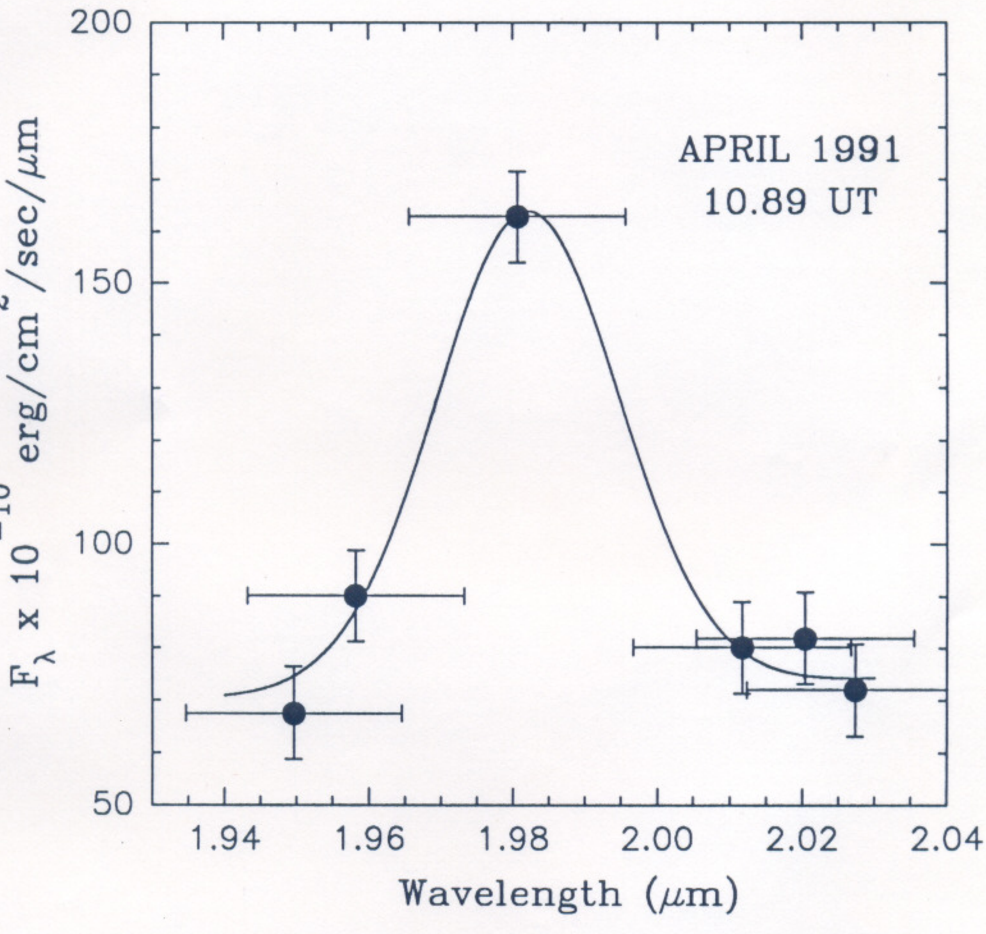

Figure 5.8: *Observed spectral line at ~ 1.98 μm from Nova Her 1991 on day 17.89 after optical maximum.*

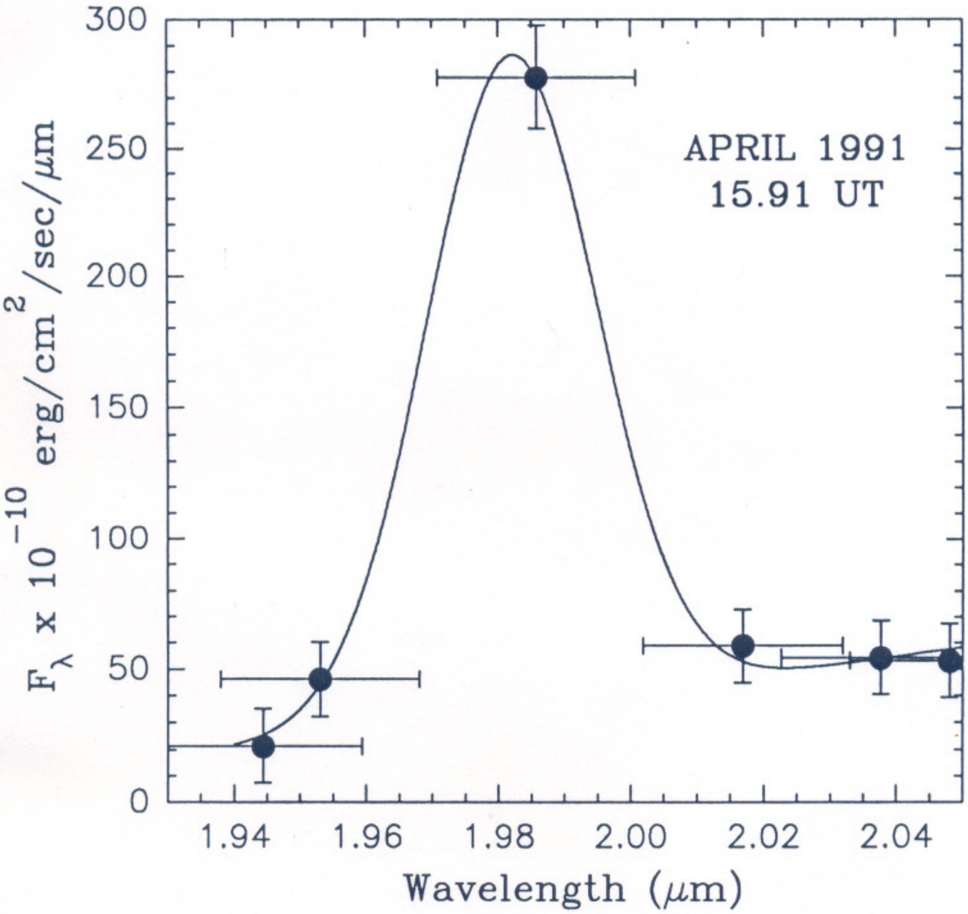

Figure 5.9: *Observed spectral line at ~ 1.98 μm from Nova Her 1991 on day 22.91 after optical maximum.*

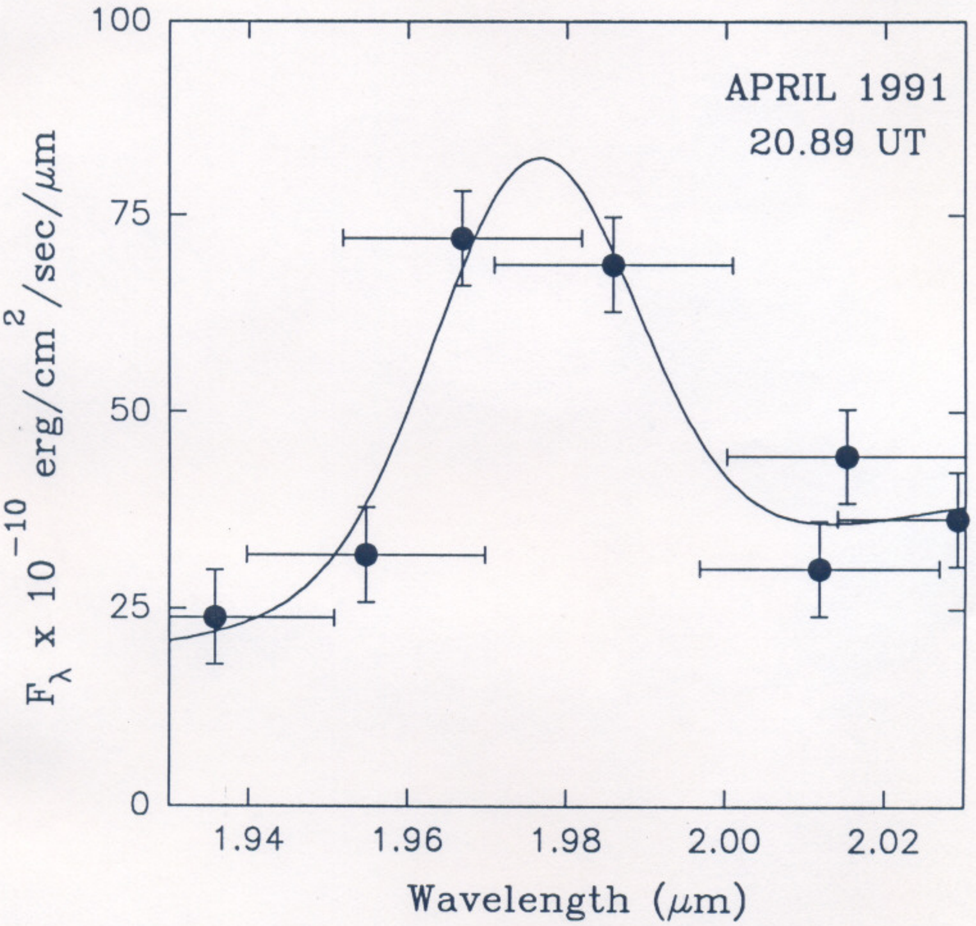

Figure 5.10: *Observed spectral line at $\sim$ 1.98 μm from Nova Her 1991 on day 27.89 after optical maximum.*

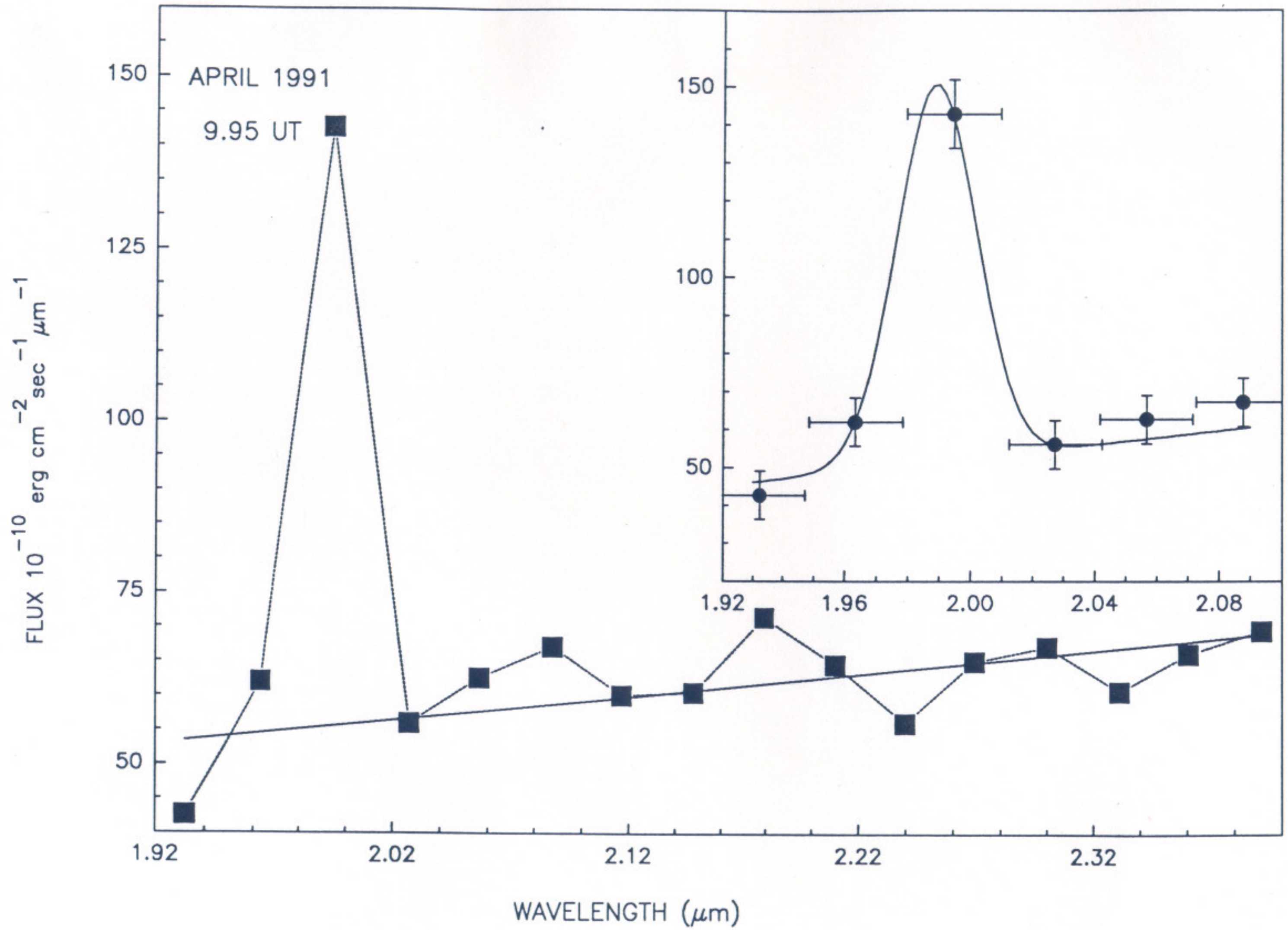

Figure 5.11: CVF observations of Nova Her 1991 on day 16.95 after optical maximum in the spectral region 1.92–2.4 μm showing the line at about 1.98 μm and the adjacent continuum.

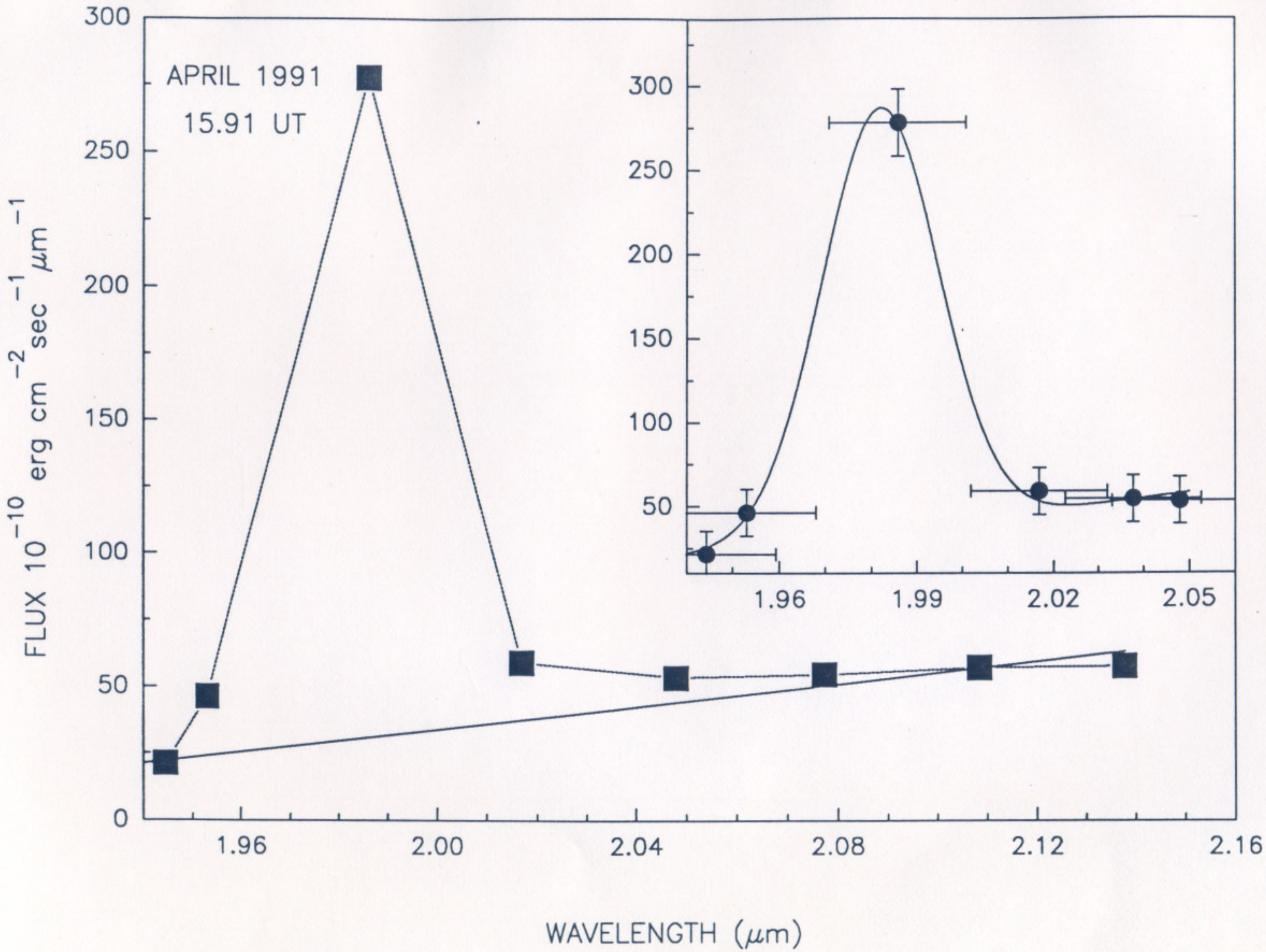

Figure 5.12: CVF observations of Nova Her 1991 on day 22.91 after optical maximum in the spectral region 1.94–2.16 μm showing the line at about 1.98 μm and the adjacent continuum.

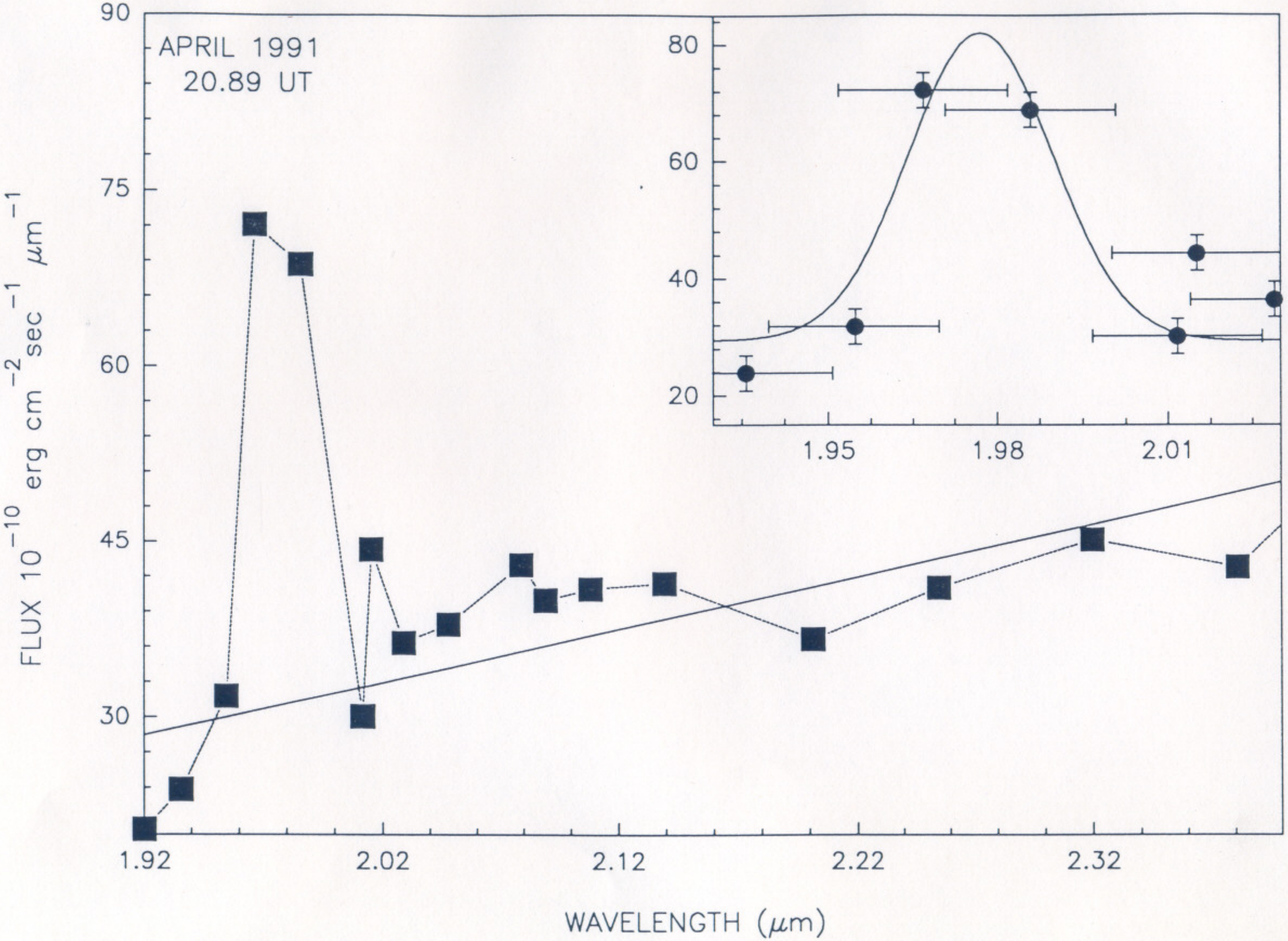

Figure 5.13: CVF observations of Nova Her 1991 on day 27.89 after optical maximum in the spectral range 1.92–2.4 μm showing the line at about 1.98 μm and the adjacent continuum.

Table 5.2: *Observations of the 1.98 μm line.*

1991 April Date UT	Days since optical maximum	Observed CVF wave-length range in μm	Line Centre wavelength ($\pm$0.02 μm)	Peak flux $\times 10^{-10}$ erg/cm^2/s/μm	Line Strength $\times 10^{-10}$ erg/cm^2/s
9.95	16.95	1.9–2.5	1.99	91$\pm$ 9	2.8$\pm$0.8
10.89	17.89	1.9–2.1	1.98	90$\pm$ 9	2.5$\pm$0.6
15.91	22.91	1.94–2.14	1.99	228$\pm$20	7.3$\pm$3
20.89	27.89	1.94–2.4	1.98	54$\pm$6	1.5$\pm$0.5

mathematical form

$$I(\lambda) = A + B\lambda + Cexp\left[-\frac{(\lambda - \lambda_o)}{2\sigma^2}\right] \tag{5.1}$$

Here σ is related to $\Delta\lambda$, the line width (Full Width at Half Maximum, FWHM) by

$$\Delta\lambda = \sqrt{8In2}\sigma. \tag{5.2}$$

A least square fit to the expression for I(λ) results in the evaluation of the parameters A, B, C and the central wavelength of the line (λ_o). A value of σ corresponding to the instrumental width (0.03 μm) has been adopted in the calculations. It can be seen from Table 5.2. that the line centre is established with reasonable accuracy at 1.98 ± 0.02 μm.

The line strength represented as the area under observed line profile above the continuum level has been determined. It is seen that on one night (1991 April 15.91) the line appears distinctly stronger with the observed flux registering more than twice the value of the previous or subsequent observations. The average value of line strength over the period of observations, $\sim (3.5 \pm 1) \times 10^{-10}$ erg/cm^2/s is adopted as a representative value for further discussions. It is to be noted from Table 5.3 that the K magnitude during this period has increased steadily by 0.5 magnitudes showing a decrease in intensity by a factor of ~ 1.6.

Table 5.3: *Near infrared Photometry, Dust temperature and Angular size of dust zone derived.*

1991 April Date UT	Days Since Optical maximum	IR Magnitude			Dust Temp. ($\pm$50K)	Calc. Angular Size of dust zone (milli arcsec)
		J	H	K		
9.95	16.95	7.71$\pm$0.08	6.16$\pm$0.10	4.51$\pm$0.03	1360	4.0
10.89	17.89	7.81$\pm$0.10	5.98$\pm$0.05	4.47$\pm$0.03	1330	4.2
15.91	22.91	8.00$\pm$0.20	6.16$\pm$0.05	4.60$\pm$0.03	1180	5.0
20.89	27.89	8.80$\pm$0.20	6.83$\pm$0.05	4.98$\pm$0.05	1080	5.7

5.7.2 Line identification

The spectral lines seen at times in novae within ± 0.1 μm of 1.98 μm are HI Brδ (1.95 μm), HeI (2.058 μm), [AlIX] (2.04 μm) and [SiVI] (1.96 μm). It is not clear if HI Brδ had been seen at all in Nova Her 1991. Paschen lines of neutral hydrogen Paβ, Paγ, and Brackett lines Brγ, Br10 $-$ Br14 with a width (FWHM) of $\sim$ 3700 km/s were seen on 1991 March 25.7 (Day 1.7) less than 2 days after optical maximum (Harrison & te Lintel Hekkert, 1991). On 1991 March 29.4 (Day 5.4) the nova showed blue continuum with broad lines of HI, Brγ Pa α, Br10, Br11 and also HeI (2.058 μm). Line intensities measured on day 5.4 were 7.5×10^{-11} erg/cm^2 /s for Brγ (2.17 μm) and 5.1×10^{-11} erg/cm^2/s for HeI (2.058 μm) (Moneti & Bouchet, 1991). Expected intensity of Brδ(1.95 μm) computed from observed Brγ intensity was $\sim 3 \times 10^{-11}$ erg/cm^2/s. With the rapid expansion of the nova and the consequent decrease in electron density the recombination lines rapidly decrease in intensity and become unobservable. Joyce (1991a), in his observations made later, did not see any hydrogen or helium emission lines. On the first and last days of our CVF observing mode, when the spectral range extended upto 2.4 μm, there was no detectable emission at 2.17 μm corresponding to HI Brγ. This implies that HI Brδ if present would also be below our detection limits.

Since the laboratory spectral calibration of the CVF allows us to pinpoint the line

Table 5.4: *Spectral Line parameters.*

Ion	Si VI
Wavelength of the coronal emission line	1.96 μm
Transition :	$^2P_{(1/2,3/2)}$
	Coronal Forbidden transition
Excitation temperature	$\sim 7.3 \times 10^3$ K
Ionization potential (E) for Si VI :	205 eV

centre within ± 0.02 μm, we can also rule out HeI (2.058 μm) and [AlIX] (2.04 μm) and ascribe the observed emission to the forbidden coronal emission due to [SiVI]. The line parameters are listed in Table 5.4. The limited spectral range of our observations (Table 5.2) precludes the observation of other coronal lines like [SiVII] (2.47 μm) which could have existed at the same time. Emissions due to [CaVII] at 2.32 μm, [AlIX] at 2.04 μm and HeI at 2.058 μm are not seen by us within detection limits.

Nova Her 1991 exhibited the coronal line emission at 1.98 μm at an unusually early phase (day 17) in its evolution. So far medium resolution near IR spectrophotometry has shown that novae enter the coronal emission phase only a few hundred days after eruption. For example Nova Vul 1984 # 2 (QU Vul) showed IR coronal emission between 500 and 800 days after optical maximum (Greenhouse et al., 1988). These authors have argued that the emission is produced by photo-ionization in a gas that exhibits a clumpy spatial distribution. Nova Cyg 1975 (V1500 Cyg), a faster nova, exhibited infrared coronal emission $\sim$ 60 days after the outburst (Grasdalen & Joyce, 1976).

Another important observation which has set Nova Her 1991 apart from other novae has been the detection of X-rays from the nova as early as day 5.4 by ROSAT satellite (Lloyd et al. 1992). Standard nova models predict X-ray emission to arise directly from nuclear burning on the white dwarf surface and do not permit X-rays in the early stages following the outburst. The best fit for the Nova Her 1991 X-ray observations require a flat spectrum of high temperature ($kT \sim 10$ KeV) thermal emission observed through a large absorbing column of neutral hydrogen with a column density (N_H) $\sim$ (3.4$\pm$1.6) $\times$ $10^{21}/cm^2$. The actual X-ray emission, the authors argue, arises from a hot shocked circumstellar material which is either pre-existing material or has been ejected during the nova eruption. A minimum density in the range 10^{-18}– 10^{-17} g/cm^3 is required for the ejecta to be heated to X-ray temperatures.

The near IR coronal line emission at 1.98 μm seen during the observations between day 17 and day 25 arises from the high temperature region in which the X-rays were detected at the periphery of the dust formation zone.

5.8 Mass of the envelope

5.8.1 Mass of gas expelled in the outburst

If we presume that the expanding nova shell went optically thin at a time t after the outburst and Thomson scattering dominated shell opacity at this time, we can estimate the gas expelled using the expression (Gehrz et al., 1988);

$$M_{gas} \sim \pi R^2(t) k_T^{-1},$$

where $R(t)$ is the shell radius at the time of onset of optical thinness and k_T is the Thomson opacity for hydrogen (0.36 cm^2 g^{-1}). Early spectroscopic observations of the nova (Della Valle & Zelinger, 1991) report hydrogen lines in emission as early as day 2.6. If we assume a time $t = 2$ d for the onset of optical thinness and an expansion velocity of 3000 km s^{-1} then

$$M_{gas} \sim 1.3 \times 10^{-5} M_{\odot}.$$

5.8.2 Mass of grains expelled in the outburst

The total grain mass in the dust shell is given by

$$M_{dust} = N \frac{4\pi}{3} \rho a^3,$$

where ρ is the density of condensed material, N is the number of dust grains and a is the grain size. Assuming the grains formed are of carbon with $a \leq 1 \mu m$ and taking $\rho \sim$

2.25 g cm^{-3}, M_{dust} can be estimated from the expression given in Gehrz et al. (1980);

$$M_{dust} = \frac{1.1 \times 10^6 (\lambda F_\lambda)_{max} D^2}{T_{BB}^6} M_\odot$$

with $(\lambda F_\lambda)_{max}$ in W cm^{-2}, D in kpc, and T_{BB} in units of 10^3 K. Taking $(\lambda F_\lambda)_{max}$ =1.7 x 10^{-15} W cm^{-2}, $T_{BB} \sim$ 1420 K and D =8.3 kpc, we get

$$M_{dust} = 1.6 \times 10^{-8} M_\odot.$$

5.8.3 Mass density of gas expelled in the outburst

Following Greenhouse et al. (1988) and Lang (1978) the line intensity of [SiVI] line from a spherical region of the nova of radius r, temperature T and distance d from earth is given by

$$I_{Si^{+5}} = \frac{(8.629 \times 10^{-6}) n_{Si^{+5}} n_e r^3 h\nu\Omega}{d^2 T^{\frac{1}{2}} g_u} cgs \tag{5.3}$$

where, $n_{Si^{+5}}$ is the number density of Si^{+5} ions, n_e is the electron density, $h\nu$ is the transition energy of [SiVI] line at 1.96 μm (0.63 eV), Ω is the collision strength and g_u is the statistical weight of its upper level.

Now,

$$n_{Si^{+5}} = \left(\frac{n_{Si^{+5}}}{n_{Si}}\right)\left(\frac{n_{Si}}{n_H} n_H\right) \tag{5.4}$$

where n_{Si} and n_H are number densities of neutral silicon and hydrogen respectively.

From the calculations of Jordan (1969) applicable to a low density plasma where radiation field is negligible, we see that for a temperature of $\sim 10^6$ K,

$$-log\left(\frac{n_{Si^{+5}}}{n_{Si}}\right) = 1.54 \tag{5.5}$$

Further,

$$-log\left(\frac{n_{Si}}{n_H}\right) = 4.48 \tag{5.6}$$

(Allen, 1973) and $n_H \sim n_e = 0.23$ (Greenhouse et al., 1988). Following Lloyd et al. (1992) a distance to nova of d = 10 ± 4 kpc is adopted. Putting in the numerical values we can rewrite Eqn. 5.3 in the form;

$$I_{Si^{+5}} = 2.86 \times 10^{-5} (\tfrac{r}{d})^3 n_e^2. \tag{5.7}$$

Taking the measured value of $I_{Si^{+5}}$ to be $\approx (3.5\pm1) \times 10^{-10}$ erg/cm^2/s

$$(\tfrac{r}{d})^3 n_e^2 \approx 1.2 \times 10^{-6} cm^{-6}. \tag{5.8}$$

The angular extent of dust-forming region for Nova Her 1991 has been estimated from broad band IR photometry to be $\sim$ 6 milliarcseconds. Further assuming the shock heated line emitting region to be located at the outer periphery of the dust forming region, we obtain $n_e \sim 2 \times 10^9$ /cm^3 and putting $n_H \sim n_e$, mass density $m_H n_H \approx 3.4 \times 10^{-15}$ g/cm^3. Further, since n_e varies as $(I_{Si^{+5}})^{\frac{1}{2}}$ it is not greatly affected by the uncertainties in the estimation of the line strength.

5.9 Early dust formation in Nova Her 1991

The most interesting aspect of Nova Her 1991 has been the rise in its IR luminosity as early as day 7 after maximum light, signifying dust formation (Feast & Carter, 1991). Since a typical 1 $M_\odot$ nova has an Eddington Luminosity $L_{Ed} \approx 2.5 \times 10^4 L_\odot$, and since it has been argued that the radiative luminosity in fast novae is limited to $L \approx L_{Ed}$, we can write an expression for the dust formation time (t_d) as

$$t_d = \frac{2}{T_g^2(0)} \left(\frac{L}{4\pi\sigma}\right)^{1/2} \frac{1}{V},$$

where $T_g(0)$ is the temperature of the grain at the time of its formation and V is the velocity of expansion such that $R = Vt_d$ gives the inner radius of the dust formation zone. It has been argued (Clayton & Wickramasinghe, 1976) that grains could condense at temperatures (T_g) as high as 2000 K. Taking $T_g(0) \sim$ 2000 K we find:

$$t_d \approx \frac{138}{V} (L/L_\odot)^{1/2} d.$$

Taking $L \approx L_{Ed} \approx 2.5 \times 10^4$ $L_\odot$ and an expansion velocity $V \approx$ 3000 km s^{-1} we get $t_d \approx$ 7.3 d.

The time when the grain temperature (T_g) reaches a value $\sim$ 1420 K is then, $t = t_d$ $[T_g(0)/T_g]^2 \sim$ 14.5 d. This value matches well with the peak K band flux reached on day 14 and an inferred blackbody temperature of $\sim$ 1400 K. Thus, early dust formation in Nova Her 1991 can be explained by the presence of refractory grains which form at temperatures close to $\sim$ 2000 K, close to the theoretical predictions (Cernuschi et al., 1967; Clayton & Wickramasinghe, 1976). Gehrz (1988) has discussed the question of why some novae produce much more dust than others. Ionization of ejecta before reaching the condensation zone, elemental underabundance of grain constituents so that nuclei are unable to accrete mantles despite high local gas densities and failure of ejecta to reach a critical density ρ_c for grain formation at the condensation point are some mechanisms which inhibit dust formation. The condition of critical density ρ_c for grain formation seems to be independently capable of explaining dust-forming scenarios in most novae. It has been shown (Gehrz & Ney, 1987) that novae developing optically thick dust shells have average shell densities of $3 \times 10^{-16} - 10^{-15}$ g cm^{-1} at the condensation point. Calculating this quantity for Nova Her 1991 we find

$$\rho_c = 1.2 \times 10^{-4}(M/M_\odot)(L/L_\odot)^{-3/2},$$

where M is the total mass ejected and L is the outburst luminosity. Earlier it has been shown that $M_{gas} \sim 1.3 \times 10^{-5} M_\odot$ and $L \approx L_{Ed} \approx 2.5 \times 10^4\ L_\odot$.

Therefore, for Nova Her 1991 we obtain

$$\rho_c = 4 \times 10^{-16} g\ cm^{-3}.$$

In Fig. 5.14 we have plotted the position of Nova Her 1991 with respect to other novae and find it located on the borderline between dust-poor and dust-rich novae.

In order that dust formation is not suppressed, the shell ionization time t_i must be $\geq t_d$. Gallagher (1977) has determined the shell ionization time as

$$t_i \approx \frac{2.2 \times 10^6}{V L^{1/3}} d.$$

Taking $V \approx 3000$ km s^{-1} and $L \approx L_{Ed} \approx 2.5 \times 10^4\ L_\odot$, we find

$$t_i \approx 25d.$$

Since in our case $t_d \sim 7$ d this condition ($t_d < t_i$) for dust formation is satisfied. Chemical abundances also play an important role in determining dust formation. Williams et al. (1978) have shown, from spectra of evolved ejecta, that DQ Her was enhanced in CNO by a factor of $\sim$ 100 compared to the solar abundance. PW Vul, in which dust

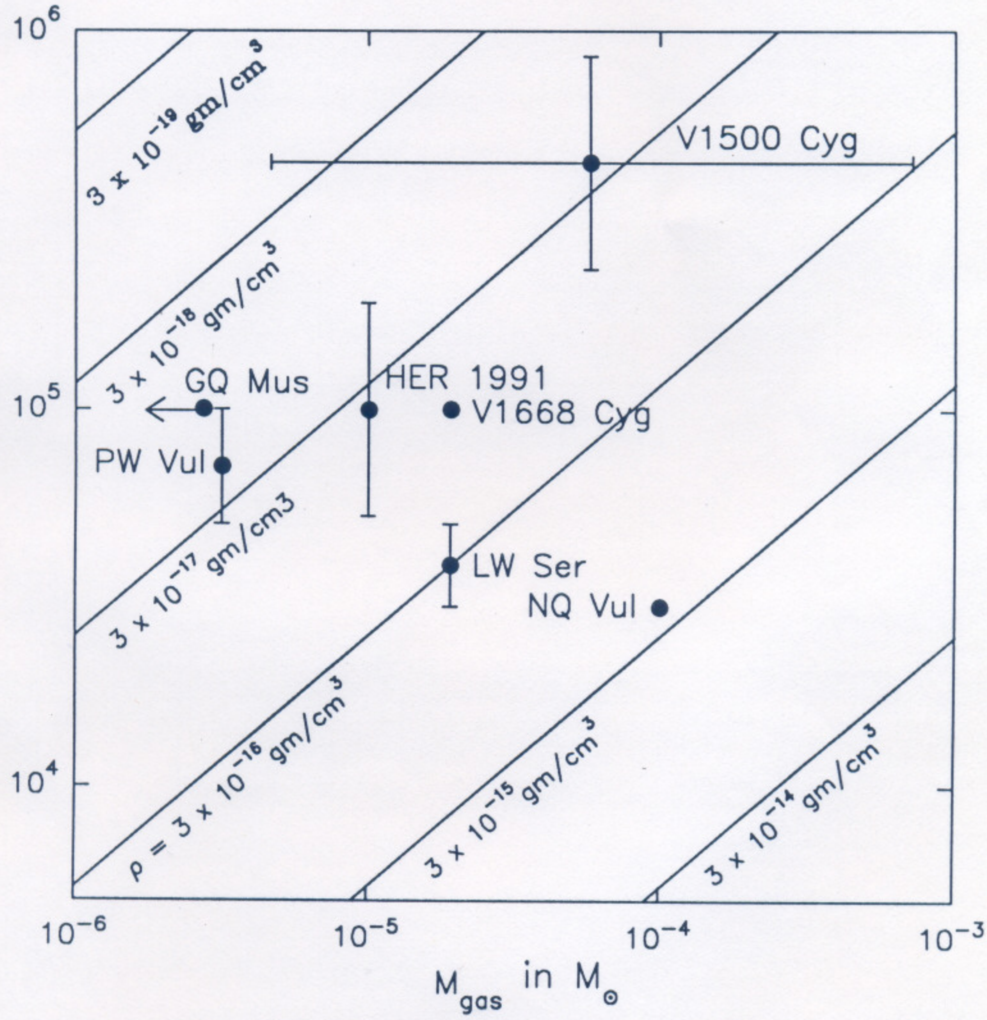

Figure 5.14: *A comparison of the outburst luminosity L_o and mass of gas ejected M_{gas} in different novae (after Gehrz, 1988). Nova Her 1991 is seen to lie in a region between dust-poor novae like PW Vul and novae which form optically thick dust shells like LW Ser and NQ Vul.*

formation was severely suppressed, did not exhibit this chemical enhancement (Gehrz et al., 1988). Nova Her 1991 is a member of the O/Ne class of objects (Dopita et al., 1991), with large neon enhancements. It would possibly also have large light-element abundances, which help dust formation. In Table 5.5 we compare the deduced physical properties of Nova Her 1991 with two other novae – Nova Ser 1978, which showed a thick dust shell, and PW Vul 1984 #1, wherein dust formation processes were severely suppressed. Nova Her 1991 emerges as a distant, luminous nova wherein the general nova evolution took place at a more rapid pace compared to other novae. The mass of gas released appears comparable to other novae, while the mass of dust condensed falls between the values for a thick dust-shell-forming nova (LW Ser) and a dust-poor nova (PW Vul).

5.10 Pre-existing material around Nova Her 1991

It has been shown (Gehrz & Ney, 1987) that novae developing optically thick dust shells have average dust shell densities in the range $3 \times 10^{-16} - 10^{-15}$ g/cm^3 at the condensation point. The critical density for grain formation in Nova Her 1991 has been shown to be $\rho_c \sim 4 \times 10^{-16}$ g/cm^3. The mass density value derived from line strength of the coronal line is above the critical density and is consistent with the argument that dust formation had begun by the time coronal emission manifested itself.

The X-ray observations require the high velocity nova ejecta to interact with some pre-existing material surrounding the nova of density in the range $\sim 10^{-18} - 10^{-17}$ g/cm^3.

It is perhaps significant that X-ray emission was detected on day 5, about 2 days before increase in IR flux indicated the onset of dust formation processes in the nova ejecta. It appears that the nova ejecta added substantially to the pre-existing material of density $\sim 10^{-18} - 10^{-17}$ g/cm^3 present at the time of X-ray emission (day 5) and reached a final value of $\sim 3.4 \times 10^{-15}$ g/cm^3 by the time dust formation processes were complete (day 25).

Is it possible that this pre-existing material has been detected in the IRAS survey indicating cold galactic dust? An elementary calculation for the angular extent of the

Table 5.5: *Comparison of Nova Her 1991 with Nova Ser 1978 and Nova PW Vul 1984.*

Parameters	Nova Her 1991	Nova Ser 1978	Nova PW Vul 1984
Day zero	JD 2448339.5$\pm$1.0	JD 2443569	JD 2445910$\pm$1.0
Expansion velocity	3000	1250	285
$V(km/s)$			
$(m_V)_{max}$	~5	7.86	6.4
A_V	0	1.0	0
	(this thesis work)	(Gehrz et al. 1980)	(Gehrz et al. 1988)
t_3 in days (for m_V)	~6	55	100
M_V	−9.6	−7.15	−7.5$\pm$1
D in kpc (from M_V)	$<$ 8.3	6.3	6.35$\pm$0.35
D in kpc (from θ_{BB},V)	$\sim$ 11.5	5	6.7
Time for dust to	7	60	158
condense t_d(days)			
M_{gas}	$10^{-5} M_\odot$	$2\times10^{-5} M_\odot$	$3.2\times10^{-6}\ M_\odot$
M_{dust}	$(1.6-2.7)\times10^{-8} M_\odot$	$3.6\times10^{-7} M_\odot$	$5.1\ \times10^{-10} M_\odot$
L (outburst luminosity)	$> 10^5 L_\odot$	$(3-5)\times10^4 L_\odot$	$10^5 L_\odot$

cold dust region can be made assuming dust at $\sim$ 30K emitting as a blackbody at a distance of $\sim$ 10 Kpc.

The sensitivity limit of IRAS point source survey at 100 μm is $\sim$ 1.5 Jy (Beichman et al., 1988). Assuming that all the emitted radiation (at 30 K) is received in the 100 μm spectral band of IRAS which has a width of $\sim$ 37 μm (83–120 μm), we obtain, for this sensitivity limit a minimum angular size ($2\theta_{min}$) given by

$$\theta^2_{min} T^4 \sim 1.25 \times 10^4 \tag{5.9}$$

$$2\theta_{min} \sim 250\mathrm{m}as \tag{5.10}$$

A search made in the two IRAS catalogs viz. the point source catalog and the extended source catalog has shown no detectable cold dust at the position corresponding to the nova in the IRAS surveys. The search puts limits on the spatial extent of pre-existing dust at a temperature of 30K or above in the pre-nova environment. The maximum angular extent of the cold dust at 30K consistent with IRAS observations is 250 milliarcseconds corresponding to 2500 A.U. at a distance of 10 kpc. At T $\sim$ 100K the extent of the dust emitting predominantly in the 25 μm IRAS band would be only $\sim$ 225 A.U. in the pre-nova environment. Cooler dust at $\sim$ 10K, however, would have been well below the sensitivity limits of IRAS to be detectable and could have existed prior to the nova, over a much larger extent.

In conclusion, Nova Her 1991 was an unusually fast nova in which grain formation processes began as early as day 7 after the eruption at a dust temperature of $\sim$ 2000K. Near infrared coronal line emission at around 1.98$\pm$0.02 μm due to [SiVI] has been detected in the spectra of Nova Her 1991 about 17 days after optical maximum. The early appearance of coronal emission is yet another unusual feature of this fast nova in which X-ray detection five days after outburst have been reported. The coronal line observations are consistent with the X-ray detection and support a hot shocked circumstellar envelope at the periphery of the dust formation zone in the nova. There is no detectable cold dust in the pre-nova environment from IRAS data, which constrains the spatial extent of dust (at 30K) in the pre-nova environment to about 2500 AU at the distance to the nova of 10 kpc.

Chapter 6

Summary and Scope for Future work

The main aim of this thesis has been to resolve the stellar photospheres and the circumstellar environment of a few evolved stars at milliarcsecond level of angular resolution in the near infrared region. A secondary objective was to investigate the processes of dust condensation and coronal emissions in Nova Herculis 1991 by near infrared photometry and spectrophotometry.

Summary

As a part of this thesis work, towards achieving the goal of high angular resolution, a reliable technique of lunar occultations in the near infrared was evolved at Physical Research Laboratory, India. A high speed near infrared photometer was designed and developed to record the occultation light curves. Occultation predictions accurate to a few seconds were made on a regular basis using the TMSS catalog of bright infrared sources. Occultation observations were carried out using 1.2 m and 0.35 m telescopes at Gurushikhar, and 1 m and 0.75 m telescopes at Kavalur. These observations include a few, difficult to observe, day time disappearance and night time reappearance events along with the relatively easier night time disappearance events. The carbon star TX Psc was observed twice, once with 0.35m telescope at Gurushikhar and again with 1 m telescope at Kavalur. Results from occultation observation of 15 late-giants/supergiants all at 2.2μm are reported in this thesis. Near infrared photometry in the J,H & K bands of the sources was also carried out with the same instrument in the photometry mode.

This data was used along with other wavelength information available in the literature and IRAS data to determine the bolometric flux and also look for infrared excess which could signify the presence of a dust shell.

A detailed analysis of all the occultation light curves was carried out to obtain the high angular resolution information. The detailed software package developed as a part of this thesis work, to analyse the observed light curves consists of a nonlinear least squares (NLS) method which provides an accurate estimation for the stellar angular size from lunar occultation light curve and the model independent algorithm (MIA) which is capable of revealing extended features in the data. The instrumental resolution was established (after a careful consideration of various factors affecting the light curve) to be ~ 2 mas.

The occultation of TV Gem constitutes the first near infrared HAR observations of this M1 supergiant. The central star and its circumstellar dust shell were resolved. The circumstellar dust envelope was found to have a radius of $\sim 20\ R_\star$ with star-to-shell flux ratio of ~ 35 at 2.2 μm. In addition, another cooler shell at $\sim 500\ R_\star$ was needed to explain the IRAS photmetric data, particularly at 60 μm. The shell dust mass was estimated from 2.2μm shell flux to be $7\times 10^{-8}\ M_\odot$. The presence of dust in two isolated shells suggests an episodic or sporadic mass loss in TV Gem. Considering these results on TV Gem and also the recent work by other HAR methods on another M1$-$M2 supergiant α Ori, it is speculated that the episodic mass loss could be a general property in early M supergiants.

A series of occultations of the bright carbon star TX Psc was predicted during 1992-1994. Knowing the rarity of a bright carbon star occultation, a co-ordinated international campaign of observing these events was organised. Two light curves, one each from Gurushikhar and Kavalur formed part of the data input from PRL, India. The stellar photosphere of TX Psc was resolved in both the light curves. Detailed analysis of the observed light curves revealed the presence of an asymmetry in the source brightness profile. This asymmetry is attributed to the presence of circumstellar material very close $\lesssim 2R_\star$) to the stellar photosphere at relatively higher temperature of < 1300 K. The stellar effective temperature of TX Psc is derived to be in the range 3000 - 3150 K.

Seven giants spanning the spectral types G8 – M7 were resolved from occultation observations. These giants have angular sizes ranging from 2.4 – 4.2 mas. In addition, occultation light curves of six giants/supergiants which had good SNR were found to be unresolved. Stringent limits were derived for their sizes. There is no evidence of companions at angular separations $\geq$ 10 mas and the K magnitude difference between the components in the range 3 - 5 magnitudes in all observed sources. Stellar effective temperatures were derived for all resolved sources and compared with the values obtained from different indirect methods. The empirical relationship that exist between stellar surface brightness in the visual (F_v) and the infrared color indices, $(V-J)$, $(V-H)$, $(V-K)$ and $(V-L)$ were investigated using a carefully selected sample of angular diameters available in the literature. Angular diameter measurements obtained from lunar occultation light curves in this thesis were compared with the estimations based on visual surface brightness and infrared colour relations and a general consistency was obtained.

Another aspect of this thesis work has been the infrared temporal studies of a fast nova, Nova Herculis 1991. Nova Her 1991 was an unusually fast nova in which grain formation processes began as early as 7 days after eruption. The spectra modeled to infrared photometric data obtained shows that the dust formed at a relatively high temperature of about 2000 K and the temperature declines with time t as $t^{-\frac{1}{2}}$. An emission line at 1.98 $\pm$ 0.02 μm, identified as the forbidden coronal line due to [Si VI] was also detected. The early appearance of coronal emission during the period 17 to 28 days after the eruption was yet another unusual feature of this fast nova. These observations are consistent with X-ray detection by ROSAT just five days after eruption and support a hot, shocked circumstellar envelope at the periphery of the dust formation zone in the nova.

Future Work

Despite its dependence on the moon and the resulting limitation in sky coverage lunar occultation, particularly in the near infrared has been well established and recognized as a technique offering great potential for HAR observations of stars at a milliarcsecond level. It has been the dominant source for stellar angular diameters, especially for the cool spectral types. The knowledge of the stellar angular sizes is used in the direct determination of the effective temperatures and calibrating the temperature scales. For the coolest spectral types (below K5) the relation between the spectrum and the T_{eff} was first determined exclusively from lunar occultation results (Ridgway et al 1980). More accurate determination of the angular diameter are possible by interferrometry, but lunar occultation still represents the only means to reach stars of spectral types beyond M5 which are not bright enough for other techniques. Multiple angular diameter measurements will also help in establishing the calibrations with much more confidence.

There are very few direct observations on the existence of circumstellar dust shells around late-type giants and supergiants.These circumstellar features are ideal targets for lunar occultation observations wherein, the circumstellar environment can be probed with very high resolution. Intriguing questions related to problems of stellar evolution, mass loss etc. can be addressed by studying these circumstellar envelopes in detail.

Lunar occultation offer very high sensitivity and resolution in detecting and studying close binary systems. Multiplicity at the early stages of stellar formation can be detected with high resolution. In comparison to other HAR techniques, lunar occultation has unrivalled capacity in terms of the limiting magnitudes involved and the large dynamic range.

The advent of CCD cameras in the visible region, while revolutionizing most fields of astronomy, has had no significant impact on the lunar occultation studies. The availability of IR arrays, has however, thrown open many unexplored vistas in astronomy particularly in relation to lunar occultation studies. They offer better sensitivity and wider applicability in the sense that many interesting astrophysical problems, like searching for low-mass companions of stars in the solar neighbourhood, can be tackled. IR arrays have been tried out in the past for few lunar occultation observations by Simon et al. (1990) and Simons et al. (1990). The major constraint was the requirement for fast readout and larger read-out noise (RON) of ~ 1000 e^- of the earlier generation arrays. However, the new generation arrays have reached a level of performance (RON ≤ 30

e^-), have the capability of reading sub arrays at fast rates and therefore can efficiently replace the conventional photometer for occultation observations. Richichi (1994b) has shown using numerical computations that the IR array is likely to improve the limiting magnitude for lunar occultation observations by about one magnitude in K band when observed with a 1 m telescope. Recently, regular occultation observations have been started using an IR array by Richichi and his co-workers. A good number of asteroids and young stellar objects will be observable with 1 m telescopes when an IR array is used for lunar occultations in the fast readout mode. A 4 m class telescope will be able to observe several active galactic nuclei at milliarcsecond levels of angular resolution to study the energetics of the sources. It should be also possible to search for brown dwarfs as a low mass companion around nearby stars.

Wavelength-resolved observations of lunar occultations should be possible with IR arrays by dispersing the light so that different parts of the array records different wavelengths. The problem of wavelength dependent angular size can therefore be efficiently addressed. From these multiwavelength observations it should be possible to easily account for the scintillation noise (if any) present in the light curve.

Scintillation noise is the major source of noise for bright star occultations with small aperture telescopes ($\lesssim$ 1m). In the presence of scintillation noise, it is very difficult to detect the signature of faint circumstellar dust envelope, if any, present around the central star. Two approaches are speculated which may enable us to overcome this problem.

Neural networks may be trained to learn the scintillation characteristics and then used to recover the HAR information present in the light curves that are severely affected by scintillation noise. Presently, there may not be enough observed light curves to train the network, nevertheless, scintillation measurements can be made within a few nights and can be used in generating large data bank by numerical simulations. Alternatively, new numerical techniques could be evolved which can take the scintillation characteristics from the measurements taken with the same telescope-instrument setup just before and after the event.

An artificial star as in the case of laser guide star adaptive optics can be placed within the isoplanatic patch around the occultation source and can be simultaneously sampled along with the event. Now from simple division of the occultation light curve with the reference light curve, the effect of scintillation on the light curve can probably be removed without assuming any model for the scintillation characteristics. This approach can be tried out with already existing laser guide star testing facilities to see the capability of this method.

Ridgway (1977) has discussed the limits imposed by various instrumental smearing effects on the angular resolution achievable by lunar occultations. Also observationally it has been shown that the achievable angular resolution is $1 - 2$ mas (White & Feierman, 1987). However, detailed numerical simulation taking into account various observational and instrumental factors is yet to be done. It will be interesting to establish such a limit for lunar occultations and compare with the present capability of optical long baseline interferometry.

Lunar occultations are one-shot events carried out at a specific position angle. It is worth following up the sources for which good quality light curves are available with other HAR techniques. Presently, complementary techniques like speckle and lunar occultations are used with the same instrument at the same telescope on the same night and such studies have given interesting results on young stellar objects. Infrared Spatial Interferometry has also resolved dust shell around a large sample of well known evolved giants. Multiwavelength observations with complementary techniques one sources like TV Gem, TX Psc and IRC+10194 can throw more light in understanding these cool giants.

Bibliography

[1] Africano, J.L., Evans, D.S., Fekel, F.C. & Ferland, G.J., 1976, AJ, 81, 650.

[2] Africano, J.L., Evans, D.S., Fekel, F.C. & Montemayor, T., 1977, AJ, 82, 631.

[3] Africano, J.L., Evans, D.S., Fekel, F.C., Smith, B.W. & Morgani, C.A., 1978, AJ, 83, 1100.

[4] Allen, C.W., 1973, Astrophysical Quantities, The Athlone press, London.

[5] Arnaud, K.A., Gilmore, G. & Cameron, A.C., 1989, MNRAS, 237,495.

[6] Ashok, N.M., Chandrasekhar, T., Sam Ragland & Bhatt, H.C., 1994, Experim. Astron., 4, 177.

[7] Babcock, H.W., 1953, PASP, 65, 229.

[8] Barnes, T.G. 1976, MNRAS, 177, 53p.

[9] Barnes, T.G. & Evans, D.S., 1976a, MNRAS, 174, 489.

[10] Barnes, T.G., Evans, D.S. & Moffett, T.J., 1978, MNRAS, 183, 285.

[11] Barnes, T.G., Evans, D.S. & Parsons, S.B., 1976b, MNRAS, 174, 503.

[12] Barnes, T.G., Dominy, J.F., Evans, D.S., Kelton, P.W., Parsone, S.B. & Stover, R.J., 1977, MNRAS, 178, 661.

[13] Bath, G.T., & Shaviv, G., 1976, MNRAS, 175, 305.

[14] Beavers, W.I., Cadmus, R.R. & Eitter, J.J., 1981, AJ, 86, 1404.

[15] Beavers, W.I., Cadmus, R.R. & Eitter, J.J., 1982, AJ, 87, 818.

[16] Beavers, W.I., Eitter J.J., Dunham, D.W. & Stein W.L.,1980, AJ, 85, 1505.

[17] Beckers, J.M., 1993, ARAA, 31, 13.

[18] Beichman, C.A., Neugebauer, G., Habing, H.J., Clegg, P.E. & Chester T.J. (Eds.), 1988, IRAS catalogs & atlases, Volume I–IV.

[19] Bell, R.A. & Gustafsson,B., 1989, MNRAS, 236, 653.

[20] Benson, J.A., Dyck, H.M., Ridgway, S.T., Dixon, D.J., Mason, W.L. & Howell, R.R., 1991, AJ, 102, 2091.

[21] Bergeat, J., Sibille, F. & Lunel, M., 1978, A&A, 64, 423.

[22] Bergeat, J., Sibille, F., Lunel, M. & Lefevre, J., 1976a, A&A, 52, 227.

[23] Bergeat, J., Lefevre, J., Kandel R., Lunel, M. & Sibille, F., 1976b, A&A, 52, 245.

[24] Bergeat, J., Lunel, M., Sibille, F. & Lefevre, J., 1976c, A&A, 52, 263.

[25] Bester, M., Danchi, W.C., Degiacomi, C.G., Townes, C.H. & Geballe, T.R., 1991, ApJ, 367, L27.

[26] Bester, M., Degiacomi, C.G., Danchi, W.C., Greenhill, L.J., Townes, C.H., Reisinger, A. & Weaver, J., 1994, IAU Symposium No.158: Very High Angular Resolution Imaging, p257.

[27] Bidelman, W.P., 1980, Pub Warner and Swasey Obs., 2, 183.

[28] Blackwell, D.E. & Lynas Gray, A.E., 1994, A&A, 282, 899.

[29] Blackwell, D.E., Petford, A.D., Arribas, S., Haddock, D.J. & Selby, M.J.,1990, A&A, 232, 396.

[30] Bloemhof, E.E., Danchi, W.C. & Townes, C.H., 1985, ApJ, 299, L37.

[31] Bloemhof, E.E., Townes, C.H. & Vanderwyck, A.H.B., 1984, ApJ, 276, L21.

[32] Bogdanov, M.B., 1979, Sov. Astron., 23, 577.

[33] Böhm-Vitesse, 1981, ARAA, 19, 295.

[34] Born, M. & Wolf, E., 1959, Principles of Optics (Pergamon Press, London).

[35] Breckinridge, J.B., 1972, Appl. Optics, 11, 2996.

[36] Brown, J.A., Sneden, C., Lambert, D.L. & Dutchover, E., 1989, ApJS, 71, 293.

[37] Buser, R. & Kuruez, R.L., 1992, A&A, 264, 557.

[38] Buss, R.H. & Snow, T.P., 1988, ApJ, 335, 331.

[39] Cernuschi, F., Marsicano, F. & Codina, S., 1967, Ann. Astrophys. 30, 1039.

[40] Chandrasekhar, T., Ashok, N.M. & Sam Ragland, 1992a, JAA, 13, 207.

[41] Chandrasekhar, T., Ashok, N.M. & Sam Ragland, 1992b, MNRAS, 255, 412.

[42] Chandrasekhar, T., Ashok, N.M. & Sam Ragland, 1993, JAA, 14, 7.

[43] Chandrasekhar T., Ashok N.M., Bhatt H.C. & Manian, K.S.B., 1984, Infrared Physics, 24, 571.

[44] Christou, J.C., Hebden, J.C. & Hege, E.K., 1988, ApJ, 327, 894.

[45] Claria, J.J., Piatti, A.E. & Lapasset, E., 1994, PASP, 106, 436.

[46] Clayton, D.D. & Wickramasinghe, N.C., 1976, Astrophys. Space Sci., 42,463.

[47] Currie, D.G., Knapp, S.L. & Liewer, K.M., 1974, ApJ, 187, 131.

[48] Danchi W.C., Bester M., Degiacomi C.G., Greenhill L.J. & Townes C.H., 1994, AJ, 107, 1469

[49] Davis, J., 1994, IAU Symposium No.158: Very High Angular Resolution Imaging, p135.

[50] de Vegt, Chr., 1974, A&A 34, 457.

[51] Della Valle, M. & Zelinger, W., 1991, IAU Circ. 5223.

[52] Deutsch A.J., 1960 in 'Stars and stellar systems', Ed. Greenstein J.L., Vol 6, chap 15

[53] Di Benedetto, G.P., 1993, A&A 270, 315.

[54] Di Benedetto, G.P. & Rabbia, Y., 1987, A&A 188, 114.

[55] Dopita, M., Ryder, S. & Vassiliadis, E., 1991, IAU Circ. 5262.

[56] Doyon, R. & Aycock, J., 1991, IAU Circ. 5224.

[57] Draine, B.T. & Lee, H.M., 1984, ApJ, 285, 89.

[58] Dunham, D.W., Evans, D.S., Silverberg, E.C., Wiant, J.R., 1975, MNRAS, 173, 61p.

[59] Dyck, H.M., Benson, J.A. & Ridgway, S.T., 1993, PASP, 105, 610.

[60] Dyck, H.M., Benson, J.A., Ridgway, S.T. & Dixon, D.J., 1992, AJ, 104, 1982.

[61] Dyck, H.M., Benson, J.A., Howell, R.R., Joyce, R.R. & Leinert, C., 1991, AJ, 102, 200.

[62] Dyck, H.M., Benson, J.A., Carlton, N.P., Coldwell, C., Lacasse, M.G., Nisenson, P., Panasyuk, A., Papaliolios, C., Pearlman, R.D., Reasenberg, R.D., 1995, AJ, 109, 378.

[63] Eddington, A.J., 1918, MNRAS, 69, 178.

[64] Eggen, O.J., 1967, ApJS, 14, 307.

[65] Eggen, O.J., 1974, PASP, 86, 129.

[66] Eggen, O.J., 1992, AJ, 104, 275.

[67] Eitter, J.J. & Beavers W.I., 1974, ApJS, 28, 405.

[68] Eitter, J.J. & Beavers, W.I., 1979, ApJS, 40, 475.

[69] Ennis, D., Becklin, E.E., Beckwith, S. Elias, J., Gatley, L. Mathews, K., Neugebauer, G. & Willner, S.P. 1977, ApJ, 214, 478.

[70] Evans, D.S. & Edwards, D.A., 1983, A.J., 88,1845.

[71] Evans, D.S., Edwards, D.A., Petterson, B.R., Robinson, E.L., Sandmann, W.H & Wiant, J.R., 1980, AJ, 85, 1262.

[72] Feast, M.W. & Carter, B.S., 1991, IAU Circ. 5230.

[73] Fluks, M.A., Plez, B., The, P.S., de Winter, D., Westerland, B.E. & Steenman, H.C., 1994, A&AS, 105, 311.

[74] Gallagher, J.S., Kaler, J.B., Olson, E.C., Hartkopf, W.I. Hunter, D.A., 1980, PASP, 92, 46.

[75] Gallagher, J.S., 1977, AJ, 82, 209.

[76] Gehrz, R.D., 1988, ARAA, 26, 377.

[77] Gehrz, R.D. & Ney, E.P., 1987, Publ. Natl. Acad. Sci. (USA) 84, 6961.

[78] Gehrz, R.D. & Woolf, N.J., 1971, ApJ, 165, 285.

[79] Gehrz, R.D., Grasdalen, G.L. & Hackwell, J.A., 1980, ApJ, 237, 855.

[80] Gehrz, R.D., Jone, T.J. & Lawrence, G., 1991, IAU Circ. 5232.

[81] Gehrz, R.D., Harrison, T.E., Ney, E.P., Mathews, K., Neugebauer, G., Elias, J., Grasdalen, G. L. & Hackwell, J.A., 1988, ApJ, 329, 894.

[82] Gezari, D.Y., Labeyrie, A. & Stachnik, R.V., 1972, ApJ, 173, L1.

[83] Gezari, D.Y., Schmitz, M. & Mead, J.M., 1987, Catalog of Infrared Observations, NASA, Reference publication 1196.

[84] Gezari, D.Y., Schmitz, M., Pitts, P.S. & Mead, J.M., 1993, Catalog of Infrared Observations, NASA, Reference publication 1294.

[85] Gillett, F.C., Merrill, K.M. & Stein W.A., 1971, ApJ, 164, 83.

[86] Gordon, K.C., 1947, ApJ, 103, 16.

[87] Gottlieb, D.M., 1978, ApJS, 38, 287.

[88] Grasdalen & Joyce, 1976, Nature, 259, 187.

[89] Greenberg J.M. & Li A., 1995, (To appear in A&A).

[90] Greenhouse, M.A., Grasdalen, G.L., Hayward, T.L., Gehrz, R.D. & Jones, T.J., 1988, AJ, 95, 172.

[91] Griffin I.P., 1993, MNRAS, 260, 831.

[92] Griffin, R.F., 1972, MNRAS, 155, 449.

[93] Hagen, W., 1982, PASP, 94, 835.

[94] Häggkvist, L. & Oja, T., 1970, A&AS, 1, 199.

[95] Häggkvist, L. & Oja, T., 1987, A&AS, 68, 259.

[96] Hanbury Brown, R., 1974, In the intensity interferometer – its application to astronomy, Taylore & Francis Ltd, London.

[97] Hanbury Brown, R. & Twiss, R.Q., 1956, Nature, 178, 1046.

[98] Hanbury Brown, R. & Davis, J. & Allen, L.R., 1974, MNRAS, 167, 121.

[99] Harrison, T.E. & Stringfellow, G., 1991, IAU Circ. 5307.

[100] Harrison, T.E. & Stringfellow, G., 1994, ApJ, 437, 827.

[101] Harrison, T.E. & te Lintel Hekkert, P., 1991, IAU Circ. 5224.

[102] Hartkopf, W.I. & McAlister, H.A., 1984, PASP,96,105.

[103] Harwood, J.M., Nather, R.E., Walker, A.R., Warner, B. & Wild, P.A.T., 1975, MNRAS, 170, 229.

[104] Hekkert, P. & Harrison, T.E., 1991, IAU Circ. 5223.

[105] Heske, A., 1990, A&A, 229, 494.

[106] Hirshfeld, A. & Sinnott, R.W., (eds.), 1982a, Sky Catalog 2000.0, Vol. I.

[107] Hirshfeld, A. & Sinnott, R.W., (eds.), 1982b, Sky Catalog 2000.0, Vol. II.

[108] Hjellming, R.M., 1991, IAU Circ. 5234.

[109] Hoffleit & Jaschek, 1982 in 'The bright star catalogue', 4^{th} revised edition, Yale University Observatory.

[110] Houk, N., 1963, AJ, 68, 253.

[111] Howell, R.R., McCarthy, D.W. & Low F.J., 1981, ApJ, 251, L21.

[112] Humphreys, R.M., Zumach, W. & Stockwey, T., 1991, IAUC, 5224.

[113] Ingram, D., Garnavich, P., Green, P. & Szkody, P., 1992, PASP, 104, 402.

[114] Johnson H.L., 1966, ARAA, 4, 193.

[115] Johnson, M.A., Betz, A.L. & Townes, C.H., 1974, Phys. Rev. Lett., 33 , 1617.

[116] Johnson, H.L., Mitchell, R.I., Iriate, B. & Wisniewski, W.Z., 1966, Comm. Lunar and Planetary Lab., 4, 99.

[117] Johnson, H.R., Ensman, L. M., Alexander, D. R., Avrett, E. H., Brown, A., Carpenter, K.G., Eriksson, K., Gustafsson, B., Jorgensen, U.G., Judge, P.D., Linsky, J.L., Luttermoser, D.G., Querci, F., Querci, M, Robinson, R.D. & Wing, R.F., 1995, ApJ, 443, 281.

[118] Jordan, C., 1969, MNRAS, 142, 501.

[119] Jorgensen, U.G., 1989, ApJ., 344, 901.

[120] Joshi, M.N. & Gopal-Krishna, 1977, MNRAS, 178, 717.

[121] Joyce, R.R., 1991a, IAU Circ. 5282.

[122] Joyce, R.R., 1991b, IAU Circ. 5297.

[123] Keenan P.C. & McNeil R.C., 1989, ApJS, 71,245.

[124] Kenyon S.J. & Fernandez-Castro T., 1987, AJ, 93, 938.

[125] Knapp, S.L., Currie, D.G. & Liewer, K.M., 1975, ApJ, 198, 561.

[126] Knoehel, G. & Van der Heide, K., 1978, A&A, 67, 209.

[127] Kukarkin, B.V., Kholopov, P.N., Efremov, Yu.N., Kukarkina, N.P., Kurochkin, N.E., Medvedeva, G.I., Perova, N.B., Fedorovich, V.P. & Frolov, M.S., 1969, General Catalog of Variable Stars, 3^{rd} edn., USSR Acad. of Sci., Moscow.

[128] Labeyrie, A., 1970, A&A, 6, 85.

[129] Labeyrie, A., 1975, A&A, 196, L71.

[130] Labeyrie, A., Schumacher, G., Dugue, M., Thom, C., Bourlen, P., Foy, F., Bonneau, D. & Foy, R., 1986, A&A, 162, 359.

[131] Lacy, C.H., 1977a, ApJS, 34, 479.

[132] Lacy, C.H., 1977b, ApJ, 213, 458.

[133] Lang, K.R., 1978, Astrophysical Formulae, Springer – Verlag, Berlin Heidelberg, New York, p.101.

[134] Lasker, B.M., Bracker, S.B., Kunkel, W.E., 1973, PASP, 85, 109.

[135] Leibowitz, E.M., Mendelson H. & Mashal, E., 1992, ApJ, 385, L49.

[136] Lena P., 1978, 'Observational techniques in Infrared Astronomy', Setti, G. & Fazio G.G. (Eds), D.Reidel Publishing Co., p.231.

[137] Lloyd, H.M., O'Brceis, T.J., Bode, M.F., Predehl, P., Schmitt, J.H.M.M., Trumper, J., Walson, M.G. & Pounds, K.P., 1992, Nature, 356, 222.

[138] Loup, C., Foryeille, T., Omont, A. & Paul, J.F., 1993, A&AS, 99, 291.

[139] Low, F.J. & Davidson, A.W., 1965, ApJ, 142, 1278.

[140] Lucke, P.B., 1978, A&A, 64, 367.

[141] Lucy L.B., 1974, AJ, 79, 745.

[142] Lynch, D.K., Hackwell, J.A. & Russel, R.W., 1992, ApJ, 398, 632.

[143] Mattei, J.A., 1991, IAU Circ. 5233.

[144] McAlister, H.A., 1985, ARAA, 23, 59.

[145] McNaught, R.H., 1991, IAU Circ 5239.

[146] McWilliam, A., 1990, ApJS, 74, 1075.

[147] Merchant, A.E., 1967, ApJ, 147, 587.

[148] Merrill, K.M. & Stein, W.A., 1976, PASP, 88, 285.

[149] Michelson, A.A., ApJ, 1920, 51, 257.

[150] Moffett, T.J., Barnes, T.G. & Evans, D.S., 1978, AJ, 83, 820.

[151] Moneti, A. & Bouchet, P., 1991, IAU Circ. 5228.

[152] Moorwood, A.F.M., 1986, Second Workshop on ESO's Very Large Telescope, D'Odorico, S. & Swing J.P., ESO conference andWorkshop Proceedings, 24, p.67.

[153] Morrison, L.V., Lukac, M.R. & Stephenson, F.R., 1981, R. Greenwich obs. Bull No: 186.

[154] Mozurkewich, D., Johnston, K.J., Simon, R.S., Bowers, P.F., Gaume, R., Hutter, D.J., Colavita, M.M., Shao, M. & Pan, X.P., 1991, AJ, 101, 2207.

[155] Nather, R.E., 1970, AJ, 75, 583.

[156] Nather, R.E. & McCants, M.M., 1970, AJ, 75, 963.

[157] Neugebauer, G. & Leighton, R.B., 1969, Two-micron SkySurvey : preliminary catalog, NASA SP-3047.

[158] Newcomb, S., 1878, Washington observations for 1875 – Appendix II, USNO.

[159] Nicolet, B., 1978, A&AS, 34, 1.

[160] Oja,T., 1987, A&AS, 71, 561.

[161] Olofsson, H., Eriksson, K. & Gustafsson, B., 1988, A&A, 196, L1.

[162] Onaka T., de Jong T. & Willems, F.J., 1989, A&A, 218, 169.

[163] Payne-Gaposchkin, C., 1957, Galactic Novae, p21, North Holland Amsterdam.

[164] Peery, B.F., Howard, U. & Wojslaw, R.S., 1976, BAAS, 8, 298.

[165] Peery, B.F., Howard, U. & Wojslaw, R.S., 1977, BAAS, 9, 365.

[166] Peterson, D.M. & White, N.M.,1984, AJ., 89, 824.

[167] Piirola, V. & Korhonen, T., 1979, A&A, 79, 254.

[168] Quirrenbach, A., Buscher, D.F., Mozurkewich, D., Hummel, C.A. & Armstrong, J.T., 1994b, A&A, 283, L130.

[169] Quirrenbach, A., Mozurkewich, D., Armstrong, J.T., Buscher, D.F. & Hummel, C.A., 1993a, ApJ, 406, 215.

[170] Quirrenbach, A., Mozurkewich, D., Hummel, C.A., Buscher, D.F. & Armstrong, J.T. 1994a, A&A, 285, 541.

[171] Quirrenbach, A., Elias II, N.M., Mozurkewich, D., Armstrong, J.T., Buscher, D.F. & Hummel, C.A., 1993b, AJ, 106, 1118.

[172] Quirrenbach, A., Mozurkewich, D., Armstrong, J.T., Johnston, K.J., Colavita, M.M & Shao, 1992, A&A, 259, L190.

[173] Radick, R.R., Henry, G.W. & Sherlin, J.M., 1984, AJ, 89, 151.

[174] Richichi, A., 1989a, A&A, 226, 366.

[175] Richichi, A., 1989b, Eds. Allion, D.M. & Mariotti, J.M. in Diffraction-limitted imaging with very large telescopes, Kluwer Academic Publishers, p415.

[176] Richichi, A., 1994a, private communication.

[177] Richichi, A., 1994b, IAU sym. 158, 'Very High Resolution Imaging', eds. Robertson J.G. & Tango W.J., p71.

[178] Richichi, A., 1995a, private communication.

[179] Richichi, A., Lisi, F. & Calamai, G., 1991, A&A, 241, 131.

[180] Richichi, A., Lisi, F., Di Giacomo, A., 1992a, A&A, 254, 149.

[181] Richichi, A., Salinari, P. & Lisi, F., 1988, ApJ, 326, 791.

[182] Richichi, A., Di Giacomo, A., Lisi, F. & Calamai, G., 1992b, A&A, 265, 535.

[183] Richichi, A., Chandrasekhar, T., Lisi, F., Howell, R.R., Meyer, C., Rabbia, Y., Sam Ragland & Ashok, N.M., 1995b, A&A, 301, 439.

[184] Ridgway, S.T., 1977, AJ, 82, 511.

[185] Ridgway, S.T. & Keady, J.J., 1988, ApJ, 326, 843.

[186] Ridgway, S.T., Wells, D.C., & Joyce, R.R., 1977, AJ, 82, 414.

[187] Ridgway, S.T., Wells, D.C., Joyce, R.R., Allen, R.G., 1979, AJ, 84, 247.

[188] Ridgway, S.T., Joyce, R.R., White, N.M. & Wing, R.F., 1980, ApJ, 235, 126.

[189] Ridgway, S.T., Wells, D.C., Joyce, R.R. & Allen, R.G., 1979, AJ, 84, 247.

[190] Ridgway, S.T., Benson, J.A., Dyck, H.M., Townsley, L.K. & Hermann, R.A., 1992, AJ, 104, 2224.

[191] Ridgway, S.T., Jacoby, G.H., Joyce, R.R., Siegel, M.J. & Wells, D.C., 1982, AJ, 87, 808.

[192] Roddier, C. & Roddier, F., 1983, ApJ, 270, L23.

[193] Roddier, F. & Roddier, C., 1985, ApJ, 295, L21.

[194] Roddier, F., Roddier, C., Petrov, R., Martin, F., Ricort, G. & Aime, C., 1986, ApJ, 305, L77.

[195] Roman, N.G., 1952, ApJ, 116, 122.

[196] Rowan-Robinson, M. & Harris, S., 1983, MNRAS, 202, 767.

[197] Russell, R. & Chatelain, M., 1991, IAU Circ. 5290.

[198] Salpeter, E.E., 1974, ApJ, 193, 585.

[199] Sam Ragland, Chandrasekhar, T. & Ashok, N.M., 1996, A&A (submitted)

[200] Sato, K. & Kuji, S., 1990, A&AS, 85, 1069.

[201] Scargle, J.D., Strecker, D.W., 1979, ApJ, 228, 838.

[202] Schmeer, P. & Royer, R., 1991, IAU Circ. 5226.

[203] Schmidt-Kaler, 1982, 'Physical parameters of the stars. In: Landolt-Bornstein New series, Volumn 2b,astronomyand astrophysics – stars and star clusters (eds. K. Schaifers, H.H. Voigt).

[204] Schmidtke, P.C., Africano, J.L., Jacoby, G.H., Joyce, R.R. & Ridgway, S.T., 1986, AJ, 91, 961.

[205] Schwarzschild, M. & Härm, R., 1962, ApJ, 136, 158.

[206] Shao, M. & Colavita, M.M., 1992, ARAA, 30, 457.

[207] Shao, M., Colavita, M.M., Hines, B.E., Staelin, D.H., Huntler, D.J. et al, 1988, A&A, 193, 357.

[208] Sharpless, S., 1956, ApJ, 124, 342.

[209] Simon, M., Chen, W.P., Forest, W.J., Garnett, J.D., Longmore, A.J., Ganer, T. & Dixon, R.I., 1990, ApJ, 360, 95.

[210] Simons, D.A., Hodapp, K.-W. & Becklin, E.E., 1990, ApJ, 360, 106.

[211] Sivaraman, K.R., Prabhu, T.P., Ghosh, K.K., Anupama, G.C. & Selvakumar, G., 1991, IAU Circ. 5236.

[212] Skinner C.J. & Whitmore B., 1987, MNRAS, 224, 335.

[213] Skinner C.J. & Whitmore B., 1988, MNRAS, 231, 169.

[214] Starrfield, S., 1988, In : Multiwavelength Astrophysics, p159, ed. Cordova, F., Cambridge University Press, Cambridge.

[215] Stencel, R.E., Pesce, J.E. & Bauer, W.H., 1989, AJ, 97, 1120.

[216] Sugano, M., Kosai, H. & Alcock, G., 1991, IAU Circ. 5222.

[217] Sutton, E.C., Storey, J.W.V. & Townes, C.H., 1978, ApJ, 224, L123.

[218] Sutton, E.C., Subramanian, S. & Townes, C.H., 1982, A&A, 110, 324.

[219] Sutton, E.C., Betz, A.L., Storey, J.W.V. & Spears, D.L., 1979, ApJ, 230, L105.

[220] Sutton, E.C., Storey, J.W.V., Betz, A.L., Townes, C.H. & Spears, D.L., 1977, ApJ, 217, L97.

[221] Toombs, R.I., Becklin, E.E., Frogel, J.A., Law, S.K., Porter, F.C. & Westphal, J.A., 1972, ApJ, 173, L71.

[222] Townes, C.H., Bester, M., Danchi, W.C., Degiacomi, C.G. & Greenhill, L.J., 1994, IAU sym. 158, 'Very High Resolution Imaging', eds. Robertson J.G. & Tango W.J., p19.

[223] Tsuji, T., 1976, PASJ, 28, 567.

[224] Tsuji, T., 1978, A&A, 62, 29.

[225] Tsuji, T., 1981a, A&A, 99, 48.

[226] Tsuji, T., 1981b, JAA, 2, 95.

[227] Turner, B.E., 1991, ApJ, 376, 573.

[228] Underhill, A.B., PASP, 1984, 96, 305.

[229] Volk, K. & Kwok, S., 1988, ApJ, 331, 435.

[230] Volk, K., Kwok, S., Stencel, R.E. & Burgel, E., 1991, ApJS, 77, 607.

[231] Warner, B., 1972, MNRAS, 158, 1p.

[232] Wesselink, A.J., 1969, MNRAS, 144, 297.

[233] White, N.M., 1978, In the HR Diagram, Eds., Philips A.G.D. & Hayes D.S. (Reidel, Dordrecht), p447.

[234] White, N.M. & Feierman, B.H., 1987, AJ, 94, 751.

[235] Whitford, A.E., 1939, ApJ, 89, 472.

[236] Williams, J.D., 1939, ApJ, 89, 467.

[237] Williams, R.E., Woolf, N.J., Hege, E.K., Moore, R.L. & Kopriva, D.A., 1978, ApJ., 224, 171.

[238] Wilson, O.C., ApJ, 1976, 205, 823.

[239] Winters, J.M., Fleischer, A.J., Gauger, A. & Sedlmayr, E., 1995, A&A, 302, 483.

[240] Woodward, C.E., Gehrz, R.D., Jones, T.J. & Lawrence, G.F., 1992, ApJ, 384, L45.

[241] Young, K., Phillips, T.G. & Knapp, G.R., 1993a, ApJS, 86, 517.

[242] Young, K., Philips, T.G. & Knapp, G.R., 1993b, ApJ, 409, 725.